

Spectroscopic and Electrochemical Studies of Di-heme Thiosulphate Dehydrogenases

Leon Paul Jenner

PhD Thesis

School of Chemistry

University of East Anglia

Norwich Research Park

Norwich

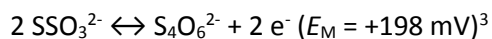
NR4 7TJ

©Leon Paul Jenner, January 2019

This copy of the thesis has been supplied on condition that anyone who consults it is understood to recognise that its copyright rests with the author and that the use of any information derived therefrom must be in accordance with current UK Copyright Law. In addition, any quotation or extract must include full attribution.

Abstract

Thiosulphate (SSO_3^{2-}) and tetrathionate ($\text{S}_4\text{O}_6^{2-}$) are found in environments where numerous bacterial species live¹. Some of these bacteria express di-heme thiosulphate dehydrogenase (TsdA)² enzymes that catalyse the interconversion of these sulphur compounds:



Electrons originate or terminate in this redox couple during respiration or photosynthesis in these bacteria. This is likely to give them a niche competitive advantage against other organisms lacking this enzyme in environments where these compounds are present. The catalytic site of TsdA enzymes is heme I which has the unusual axial ligand pairing His/Cys⁻. Heme II is an electron transfer site which has His/Met ligation in most TsdA enzymes (*eg. Campylobacter jejuni* (*Cj*) TsdA⁴), but which has a redox-driven switch between His/Lys and His/Met ligation in two known TsdA enzymes (*eg. Allochromatium vinosum* (*Av*) TsdA²).

This work uses magnetic circular dichroism (MCD) to identify the heme ligation states for recombinant TsdA enzymes *Cj* TsdA and *Av* TsdA in solution and several variants where these ligands are substituted. Protein film electrochemistry (PFE) also characterised the electroactivity of the TsdA hemes in these proteins. This, in combination with electrochemically-poised MCD samples, was used to determine the mid-point potentials of native and variant hemes. Additionally these techniques confirmed the *Av* TsdA heme II ligand switch and permitted investigation of its kinetics. Remarkably, the number of electrons transferred by *Cj* TsdA heme I in PFE is different to the number transferred by heme II. In comparison, the number of electrons transferred by the *Av* TsdA hemes are equal, although introducing *Cj* TsdA-like heme II ligation, introduces unequal electron transfer. Replacing the heme I cysteine ligand with methionine in *Cj* TsdA causes both hemes to have equal electron transfer. Liquid chromatography mass spectrometry (LC-MS)-resolved native covalent adducts to the heme I cysteine ligand, which modulate the electroactivity of heme I.

A catalytic mechanism proposed for TsdA enzymes features covalent modification of the heme I cysteine ligand⁵. Chemical treatments, substrates and substrate analogues have been used to change these modifications in a predictable manner, allowing for the characterisation of TsdA with defined heme I cysteine modifications. Combining data from PFE, MCD and LC-MS the previously-proposed catalytic mechanism is expanded further. Evidence suggests that the substrate-augmented site has adducts to the heme I cysteine which also control electron transfer to the TsdA hemes. This electron transfer is not adequately explained by conventional theory of redox centres in proteins⁶ suggesting that the reality in TsdA enzymes is more complex than this typically assumed model.

Acknowledgements

First and foremost, this project has been exciting and enjoyable every step of the way due to the support, tutelage and enthusiasm of my supervisory team. So heartfelt thanks to...

Prof. Julea Butt for being able to read a draft thesis in a weekend, for introducing me to electrochemistry and then fixing it when it doesn't work and for being the thermodynamic driving force for the whole project.

Dr. Myles Cheesman for introducing me to the world of hemes, spectroscopy and having fun while pretending to do work, for teaching me MCD and checking I didn't asphyxiate, for providing doughnuts and scrap metal and for clarifying some points on the reduction potential of ascorbate.

Dr Justin "Make Workey" Bradley for showing me how everything else works in a lab, for winding up Myles, for also teaching me MCD and checking I didn't asphyxiate, for having all the good ideas first and for being the first port-of-call when something doesn't work or make sense.

Dr. Nick Watmough for letting me have a go on his stopped-flow spectrophotometer, for tracking my progress as a researcher, for making sense of my garbled presentations in the early days, for never being afraid to let me know about my progress as a researcher.

Massive thanks also to...

Dr. Jason Crack for turning an innocent question about MS methods into a major part of my PhD, for being the first port-of-call when the mass spectrometer or anything related to a glove box doesn't work and for turning up, kids in tow, to bail me out when the nitrogen supply failed over Christmas.

Dr. Jess van Wonderen for showing me how Nova works, being 90% of my undergraduate demonstrators and aiding and abetting in the use of the Mass Spectrometer.

Many thanks to the colleagues who have popped in and out of CHE 2.24...

Prof. Nick le Brun for letting me use his Mass Spectrometer and his post-Docs, **Dr. Sophie Bennett** for putting up with me trying to grow *Paracoccus pantotrophus* as an undergraduate and going through the whole PhD process just before me, **Dr. Sam Rowe** for making snapping glass electrodes look so easy, **Dr. Tony Blake** for spending an insane amount of time doing potentiometric titrations and for instantly identifying icosahedra, **Dr. Daobo Li** for considering only working until 10 pm basically a holiday and leaving behind a very colourful electrode, **Dr. Colin Lockwood** for letting me inherit his box and rusty razorblade, **Melissa Stewart** for being a back-up Jason, **Stella Foster** for chronoamperometry and catnip and **Sam Piper** for taking over keeping CHE 2.18 running and for making conductive jigsaw puzzles.

This project would not *have* been possible without collaboration with the group of **Dr. Christiane Dahl** of the Rheinische Friedrich Wilhelms Universität Bonn. If I *have* seen far, it is because I have stood on the shoulders of Germans. Specifically...

Dr. Julia M. Kurth who *not* only grew and purified most of the TsdA enzymes and variants featured in this thesis, but who recorded vast quantities of data at Bonn and the UEA, produced even more variants, responded with alarming speed to emails and participated in extensive discussion and speculation about this enzyme system.

Sebastian van Helmont who grew and purified almost all of the rest of the TsdA enzymes and variants featured in this thesis and also helped lay a lot of the *groundwork* for their electrochemistry. It was a pleasure working *with* you and I'm not sure I can print any of the gags you cracked!

Special thanks also to last-minute saviour **Linda Brandt**, who was able to supply me just a little bit more protein to finish this work!

Thanks to the group of **Prof. Erwin Reisner** at Cambridge University, in particular **Katarzyna Sokół** who produced all IO-ITO electrodes used for the voltammetry presented in this thesis and was able to keep me supplied despite physical injury (!).

Thanks to visiting Erasmus student **Fabien Chappert** for being an assay-recording machine and for being so utterly distracted by the football game that he *didn't* notice the flags Julea snuck onto his glove box.

And finally, I am indebted to the visiting researchers from prof. Miroslav Fojta's group in Masarykova Univerzita and Biofyzikální Ústav, Brno, in particular...

Mgr. Martin Ženka for always being *cheerful* even after weeks of being sent non-electroactive samples, for finally giving up and instead working on the much more electroactive TsdA enzymes and for a strange bottle of Czech spirit.

Mgr. Zuzana Bábková for being a voltammetry recording machine, for perfecting the electrode scratching technique, for not mocking me when the peaks were actually the other way around from my predictions and for providing me with beer and a saucepan.

And finally, finally thanks to fellow Dungeon Master **Mgr. Anna Ondráčková** for making me realise snapping glass electrodes isn't actually that easy, for cheering me towards the finish line, for treemen and for a strange bottle of Czech spirit.

And of course... thanks to **Dad** – I'll get a real job now I promise! and **Mum** – thanks for wishing me luck with my thesaurus!

Contents

1. Introduction	15
1.1. Cytochromes: Defining Features.....	15
1.2. TsdA: A Novel Family of Hemoproteins	18
1.2.1. Catalytic Activity of TsdA Enzymes	19
1.2.2. Structures of TsdA Enzymes	21
1.2.3. Cysteine Conjugations and Catalysis by TsdA Enzymes.....	24
1.3. Optical Spectroscopy of Hemes for Assignment of Ligation, Oxidation and Spin States	26
1.3.1. Electronic Absorbance Spectroscopy of Hemes.....	26
1.3.2. Magnetic Circular Dichroism (MCD) of Hemes.....	29
1.4. Electrochemistry for Resolution of Heme Redox Behaviour	32
1.4.1. Potentiometry	33
1.4.2. Dynamic Protein Film Electrochemistry	34
1.5. Aim of Study.....	40
2. Materials and Methods	41
2.1. Reagents.....	41
2.2. Proteins	41
2.3. Optical spectroscopy.....	43
2.3.1. Electronic Absorbance.....	43
2.3.2. Magnetic Circular Dichroism	43
2.3.3. MCD Instrumentation.....	44
2.4. Potentiometry	46
2.5. Protein Film Voltammetry.....	46
2.6. Liquid Chromatography Mass Spectrometry	47
2.6.1. LC-MS Instrumentation	48
3. MCD and PFE of WT <i>Cj</i> and <i>Av</i> TsdA Proteins and their Variants	51
3.1. Wild-Type TsdAs.....	51

3.1.1. MCD of Oxidised TsdAs.	51
3.1.2. PFE of TsdAs.	54
3.1.3. MCD of Semi- and Fully Reduced TsdAs.....	56
3.2. MCD and PFE of TsdA Variants.	61
3.2.1. <i>Cj</i> TsdA Heme I Environment Cys-138 → Met and His Variants.	61
3.2.2. <i>Av</i> TsdA Heme I Environment Cys-96 → Met and His Variants.	66
3.2.3. <i>Av</i> TsdA Heme II Environment Lys-208 → Asn Variant.....	72
3.2.4. <i>Cj</i> TsdA Heme II Asn-254 → Lys Variant.....	74
3.3. Discussion	79
3.3.1. Heme Ligation States and E_M Values.....	79
3.3.2. Ligand switch at heme II.	81
3.3.3. Unequal Electroactive Populations between Heme I and Heme II.....	82
4. Cysteine Modifications of <i>Cj</i> WT and their Contributions to Spectroscopy and Electrochemistry.....	85
4.1. An Overview of Post-Translational Cysteine Modifications	85
4.1.1. Methods that Identify Cysteine Modifications	85
4.1.2. Cysteine Reactivity	88
4.1.3. Cysteine Chemistry of Sulphur-Cycle Enzymes	90
4.2. LC-MS Reveals Multiple Cys-138 Modifications in <i>Cj</i> WT as Prepared, which are Removed by TCEP Treatment	91
4.3. (Magneto) Optical Spectroscopy of <i>Cj</i> WT with no Cys-138 Modifications.....	96
4.4. PFE of <i>Cj</i> WT with no Cys-138 Modifications.....	98
4.5. Correlating Electroactivity and Cys Modification in <i>Cj</i> WT	102
4.6. Discussion	107
5. Preparing and Characterising Catalytic Intermediates of <i>Cj</i> WT	110
5.1. Catalytic Activity of TsdA.	110
5.1.1. PFE Investigations of <i>Cj</i> WT Catalysis and Sulphite Inhibition	111
5.1.2. Catalytic Activity of TsdA-Coated IO-ITO Electrodes.....	112

5.1.3. The Effect of Cysteine Adducts on TsdA Catalytic Activity.....	114
5.2. LC-MS of <i>Cj</i> WT Reveals Cys-138 Covalent Modification by Sulphite.	117
5.2.1. (Magneto) Optical Spectroscopy of Sulphite-Bound <i>Cj</i> WT.	120
5.2.2. Mechanism of Sulphite Binding to <i>Cj</i> WT.....	123
5.3. Electroactivity of Sulphite-Bound <i>Cj</i> WT.....	124
5.4. LC-MS and MCD of <i>Cj</i> WT Reveals Modification of Cys-138 by Substrates.	126
5.5. PFE used to Characterise Substrate-Bound <i>Cj</i> WT.....	131
5.6. Re-Evaluation of the Origin of <i>Cj</i> TsdA PFE.....	132
5.7. Discussion.....	137
6. Conclusions and Implications for the Catalytic Mechanism of <i>Cj</i> TsdA.....	139
6.1. The Catalytic Mechanism of <i>Cj</i> -Type TsdA.....	139
6.2. The Catalytic Mechanism of <i>Av</i> -Type TsdA.....	143
6.3. Further Studies.....	146
References	149

Abbreviations

All potentials throughout this thesis are quoted versus the standard hydrogen electrode (SHE)

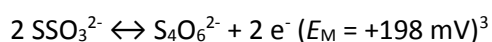
A	absorbance
AC	alternating current
A_e	geometric electrode area
A_v	<i>Allochromatium vinosum</i>
CT	charge transfer
C_j	<i>Campylobacter jejuni</i>
CV	cyclic voltammetry
DC	direct current
E	sample potential
E_M	mid-point potential
E_p	peak potential
E_{cat}	catalytic potential
ESI	electrospray ionisation
F	the Faraday constant, 96485.3 C mol ⁻¹
G	Gibbs free energy
H	magnetic field strength
h	Planck's constant, 6.62607004 x 10 ⁻³⁴ m ² kg s ⁻¹
IO-ITO	inverse-opal indium tin oxide
i	current
i_{max}	maximum current
K_d	binding constant
K_M	Michaelis constant
k°	heterogenous electron transfer rate constant
k_{cat}	maximum turnover frequency
k_{ox}	oxidative equilibrium rate constant

k_{red}	reductive equilibrium rate constant
LCMS	liquid chromatography mass spectrometry
LCP	left-handed circularly-polarised light
<i>Mp</i>	<i>Marichromatium purpuratum</i>
MCD	magnetic circular dichroism
N_{mol}	numbers of moles of electrons
n	electron stoichiometry
nIR	near infra-red
ox	oxidised
PFE	protein film electrochemistry
PGE	pyrolytic graphite edge
pH*	the apparent, measured pH of a solution in D ₂ O
Q	charge
R	the gas constant, 8.31446 J mol ⁻¹ K ⁻¹
RCP	right-handed circularly-polarised light
red	reduced
RF	radio frequency
SAM	self-assembled monolayer
SHE	standard hydrogen electrode
<i>Sl</i>	<i>Sideroxydans lithotrophicus</i>
T	absolute temperature
t	time
TCEP	tris (2-carboxyethyl) phosphine
TCEPO	tris (2-carboxyethyl) phosphine oxide
TCO	transparent conducting metal oxide
TOF	time-of-flight
TsdA	thiosulphate dehydrogenase
TsdBA	thiosulphonate dehydrogenase fusion protein

UV	ultraviolet
V	velocity
V_{\max}	maximum velocity
ν	scan rate
Ws	<i>Wolinella succinogenes</i>
WT	wild-type
X	amplitude
α	electron transfer coefficient
Γ_0^*	electroactive surface population
δ	peak half-height width
ε	extinction coefficient
θ	optical rotation
λ	wavelength
ν	frequency

1. Introduction

Cytochromes are a family of metalloproteins, ubiquitous in living organisms, which have diverse functionality thanks to the presence of the heme cofactor. Hemes can act as electron relays or provide a site for the binding or catalytic transformation of substrate molecules. The biogeochemical oxygen⁷ and nitrogen⁸ cycles are possible thanks to many well-studied cytochromes which commonly feature His/His and His/Met ligated hemes or hemes with an accessible co-ordination site. Fewer details are known about the contribution of cytochromes towards the sulphur cycle; a case in point is the recently discovered thiosulphate dehydrogenase (TsdA) bacterial enzyme family² that forms the subject of this thesis. TsdA enzymes contain c-type hemes and catalyse the following interconversion:



The active site for this catalysis is a heme with unusual His/Cys⁻ ligation^{5,9}. A second heme with His/Met ligation is thought to facilitate electron transfer, however in some TsdA enzymes this heme switches to His/Lys ligation⁹ upon oxidation. This chapter introduces TsdA enzymes and the techniques of optical spectroscopies and electrochemistry as they relate to the study of cytochromes. Chapter 3 reports the use of these techniques to characterise TsdA enzymes from *Allochromatium vinosum* (*Av*) and *Campylobacter jejuni* (*Cj*). Chapters 4 & 5 explore the consequences of post-translational Cys⁻ modifications in TsdA which parallel mechanistic intermediates found in another sulphur cycle enzyme system. All findings are then brought together in Chapter 6, where a catalytic mechanism for *Av* and *Cj* TsdA is proposed.

1.1. Cytochromes: Defining Features

The discovery of cytochromes was largely the work of David Keilin who first observed these cellular pigments in the mitochondrial respiratory chain. Keilin observed that different cytochromes could be distinguished by their electronic absorbance spectra (see below 1.3.1) and assigned them letters of the alphabet in decreasing order based on their longest wavelength absorbance bands under reducing conditions, hence cytochromes *a*, *b* and *c*. Keilin went on to observe more cytochromes in bacteria, analogous to those in mitochondria¹⁰. The naming convention he initiated has since been expanded to better distinguish similar cytochromes by the position of their longest wavelength electronic absorbance bands when reduced, for example cytochrome *c*₅₅₁¹¹ and cytochrome *b*₅₆₂¹². Alternatively some cytochromes, such as P450¹³ and P460¹⁴ are named for the wavelength of their most intense electronic absorbance band when reduced and incubated with carbon monoxide. Over time, it has become apparent that heme-binding metalloproteins and metalloenzymes are widespread in biology and have a variety of *in*

vivo functions. As a result, cytochromes are now often named according to their function, such as cytochrome *cd*₁ nitrite reductase¹⁵ and hydroxylamine oxidoreductase¹⁶. The International Union of Biochemistry and Molecular Biology Enzyme Commission (EC) classification can also be used for cytochromes which are enzymes. The TsdA enzymes for example would typically have the designation EC 1.2.8, denoting oxidoreductases that act on sulphur donors with a cytochrome as an acceptor.

Both the colour of cytochromes and much of their redox activity is the result of the heme prosthetic group. This cofactor is found in virtually all organisms and consists of an iron ion bound in a tetradentate manner by an equatorial porphyrin ring *via* its four nitrogen heteroatoms. The central iron also has two axial coordination sites, giving an octahedral geometry when these are occupied. In folded proteins, the proximal axial site is almost exclusively occupied by the side chain of an amino acid residue, typically histidine. P450s differ in that they invariably have cysteinate¹⁷ as their proximal ligand. The distal axial site can be vacant as with peroxidases¹⁸ although mostly it is occupied by a sixth ligand. This ligand is either the side chain of an amino acid residue, typically methionine or histidine, or an exogenous molecule, as with solvents or substrates binding to globins and P450s. The distal ligand can also be the amine group of the N-terminus of a peptide chain such as with cytochrome *f*¹⁹, but such instances are rare.

Several different hemes exist which are classified based on Keilin's original nomenclature¹⁰ according to the structure of their porphyrin rings and how they attach to their corresponding apoprotein. Heme *b* is the simplest of these, being an iron ion in protoporphyrin IX attached to a host protein by non-covalent interactions (Figure 1.1, Left). Heme *c* is similar but is covalently linked to cysteine residues in the host protein *via* thioether bonds from two vinyl groups on the porphyrin ring (Figure 1.1, Right). Such cysteine residues are often found in the structural motif CXXCH where the histidine residue typically serves as the proximal heme ligand²⁰.

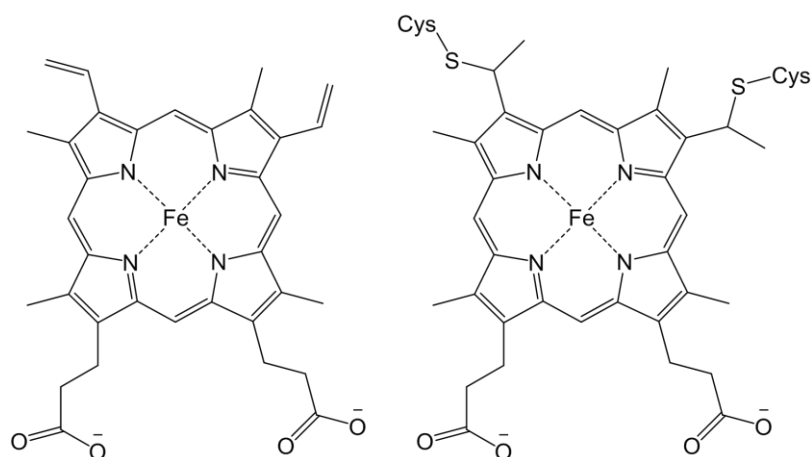


Figure 1.1 – Structures of heme *b* (left) and heme *c* (right).

Hemes display a diverse range of chemical activities depending on their environment. They can be classified as:

- i) catalytic centres for the redox transformation of molecules or ions
- ii) sites for the reversible binding of small molecules or ions
- iii) electron transfer centres

Proteins often contain multiple hemes, with axial ligation appropriate to their function within that protein. One example of this is *Nitrosomonas europaea* hydroxylamine oxidoreductase where six His/His ligated *c* hemes (Figure 1.2, blue) accompany a His/H₂O ligated P460 heme²¹ (Figure 1.2, red). P460 hemes are similar to *c* hemes but have an additional residue covalently bound to the porphyrin ring, which is tyrosine in the *N. europaea* enzyme²². Catalytic oxidation of hydroxylamine to nitrite is believed to occur with hydroxylamine binding to the P460 heme, displacing and consuming a water molecule to produce nitrite, five protons and four electrons. Nitrite is then released from the P460 heme, while the four liberated electrons are relayed across a bifurcated chain of His/His ligated hemes.

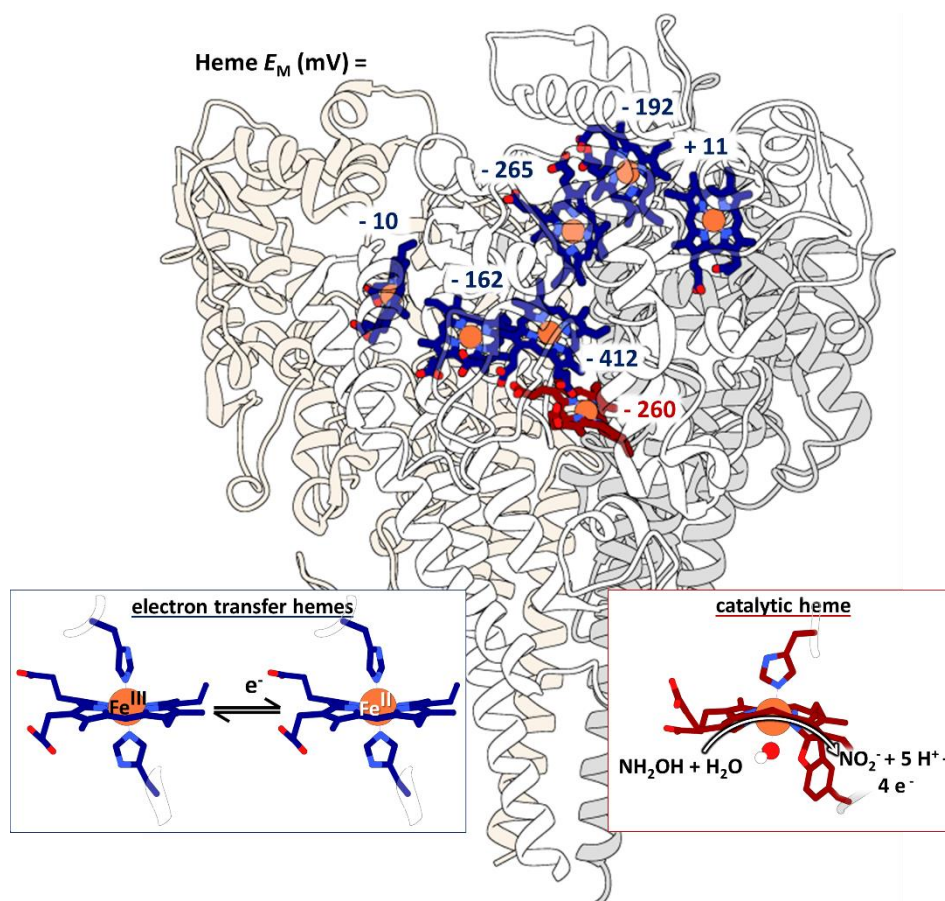


Figure 1.2 – Catalytic and electron transfer hemes within a multiheme cytochrome, *Nitrosomonas europaea* hydroxylamine oxidoreductase. Protein structure as resolved by X-ray crystallography²³ (PDB: 4N4N). Electron transfer hemes (blue) and catalytic heme (red) are shown for one monomer of the homotrimeric enzyme, three smaller subunits omitted for clarity. **Inset:** Details of coordination and reactivity of electron transfer hemes (blue) and catalytic heme (red). Structure rendered using UCSF Chimera 1.10.2²⁴.

As with the P460 heme in hydroxylamine reductase, most hemes that bind exogenous species or which serve as catalytic sites have a labile sixth ligand easily displaced by substrates. In contrast, the ligands to hemes involved in electron transfer are typically not displaced; common ligand pairings are His/His and His/Met. The iron centre in such hemes can cycle between the ferric (Fe^{III}) and ferrous (Fe^{II}) oxidation states in order to act as an electron relay. The heme environment and the chemical identity of the axial ligands define the midpoint potential (E_M) of the $\text{Fe}^{\text{II}}/\text{Fe}^{\text{III}}$ couple which in turn defines the driving force for electron transfer to other redox centres. Knowledge of the axial ligands provides some indication of the likely E_M value of a given heme; examples of His/Met heme potentials range from +20 to +370 mV, whilst examples of His/His ligated hemes have potentials between -412 and +130 mV²⁵.

From the information above it should be apparent that when characterising a novel heme enzyme, the role of each heme can often be inferred from the identity of the axial ligands. This information can be resolved using X-ray diffraction of the crystallised protein. However, even if this is possible at atomic resolution, the process of crystallising a protein is complex and time consuming; over this time proteins may become modified by oxygen or additives necessary for efficient crystallisation²⁶. In addition, as a synchrotron X-ray source is often necessary to collect high quality diffraction data, proteins can be subjected to intense radiation *in crystallo* which may photolyse bonds or photoreduce metal-containing cofactors²⁷. As such there is a concern that the structure of a protein crystal might differ from the natural protein in solution²⁸. In this context it is significant that (magneto-) optical spectroscopy can be used to assign heme ligation as well as oxidation and spin states as presented in Section 1.3. These spectroscopies can be combined with potentiometric titration to resolve heme reduction potentials as described in Section 1.4. That section also introduces protein film electrochemistry as a complementary tool for studying redox proteins. In the following section (1.2) the heme-containing TsdA enzymes are introduced along with justification for using magneto-optical and multiple electrochemical approaches to gain new insights into enzyme structure-function.

1.2. TsdA: A Novel Family of Hemoproteins

TsdA enzymes are found in the periplasm of several species of bacteria. In many species, thiosulphate is oxidised by TsdA to provide a source of electrons for aerobic respiration (Figure 1.3, right). Also, photosynthetic bacteria use TsdA-catalysed thiosulphate oxidation to provide electrons during anaerobic photosynthesis, possibly to offset electrons leaving the quinone pool to fuel the Calvin cycle (Figure 1.3, centre). The purple sulphur bacteria *Allochromatium vinosum* (*Av*)²⁹ and *Marichromatium purpuratum* (*Mp*)³⁰ feature both of these activities. Microaerophilic gut bacteria of the order Campylobacteriales, such as the human pathogen *Campylobacter jejuni*

(Cj), instead employ TsdA so that tetrathionate can be used as an alternative terminal electron acceptor during anaerobic respiration⁴ (Figure 1.3, left).

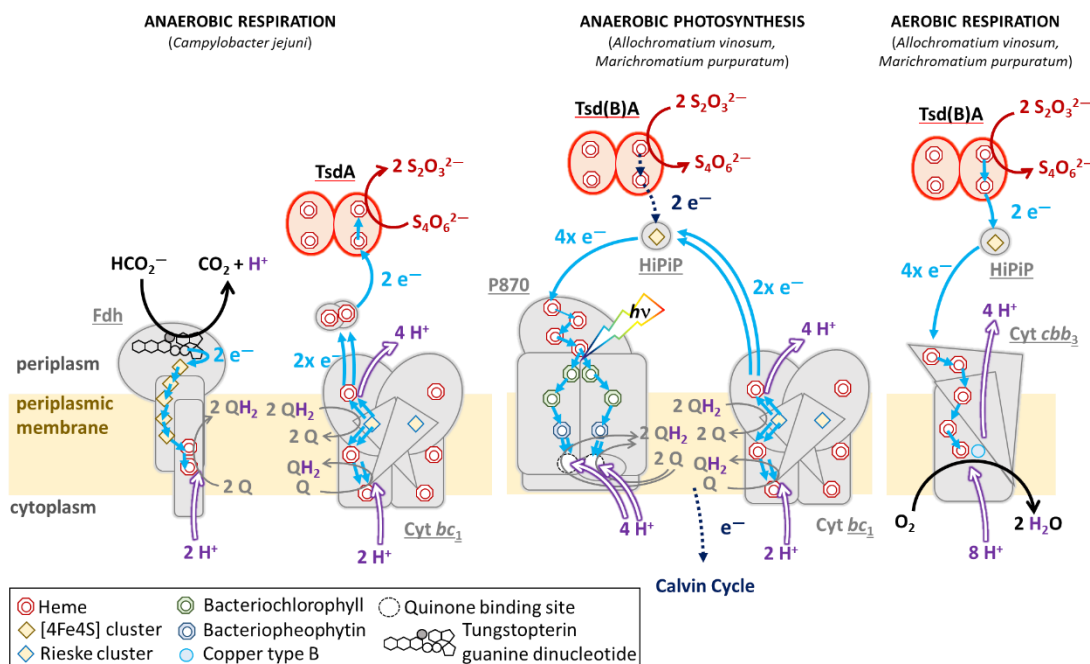


Figure 1.3 - TsdA enzymes in bacterial metabolism. (Left) In *Campylobacter jejuni*, TsdA receives electrons from cytochrome bc_1 which are used to reduce tetrathionate⁴. **(Right)** In *Allochrochromatium vinosum* and *Marichrochromatium purpuratum*, Tsd(B)A oxidises thiosulphate to provide electrons to cytochrome cbb_3 for the reduction of oxygen via a high-potential iron-sulphur protein (HiPIP) during aerobic respiration³⁰. **(Centre)** Alternatively electrons from HiPIP are transferred to the photosystem P870 to be photoexcited during anaerobic photosynthesis.

1.2.1. Catalytic Activity of TsdA Enzymes

Ferric cytochrome c or ferricyanide act as both electron acceptor and chromophore for thiosulphate oxidation by purified TsdA, permitting spectrophotometric monitoring of the course of this reaction *in vitro*. Tetrathionate reduction by purified TsdA has been assayed in a similar manner, using the methyl viologen cation radical as both a chromophore and an electron donor. From these assays, the maximum turnover number (k_{cat}) and Michaelis constant (K_M) of TsdA from several organisms have been reported^{5,9,31,32}. k_{cat} represents the maximum number of substrate molecules each enzyme molecule can convert per second during catalysis and K_M is the substrate concentration where half of the active sites in a sample are bound, giving a measure of the affinity an enzyme has for its substrate. Use of these parameters enables comparison of TsdA from different source organisms.

Regardless of their proposed *in vivo* role, purified recombinant wild-type (WT) TsdA enzymes catalyse both thiosulphate oxidation and tetrathionate reduction at measurable rates *in*

vitro. To date, the k_{cat} for thiosulphate oxidation (Figure 1.4, middle panel, blue bars) does not vary by more than one order of magnitude across organisms. However, for tetrathionate reduction (Figure 1.4, middle panel, red bars) TsdA enzymes from *Av* and the iron-oxidising autotroph *Sideroxydans lithotrophicus* (*Sl*) have k_{cat} values approximately 40-fold lower than TsdA from *Cj* and the related microaerophile *Wolinella succinogenes* (*Ws*). Similar experiments have also been performed using catalytic voltammetry of *Av* and *Cj* WT enzymes and the trends in activity are consistent with solution experiments³. The ratio k_{cat}/K_M , often termed the specificity constant, often reflects catalytic activity in cellular conditions. Specificity constant values for thiosulphate oxidation (Figure 1.4, right panel, blue bars) by wild-type enzymes fall within an order of magnitude with the exception of *Ws* WT which is approximately 20-fold lower. For tetrathionate reduction (Figure 1.4, right panel, red bars) k_{cat}/K_M is similar for *Ws* WT and *Cj* WT, but 200-fold less for *Sl* WT and 1000-fold less for *Av* WT.

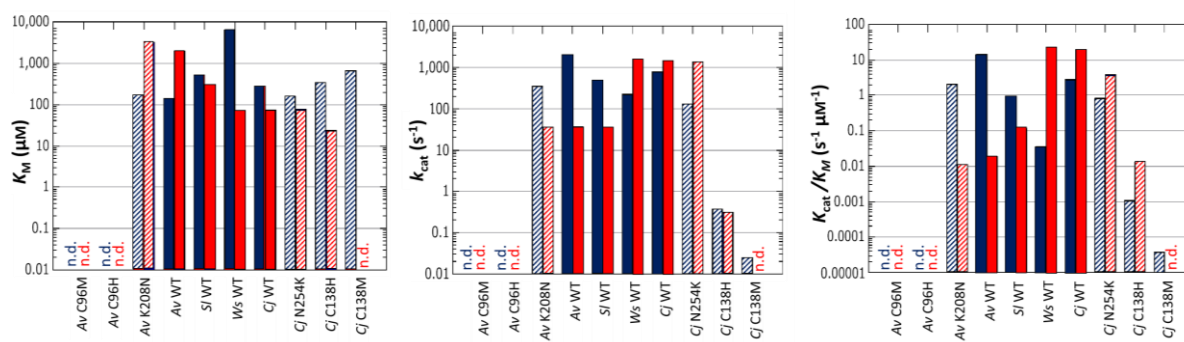


Figure 1.4 – Kinetic parameters for thiosulphate oxidation (blue) and tetrathionate reduction (red) in TsdA enzymes and variants. k_{cat} and K_M for thiosulphate oxidation was determined by *in vitro* spectrophotometric enzyme activity assays, ‘n.d.’ denotes no measurable activity. *Allochromatium vinosum* (*Av*) and variants pH 5.0, T = 303 K^{5,9}; *Sideroxydans lithotrophicus* (*Sl*) pH 5.0, T = 293 K³¹; *Wolinella succinogenes* (*Ws*) pH 5.5 (ox.) 6.5 (red.), T = 312 K³¹; *Campylobacter jejuni* (*Cj*) and variants pH 6.5 (ox.) 5.0 (red.), T = 315 K³². Donor/acceptor is 1 mM ferricyanide (thiosulphate oxidation) or 80 μM cytochrome *c* (*Cj* and variants) or 300 μM methyl viologen (tetrathionate reduction).

Similarly, the K_M values for thiosulphate oxidation (Figure 1.4, left panel, blue bars) all fall within an order of magnitude of one another, except for *Ws* WT which is more than 20-fold higher. The K_M values for tetrathionate reduction (Figure 1.4, left panel, red bars) are comparable for *Cj* WT and *Ws* WT but are approximately 4-fold higher and 30-fold higher for *Sl* WT and *Av* WT, respectively. This suggests that whilst only *Ws* WT has a different (decreased) affinity for thiosulphate, the affinity for tetrathionate between TsdA enzymes is more varied. Overall, kinetic parameters from *in vitro* activity assays suggest that there are differences in the catalytic activity of recombinant TsdA enzymes from different organisms which are more pronounced in the direction of tetrathionate reduction. It is therefore of interest to investigate the molecular basis of these differences.

1.2.2. Structures of TsdA Enzymes

TsdA monomers have a molecular mass of ~30 kDa and possess two domains, each of which features a CXXCH motif that binds a *c* type heme. The best characterised member of the family to date is *Av* WT for which X-ray crystallography has resolved the structure along with several variants under a variety of conditions^{5,9,33}. The structure of the di-ferric form of *Av* WT as-purified (Figure 1.5, left) resolves the two heme cofactors with an edge-to-edge distance of 8.1 Å, implying facile electron transfer can occur between them⁶. One heme (I) binds to the first CXXCH motif in the *Av* WT sequence, with His-53 from the motif providing the proximal heme ligand and Cys-96 providing the distal heme ligand (Figure 1.6, A). A solvent channel lined by positively charged arginine residues surrounds Cys-96. Two of these surrounding residues, Arg-82 and Arg-92 are implicated in binding negatively charged substrate molecules⁵ together with the hydrogen bond donor Ser-100 (Figure 1.5, brown residues). Heme I is proposed to be the active site for catalysis^{5,9}. Consistent with this, electron density modelled as sulphite (Figure 1.6, B) or thiosulphate (Figure 1.6, C) molecules is present near to the sulphur of Cys-96 in sulphite and dithionite-soaked crystal structures respectively⁹. Additionally, in both structures the sidechains of Arg-82, Arg-92 and Ser-100 are orientated towards these molecules in a manner consistent with electrostatic binding.

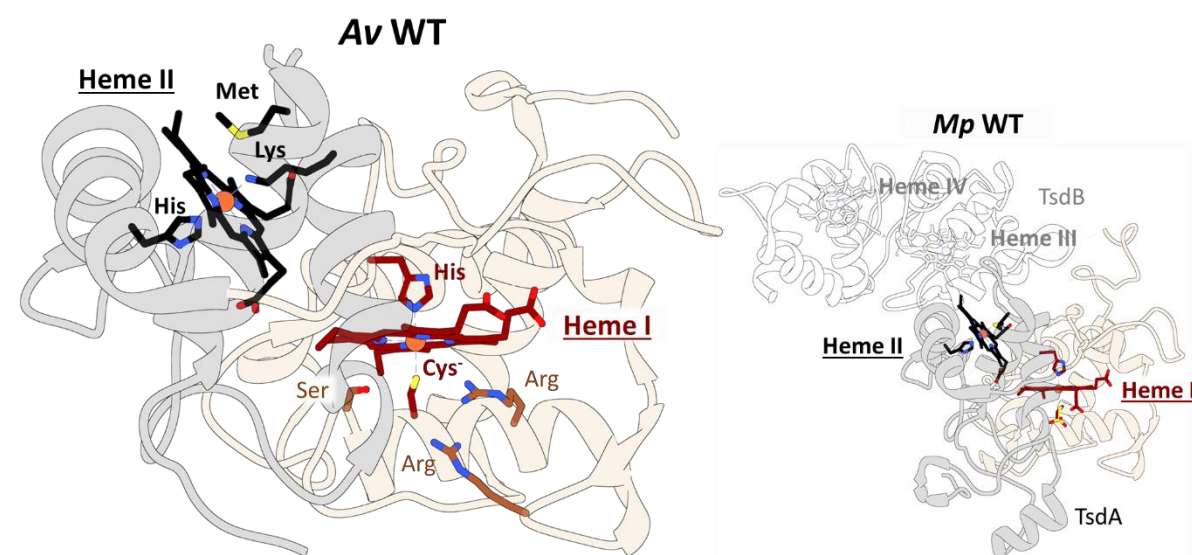


Figure 1.5 – 1.98 Å resolution structure of *Av* WT as-isolated⁹ (left, PDB 4WQ7) and 2.75 Å structure of *Mp* WT as-isolated³⁰ (right, PDB 5LO9) resolved by X-ray diffraction. Heme I cofactors in red, domains in beige. Heme II cofactors in black, domains in grey. *Mp* TsdB, a fused redox partner with two His/Met ligated hemes, shown in white. Structures rendered using UCSF Chimera 1.10.2²⁴.

The second heme (II) in the di-ferric *Av* WT structure is bound to the second CXXCH motif in the polypeptide sequence, with His-164 in the motif providing a proximal heme ligand and Lys-209 providing the distal heme ligand (Figure 1.6, E). It is proposed that this heme functions as an electron transfer site, so that the two hemes can each accept or donate one of the two electrons for interconversion of thiosulphate and tetrathionate^{5,9}.

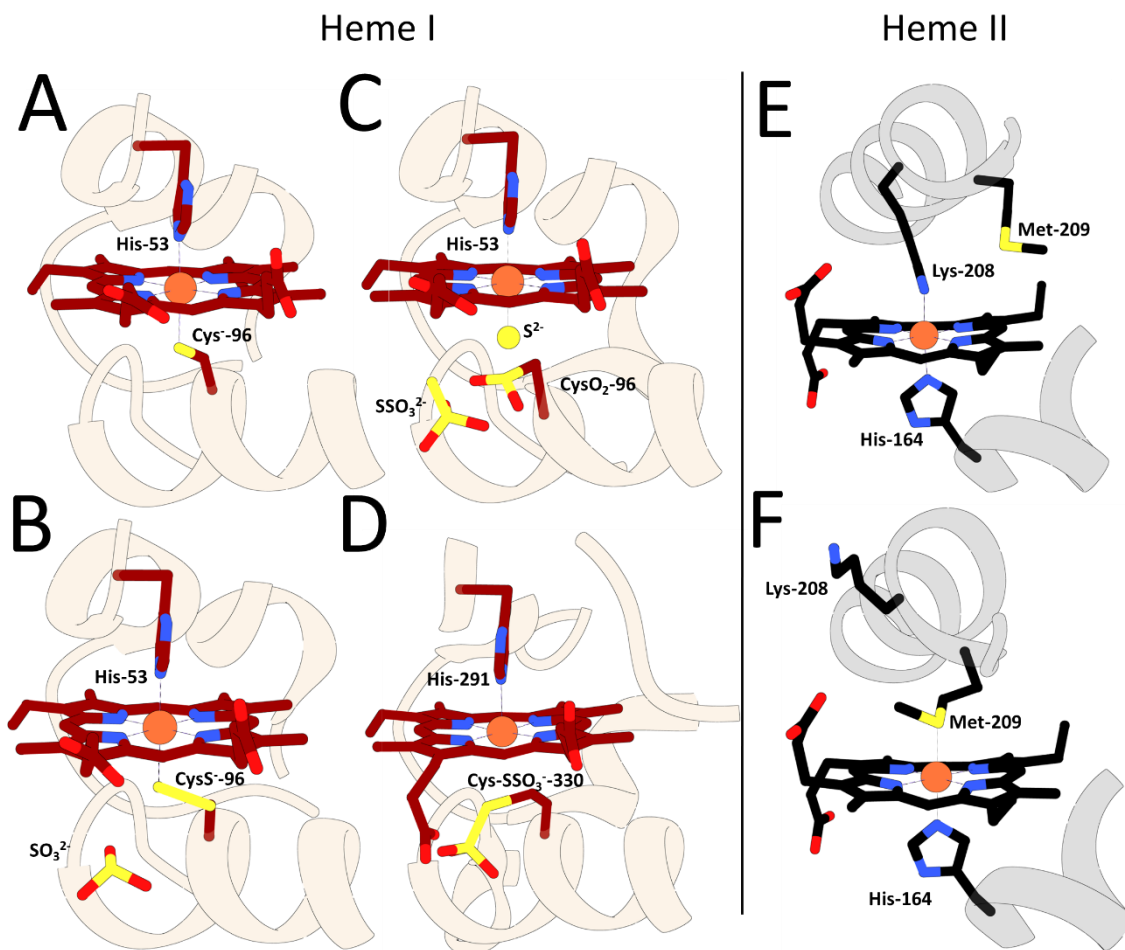


Figure 1.6 - Details of Heme Ligation in TsdA structures resolved by X-ray diffraction^{9,30}. **A)** *Av* WT 'as isolated' (4WQ7) heme I with His-53/Cys-96 ligation **B)** 'sulphite soak' (4WQB) with cysteine persulphide ligation and bound sulphite **C)** 'dithionite soak' (4WQ9) with sulphide ligation, bound thiosulphate and cysteine sulphenic acid, **D)** *Mp* WT 'as isolated' heme I with His-291/- ligation and Cys-330 modelled as cysteine thiosulphonate. **E)** *Av* WT 'as isolated' heme II with His-164/Lys-208 ligation. **F)** *Av* WT 'dithionite soak' heme II with His-164/Met-209 ligation. Structures rendered using UCSF Chimera 1.10.2²⁴.

The heme I binding motif and distal cysteine ligand are conserved in all known and putative TsdA enzymes (Figure 1.7, blue shading). The heme II binding motif is also conserved, however the lysine ligand is only present in *Av* TsdA and predicted in the TsdA of permafrost-dwelling bacterium *Psychrobacter arcticus* (Figure 1.7, orange shading). All other TsdA enzymes have non-ligating residues in this position making the prediction of heme II ligands from sequence alignments ambiguous.

<i>Parachlamydia acanthamoebae</i>	-----	0
<i>Campylobacter jejuni</i>	-----LDPNL-----	5
<i>Wolinella succinogenes</i>	-----FERWT-----	5
<i>Marichromatium purpuratum</i>	PACVCRCHGPGGVGAGAVFPPLAGQPYSYLLAQLQAWGTGRRRHGPEMALMGAVAGRLDADE	180
<i>Thiomonas intermedia</i>	-----	0
<i>Sideroxydans lithotrophicus</i>	-----	0
<i>Pseudomonas stutzeri</i>	-----	0
<i>Allochromatium vinosum</i>	-----	0
<i>Psychrobacter arcticus</i>	-----SDNTE-----	5
<i>Parachlamydia acanthamoebae</i>	-----SSN-----	3
<i>Campylobacter jejuni</i>	-----EK-----TKSATGIDLPTAKWNLPKALNED-----	30
<i>Wolinella succinogenes</i>	-----LE-----ARGKSGYDAPKLEWVEGKTIINEIKNPITI	35
<i>Marichromatium purpuratum</i>	QRALAAAYFATRPLAVADPADDLDPSPPPATASVSTPAMTVAGANAVVPEHLGAV-----	235
<i>Thiomonas intermedia</i>	-----ADAPMAP-PKSEI-----	12
<i>Sideroxydans lithotrophicus</i>	-----ASET-----	4
<i>Pseudomonas stutzeri</i>	-----AEIKMDDQSQTLTQ-----	13
<i>Allochromatium vinosum</i>	-----	0
<i>Psychrobacter arcticus</i>	TKAVERVEEAAALA---RVKDLLEA---RAEALKS---NMPAANDMTA---TAG---	46
<i>Parachlamydia acanthamoebae</i>	--GMSSNDTQEWRTLLDPEMAPENIKPLVMQGFRI LFDTKK-----HAPQYAGDE	53
<i>Campylobacter jejuni</i>	-----GTIDETKMPKNSSEYSKMWILGNKILNETSKYVGPQAKDPKKRFAGNN	77
<i>Wolinella succinogenes</i>	QYALPKFEGDVFDWTINAKPVVPSIYGEFVQYGYELFVNTQAVI GPEVADPNMRYSGNN	95
<i>Marichromatium purpuratum</i>	--PAGRAEAAAS-RFTPPSRDALPEGLPEGMVRLGARLFRHTNTD-----PRSA PHVGN	286
<i>Thiomonas intermedia</i>	--NA-AVGTGA-KFTPPPESAIPDDDFGKMKVLLGRDIMLDTPK-----YAKDYVNTD	60
<i>Sideroxydans lithotrophicus</i>	--STPTAAKAL-VFTPPNDEEIPNNEFGKIVRQGNKNI FEDTQH-----YAKQYVGN	53
<i>Pseudomonas stutzeri</i>	--KAGKGAGES-YFQPPQEKDLPANAYGELVQQGRAIFVDTQK-----YAAEYVGN	62
<i>Allochromatium vinosum</i>	-----EEPTTV-ALTVPAAALLPDGALGESIVRGRYLSDTPA-----QLPFDVGN	46
<i>Psychrobacter arcticus</i>	--GTD TASGKP-TIKMPDESTIPDDEFGAAVRRGLQISNHTYK-----ELPNFVGNQ	95
Heme I		
<i>Parachlamydia acanthamoebae</i>	ISCTNCHFNCGNTFGGENNGISLVGVTKKYPRAILD-NPHYTLEERINACFTKSLNG---	109
<i>Campylobacter jejuni</i>	LSCSSCHANGG---SVQNQSGFVGIWARFPQYNARGDKVITLADRINGCFERSMNG---	130
<i>Wolinella succinogenes</i>	LSCNSCHLGAG---TAKYAAPLVNDHANFPQYRNRENSLGTMAARVNGCMQRSMNG---	148
<i>Marichromatium purpuratum</i>	QTCAGCHLDNG---RRADASPMWAAWVAYPAYRGKNQRVDTMAERIQCFFRYSMNAQDS	342
<i>Thiomonas intermedia</i>	LSCVNCHTDAG---RMAGSAPLWAAVVSYPAYRGKNNKVNTFEERLQGCFFKFSQNG---	113
<i>Sideroxydans lithotrophicus</i>	LNCVNCHLASG---RKNSSPLWAAVRYPAYRAKNNKVNTYEERIQCCKFYSLNG---	106
<i>Pseudomonas stutzeri</i>	MNCTNCHLEQG---RKNASAPLWAGAYPMYPAYRKKNKVNYSYAEYVQGCFFRYSMNG---	115
<i>Allochromatium vinosum</i>	LACRHCHPGRDGEVGTANAAFPVGVGRFPQYSARHGRLITLEQRIGDCFFERSLNG---	103
<i>Psychrobacter arcticus</i>	LNCTSCHLGNG---SEAYAAPWNNTPSVYPNYSKRTGRINTIQERINDCFERSLNG---	148
<i>Parachlamydia acanthamoebae</i>	---KPVPLKSKEMKAMIAYLEWISKGVSNQA---PWLGLKRLS---HAI PNAEKGNAL	159
<i>Campylobacter jejuni</i>	---KRMPSDTPEMKAMLTMYQWLSQGVVPGA-KIEGQGLKIDF---ISRAADPKKGA	183
<i>Wolinella succinogenes</i>	---YPLPAEGKEMKAFLAYIHWLGGQIPVGA-KIEGRSLKTVDKRMVQQNAADVKNAGEV	204
<i>Marichromatium purpuratum</i>	VSGQVPTENGLVLDALQSYIFWLATGAPTGDAMSGRGPRLQP---PAEGFDRTRGAAL	399
<i>Thiomonas intermedia</i>	---KAPPLGSKTLVALESYSYWLKGLPVDE-KVAGRGPNLPE---PQQAPDYVRGQK	166
<i>Sideroxydans lithotrophicus</i>	---KAPAVDSPEMVALVITYSYWLATGAPVGA-KLKGAGYPEVPK---PGLIPDANRGT	159
<i>Pseudomonas stutzeri</i>	---TPPAADSHVINALTAYSYWLSTGAPTQ---ELPGRAYPEVPO---PQQGFDIAGKGI	168
<i>Allochromatium vinosum</i>	---RALALDHPALIDMLAYMSWLSQGVVPGA-VVAGHGPITLTL---E-REPDGHWGEAL	155
<i>Psychrobacter arcticus</i>	---KALDLNSDDMNAMVSYMSWLSQDMFPGV-SPEGSGFVKVVK---T-LEPNTDNGK	200
Heme II		
<i>Parachlamydia acanthamoebae</i>	YQHCACCHGKDEGQLRPD-----NLKYPPLWGN-HS FNQAAGMNDLPTLAAFIYDNM	212
<i>Campylobacter jejuni</i>	YMDKCAVCHQENGLGLKNEDSA--GAYLYPPLWGD-DSYNTGAGMYRLIKAASYIKENM	240
<i>Wolinella succinogenes</i>	YARDCASCHGAEGERLRRESKDGKPAYEFPPLWGSDDTYNTGAGMYRFLKAADFIKSTM	264
<i>Marichromatium purpuratum</i>	YAEHCALCHGAEGERLL-VD-----GEVVFPLWGP-RSYNWGAGMHRVDTAAAFIAANM	452
<i>Thiomonas intermedia</i>	YEAACKILCHAANGEGQY-VN-----GETVFPPLWGP-KS FNWAGAGMSYKNAKFIYANM	219
<i>Sideroxydans lithotrophicus</i>	FVENCQVCHGSGNGEGK-VD-----GKYIFPPLWGS-ESFNWAGAGMHRINTAAAFIKANM	212
<i>Pseudomonas stutzeri</i>	YAEQCAVCHGDDGGQK-AG-----GGYVFPLWGP-DSFNWAGAGMHRINTAAAFIKE	221
<i>Allochromatium vinosum</i>	YQARCLA CHGADGSGTLDAD-----GRYLFPLWGP-RS FNWAGAGMNRQATAAGFIKHKM	209
<i>Psychrobacter arcticus</i>	FAEKCSVCHGATGEGQYND-----GTYYVPAIAGD-KS FNDGAGMARTYTAASFIKGKM	254
<i>Parachlamydia acanthamoebae</i>	PYQEP-RLTVEEVLDAIAAYITSQ--PRPIEIRTP-----	243
<i>Campylobacter jejuni</i>	PQGAP-DLSLEDAYDVAAAYMNSQ--ARPIKANRDKDFPDRKVK---PLDMD---VGPYDD	291
<i>Wolinella succinogenes</i>	PKGAP-TLSDKDAYDVAAFINDYSHYRTVVKLNRQNDVDPKVR---VPDHDQ---PGPYGP	318
<i>Marichromatium purpuratum</i>	PLLDTVRLTPQEAWDVAAYINAH--ERPQDPRF---DG-SVERTAARFHASP-FDLYGE	504
<i>Thiomonas intermedia</i>	PYGMSYSLSPQEAWDVAYFMDAQ--ERPQDPRW---QG-SVAATRAKFDHDK-FSLYGT	271
<i>Sideroxydans lithotrophicus</i>	PLSKGGTLTDQEAWDVAFVMSH--ERPQDPRF---KG-NVAQTKEYHDE--NCRYGE	263
<i>Pseudomonas stutzeri</i>	PLGKGSLSADAWHVAAYMNSH--ERPQDPRL---IEGSVEKTRLYKHANDGNVLYGQ	275
<i>Allochromatium vinosum</i>	PLGADDSLSDEEAWDVAGFVLT--PRPLFQEPETGD-----	243
<i>Psychrobacter arcticus</i>	PFGQGSLSQEAVDIA SYFTHL--PRPIKANKDKDWPNGDAPKDVRR-----	300
<i>Parachlamydia acanthamoebae</i>	-----	243
<i>Campylobacter jejuni</i>	S-----FSTTQHRYPYTNMIKK-----	309
<i>Wolinella succinogenes</i>	EGSYIFPDEGKTQMDYKVGYPYKGI IKQKPAAK--	350
<i>Marichromatium purpuratum</i>	P-----LGVDGAVLGGQVAKD--	520
<i>Thiomonas intermedia</i>	K-----VNGKLLGDIGAPKPR	287
<i>Sideroxydans lithotrophicus</i>	T-----VNGKVLGGKHQTAAK	279
<i>Pseudomonas stutzeri</i>	Q-----VDGALLGQGVK----	287
<i>Allochromatium vinosum</i>	-----	243
<i>Psychrobacter arcticus</i>	-----	300

Figure 1.7 – Sequence alignments of known and putative TsdA enzymes. Heme I and II binding motif and corresponding ligands in blue or orange, respectively⁹. Residues implicated in substrate binding in yellow⁵.

An example is the enzyme TsdBA from *Mp* for which a crystal structure is available³⁰ (Figure 1.5, right). This enzyme is a fusion with a diheme redox partner TsdB which features two domains with clear sequence (Figure 1.7) and structural homology to the diheme *Av* TsdA. The residue equivalent to *Av* TsdA Lys-208 that ligates heme II is the non-ligating residue Asn-449 in *Mp* TsdBA. Instead, in *Mp* TsdBA the heme II ligands are His-406 of the CXXCH motif and Met-450. The flexible nature of the distal ligand in heme II is significant given the apparent conservation of Met and not Lys in the sequences of all known TsdA enzymes (Figure 1.7, orange shading). Furthermore the crystal structure of the presumed diferrous *Av* TsdA prepared by dithionite soaking has Lys-208 replaced by Met-209 as the distal heme II ligand (Figure 1.6, F). The significance of the Lys to Met ligand switch in heme II of *Av* TsdA is not clear. There is precedent for similar behaviour in the alkaline form of cytochrome *c*³⁴ and an analogous His/His to His/Met switch is proposed for the *c*-type electron transfer heme of the diheme *cd*₁ nitrite reductase³⁵. A further feature of interest in the *Mp* TsdBA structure is modification of the conserved Cys-330 that is resolved as a Heme I ligand in *Av* TsdA (Figure 1.6, D). In *Mp* TsdBA this cysteine is present as cysteine thiosulphonate. The closest iron to sulphur distance is 2.9 Å and there is no intervening electron density, suggesting that heme I has no distal ligand. Possible implications of these observations for the catalytic mechanism of TsdA are discussed below.

There is a second diheme TsdA enzyme described in the literature, that from *Cj*^{3,32}, however there are currently no published crystal structures of this. At present, studies of *Cj* TsdA have focused on catalytic activity and electronic absorbance spectroscopy of the purified enzyme. Based on sequence alignments (Figure 1.7), His-98/Cys-138 are proposed as heme I ligands and His-207/Met-255 as heme II ligands for this enzyme (equivalent to Lys-208 in *Av* WT is non-ligating Asn-254). Consistent with this, the electronic absorbance spectrum of *Cj* WT confirms only high field strength heme ligands (*eg.* His, Cys or Met) are present, whereas this is not the case for variants where Cys-138 or Met-255 are replaced by non-ligating glycine³². Section 1.3.1 has more detail on electronic absorbance spectroscopy of hemes.

1.2.3. Cysteine Conjugations and Catalysis by TsdA Enzymes

The heme irons in the majority of *Av* TsdA structures are six co-ordinate; this is typical for electron transfer hemes, but does not reveal an obvious site for catalysis. In the catalytic mechanism proposed by Grabarczyk *et al.*, one molecule of thiosulphate (Figure 1.8, red) binds near to Cys-96 of the fully oxidised enzyme, stabilised by hydrogen bonds from Arg-82 and Arg-92 (Figure 1.8, top left). A covalent bond then forms between the sulphane sulphur of thiosulphate and the thiolate of Cys-96, releasing two electrons which reduce both hemes. An electron acceptor reoxidises the hemes before a second molecule of thiosulphate binds (Figure 1.8, blue),

stabilised by a hydrogen bond from Ser-100. The thiosulphonate group bound to Cys-96 is then transferred to the sulphane sulphur of the second thiosulphate molecule, forming a molecule of tetrathionate, which is released leaving an empty active site.

Variants of *Av* TsdA⁹ and *Cj* TsdA³² where Cys-96 or Cys-138 have been substituted by His or Met are all but inactive in thiosulphate oxidation or tetrathionate reduction activity assays (Figure 1.4) consistent with the proposal that interconversion of thiosulphate and tetrathionate proceeds *via* covalent modification of the heme I cysteine ligand, rather than binding to a vacant heme I iron co-ordination site.

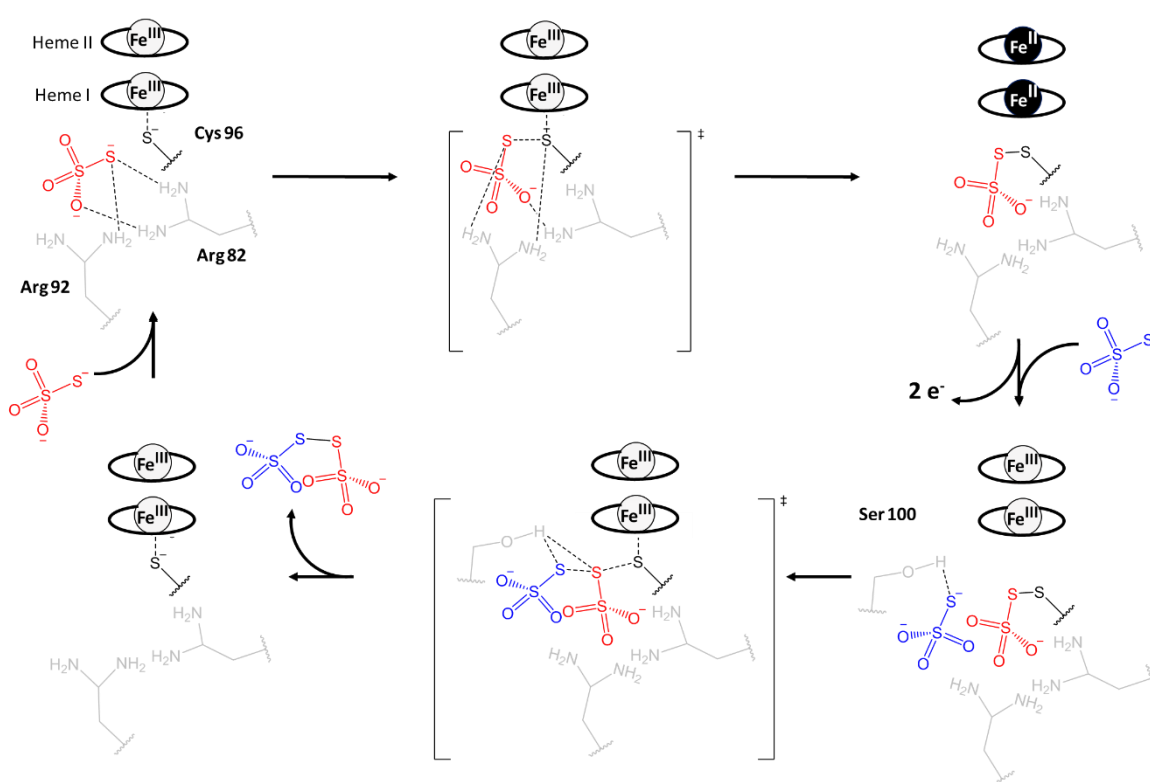


Figure 1.8 – TsdA catalytic mechanism for thiosulphate oxidation proposed by Grabarczyk *et al.*⁵ Residue numbers apply to *Av* TsdA.

As proposed for the first and last steps of this reversible mechanism, *Av* WT incubated with thiosulphate or tetrathionate shows a mass increase detected by mass spectrometry consistent with the formation of a covalent bond between Cys-96 and one thiosulphonate moiety⁵. This modification does not inhibit catalysis, but is not further modified by substrate without the presence of an electron acceptor. Electronic absorbance (see below, 1.3.1) of thiosulphate incubated protein also shows reduction of the *Av* WT hemes and spectral features consistent with the removal of one of the heme ligands⁵. This is consistent with the formation of a cysteine adduct, releasing electrons to the hemes and causing Cys-96 to be displaced as a heme ligand by

solvent. The structure of *Mp* WT similarly has Cys-330 covalently thiosulphonated (Figure 1.6, D) and not ligating heme I³⁰. The reactivity of the heme I cysteine ligand is further revealed in other *Av* TsdA structures where Cys-98 is displaced or post-translationally modified (see below, 4.1) in ways that do not feature in the Grabarczyk mechanism^{5,9} (Figure 1.6, B, C). However, the relevance of any of these species to catalysis remains to be established. Cysteine modifications could also have occurred during the crystallisation process as the result of oxidative⁹ damage or X-ray cleavage of bonds³⁶.

The axial ligands of heme II are not specified in the mechanism proposed by Grabarczyk *et al*⁵, however in most TsdA enzymes including *Cj* WT³² these are inferred to be His/Met as with *Mp* WT³⁰. The presence of an additional heme II ligand in *Av* WT could therefore be a mechanistic feature specific to that organism's enzyme, possibly contributing to its low rate of tetrathionate reduction (Figure 1.4). As a counterpoint, when Lys-208 is replaced by Asn in *Av* K208N or *Sj* WT, k_{cat} for thiosulphate oxidation is approximately 5-fold less, but tetrathionate reduction is unaffected³² (Figure 1.4). Likewise a *Cj* TsdA variant introducing Lys in an equivalent position in *Cj* N254K decreases k_{cat} for thiosulphate oxidation modestly, but does not change the rate of tetrathionate reduction. Further investigation of *Av* TsdA in solution is therefore necessary to determine if this unusual ligation state is artefactual, or if it serves a mechanistic or regulatory role not required by other members of the TsdA enzyme family.

To gain greater insight into the properties of these enzymes and to complement crystallographic data, it is necessary to resolve the heme I and II ligands with defined oxidation states and with defined cysteine modifications. Much of this can be achieved for samples in solution using (magneto) optical spectroscopy, which is detailed in the following section.

1.3. Optical Spectroscopy of Hemes for Assignment of Ligation, Oxidation and Spin States

1.3.1. Electronic Absorbance Spectroscopy of Hemes

Electronic absorbance occurs when a chromophore absorbs a photon with the correct energy to raise the ground state of that species to an excited state. Each optical transition gives rise to a peak in electronic absorbance centred on the wavelength (λ) of light corresponding to the transition energy; such peaks have a Gaussian shape and positive intensity. The spectra of hemes are dominated by $\pi - \pi^*$ transitions, from the heavily conjugated porphyrin macrocycle, and ligand-to-metal charge transfer (CT) transitions. The intense red-brown colours of hemes *b* and *c* in solution are predominately due to the former transitions which occur in two separate wavelength regions^{37,38} referred to as the Soret (~400 nm) and the $\alpha\beta$ band (~550 nm) (Figure 1.9,

lower panels). Variations in these bands can often be used to distinguish heme spin- and oxidation state in electronic absorbance spectra.

In a strictly octahedral environment, iron d orbitals have e_g and t_{2g} symmetry. In hemes, these are tetragonally distorted causing further splitting (Figure 1.9, upper panels). The electrons occupying these orbitals can either overcome the pairing energy to occupy only the three lowest energy d orbitals (Figure 1.9, left) or otherwise occupy all five d orbitals to minimise pairing (Figure 1.9, right). These are the low- and high-spin states respectively. Spin states in hemes are dictated by the field strength of the axial ligands as described by the spectrochemical series. Strong ligands include imidazole, histidine and methionine and hemes with two of these ligands are typically low-spin. Weak ligands include fluoride and water and hemes with one or more of these ligands are typically high-spin. It is therefore possible to derive information on heme axial ligation from the spin state.

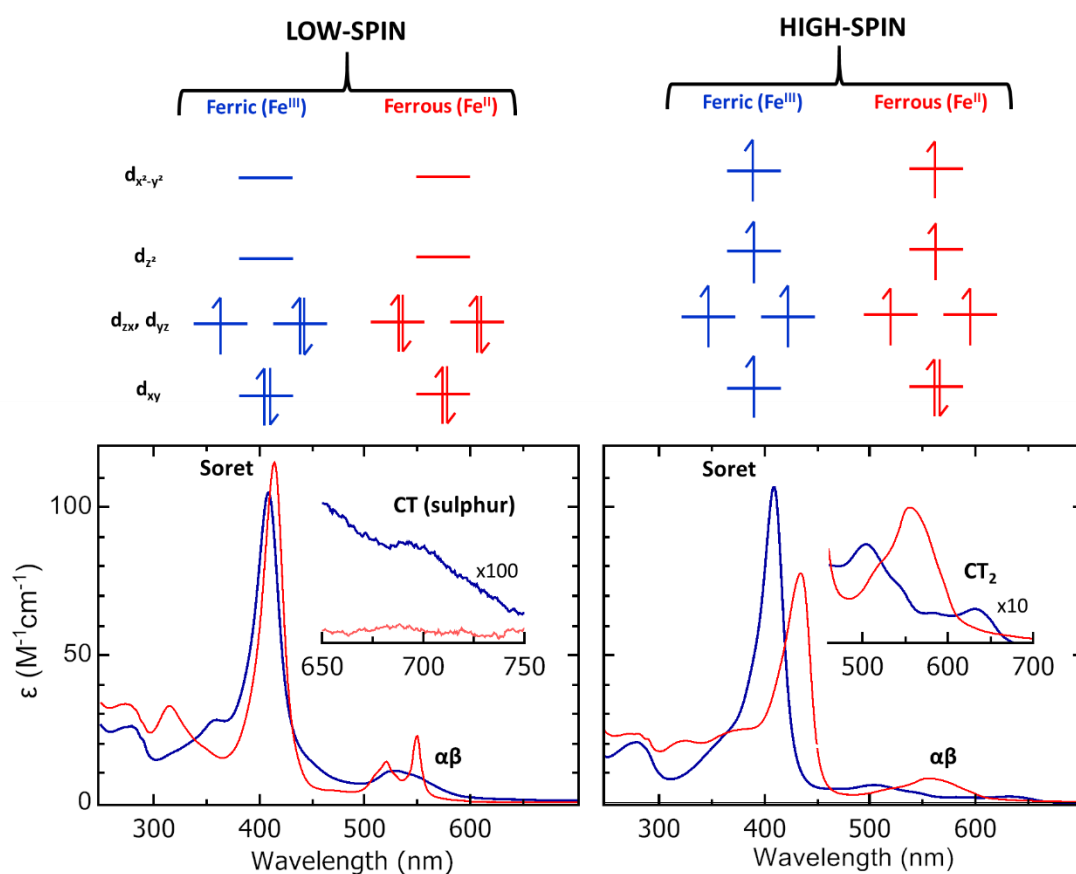


Figure 1.9 – The effect of spin and oxidation state on the UV/visible electronic absorbance spectra of *b* and *c* hemes. **(Top)** d orbital occupancy by electrons (arrows) in low-spin (left), high spin (right), ferric (blue) and ferrous (red) hemes. **(Bottom)** Spectra of 30 μ M horse-heart cytochrome *c* before (low-spin ferric, blue line) and after (low-spin ferrous, red line) incubation with excess sodium dithionite. (Right) Spectra of 140 μ M horse-heart myoglobin before (high spin ferric, blue line) and after (high-spin ferrous, red line) incubation with excess sodium dithionite.

The spectra of low-spin ferric hemes feature broad, low-intensity $\alpha\beta$ bands which become sharper upon reduction to the ferrous state with a simultaneous red-shift and increase in intensity of the Soret peak (Figure 1.9, bottom left). Subtle differences in heme environment can modify the energy of these electronic transitions, hence Keilin's original differentiation between *b* and *c* hemes based on their shifted $\alpha\beta$ bands in the low-spin ferrous state¹⁰. Cysteinate-ligated ferric hemes are unusual in that they exist in a resonant state with a cysteinyl-radical-ligated ferrous heme with the unpaired electron on sulphur 30-40% of the time³⁹. This influences the porphyrin $\pi - \pi^*$ transitions such that both the Soret and $\alpha\beta$ bands are broader and of lower intensity than for other ligand sets.

CT transitions can occur between the p orbitals of axial heme ligands and the d orbitals of iron when there is a vacancy in the d_{zx} or d_{yz} orbitals for a promoted electron, *ie.* not low-spin ferrous hemes (Figure 1.10, left). Where the axial ligand contains oxygen or nitrogen, these bands appear in the UV or visible region and are usually obscured by the more intense Soret or $\alpha\beta$ peaks (Figure 1.10, right). However axial ligands containing sulphur have higher energy p orbitals, reducing this energy gap so that bands for these species occur at ~ 700 nm. It is often possible to infer the nature of a sulphur heme ligand from the λ_{\max} and shape of this band, such as the 695 nm 'Methionine band' (Figure 1.9, bottom left inset) typical in spectra of cytochrome *c*⁴⁰ or the ~ 750 nm bis-Met band in bacterioferritin⁴¹.

CT transitions can also occur between the porphyrin π orbitals and the d orbitals of iron. In high-spin hemes there are two transitions which give rise to the CT_1 band in the ~ 900 -1600 nm region and the CT_2 band in the ~ 600 -680 nm region. Low spin hemes give rise to a single CT_{LS} band in the 900-2500 nm (NIR) region. CT transitions are highly sensitive to the nature of the heme axial ligands, however the absorbance features that arise from these are broad due to vibrational contributions and have low-intensity. H_2O also has broad bands at 1450 nm and 2000 nm⁴², so electronic absorbance is unable to detect CT_1 and CT_{LS} bands in aqueous solution as these are obscured by absorbance from the solvent.

Electronic absorbance spectroscopy has previously been used to identify the presence and number of heme cofactors in some TsdA enzymes and can go some way towards distinguishing heme spin- and oxidation states^{5,9,32}. However, to resolve the individual contributions of multiple hemes reliably and to identify heme axial ligands from NIR CT bands requires magnetic circular dichroism (MCD) spectroscopy.

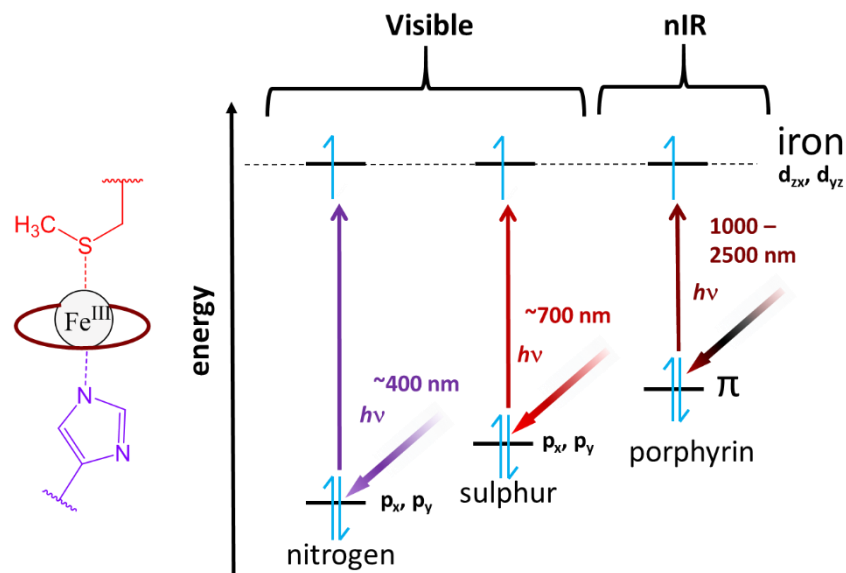


Figure 1.10 – Charge transfer (CT) transitions in hemes relevant to (magneto-) optical spectroscopy. Example illustrates bands present for a low-spin ferric heme with His/Met coordination.

1.3.2. Magnetic Circular Dichroism (MCD) of Hemes

MCD spectroscopy involves recording the apparent circular dichroism (CD) spectra of samples in the presence of a longitudinal magnetic field (H). MCD signals arise from the same optical transitions as electronic absorbance spectra, however the intensities of different MCD signals can vary by orders of magnitude between spin- and oxidation-state and many signals have a signed nature, often making it possible to distinguish between chemically different hemes in one sample.

In the classical Buckingham and Stephens model there are three possible sources of MCD intensity, the A, B and C terms⁴³. The major contributor to heme spectra at room temperature is the A term. This arises when excited energy states lose their degeneracy in the presence of the applied magnetic field due to the Zeeman Effect so that now there is a small difference in the photon energy required to excite transitions into these states (Figure 1.11, left). This difference in energy may be such that circularly polarised light can preferentially cause one of the two transitions and the extinction coefficients for left- (ϵ_{LCP}) (Figure 1.11, red dashed line) and right-handed (ϵ_{RCP}) (Figure 1.11, blue dashed line) circularly polarised light peak at different wavelengths (λ). Circular dichroism ($\Delta\epsilon$) is defined as:

$$\Delta\epsilon = \epsilon_{LCP} - \epsilon_{RCP}$$

In the simplest case LCP will excite one transition and RCP will excite the other. When $H = 0$ and excited levels are degenerate, $\Delta\epsilon = 0$. When $H \neq 0$, $\Delta\epsilon$ will have a positively-signed peak at λ_{max}

for ϵ_{LCP} and a negatively signed peak at λ_{max} for ϵ_{RCP} giving rise to a bisignate feature with $\Delta\epsilon = 0$ between these points (Figure 1.11, thick black line).

The B term can also influence the appearance of room-temperature heme MCD spectra and arises when excited energy levels mix in the presence of a magnetic field, so that previously disallowed transitions become allowed. Unlike the A and B terms, the C term is temperature dependent and so is not a significant contributor to the room-temperature spectra featured in this thesis.

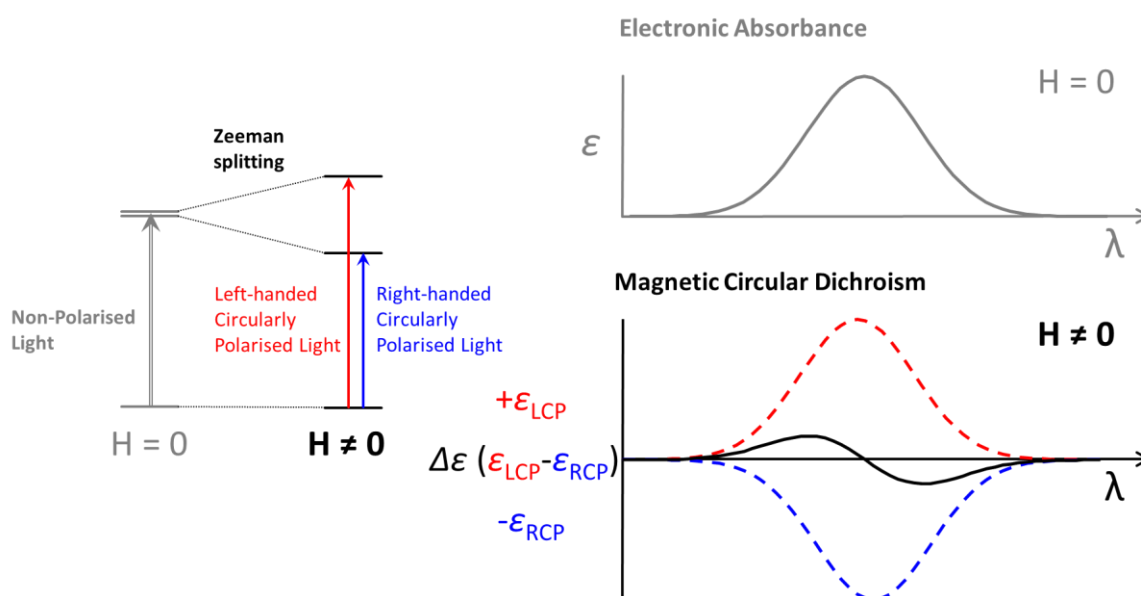


Figure 1.11 – Signals in (Magneto) Optical Spectra. Gaussian peaks (right, grey line) arise from optical transitions (left, grey arrow) in electronic absorbance spectroscopy. When the A-term dominates, the same transitions (left, red and blue arrows) in the presence of an external magnetic field (H) have shifted absorbances of left- (ϵ_{LCP}) and right-handed (ϵ_{RCP}) circularly-polarised light, giving rise to bisignate signals ($\Delta\epsilon$, right, black line) when monitored by magnetic circular dichroism (MCD).

MCD of low-spin ferric hemes (Figure 1.12, upper black lines, 350-450 nm) has a bisignate Soret feature with equal positive and negative intensity, for ferrous hemes this is red-shifted with more positive than negative intensity (Figure 1.12, red lines, 350-450 nm). High-spin ferric hemes have Soret features almost 10-fold less intense than these, so it is often possible to quantify low-spin heme content from the peak-to-trough intensity of this feature and to estimate oxidation state from its shape. High-spin ferrous hemes give rise to intense Soret features with mostly positive intensity even further red-shifted compared to low-spin ferrous hemes. The $\alpha\beta$ signals of ferric hemes are of low intensity, but the bisignate α feature of low-spin ferrous heme is sharp and intense, permitting clear resolution of even trace reduction in a low-spin heme sample (Figure 1.12, red lines, 450-600 nm).

As with electronic absorbance, the MCD of cysteinate-ligated ferric hemes give rise to slightly red-shifted signals which are broader and less intense due to their hybrid oxidation state^{39,44,45}. To a lesser extent, the same is true for methionine-ligated hemes. Overall the combination of a signed spectrum and significant intensity variations afforded by MCD allows for better deconvolution of multiple heme species and a more reliable diagnosis of spin- or oxidation-state. Furthermore, as described below, axial heme ligands can also be resolved using near infra-red (nIR) MCD of samples prepared in D₂O to minimise the 1450 nm and 2000 nm absorbance bands from water⁴².

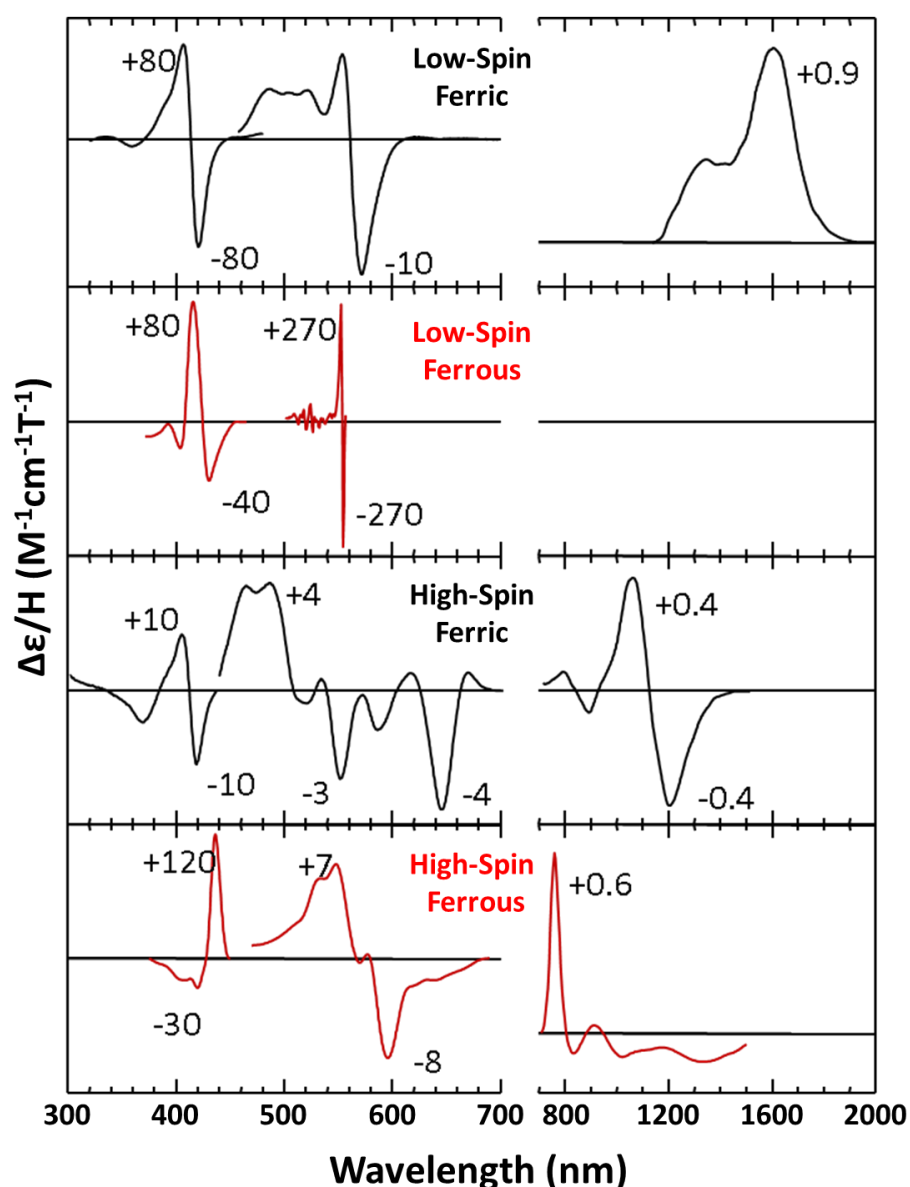


Figure 1.12 – Example Room Temperature MCD Spectra of Hemes. Spectra of cytochrome *c* (low-spin) or myoglobin (high-spin) in the ferric or ferrous states as annotated. Signals recorded in the UV/visible (left) and near infra-red (right) regions annotated with typical intensities in extinction coefficients per tesla.

Low-spin ferrous hemes do not give rise to CT_{LS} bands as there is no hole available for a promoted electron in the appropriate d_{zx} or d_{yx} orbitals (Figure 1.9, top left). The CT bands of hemes in other spin- and oxidation states occur in the visible and nIR regions (Figure 1.12, 600-2000 nm). MCD-resolved CT_{LS} bands for ferric hemes are broad, positively signed and have low intensity (Figure 1.12, black lines, 700-2000 nm). Bands are often accompanied by one (or more) vibrational side-band(s) visible as a lower-wavelength shoulder on the main band. High-spin hemes typically have bisignate CT₁ bands at shorter nIR wavelengths (Figure 1.13, bottom right) and corresponding CT₂ signals in the ~600-680 nm region (Figure 1.13, bottom left)^{46,47}. The wavelengths at which CT transitions occur is often diagnostic of heme axial ligation (Figure 1.13).

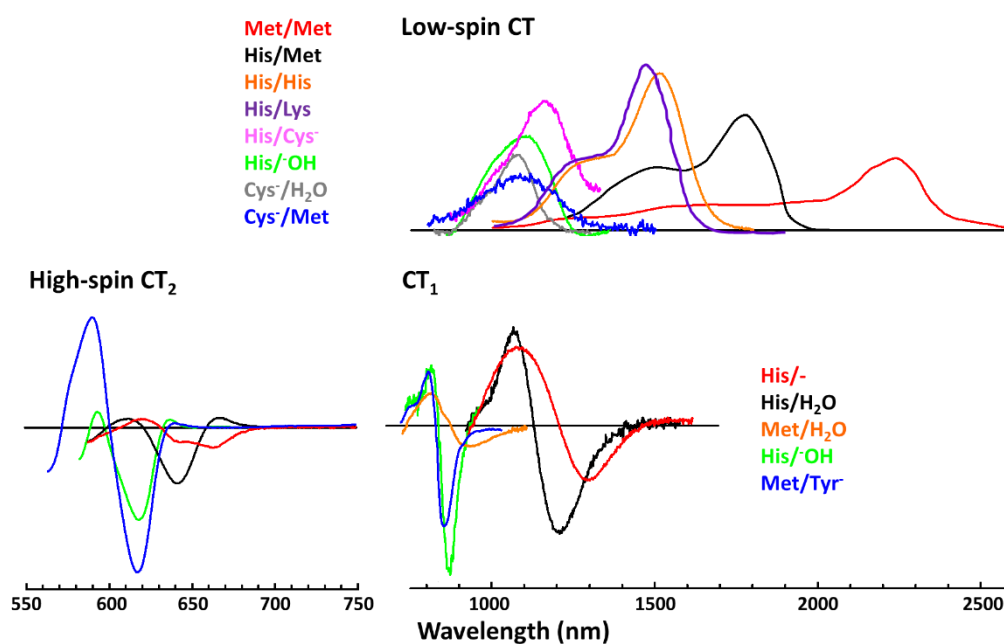


Figure 1.13 – Representative MCD of Ferric CT bands. Wavelengths of these bands are often diagnostic of Heme axial ligation as annotated.

As explained above, MCD spectroscopy allows identification of heme axial ligation in addition to spin- and oxidation-state. In combination with potentiometry (see below, 1.4.1) this can be used to investigate the redox activity of heme proteins^{48,49}, such as TsdA and to identify any conformational changes that occur in response to changes in heme oxidation state.

1.4. Electrochemistry for Resolution of Heme Redox Behaviour

Protein cofactors, such as hemes can function as redox centres, exchanging electrons with other cofactors^{30,50}, amino acid sidechains^{51,52} or small redox active molecules⁵³. Facile electron transfer to, or from, biological redox centres typically occurs over ≤ 14 Å distances⁶ and the relative mid-point potential (E_M) value of each centre defines the thermodynamic driving force. E_M

describes the potential at which a redox couple has equal concentrations of oxidised and reduced species. Knowledge of heme E_M values is therefore desirable for predicting favourable electron transfer or the driving force for oxidation or reduction of a substrate⁵⁴. With the exception of peroxidases⁵⁵ and P450s¹⁷, it is typically the Fe^{II}/Fe^{III} couple which is of biological relevance in hemes and all references to heme E_M values in this thesis refer to this redox transition.

1.4.1. Potentiometry

When a heme (or other redox centre) is equilibrated at an electrochemical potential (E) the E_M value can be calculated from the resulting concentrations of reduced ([red]) and oxidised ([ox]) species using the Nernst equation:

$$E = E_M - \frac{RT}{nF} \ln \left(\frac{[\text{red}]}{[\text{ox}]} \right) \quad \text{Equation 1.1}$$

where R is the gas constant, T is absolute temperature, n is the number of electrons involved in the redox transition and F is the Faraday constant. The Nernst equation applies when electron transfer to a redox centre is facile in both directions (*i.e.* reversible) relative to the experimental measurement time so that a thermodynamic equilibrium is reached. Experimentally, chemical oxidants or reductants can be added to a sample to define the potential; often with soluble redox mediator(s) active over the potential range studied to ensure facile equilibration. If known concentrations of a redox agent with a well-defined E_M close to the E_M of interest is used, there is no need to monitor potential independently⁵³. Typically, however potential is monitored relative to an internal reference couple (such as Ag/AgCl) using a combination electrode, or a working electrode is used to define a potential instead of using chemical agents⁵⁶. Either [ox] or [red] must be measurable at each defined potential, for example optical spectroscopy can be used to monitor heme oxidation state (see 1.3.1). Appropriate re-arrangement of the Nernst Equation, noting that for a simple redox couple [ox] + [red] = 100%, allows plots of [ox] (or [red]) versus E to be fit to quantify E_M and n for the corresponding half-reaction (Figure 1.14).

Potentiometric determination of E_M becomes challenging when the sample has multiple redox centres with similar spectroscopic properties, as is the case for diheme cytochromes such as TsdA³⁰. In this case, E_M is readily determined only if [ox] and/or [red] can be independently quantified for each chromophore or if the E_M values are separated enough that each transition is resolved discretely and there is some method to assign each E_M value to a specific centre. If a precise E_M is not determined for a centre, it is still possible to identify a potential window of redox activity based on potential values that cause oxidation or reduction of that centre.

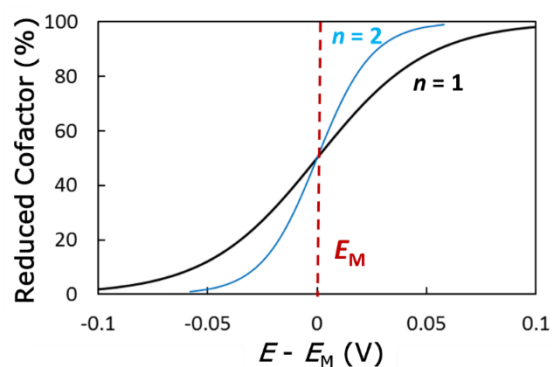


Figure 1.14 – Behaviour predicted for Nernstian process with the indicated properties⁵⁷. Resolution of these data requires an experimental method of determining [ox] and/or [red] at defined E values.

Electronic absorbance spectroscopy was previously used to monitor Av WT adsorbed on an optically transparent SnO₂ working electrode. The change in absorbance at 418 nm was used as an estimate of total low-spin ferrous heme concentration (see above, 1.3.1). As the thiolate-ligated and non-thiolate ligated hemes in Av WT have different $\Delta\epsilon$ values in this region, the contribution of each heme to this overall absorbance change could be deconvoluted. Based on these assignments, a -350 to -100 mV range was identified for the reversible redox activity of the His/Cys⁻ ligated heme I. Heme redox activity over -100 to +150 mV was assigned to the His/Lys ligated heme II³⁰. However, non-reversibility of electron transfer was observed, preventing the use of the Nernst equation to determine E_M values for the Av WT hemes as equilibrium was not reached in this study. It is possible that the heme II ligand switch to His/Met ligation seen in Av WT crystals⁹ rationalises the slow electron transfer observed upon reoxidation in this study, as hemes with this ligation state typically have high E_M values²⁵.

One method suited to dynamic investigation of redox centres is protein film electrochemistry (PFE). With PFE, [ox] and [red] can be directly calculated from the flow of current between a redox centre and a working electrode without the need for a chromophore. The E values over which this current flows can then be used to determine E_M and n for each centre.

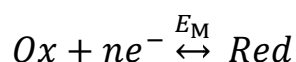
1.4.2. Dynamic Protein Film Electrochemistry

When the electroactive centres of a protein are in direct communication with a working electrode, oxidation or reduction cause a current flow that can be measured in real-time. Such experiments can be performed using a standard three-electrode cell (Figure 1.15) where a potentiostat is used to set the potential at a working electrode, relative to the standard potential

of a reference electrode. Protein electroactive centres within 14 Å of the working electrode⁶ can undergo redox transformations with the electrode acting as an electron donor and/or acceptor. This in turn causes measurable current flow between the working and counter electrodes. Proteins investigated by these experiments may be freely diffusing in solution⁵⁸, alternatively they may exist as an electroactive film adsorbed on the surface of the working electrode⁵⁹. It can be argued that the latter experiment, often termed protein film electrochemistry (PFE) offers several advantages over the former. For example:

- i) economy of sample; protein films can provide measurable current with \leq nmol of protein⁶⁰
- ii) instant dialysis; with a stable adsorbed protein film on a solid electrode it is possible to replace the buffer-electrolyte with ease. This way a single protein film can be examined as pH or temperature are varied, possibly identifying chemical changes in the environments of the electroactive cofactors under these conditions^{61,62}
- iii) ease of analysis; contributions due to diffusion are eliminated making analysis of multiple signals easier and electron transfer with the protein is not limited by the typically much slower rate of diffusion⁶³
- iv) access to extreme conditions; a protein film may be more stable to conditions that would denature the same protein in solution^{64,65}
- v) *in vivo*-like conditions; electrode surfaces may be tailored to mimic the crowded conditions inside a living cell⁶⁶.

In an ideal case, an adsorbed protein would retain its native conformation and functionality on the surface of a working electrode (Figure 1.15, inset bottom). Cyclic voltammetry (CV) is a simple, but highly informative experiment that can then be used to visualise its redox activity. In CV, the potential at a working electrode is varied in a linear/saw tooth manner between set upper and lower values at a user defined scan rate (ν) (Figure 1.15, inset left). The resulting current (i) is recorded and output as a voltammogram which plots i vs. E . When all protein redox centres are capable of identical, rapid and independent electrical transfer with the electrode, a Nernstian equilibrium can be attained at each applied potential. For a reversible redox transformation of the type:



there are a pair of peaks in the voltammogram in addition to any baseline current that results from charging and discharging the electrode. One peak has a positive current and one has a negative current corresponding to oxidation or reduction respectively (Figure, inset right).

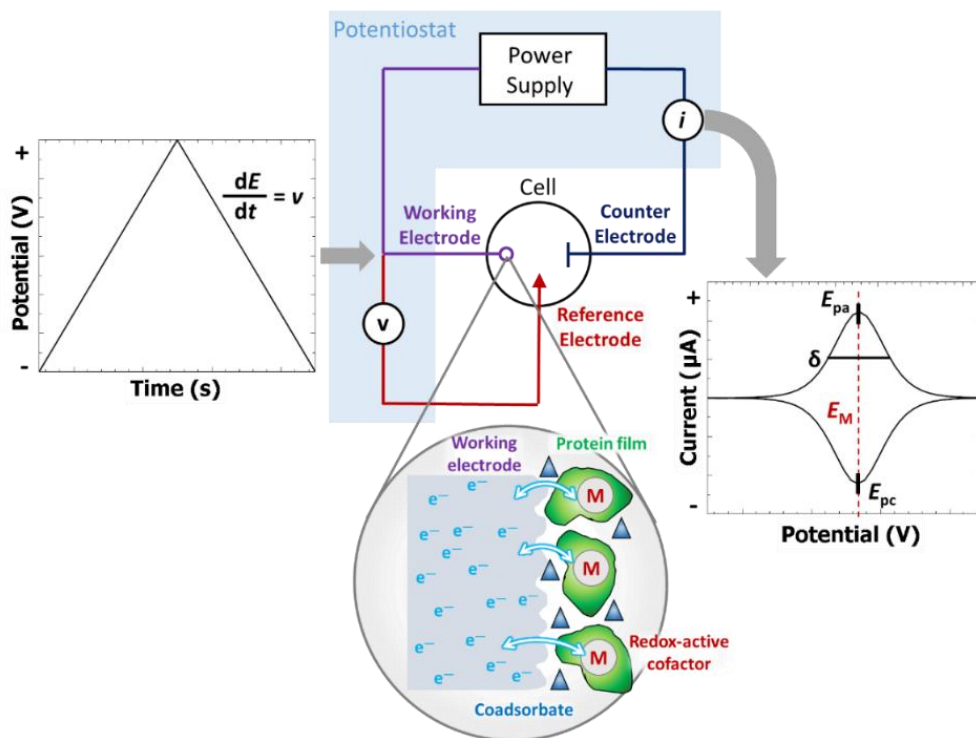


Figure 1.15 – Schematic of a metalloprotein adsorbed onto the working electrode of a standard 3-electrode assembly. (Inset bottom) Protein molecules (green) are adsorbed onto the working electrode surface, possibly with a coadsorbent molecule (blue triangles) to stabilise the protein film. Exchange of electrons is then possible between a redox-active cofactor (M) and the working electrode. (Left) Saw-tooth excitation profile of cyclic voltammetry (Right) Form of the resulting voltammogram showing peak potentials (E_p) and half-height width (δ).

Under ideal conditions with facile, fully reversible electron transfer, these peaks have maximum current (E_{pa} for oxidation, E_{pc} for reduction) when $E = E_M = E_{pa} = E_{pc}$. The symmetrical peaks observed in this case are described by the equation:

$$i = \frac{n^2 F^2 \nu A_e \Gamma_0^* \exp\left(\frac{nF}{RT}(E - E_M)\right)}{RT (1 + \exp\left(\frac{nF}{RT}(E - E_M)\right))^2} \quad \text{Equation 1.2}$$

where Γ_0^* is the surface population (mol cm^{-2}) of adsorbed redox active species at time 0 and A_e is the electrode area (cm^2).

The width in volts of the peak at half its height (δ) (Figure 1.15, right) defines n through the relationship:

$$\delta = 3.53 \left(\frac{RT}{nF}\right) \quad \text{Equation 1.3}$$

If the potential axis is converted to time (t) using the relationship:

$$\Delta t = \frac{\Delta E}{\nu} \quad \text{Equation 1.4}$$

the area of each peak quantifies the charge (Q) exchanged between electrode and redox cofactor. Knowledge of Q can then be used to calculate the number of moles of electrons (N_{mol}) passed to or from the electrode according to the formula:

$$N_{mol} = \frac{Q}{nF} \quad \text{Equation 1.5}$$

Knowledge of the electron stoichiometry (Equation 1.3) can then be used to determine exactly the amount of redox active cofactor present on the electrode.

Cyclic voltammetry under conditions where the adsorbed centre behaves in a Nernstian manner at all values of E will give rise to a pair of symmetrical peaks with $E_M = E_{pa} = E_{pc}$ as described above (Figure 1.15). However, above a certain value of scan rate the rate of interfacial electron transfer will be too slow to allow equilibration of all electroactive centres with the applied potential. Under these conditions the electrochemical response becomes smeared along the potential axis such that $E_{pa} > E_M$ and $E_{pc} < E_M$, (Figure 1.16). This results in a peak separation ($E_p - E_M$) that becomes bigger in magnitude as scan rate increases. The E_M is given by the average of the peak potentials. The values of the interfacial electron transfer coefficients (k_{ox} and k_{red}) that describe electron transfer between electrode and redox cofactor during oxidation and reduction respectively, are given by the Butler-Volmer equations⁵⁷:

$$k_{ox} = k^\circ \exp[-\alpha(F/RT)(E-E_M)]$$

$$k_{red} = k^\circ \exp[(1-\alpha)(F/RT)(E-E_M)] \quad \text{Equation 1.6}$$

In these equations, k° is the interfacial electron transfer rate constant when $E = E_M$ and α is the electron transfer coefficient describing the reversibility of the system, often assumed to be 0.5 representing full reversibility⁶³. The effect of k° can be visualised by plotting E_p vs. v , often termed a ‘Trumpet’ plot (Figure 1.16, right) however obtaining a value for k° is not straightforward and generally requires the algorithmic simulation of theoretical lineshapes which are fitted to experimental data as part of an iterative process⁶⁷.

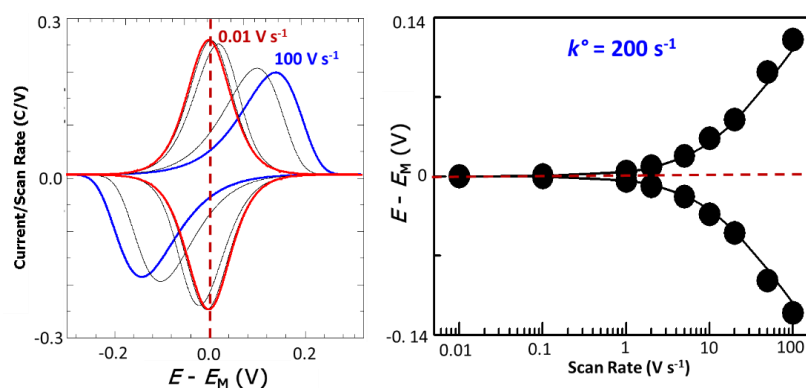


Figure 1.16 – Scan rate dependence of CV response for adsorbed species. (Left) CVs simulated for scan rates of 0.01, 0.1, 1, 10 and 100 $V s^{-1}$ for an $n = 1$ half-reaction with $k^\circ = 200 s^{-1}$ (Right) Variation of E_p with v for the system described in the left panel.

Achieving stable electroactive protein films, where cofactors are close enough to the electrode to allow direct electron transfer, can often be achieved by spontaneous adsorption^{66,68}. This process relies on serendipitous hydrophobic and electrostatic interactions between the protein and the electrode surface. As a result, much prior work has gone into identifying optimal electrode materials for various experimental applications.

Graphite (Figure 1.17, A) is a standard biocompatible electrode material which can be condensed from hydrocarbon vapour to create a highly regular structure and then abraded perpendicular to the plane of the stacked graphene layers to form pyrolytic graphite edge (PGE) electrodes. Freshly abraded PGE surfaces have a range of oxygen-containing functional groups thought to be complementary to protein surfaces and electroactive pores and clefts between damaged layers where adsorption can take place⁶⁹. Although PGE electrodes can certainly adsorb protein films where non-turnover signals are detectable^{52,70–73}, electroactive coverage is generally thought to be sub-monolayer and confined to pores and clefts. As a result these electrodes are well suited for catalytic experiments where sparse electroactive coverage allowing hemispherical diffusion is advantageous. Coverage of PGE electrodes and others may be improved by using a coadsorbate, such as the amino sugar neomycin. These small molecules are electrochemically inactive, but positively charged at neutral pH and are thought to make an electrode surface less repulsive to negatively-charged proteins⁶¹. Electroactive surface area can be increased and direct electron transfer to less accessible redox centres improved by using graphite structures (Figure 1.17, B) with dimensions closer to those of proteins; nanomaterials, such as single-walled nanotubes are popular electrode materials⁷⁴, alternatively, compacted porous carbon⁷¹ has the added benefit of protecting deeply buried oxygen-sensitive protein from an aerobic atmosphere.

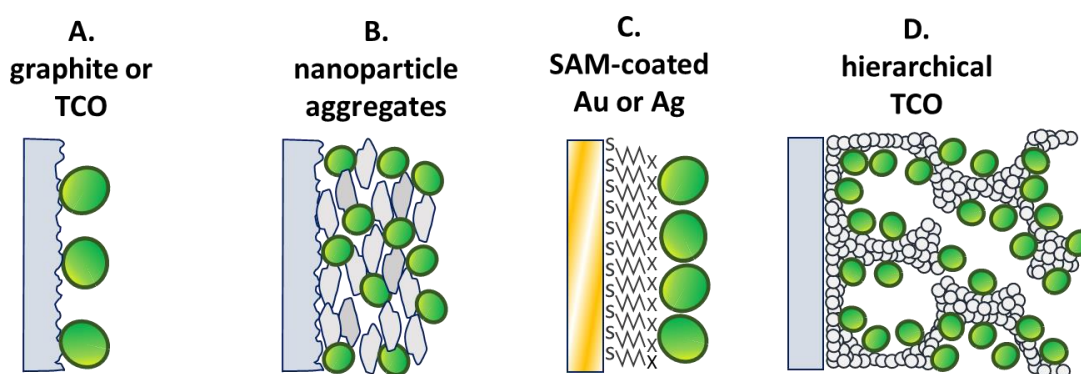


Figure 1.17 – Some electrode materials suitable for PFE. Spontaneous protein film (green) adsorption is possible on (A) pyrolytic graphite or transparent conducting metal oxides, (B) nanoparticles of gold or carbon, (C) Gold or silver coated with ω -terminated alkane thiols or (D) Hierarchichally-structured ITO.

Gold and silver have good conductive properties, but are highly hydrophobic and can denature proteins at their surface. Coating a gold or silver electrode (Figure 1.17, C) with a self-assembled monolayer (SAM) of thiol-functionalised organic compounds⁷⁵ mitigates against this and the exact composition of the SAM can be tailored to create an optimised surface for protein adsorption. The main advantage of these electrodes is their amenability to other techniques that can be used to quantify adsorbed protein such as atomic force microscopy, quartz crystalline microbalance or surface plasmon resonance^{76–78}. These techniques provide measurements for total protein adsorption, which can be a useful comparison to the amount of electroactive protein present on an electrode.

Transparent conducting oxides (TCO) such as (antimony doped) tin oxide, titanium oxide and indium tin oxide (ITO) can be deposited on conductive glass to make electrodes where *in-situ* optical spectroscopy is possible^{30,70,77,79}. As with porous and nanostructured carbon, TCO electrodes can be made with a three-dimensional structure to improve surface area. Highly periodic architectures are possible and pore dimensions in the order of nm to μm can be formed⁸⁰. Good non-turnover signals and catalytic currents proportional to electrode thickness are possible on hierarchically-structured inverse-opal ITO (IO-ITO) (Figure 1.17, D)⁷⁹ and the optical transparency of these materials allows adsorbed photosystems to generate measurable photocurrent when illuminated^{76,81,82}. Such electrodes have macro-scale pores to allow for diffusion through the electrode material and micro-scale pores to increase the surface area for protein adsorption. Thicker electrodes can adsorb more protein for larger Faradaic currents at the expense of increased opacity; the electrodes used in Chapters 3-5 are of this type.

From the above discussion it is apparent that potentiometry in combination with (magneto) optical spectroscopy offers the opportunity to determine oxidation- spin- and ligand states of the TsdA hemes at defined potential. Complemented by PFE on a suitable electrode material, the electroactivity and E_M values of the hemes in TsdA can also be determined. The following section details the specific questions about TsdA enzymes that these techniques may go some way towards answering, as addressed in this thesis.

1.5. Aim of Study

The work presented in this thesis aims to do the following:

Determine the axial ligands to the hemes in *Av* TsdA and *Cj* TsdA in solution. The hemes are the major part of TsdA enzymes that are likely to be responsible for its catalytic activity. The axial ligands of hemes define much of their chemistry, so this knowledge may give a good initial idea of the function of each heme. The major difference between *Av* TsdA and *Cj* TsdA so far appears to be in the ligation state of one of the hemes, so confirming this difference is an important first step in knowing why these enzymes are different.

Investigate the redox chemistry of the TsdA hemes. The hemes are also the part of TsdA enzymes likely to exchange or carry electrons. They will need to do this so that TsdA can catalyse the two-electron interconversion of thiosulphate and tetrathionate. Being able to define the oxidation states of the hemes will be essential in determining if there is any redox-linked conformational change in the TsdA structure. Determining the E_M values for each heme within TsdA will give thermodynamic information for how electrons travel between these hemes and to redox partners.

Investigate the chemistry of the active site heme I cysteine ligand. This ligand is unusual in that it directly reacts with substrate molecules when typically most heme ligands either stay bound to the heme or are displaced so that substrate molecules can bind to the heme iron. All TsdA enzymes to date need this ligand for catalytic activity to occur, so it is likely to be central to the reaction mechanism of these enzymes.

Determine the reaction mechanism of TsdA enzymes. Consideration of the above points in combination may start to give some idea of how TsdA might work. Experiments to test this further can then be performed to gradually develop a model for the TsdA mechanism. Performing key experiments with *Av* TsdA as well may help to identify if this enzyme has a different mechanism compared to its counterparts that would account for its different rate of tetrathionate reduction.

2. Materials and Methods

The following Chapter details the materials and methods used for experiments presented in Chapters 3-6 of this thesis. In addition, details are given of the instrumentation employed for MCD spectroscopy and for the mass spectrometry experiments introduced in Chapters 4 & 5.

2.1. Reagents

Buffer-electrolyte solutions were prepared by dissolving the required mass of reagents in an appropriate volume of deionised water (resistivity = 18.2 M Ω -cm, Milli-Q) or D₂O (Aldrich). Solution pH was measured using an Accumet AE 150 electrode (Fisher) and microlitre additions of 5 M NaOH/HCl (Sigma-Aldrich) were used to adjust this. The buffer-electrolyte used at pH 7 was 50 mM HEPES (Fisher), 50 mM NaCl (Fisher). Where an anaerobic chamber (Belle Technology) was used, this was filled with N₂ and kept under positive pressure. The chamber atmosphere was maintained at <10 ppm O₂ at all times by circulation through metal oxide filled O₂-reactive columns. Buffer-electrolyte solutions (typically 200 mL) were sparged with N₂ gas for >20 minutes before being transferred to the anaerobic chamber and typically left overnight to equilibrate with the chamber atmosphere prior to use. Stock solutions of sodium ascorbate (Fluka), potassium ferricyanide (Aldrich), sodium iodoacetate, sodium sulphite, sodium thiosulphate and sodium tetrathionate dihydrate (Sigma-Aldrich) were all prepared by transfer of the desired mass to an anaerobic chamber where they were dissolved in anaerobic buffer-electrolyte to make 100 mM stock solutions. These were prepared fresh for each day of experimentation. Sodium dithionite (Sigma-Aldrich, 20 mg/mL \approx 100 mM) and europium (II) chloride (Sigma) were handled similarly with the exception that these were stored in the anaerobic chamber as solids and aliquots were transferred to N₂-filled vessels and then sealed to limit O₂ exposure prior to weighing. Tris (2,-carboxyethyl) phosphine (TCEP) hydrochloride (Sigma) was purchased as a 0.5 M aqueous solution adjusted to pH 7 with ammonium hydroxide, stored in sealed ampoules under argon gas. Ampoules were opened in an anaerobic chamber and aliquots were either stored within the chamber or flash-frozen in liquid N₂ to limit O₂ exposure. Neomycin sulphate (Sigma) was prepared as a 5 mM stock in deionised water and frozen between uses.

2.2. Proteins

TsdA enzymes and variants were prepared and provided by Julia M. Kurth, Sebastian van Belmont and Linda Brandt from Christiane Dahl's group at the Rheinische Friedrich Wilhelms Universität Bonn, Germany using the method described in Brito *et al.* 2015 for Av TsdA enzymes and Kurth *et al.* 2016 for Cj TsdA enzymes. Gel electrophoresis was used to assess the purity of

purified TsdA (data not shown). The appearance of gels was consistent with previously published data for *Av* WT³ and *Cj* WT and variants³². Recombinant *Av* TsdA enzyme⁹ overexpressed in *Escherichia coli* contains the 243 amino acids predicted from the Alvin_0091 gene without a signal peptide and with a single residue linking the C-terminus to a Strep II tag. The predicted mass of the *Av* WT monomer with two *c*-hemes is 28,141 Da. Throughout this thesis amino acids are numbered from the first residue of the mature protein (Figure 2.1, lower). Recombinant *Cj* TsdA enzyme³² overexpressed in *E. coli* contains the 309 residues predicted from c8j_0815 without a signal peptide and with a four-residue linker to a Strep II tag followed by three more residues at the N-terminus. The predicted mass of the *Cj* WT monomer with two *c*-hemes is 37,103 Da. Throughout this thesis amino acids are numbered from the first of the three residues prior to the Strep tag on the predicted N-terminus of the mature protein (Figure 2.1, upper).

Cj TsdA WT

```

10      20      30      40      50      60      70
MASWSHPQFE KGAGSLDPNL ETKSATGID LPTAKWNLPK ALNEDGTIDE TKMPKNSEYS KMVILGNKIL
80      90      100     110     120     130     140
NETSKYVGPO AKDPKKRFAG NNLSCSSCHA NGGSVQNSG FVGIWARFPQ YNARGDKVIT LADRINGCFE
150     160     170     180     190     200     210
RSMNGKRMPS DTPEMKAMLT YMQWLSQGVV VGAKIEGQGL KKIDFISRAA DPKKGKAIYM DKCAVCHQEN
220     230     240     250     260     270     280
GLGLKNEDSA GAYLYPPLW GDSYNTGAG MYRLIKAASY IKENMPQGAP DLSLEDAYDV AAYMNSQARP
290     300     310     320     324
IKANRDKDFP DRKVKPLDMD VGPYDDSFST TQHRYGPYTN MIKK

```

Av TsdA WT

```

10      20      30      40      50      60      70
EPPPTVALTV PAAALLPDGA LGESIVRGRR YLSDTPAQLP DFVGNGLACR HCHPGRDGEV GTEANAAPFV
80      90      100     110     120     130     140
GVVGRFPQYS ARHGRLITL QRIDGCFERS LNDRALALDH PALIDMLAYM SWLSQGVVPG AVVAGHGIPV
150     160     170     180     190     200     210
LTLREPDGV HGEALYQARC LACHGADGSG TLDADGRYLF PPLWGPFSFN TGAGMNRQAT AAGFIKHKMP
220     230     240     250     252
LGADDSLSDE EAWDVAGFVL THPRPLFQEP TGDAWSHPQF EK

```

Figure 2.1 – Sequences of *Cj* (above) and *Av* (below) TsdA wild-type enzymes. Ochre residues are linkers, purple residues are Strep tags and green residues are heme binding motifs and proposed heme ligands.

The concentration of TsdA in solution was determined from the intensity of the heme Soret peak in oxidised proteins using electronic absorbance (see above, 1.3.1) and extinction coefficients (ϵ) (Table 2.1) calculated from pyridine hemochrome experiments^{9,32} and comparison of MCD and absorbance intensities. Proteins were stored frozen at -80 °C, thawed before use and afterwards flash-frozen in liquid N₂ before being returned to -80 °C storage. Proteins provided as 80-150 μ M solutions in various buffers were transferred to the desired buffer-electrolyte using 10,000 MWCO spin concentrators (Thermo Fisher) and a Spectrafuge mini-centrifuge (Sigma-Aldrich) or an AccuSpin micro 17 centrifuge (Thermo Fisher). Prior to electrochemical measurements, exchange of the original buffer was repeated extensively until >0.1% remained.

Table 2.1 – Soret peak wavelengths (λ) and extinction coefficients (ϵ) of fully oxidised TsdA enzymes and variants featured in this thesis. * Denotes estimates based on other TsdA variants.

Variant	λ_{Soret} (nm)	ϵ_{Soret} ($\text{M}^{-1} \text{cm}^{-1}$)
<i>Cj</i> WT	415	190,000
<i>Cj</i> C138M	413	210,000
<i>Cj</i> C138H	411	230,000
<i>Cj</i> N254K	408	200,000
<i>Av</i> WT	407	208,000
<i>Av</i> K208N	409	200,000
<i>Av</i> C96M	412	210,000*
<i>Av</i> C96H	411	210,000*

2.3. Optical spectroscopy

2.3.1. Electronic Absorbance

UV-visible electronic absorbance spectra of protein samples were recorded using a model 4100 UV-visible-nIR spectrophotometer (Hitachi) or a model V-650 UV-visible spectrophotometer (JASCO). Samples were exchanged into 50 mM HEPES, 50 mM NaCl at pH 7.0 and then transferred to an anaerobic chamber. Sample concentrations are indicated in figure legends and all spectra were recorded using sealed type 21 quartz cuvettes with an optical pathlength (l) of 0.1 cm. Electronic absorbance spectra were also recorded for all samples prior to MCD measurements to determine heme concentration and sample quality. Where traces of autoreduction were apparent, sub-stoichiometric quantities of potassium ferricyanide were added to the sample until the spectrum indicated full oxidation.

2.3.2. Magnetic Circular Dichroism

Samples were exchanged into 50 mM HEPES, 50 mM NaCl at pH 7.0 for spectra in the range 250-800 nm and pH* 7.0 for spectra in the range 800-2000 nm (pH* being the apparent pH recorded using a glass electrode for a solution in D₂O). Samples were transferred to an anaerobic chamber (unless fully oxidised) and spectra were recorded using sealed (or open) quartz cells with $l = 0.1$ cm. Typical sample concentrations were 90-150 μM for spectra in the range 450-2000 nm,

or 10-50 μm dilutions of these for spectra of oxidised (reduced) samples in the range 250-450 nm (250-800 nm). Full details of sample concentrations are indicated in corresponding figure legends.

MCD spectra were recorded using JASCO spectropolarimeters; model J810 for the wavelength range 250-800 nm and model J730 for the range 800-2000 nm. An 8T magnetic field was generated using a Special Spectromag 1000 split coil superconducting solenoid (Oxford Instruments) with a 50 mm ambient temperature bore. Instrumental control of the slit width to achieve a spectral band width of 2 nm was used for spectra in the range 250-480 nm. A set slit width of 120 μm (90 μm) was used for oxidised (reduced) samples in the range 480-800 nm.

2.3.3. MCD Instrumentation

In MCD a circular dichroism spectropolarimeter is used to pass oscillating left- and right-handed circularly-polarised light through a sample where there is an external magnetic field parallel to the path of incident light (Figure 2.2). Linearly-polarised light is converted to circularly-polarised light using a photoelastic modulator consisting of two crystalline quartz prisms held together by a flexible adhesive. Regular piezoelectric vibration in response to an applied alternating current (AC) is stimulated by electrodes attached to one crystal. This vibration is transferred through to the second crystal, compressing across one crystalline plane and causing birefringence. Linearly-polarised light travelling through this prism at a 45 ° incident angle experiences a different refractive index when travelling through one plane compared to the other, resulting in circular polarisation. This polarity is reversed with a regular frequency as it passes through the sample to a detector. The detector records the peak-to-trough difference of the photomultiplier voltage or photodiode current, either of which are proportional to the difference in absorbance of left- and right-handed circularly-polarised light.

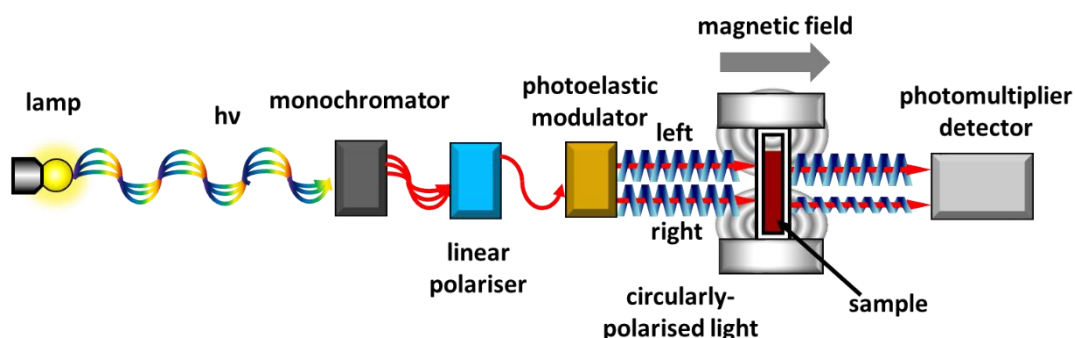


Figure 2.2 - Schematic of a typical MCD experiment. A tungsten deuterium arc lamp (UV/visible region) or a tungsten halogen bulb (nIR region) is used as a broad-emission light source; specific wavelengths are then selected using a monochromator. A photoelastic modulator polarises light in an oscillating circular left/right manner which passes through a sample mounted in a quartz cell before being registered by a photomultiplier or photodiode detector which is effective over the wavelength range being used.

The amplitude of room-temperature MCD signals is proportional to the strength of the external magnetic field (H), so a superconducting electromagnet is used to obtain a good signal-to-noise ratio (Figure 2.3). To maintain superconductive temperatures, the magnet coils are cooled by liquid helium. In addition, a split coil design allows for the positioning of samples in a bore between the coils where the direction of the forward magnetic field is collinear with light passing along the bore. Typical MCD spectra are recorded with the magnetic field in both the forward and reverse directions, resulting in two identical spectra with opposite-signed intensities. The difference between forward and reverse signals is then halved to give a spectrum of optical rotation (θ) in millidegrees, which is converted to a change in extinction coefficient ($\Delta\varepsilon$) using the following manipulation of the Beer-Lambert Law:

$$\Delta\varepsilon = \frac{\theta}{32980 \cdot H \cdot c \cdot l}$$

where H is the external magnetic field strength in tesla, c is concentration and l is the optical pathlength.

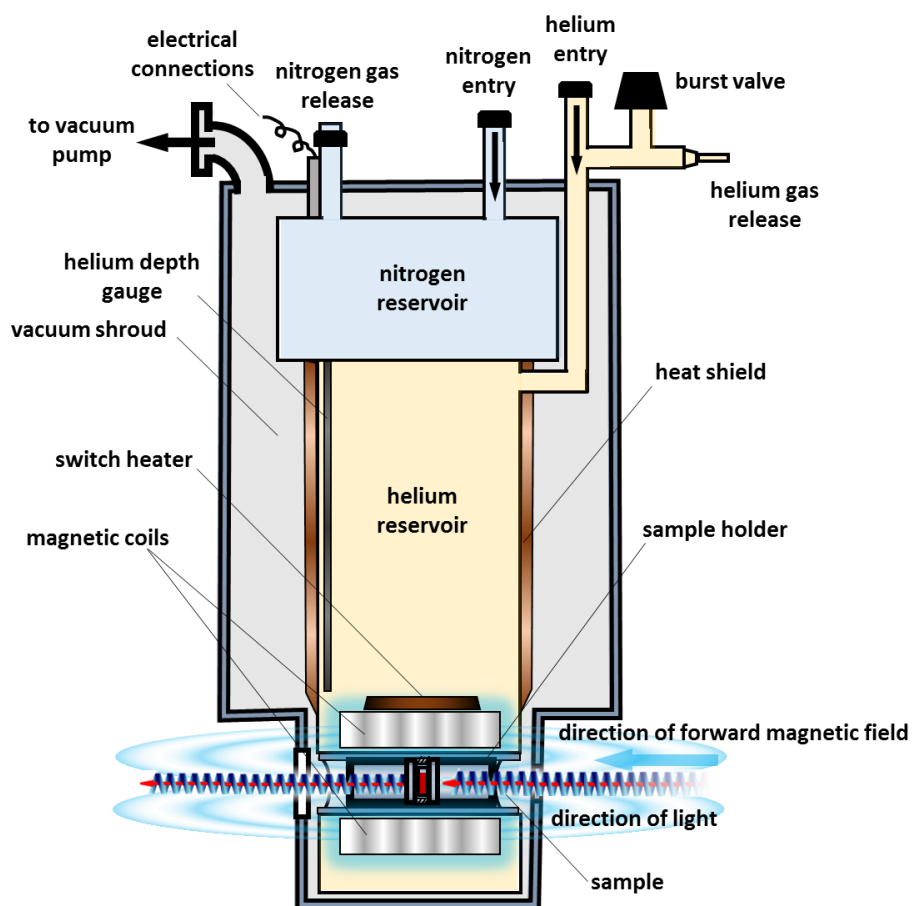


Figure 2.3 – Simplified schematic of a split-coil superconducting electromagnet suitable for room-temperature MCD experiments. Magnetic field is shown in a forward direction; measurements for a single sample are typically recorded in both the forward and reverse directions.

2.4. Potentiometry

Aliquots from a freshly-prepared ascorbate stock solution were added to protein solutions within an anaerobic chamber to achieve the desired ascorbate concentration (1.5 mM). A combination electrode (Metrohm) placed in an equivalent solution with no protein under an argon atmosphere recorded a potential of $+59 \pm 12$ mV. This solution also contained a mediator cocktail (2 μ M each) of 3,6 -diaminodurene (DAD) ($E_M = +276$ mV), 2-((3-(3,6-dichloro-9H-carbazol-9-yl)-2-hydroxypropyl)amino)-2-(hydroxymethyl)propane-1,3-diol (DCAP) ($E_M = +217$ mV), 2,6-dichloroindophenol sodium salt hydrate (DCPIP) ($E_M = +217$ mV), phenazine methosulphate (PMS) ($E_M = +80$ mV), phenazine ethosulphate (PES) ($E_M = +55$ mV), juglone ($E_M = +30$ mV), methylene blue ($E_M = +11$ mV), duraquinone ($E_M = +5$ mV), menadione ($E_M = -70$ mV), indigo carmine ($E_M = -125$ mV), anthraquinone-2,6-disulphonic acid disodium salt (ADQS) ($E_M = -185$ mV), anthraquinone-2-sulphonic acid sodium salt monohydrate (AQS) ($E_M = -225$ mV), phenosafranine ($E_M = -252$ mV), safranine-O ($E_M = -280$ mV), benzyl viologen ($E_M = -350$ mV) and methyl viologen ($E_M = -440$ mV). A saturated aerobic solution of quinhydrone ($E_M = +295$ mV) was used for calibration of solution potential.

Complete reduction of the protein samples used sodium dithionite (0.3 mg/mL, approximately 1.5 mM) titrated from a stock solution under anaerobic conditions monitored initially by electronic absorbance, then by MCD. Samples of *Cj* N254K and the *Av* K208N prepared in this way had residual signals from ferric heme in their MCD spectra which were absent after increasing the dithionite concentration to 1 mg/mL.

2.5. Protein Film Voltammetry

Voltammetric measurements were performed inside a Faraday cage within an anaerobic chamber using a PGSTAT12 or 30 (Autolab) connected to a thermostated electrochemical cell with a standard 3 electrode configuration⁸³ (Figure 2.4). The electrodes used were a Ag/AgCl reference electrode in saturated KCl solution (Radiometer Analytical), a platinum counter electrode and working electrodes comprised of IO-ITO⁸⁴ ($A_e = 0.25$ cm², 20 μ m thickness, 750 nm pore diameter) on fluoride-doped tin oxide glass provided by Katarzyna Sokół and Erwin Reisner from the University of Cambridge. Concentrated (60-120 μ M) purified TsdA enzyme in 50 mM HEPES, 50 mM NaCl, pH 7 with 1.25 mM neomycin sulphate was applied to a fresh IO-ITO electrode to form the protein film for each set of experiments. This was left in an aerobic atmosphere on ice for ~40 minutes before being transferred to an anaerobic chamber, rinsed with anaerobic buffer to remove loosely-bound materials and transferred to the electrochemical cell.

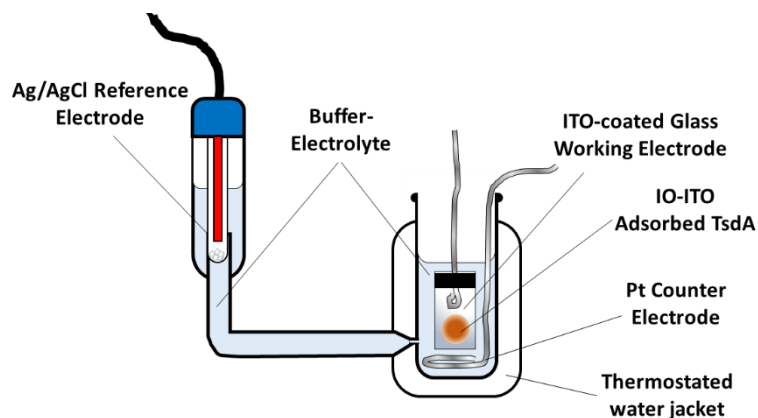


Figure 2.4 – Typical arrangement of an IO-ITO electrode in a standard 3-electrode cell.

For each enzyme, multiple cyclic voltammograms were recorded at scan rates of 5, 7, 10, 30, 50, 70, 100 mV s^{-1} in an arbitrary, non-sequential order to distinguish signals changing over time from signals changing with scan rate. Before the first scan at each scan rate the electrode was poised at $E = +500$ mV for 5 minutes to fully oxidise the protein film. Experiments were performed in 50 mM HEPES, 50 mM NaCl, pH 7 buffer-electrolyte and a new electrode was used for each film of each enzyme. Potentials recorded using the Ag/AgCl reference electrode were converted to potentials versus standard hydrogen electrode (SHE) by adding +0.197 mV. Baselines were drawn manually on raw voltammograms using Nova 1.11 software (Autolab) using voltammograms recorded with a neomycin-coated electrode as a guide. Baseline-subtracted Faradaic currents were then analysed for Nernstian redox behaviour (Equation 1.2) as fully described in Chapters 3, 4 and 5.

2.6. Liquid Chromatography Mass Spectrometry

Protein samples (~ 30 μM) in 50 mM HEPES, 50 mM NaCl, pH 7 were transferred to an anaerobic chamber and incubated with substrates or chemical agents where indicated, typically for 10 minutes. All samples except *Cj* C138H/M and *Av* C96H/M were subsequently incubated with 20 mM sodium iodoacetate for 2 minutes to alkylate free thiols so they are unable to react further during denaturation and liquid chromatography mass spectrometry (LC-MS) analysis. Samples containing excess sulphite or ferricyanide were then buffer exchanged using 10,000 MWCO spin concentrators (Thermo Fisher) and an AccuSpin micro 17 centrifuge (Thermo Fisher). Samples were then diluted 10-fold in 2% acetonitrile (MS grade, Honeywell), 0.1% formic acid (Fluka) in water (MS grade, VWR) and transferred into 2 mL chromatography vials with 250 μL inserts (Agilent).

For LC-MS of protein recovered from IO-ITO electrodes, the electrode was removed from its buffer-electrolyte following voltammetry and kept within the anaerobic chamber. A 5 μL drop of 100 mM sodium iodoacetate was placed on the IO-ITO surface and left to incubate for 2 minutes. Following this 200 μL of 2% acetonitrile, 0.1% formic acid was dropped onto the electrode surface with a gas-tight syringe (Hamilton), and the syringe tip was used to remove the IO-ITO coating forming a suspension in the solvent drop. This suspension was transferred to an Eppendorf tube and allowed to sediment under gravity for 5 minutes, after which the supernatant containing desorbed protein but no ITO particles was transferred into a 2 mL chromatography vial with a 250 μL insert.

For LC-MS measurement, 8 μL of a sample was robotically loaded into a Dionex Ultimate 3000 (Thermo) liquid chromatography system feeding into the electrospray ionisation (ESI) source of a MicroTOF-QIII (Bruker) mass spectrometer controlled by HyStar 3.11 software (Bruker). LC-MS measurements to detect ions over a 50-3000 m/z range were made in positive ion mode with capillary (end plate) potentials of -4500 V (-4000 V). Nebuliser gas pressure was 0.8 Bar, dry gas (8 L min^{-1}) was heated to 240 $^{\circ}\text{C}$, funnels 1 and 2 had a radio frequency (RF) potential of 400 V per plate with no in-source collision induced dissociation (isCID) energy. The hexapole RF potential was 600 V per plate, the analytical quadrupole had an ion energy of 5 eV, neutral gas collision energy was set to 10 eV, the collision cell RF potential was 650 V per plate, transfer time to the time-of-flight (TOF) chamber was 143 μs and pre-pulse storage time was 1 μs . The ESI-TOF was calibrated using ESI-L low concentration tuning mix (Agilent) which in positive ion mode has m/z peaks from 118-2722.

The m/z peaks of intact TsdA proteins were selected using Compass Data Analysis 4.1 (Bruker) software from chromatograms monitored by total mass intensity and absorbance at 280 nm. These peaks were smoothed using a Gaussian algorithm over a 0.1 m/z window then the ESI Compass 1.3 Maximum Entropy Deconvolution algorithm was used to deconvolute the m/z data into mass spectra over a 35,000 – 40,000 Da range (*Cj* TsdA) or a 25,000 – 35,000 Da range (*Av* TsdA).

2.6.1. LC-MS Instrumentation

In time-of-flight (TOF) mass spectrometry (MS) a charged molecule is electrostatically propelled through vacuum to a detector. If the kinetic energy of propulsion and the distance of travel are constant, the time of travel can be related to the mass and the charge of the molecule⁸⁵. There are many methods used to ionise MS samples so that they have charge, the method used in this study is electrospray ionisation (ESI), a 'soft' method suitable for use on proteins⁸⁶. The presence of small, easily ionised molecules such as buffers and salts can often

make the ionisation of proteins difficult, so prior to ESI-MS, liquid chromatography (LC) was used to remove these for the work presented here⁸⁷.

After LC removal of unwanted ions, proteins in solution are pumped at high pressure through a nebuliser (Figure 2.5), consisting of a very fine needle, sheathed in a neutral gas such as N₂. At the tip of the needle, a fine spray of solution is produced, which is spread and desolvated by gas pressure within a sealed electrospray chamber. The nebuliser is electrically grounded, spraying towards an end plate/spray shield which has an extremely low potential (-4000 V). This potential difference causes many of the sample molecules to gain positive charge, making them repel each other once desolvation has reached a critical point (Rayleigh limit). These positive ions are attracted to the spray shield which has a central hole, behind which there is a capillary with an even lower potential (-4500 V) which draws in the ions. Heated gas pumped in the opposite direction serves to repel neutral molecules and prevent them from entering the capillary. All chambers of the instrument behind the capillary are evacuated, so pressure difference and electromagnetic attraction draw positive ions along the capillary into the first of two funnels.

Funnel 1 consists of stacked metal plates with consecutively narrower concentric holes to which a radio frequency (RF) potential is applied. This rapidly oscillating current both attracts and repels the positive ions, with the net effect that they are constrained to the central axis of the funnel. A positive direct current (DC) potential bias is applied to the first (widest) plate, propelling the ions further into the funnel, a lower potential bias at the last plate and the funnel base focuses the ions. Funnel 1 is offset from the capillary axis, so that neutral species will be propelled onto the sides of the funnel or drawn away by vacuum rather than travelling further into the instrument. Funnel 2 is similarly constructed, and guides the positive ions through a RF hexapole with a gating lens and a focusing lens at the end, which combine to shape a narrow ion beam.

The ion beam then passes through an analytical quadrupole into a collision cell filled with a pressure of neutral gas such as N₂. A gate lens halts the path of the ions for a matter of μ s before transfer and focussing lenses propel an ion pulse into the TOF chamber. A small percentage (>5%) of the pulsed ion beam entering the TOF chamber strikes a secondary electron multiplier (SEM) and detector which is used for monitoring and calibration purposes rather than mass determination. The remaining ions are electromagnetically accelerated by a stack of concentric electrodes positioned orthogonally to the ion beam. This acceleration stage applies a set kinetic energy to the ions, which travel towards a second stack of electrodes, the reflector. The reflector then propels the ions back towards a detector, minimising any variations in kinetic energy applied to each molecule. The time it takes for the electrons to reach the detector from the acceleration stage is recorded and then digitised as m/z peaks which can be monitored in real-time and subsequently analysed using the Compass (Bruker) software suite.

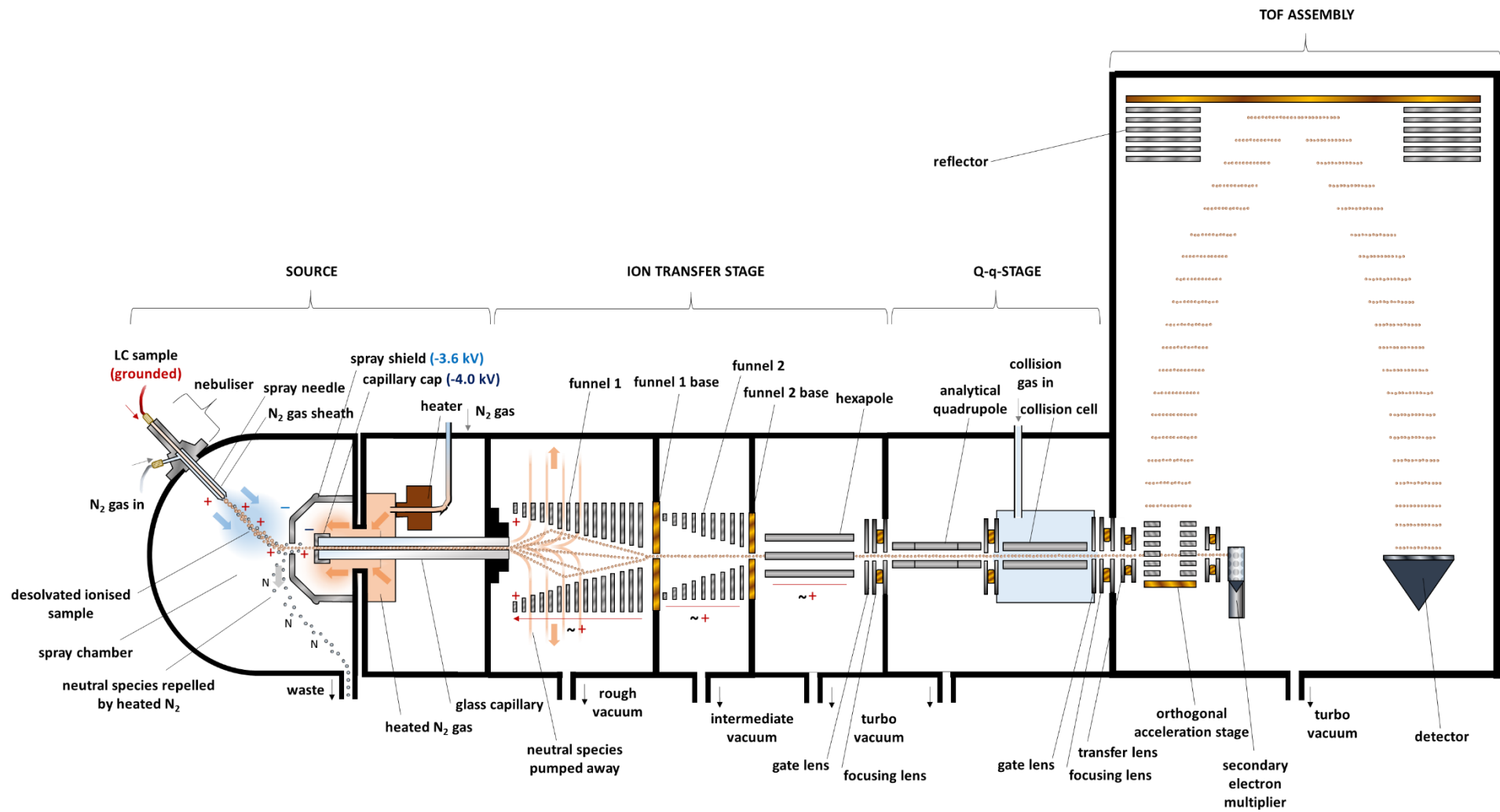


Figure 2.5 - Simplified schematic of a microOTOF-QIII Mass Spectrometer.

3. MCD and PFE of WT *Cj* and *Av* TsdA Proteins and their Variants

The structure of *Av* WT (Figure 1.5) identifies the binding of two *c*-hemes to the conserved CXXCH motifs in the amino acid sequence^{5,9,33} (Figure 1.7, blue and orange shading). Heme I is ligated by His-53 and Cys-96 in oxidised crystals, however Cys-96 is modified and/or occupies a position where it can no longer ligate the heme iron in crystal structures where sulphur oxyanions are present⁹ (Figure 1.6, B, C). Heme II is proximally ligated by His-164 but the distal ligand is either Lys-208 or Met-209 depending on the inferred heme iron oxidation state of the crystalline protein^{9,30}. It is therefore of interest to resolve the axial ligands of the *Av* WT hemes in solution and in defined oxidation states. Sequence alignments (Figure 1.7, orange shading) indicate the Lys ligand (208 in *Av* WT) is not conserved in the majority of di-heme TsdA enzymes, for which no crystal structures exist. Consequently it is also of interest to resolve the heme axial ligands of a representative of these more numerous family members. *Cj* WT is the best characterised of this latter group of enzymes and it is proposed to have His-98/Cys-138 heme I ligation and His-207/Met-255 heme II ligation³².

This chapter presents data from MCD spectroscopy that has been used to identify the heme ligation states of *Av* and *Cj* WT in solution where the hemes are in defined oxidation states. PFE is presented which complements MCD to define E_M values for hemes with defined ligation states in both proteins. PFE was performed with proteins adsorbed on IO-ITO electrodes (see above, 2.5). Both PFE and MCD were performed in 50 mM HEPES, 50 mM NaCl, pH 7 or the same buffer in D₂O, pH* 7 for nIR MCD. Similar data is presented for *Av* and *Cj* variants in which the proposed Cys ligand of heme I is replaced by His or Met and *Av* and *Cj* variants where the proposed Lys ligand of heme II is replaced or introduced respectively. Together these results allow full description of the redox chemistry in these purified TsdA proteins.

3.1. Wild-Type TsdAs

3.1.1. MCD of Oxidised TsdAs.

The MCD spectrum of oxidised ***Cj* WT** in the nIR region has two clear CT_{LS} bands indicating the presence of two chemically-distinct low-spin ferric hemes (Figure 3.1, top right). The band with a maximum at 1830 nm accompanied by a vibrational shoulder at 1560 nm can be unambiguously assigned as arising from heme with His/Met axial ligation based on previous examples of His/Met hemes^{34,47}. With an intensity of 0.8 M⁻¹cm⁻¹T⁻¹ it is likely that this band represents one heme per monomer of the *Cj* WT protein. Another band with a maximum at 1210 nm appears in the region where signals from His/Cys⁻ co-ordinated hemes have previously

been observed^{49,88}; with an intensity of $0.6 \text{ M}^{-1}\text{cm}^{-1}\text{T}^{-1}$ this is likely to represent the second heme per *Cj* WT monomer.

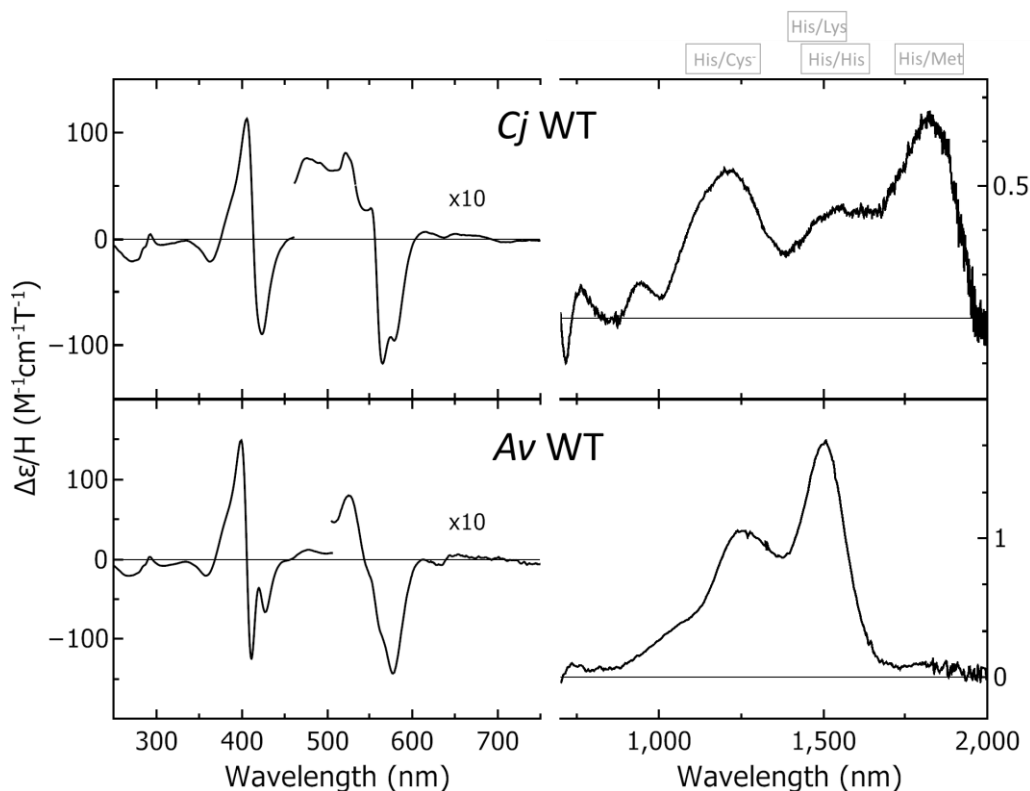


Figure 3.1 – MCD of oxidised *Cj* and *Av* WT. Room-temperature (left) UV/visible and (right) nIR MCD spectra of $17.6 \mu\text{m}$ (250–450 nm), $163 \mu\text{m}$ (450–700 nm) and $123 \mu\text{m}$ (700–2000 nm) *Cj* WT and $33.4 \mu\text{m}$ (250–450 nm) and $175 \mu\text{m}$ (700–2000 nm) *Av* WT. Samples have been fully oxidised by substoichiometric potassium ferricyanide. All data recorded at room temperature in 50 mM HEPES, 50 mM NaCl, pH 7 or the same buffer in D_2O pH* 7 for nIR MCD.

The UV/visible MCD of oxidised *Cj* WT has a Soret feature centred on 415 nm with approximately equal positive and negative intensity. This is consistent with only low-spin ferric hemes being present (Figure 3.1, top left). The peak-to-trough intensity of $200 \text{ M}^{-1}\text{cm}^{-1}\text{T}^{-1}$ for the protein is lower than would be expected for two low-spin hemes, which typically have intensities of $150 \text{ M}^{-1}\text{cm}^{-1}\text{T}^{-1}$ per heme when ligated by some combination of His, Lys or Met. This value is consistent with there being one thiolate-ligated heme with a peak-to-trough intensity of $50 \text{ M}^{-1}\text{cm}^{-1}\text{T}^{-1}$ ^{44,89} together with one ‘typical’ heme⁴⁷. The $\alpha\beta$ region has two overlaying low-spin ferric signals and the negatively-signed features of each of these are resolved. The trough at 566 nm corresponds to the ‘typical’ ligation heme species and the red-shifted broader, lower-intensity trough at 580 nm arises from thiolate-ligated heme^{44,89}.

In the MCD there are broad, low-intensity negative signals at 635 nm and 720 nm, the latter of which appears in both UV/visible and nIR MCD spectra. These bands could tentatively be assigned as arising from the His/Cys⁻ and His/Met $\text{S}(\text{p}) - \text{Fe}(\text{d})$ transitions respectively⁸⁸, although

the former could also represent the CT₂ band of a trace (<10%) population of high-spin His/H₂O ligated heme with the positive shoulder at 940 nm being part of the corresponding CT₁ band⁴⁷. The assignment of these minor features is unnecessary as the rest of the MCD spectrum in both regions is entirely consistent with oxidised *Cj* WT in solution having His/Cys⁻ ligation at heme I and His/Met ligation at heme II, confirming the previous inferences made from site-directed mutagenesis and electronic absorbance spectroscopy³².

The nIR MCD of **Av WT** has a CT_{LS} band at 1250 nm consistent with His/Cys⁻ ligated heme (Figure 3.1, bottom right) consistent with the structure of the oxidised protein^{9,33}. However there is no band at 1830 nm, ruling out His/Met ligation. Instead, there is a CT_{LS} band at 1510 nm in a region where examples of bis-nitrogen ligation have been previously observed⁴⁷; this 1510 nm band can be specifically assigned as His/Lys due to the absence of a plausible distal histidine ligand in crystallographic data⁹ and the sharp appearance of the band^{34,90}. The intensity of this feature is 1.7 M⁻¹cm⁻¹T⁻¹, consistent with one His/Lys heme per Av WT monomer. Although the His/Cys⁻ band is more intense than would be expected for a single heme, this is likely due to overlapping intensity from the vibrational shoulder of the His/Lys band and so His/Cys⁻ heme cannot be unambiguously quantified from the oxidised nIR MCD.

The Av WT Soret feature has a peak-to-trough intensity of 280 M⁻¹cm⁻¹T⁻¹, more intense than from *Cj* WT consistent with His/Lys in the place of His/Met ligation (Figure 3.1, bottom left). Although this signal has greater positive than negative intensity, it is likely that this is due to unresolved ferric signals rather than ferrous heme. There is a negative shoulder at 430 nm, likely to be the separately resolved negative lobe of a red-shifted, lower intensity thiolate-ligated Soret feature. Unlike for *Cj* WT, there is no clear resolution of two separate signals in the αβ region and no indication of a His/Met S(p) - Fe(d) CT band. There is also a broad, low-intensity feature at 633 nm which could either be a trace (<10%) population of high-spin heme or the S(p) - Fe(d) CT band for His/Cys⁻ ligated heme. Again, the assignment of this minor feature is not critical as the rest of the spectrum accounts for >90% of the sample. MCD is entirely consistent with His/Cys⁻ ligation at heme I and His/Lys ligation at heme II in agreement with crystallography of the as-isolated (oxidised) enzyme⁹. Table 3.1 presents a summary of spectroscopic features for *Cj* WT, Av WT and all proteins studied in this work.

Based on previously reported examples of hemes with His/Cys⁻ ligation; human cystathione-β synthase ($E_M = -350$ mV)⁹¹, the novel cyanobacterial cytochrome TII0287 ($E_M = -255$ mV)⁹² and the bacterial thiosulphate oxidase SoxA ($E_M = -432$ to -340 mV)^{49,93} it is likely that heme I in both enzymes has $E_M < -250$ mV. With His/Met ligation, heme II in *Cj* WT is likely to have a higher E_M value as previously reported examples of these hemes range from $E_M = +20$ to $+390$ mV^{94,95}. Whilst there are few examples of hemes with His/Lys ligation in both ferric and

ferrous states, that in the *Thiobacillus versutus* cytochrome c_{550} M100K variant also has a lower E_M value ($E_M = -77$ mV)⁹⁶ than most His/Met hemes. It is therefore predicted that *Cj* WT with His/Cys⁻ and His/Met hemes will be electroactive over a larger potential range than *Av* WT with His/Cys⁻ and His/Lys hemes. If the proposed His/Lys to His/Met heme II ligand switch⁹ does occur in the latter protein it is likely that both enzymes will be electroactive over a similar potential window. To investigate the redox properties of the hemes and assign E_M values, PFE has been employed.

Table 3.1 – (Magneto) optical bands for TsdA enzymes and variants. Data recorded at pH 7, 293 K. Soret, CT_{LS} bands were resolved at the wavelengths (λ_{Soret} , λ_{LS}) and intensities (ϵ , $\Delta\epsilon$) indicated. * = inferred heme ligands, † = heme II assumed to be identical to *Cj* WT, heme I calculated by subtraction, ‡ = calculated by subtraction.

Variant	$\lambda_{\text{Soret}} (\epsilon)$ nm (mM ⁻¹ cm ⁻¹)	Heme I CT _{LS}		Heme II CT _{LS}	
		Ligation	$\lambda_{\text{LS}} (\Delta\epsilon)$ nm (mM ⁻¹ cm ⁻¹ T ⁻¹)	Ligation	$\lambda_{\text{LS}} (\Delta\epsilon)$ nm (mM ⁻¹ cm ⁻¹ T ⁻¹)
<i>Cj</i> WT	415 (190)	His/Cys ⁻	1215 (0.50)	His/Met	1825 (0.74)
<i>Cj</i> C138M	413 (210)	His/Met	1735 [†] (0.51)	His/Met	1825 [‡] (0.74)
<i>Cj</i> C138H	411 (230)	His/His	1480 (1.03)	His/Met	1820 (0.82)
<i>Cj</i> N254K	407 (200)	His/Cys ⁻	1250 (0.40)	His/Lys or His/Met	1530 [‡] (0.64) 1830 (0.47)
<i>Av</i> WT	407 (208)	His/Cys ⁻	1240 (0.42)	His/Lys or His/Met	1505 (1.6) -
<i>Av</i> C96M	412 (210)	His/Met*	-	His/Lys* or His/Met*	- -
<i>Av</i> C96H	411 (210)	His/His*	-	His/Lys*	-
<i>Av</i> K208N	407 (190)	His/Cys ⁻	1140 (0.45)	His/Met	1790 (0.83)

3.1.2. PFE of TsdAs.

In the following sections PFE of *Av* and *Cj* WT proteins is presented as black lines. The behaviour predicted by a single, reversible, Nernstian $n = 1$ redox process (Equation 1.2) is indicated by coloured lines and assigned as either X, Y or Y' to aid their description. The sum of modelled contributions is presented as black circles. A similar format is used throughout this thesis and all potentials are quoted versus the standard hydrogen electrode (SHE).

Representative PFE of **Cj WT** on an IO-ITO electrode is presented in the upper panel of Figure 3.2. In the absence of protein the CV shows only current from charging and discharging the electrode and no peaks. Although the charging current recorded in the first voltammogram differs from subsequent scans, the signals assigned to Faradaic processes do not change over >20 cycles. At $\nu = 10 \text{ mV s}^{-1}$ two pairs of peaks (X and Y) are observed which are well described by the theoretical response for two independent, reversible $n = 1$ processes. Taking the average of E_{pa} and E_{pc} for each process gives $E_M = -186 \text{ mV}$ and $E_M = +172 \text{ mV}$ for X and Y respectively. MCD has identified two hemes (Figure 3.1, upper panel) with different chemical environments in the oxidised protein, consistent with two centres having different E_M values. If all hemes were to exchange electrons with the electrode equally, the areas of each pair of signals would be equal. However this is not the case and the areas of the lower potential peaks (X) are only approximately 25% those of the higher potential peaks (Y). This feature of the voltammetry is considered further below.

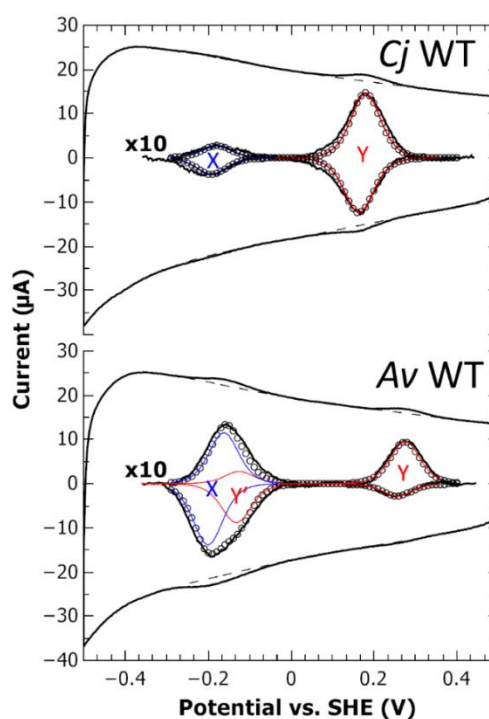


Figure 3.2 – Representative CV of wild-type **Cj** and **Av** TsdA adsorbed on IO-ITO. Raw data (outer black line) with baselines (dashed line) used to prepare baseline-subtracted CVs (inner black line) of TsdA enzymes in 50 mM HEPES, 50 mM NaCl, pH 7, $\nu = 10 \text{ mV s}^{-1}$, $T = 277 \text{ K}$. Each peak has been fitted to predicted $n=1$ theoretical responses (red and blue lines). The sum of these contributions is also shown (black circles).

PFE of **Av WT** is also unchanged over >20 cycles once the initial charging currents have stabilised. A representative CV recorded at $\nu = 10 \text{ mV s}^{-1}$ (Figure 3.2, lower panel) features a more complex Faradaic response than **Cj WT**. For **Av WT** there is a pair of peaks at high potential which is well described as an $n = 1$ redox centre with $E_M = +266 \text{ mV}$ (Y). However, for Y the area of the

oxidative peak is much larger than the reductive peak. There is also a signal at low potential which is too broad to be a single $n = 1$ process and there is structure in the reductive current suggestive of two overlapping peaks. This signal is well-described as the sum of an $n = 1$ process with $E_M = -181$ mV (X) having equal oxidative and reductive areas and an $n = 1$ redox centre with $E_M = -129$ mV (Y') where the area of the reductive peak is much larger than the area of the oxidative peak. The total area of X is approximately equal to the sum of Y and Y'. This suggests the latter two signals arise from the same redox centre and consequently equal electroactive populations of centres give rise to X and (Y + Y').

The Faradaic response of the Av WT film is rationalised as arising from two redox centres. One redox centre, *i.e.* heme, undergoes reversible, Nernstian oxidation and reduction centred on $E_M = -181$ mV giving rise to peaks X. The second redox centre, *i.e.* heme, has most of its electroactive population reduced at -129 mV (Y') and then oxidised at +266 mV (Y). This indicates a redox-driven change in chemical environment at the Av WT heme which gives rise to Y and Y'.

Voltammetry was also recorded using Av and Cj WT coated IO-ITO electrodes in 100 mM Ammonium Acetate, 50 mM NaCl, pH 5; 50 mM MES, 50 mM NaCl, pH 6 and 50 mM TAPS, 50 mM NaCl, pH 8 (data not shown). Although Faradaic peaks were centred on different E_M values, the overall appearance of voltammograms and the relative areas of X, Y (and Y' for Av WT) were unchanged from pH 7, suggesting that the ligation of the TsdA hemes does not vary over pH 5-8.

It will be seen in Chapter 5 that thiosulphate (tetrathionate) added to electrodes coated with Av and Cj WT results in positive (negative) catalytic currents due to substrate oxidation (reduction) (Figure 5.2). This suggests that adsorption onto IO-ITO does not significantly perturb the TsdAs from their native form and that both MCD and PFE are interrogating the same form of the enzyme. To assign peaks in the PFE to redox activity of the hemes I (II) with a specific ligand set, solutions of the enzymes were chemically poised at potentials that PFE suggests will reduce only one of the TsdA hemes. MCD was then recorded to identify the ligand set of the heme that remains oxidised, as described below. This potentiometric interrogation also served to identify the chemical change in Av WT heme environment upon reduction that can account for the peaks Y and Y'.

3.1.3. MCD of Semi- and Fully Reduced TsdAs.

In the following sections, MCD of TsdA fully oxidised by ferricyanide is presented as black lines, MCD of samples poised at $E = +60$ mV with ascorbate (see above, 2.4) is presented as red lines and that of samples poised at $E \approx -500$ mV⁹⁷ by subsequent incubation with dithionite is presented as grey lines. A similar format is used throughout this thesis.

MCD of *Cj* WT incubated with ascorbate shows no trace of the 1830 nm His/Met CT_{LS} band showing that low-spin ferric His/Met heme is no longer present (Figure 3.3, top right). The 1210 nm CT_{LS} band is largely unaffected in intensity, but there is now clear resolution of its vibrational sideband at 1060 nm which may be diagnostic of a subtle change in the chemical environment of heme I. In the UV/visible spectrum the ferric Soret feature is broader and less intense than in the fully oxidised enzyme (Figure 3.3, top left), consistent with only thiolate-ligated heme remaining in the ferric state. A more intense red-shifted Soret with greater positive than negative intensity has appeared and there is a sharp α band at 552 nm, both of which indicate the presence of low-spin ferrous heme. The peak-to-trough intensity of the α band is $370 \text{ M}^{-1}\text{cm}^{-1}\text{T}^{-1}$, consistent with one His/Met heme per *Cj* WT monomer being reduced to the ferrous state at $E = +60 \text{ mV}$.

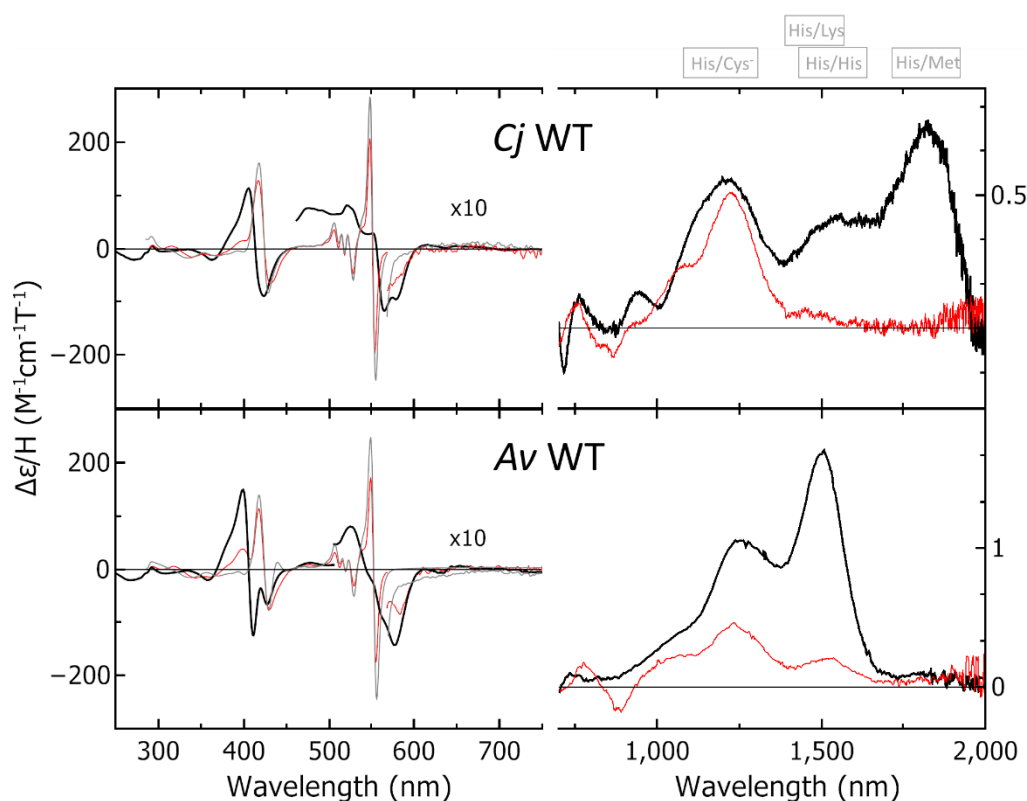


Figure 3.3 - MCD spectra of oxidised, semi-reduced and reduced *Cj* and *Av* WT. Room-temperature (left) UV/visible and (right) nIR MCD spectra of 17.6 μM (250-450 nm or 250-700 nm reduced), 163 μM (450-700 nm) and 123 μM (700-2000 nm) *Cj* WT or 30 μM (250-700 nm) and 170 μM (700-2000 nm) *Av* WT. Samples have been fully oxidised by sub-stoichiometric potassium ferricyanide (black), poised at +60 mV with 1.5 mM sodium ascorbate (red) or poised at <-300 mV with 1.5 mM sodium dithionite (grey). All data recorded at room temperature in 50 mM HEPES, 50 mM NaCl, pH 7 or the same buffer in D₂O pH* 7 for nIR MCD.

The addition of dithionite removes all traces of low-spin ferric signals in the UV/visible MCD spectrum and increases the intensity of the low-spin ferrous signals. The peak-to-trough intensity of the 552 nm feature is now $470 \text{ M}^{-1}\text{cm}^{-1}\text{T}^{-1}$. The $100 \text{ M}^{-1}\text{cm}^{-1}\text{T}^{-1}$ increase compared to the

ascorbate-treated sample is unusually high for one population of thiolate-ligated low-spin ferrous heme, so may indicate the presence of some thiol⁹⁸ or (bi)sulphide ligation (Figure 1.6, C).

Taken together the MCD spectra of oxidised and ascorbate-incubated *Cj* WT indicate that at $E = +60$ mV the His/Met heme II of this enzyme is fully reduced and the His/Cys⁻ heme I fully oxidised. At $E \approx -500$ mV both hemes are fully reduced. Therefore the high potential signals in PFE (Y, Figure 3.2, top panel) represent the electroactivity of heme II and the low potential signals (X, Figure 3.2, top panel) relate to the electroactivity of heme I. In addition, it is concluded that no heme has electroactivity outside of the potential window chosen for PFE experiments and PFE and MCD experiments provide consistent data. The assignments of E_M and ligand sets for *Cj* WT are summarised in Table 3.2 together with those for all proteins studied in this work.

Table 3.2 – Heme ligation states and E_M values for TsdA enzymes and variants. Data recorded at pH 7, 277 K, $v = 10$ mVs⁻¹. Average of oxidative and reductive E_P values from baseline-subtracted voltammograms have been used to calculate E_M . Fitted $n = 1$ areas of oxidative (Q_{ox}) and reductive (Q_{red}) peaks are presented as pmol of electrons. * = inferred heme ligands.

Variant	Heme I			Heme II		
	Ligation	E_M mV	$Q_{ox}(Q_{red})$ pmol	Ligation	E_M mV	$Q_{ox}(Q_{red})$ pmol
<i>Cj</i> WT	His/Cys ⁻	-186	27 (38)	His/Met	+172	145 (122)
<i>Cj</i> C138M	His/Met	+94	177 (170)	His/Met	+174	177 (145)
<i>Cj</i> C138H	His/His	-100	123 (110)	His/Met	+160	220 (220)
<i>Cj</i> N254K scans 9+	His/Cys ⁻	-115	45 (55)	His/Lys	-171	16 (45)
				or His/Met	+205	120 (45)
scan 1	His/Cys ⁻	-115	50 (35)	His/Met	+203	125 (103)
<i>Av</i> WT	His/Cys ⁻	-181	115 (138)	His/Lys	-129	27 (87)
				or His/Met	+266	95 (27)
<i>Av</i> C96M	His/Met*	+94	160 (135)	His/Lys*	~-172	~100 (~130)
				or His/Met*	+270	95 (9)
<i>Av</i> C96H	His/His*	-211	85 (85)	His/Lys*	-158	85 (85)
<i>Av</i> K208N	His/Cys ⁻	-173	55 (55)	His/Met	+264	168 (140)

In the MCD of the ascorbate-incubated **Av WT** sample, the 1510 nm His/Lys CT_{LS} band has diminished to only ~10% of the intensity in the di-ferric form (Figure 3.3, bottom right); this now permits clear resolution of the His/Cys⁻ CT_{LS} band at 1230 nm with an intensity of 0.5 M⁻¹cm⁻¹T⁻¹, similar to the band in *Cj* WT and consistent with one ferric His/Cys⁻ heme per monomer. In the UV/visible region a broad, low-intensity Soret feature typical of thiolate-ligated low-spin ferric heme is present with a peak-to-trough intensity of 110 M⁻¹cm⁻¹T⁻¹ (Figure 3.3, bottom left), consistent with a small (~10%) population of non-thiolate ligated low-spin ferric heme in addition to one thiolate-ligated heme. A red-shifted, asymmetric Soret peak has appeared along with a sharp α band at 553 nm indicating low-spin ferrous heme. This α band has a broader appearance than is typical for hemes with bis-nitrogenous ligation, but is explained if there has been a switch to His/Met ligation. Consistent with this proposal, the α peaks of ascorbate-incubated *Av* WT and *Cj* WT have a similar appearance. From the peak-to-trough intensity of this band (348 M⁻¹cm⁻¹T⁻¹) ascorbate-incubated *Av* WT is therefore assigned as having ~90% of one heme population both ferrous and His/Met ligated.

At 830 nm there is a low-intensity bisignate CT₁ band indicating that the previously-detected minor (<10%) high-spin ferric heme population is unaffected by ascorbate. Incubation with dithionite removes all trace of low-spin ferric heme in both the Soret and $\alpha\beta$ regions and increases the intensity of the low-spin ferrous signals. The peak-to-trough intensity of the α band is now 490 M⁻¹cm⁻¹T⁻¹, consistent with one thiolate-ligated ferrous heme and one methionine-ligated ferrous heme.

The MCD of semi-reduced ($E = +60$ mV) *Av* WT shows ~90% His/Lys heme II is reduced and switches to His/Met ligation, while His/Cys⁻ heme I remains fully oxidised. All hemes are reduced by excess dithionite ($E_M \approx -500$ mV). The low potential signals (X, Figure 3.2, bottom panel) in PFE are therefore assigned to the redox activity of heme I as their electroactivity is entirely below +60 mV. The remaining signals (Y and Y', Figure 3.2, bottom panel) are assigned as both arising from the redox activity of heme II, with the following rationalisation. His/Lys ligated ferric heme II is reduced to the ferrous state (Y'), Met-209 then displaces Lys-208 as a heme II ligand in much of the protein as suggested by crystallography⁹. This ligand switch increases the E_M of this heme (Figure 3.4, top left grey arrow) so that this ferrous His/Met ligated heme II population is oxidised at a higher potential (Y). Met-209 is then displaced by Lys-208 in ferric heme II, lowering the E_M of this heme again (Figure 3.4, bottom right grey arrow). This behaviour is consistent with *Av* WT crystallography data and confirms that the heme II ligand switch proposed by Brito *et al.*³³ occurs in an IO-ITO adsorbed enzyme film.

When E_M is known for a heme, the change in Gibbs free energy (ΔG) for that redox transition can be calculated from the following relationship:

$$\Delta G = -nFE_M \quad \text{Equation 3.1}$$

The binding constant (K_d) for Lys or Met as heme ligands can also be described in terms of free energy change:

$$\Delta G = -RT \ln K_d \quad \text{Equation 3.2}$$

Each of the four possible transitions between heme II ligand sets and oxidation states can then be arranged as a square scheme (Figure 3.4) and the sum of ΔG in a clockwise direction calculated. Rearranging the resultant expression gives the ratio of the His/Lys to His/Met binding constants for ferrous heme (K_d^{red}) and ferric heme (K_d^{ox}). The ratio ($K_d^{\text{red}}/K_d^{\text{ox}} = 5 \times 10^6$) is positive for Av WT emphasising that at heme II, this enzyme has a thermodynamic preference for His/Lys ligation in the ferric state and His/Met ligation in the ferrous state.

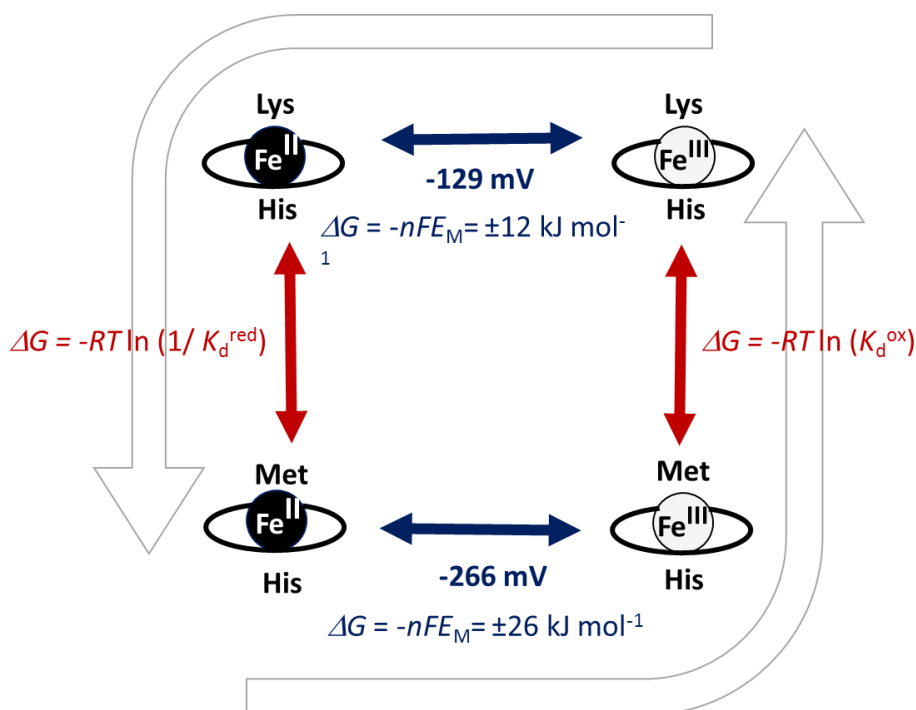


Figure 3.4 – Heme II ligation in Av WT. Oxidation of the heme II iron causes displacement of methionine by lysine as a heme ligand, the reverse occurs upon reduction. The ratio of binding constants ($K_d^{\text{red}}/K_d^{\text{ox}}$) can be calculated for the Lys-208 \rightarrow Met-209 ligand switch. Grey outlined arrows show redox-driven events resolved by PFE.

As described above, fully reduced Av and Cj WT were prepared using dithionite as it has a suitably low potential⁹⁷, is the same agent used in crystallographic studies previously⁹ and has absorbance only at 314 nm, unlikely to obscure any heme signals. However dithionite ($S_2O_4^{2-}$) is also a substrate mimic for TsdA enzymes, so electronic absorbance spectroscopy was used to investigate evidence of any change in heme environment caused by dithionite other than reduction of the hemes.

The electronic absorbance spectrum of *Av* WT incubated with excess dithionite was compared to that of the same enzyme incubated with europium (II) chloride in complex with ethylene glycol bis(β -aminoethyl ether)-*N,N,N',N'*-tetraacetic acid (EGTA) ($E_M = -880$ mV)⁹⁹. Similarly, the electronic absorbance spectrum of *Cj* WT with excess dithionite was compared to that of *Cj* WT incubated with excess europium (II) chloride ($E_M = -350$ to -430 mV⁹⁹). The heme peaks in the two *Av* WT spectra are virtually identical and the same is true for *Cj* WT (Figure 3.5). This suggests that the presence of dithionite or its sulphur-containing breakdown products is not modifying the TsdA enzymes in any way other than acting as a reducing agent.

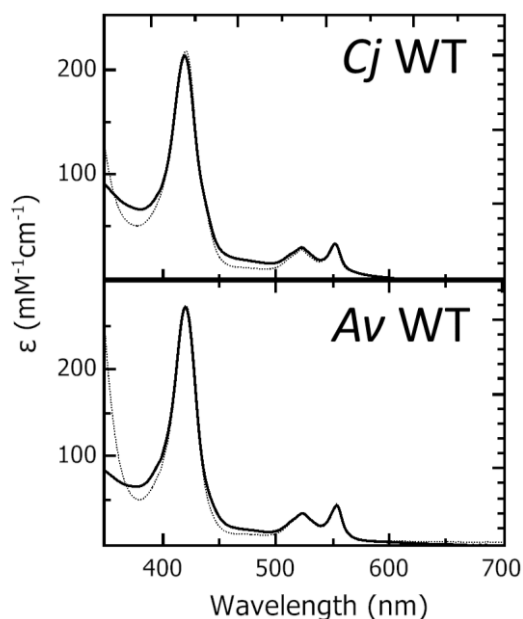


Figure 3.5 – Electronic absorbance spectra of fully reduced *Cj* and *Av* WT. Samples incubated with excess sodium dithionite (grey lines) or excess EuCl_2 (*Cj* WT, top black line) or EuCl_2 -EGTA (*Av* WT, bottom black line) in 50 mM HEPES, 50 mM NaCl, pH 7.

3.2. MCD and PFE of TsdA Variants.

The combination of MCD and PFE data used to characterise *Av* and *Cj* WT has led to a proposal for heme ligation states and E_M values. For *Av* WT it has provided evidence for redox-driven ligand switching at heme II. For *Cj* WT it has also provided evidence of unequal electroactive populations of hemes I and II. To test the validity of these proposals and shed greater insight into the redox chemistry of these enzymes, variants of both proteins were studied by the same approach; the results from these investigations are described below.

3.2.1. *Cj* TsdA Heme I Environment Cys-138 \rightarrow Met and His Variants.

Cj TsdA variants were investigated where the heme I cysteine ligand is substituted by the coordinating residues histidine or methionine³² that are unlikely to be modified by sulphur

chemistry and which typically give rise to low or high E_M hemes respectively²⁵. These variants are catalytically inactive in solution assays³² (Figure 1.4) and also on IO-ITO electrodes (data not shown), consistent with an essential mechanistic role for the heme I cysteine⁵. MCD spectra were recorded for both fully oxidised variants (Figure 3.6). In the nIR region, both have a ~ 1800 nm CT_{LS} band indicative of low-spin ferric heme with His/Met ligation similar to that observed for *Cj* WT (Figure 3.1, top panels). As with the wild-type enzyme, these bands disappear when the sample is incubated with ascorbate ($E = +60$ mV).

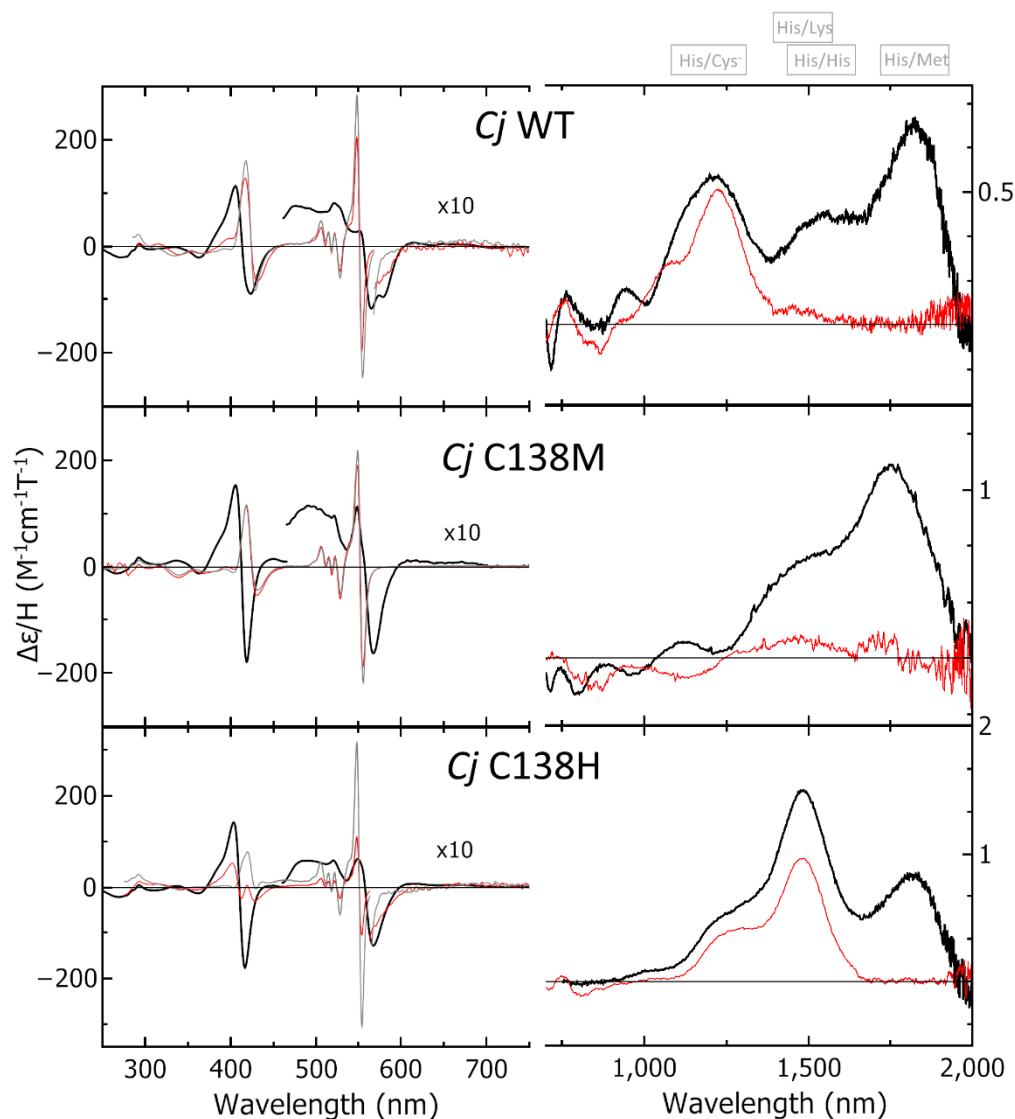


Figure 3.6 – MCD spectra of *Cj* TsdA heme I variants. Room-temperature (left) UV/visible and (right) nIR MCD spectra of 17.6 μM (250-450 nm or 250-700 nm reduced), 163 μM (450-700 nm) and 123 μM (700-2000 nm) *Cj* WT; 160 μM (700 nm – 2000 nm) and 40 μM (250 – 700 nm) or 25 μM (250 – 700 nm dithionite) *Cj* C138M; 170 μM (450 – 2000 nm) and 18 μM (250 - 450 nm or 250 – 700 nm reduced) *Cj* C138H. Samples are oxidised by sub-stoichiometric potassium ferricyanide (black) or reduced by 1.5 mM sodium ascorbate (red) or 1.5 mM sodium dithionite (grey). All data recorded in 50 mM HEPES, 50 mM NaCl, pH 7 or the same buffer in D_2O pH* 7 for nIR MCD.

Representative voltammograms recorded at $v = 10 \text{ mVs}^{-1}$ for both *Cj* C138M and C138H (Figure 3.7, left) feature a pair of peaks (Y) with $E_M \approx +200 \text{ mV}$ which are well described by the theoretical response for a reversible $n = 1$ process (Equation 1.2). These are largely identical to the peaks assigned to heme II in *Cj* WT (Figure 3.2, top panel) confirming that these variants have retained wild-type His/Met ligation at heme II, as expected when only a predicted heme I ligand has been substituted (Table 3.2).

The His/Met CT_{LS} band for the **C138M** variant (Figure 3.6, middle panel) has λ_{max} at 1750 nm and a vibrational shoulder at 1460 nm and is the only signal resolved in the nIR region. The broad appearance of this feature and intensity of $1.13 \text{ M}^{-1}\text{cm}^{-1}\text{T}^{-1}$ suggests two non-identical His/Met heme populations give rise to largely overlapped CT_{LS} bands. The UV/visible MCD is consistent with this, resolving only signals for low-spin ferric heme. The Soret has a peak-to-trough intensity of $337 \text{ M}^{-1}\text{cm}^{-1}\text{T}^{-1}$ consistent with two ferric methionine-ligated hemes per TsdA monomer. When this sample is incubated with ascorbate, all signals disappear from the nIR region and a sharp α band appears at 552 nm in the UV/visible region. This band has a peak-to-trough intensity of $378 \text{ M}^{-1}\text{cm}^{-1}\text{T}^{-1}$ consistent with two low-spin methionine-ligated ferrous hemes. Further incubation with dithionite does not change the spectrum any further suggesting a lack of redox activity at $E < +60 \text{ mV}$ and implying no electroactivity below +60 mV in PFE. Voltammetry of the C138M film (Figure 3.7, centre left) features two pairs of peaks; Y as described above is overlapped by peaks (X) with a similar area, centred on a slightly lower potential ($E_M = +94 \text{ mV}$) well described by $n = 1$ processes. Assuming Heme II is unchanged from *Cj* WT, the C138M variant is therefore assigned as having His/Met ligation and $E_M = +94 \text{ mV}$ at heme I (Table 3.2).

MCD of the **C138H** variant (Figure 3.6, bottom panel) has a prominent CT_{LS} band at 1480 nm, with a vibrational shoulder at 1220 nm typical of low-spin ferric heme I with bis-nitrogenous co-ordination. Some of the apparent intensity of this band is likely to arise from overlap with the vibrational shoulder of the 1820 nm His/Met CT_{LS} band. In the UV/visible region only low-spin ferric heme signals are present and the Soret feature has a peak-to-trough intensity of $320 \text{ M}^{-1}\text{cm}^{-1}\text{T}^{-1}$ consistent with two non-thiolate ligated hemes. Incubation with ascorbate eliminates all trace of the His/Met CT_{LS} band and the bis-nitrogenous CT_{LS} band is clearly resolved at 1480 nm, with an intensity of $0.96 \text{ M}^{-1}\text{cm}^{-1}\text{T}^{-1}$ consistent with a single remaining ferric heme population. The UV/visible region of the spectrum features a sharp α band at 552 nm with a peak-to-trough intensity of $212 \text{ M}^{-1}\text{cm}^{-1}\text{T}^{-1}$ consistent with a single low-spin ferrous heme population with His/Met ligation. Incubation with dithionite eliminates all signals indicative of ferric heme and increases the size of the ferrous α band to $622 \text{ M}^{-1}\text{cm}^{-1}\text{T}^{-1}$, consistent with the presence of one additional nitrogen-ligated ferrous heme population. In the crystal structures of *Av* and *Mp* WT there are no nitrogenous residues that would commonly be considered as heme ligands in the

vicinity of heme I³⁰. Assuming the folding of this region is similar in *Cj* C138H, from sequence comparisons (Figure 1.7) the only nitrogenous ligand present would be the introduced His-138. Therefore, heme I can be assigned as having His/His ligation.

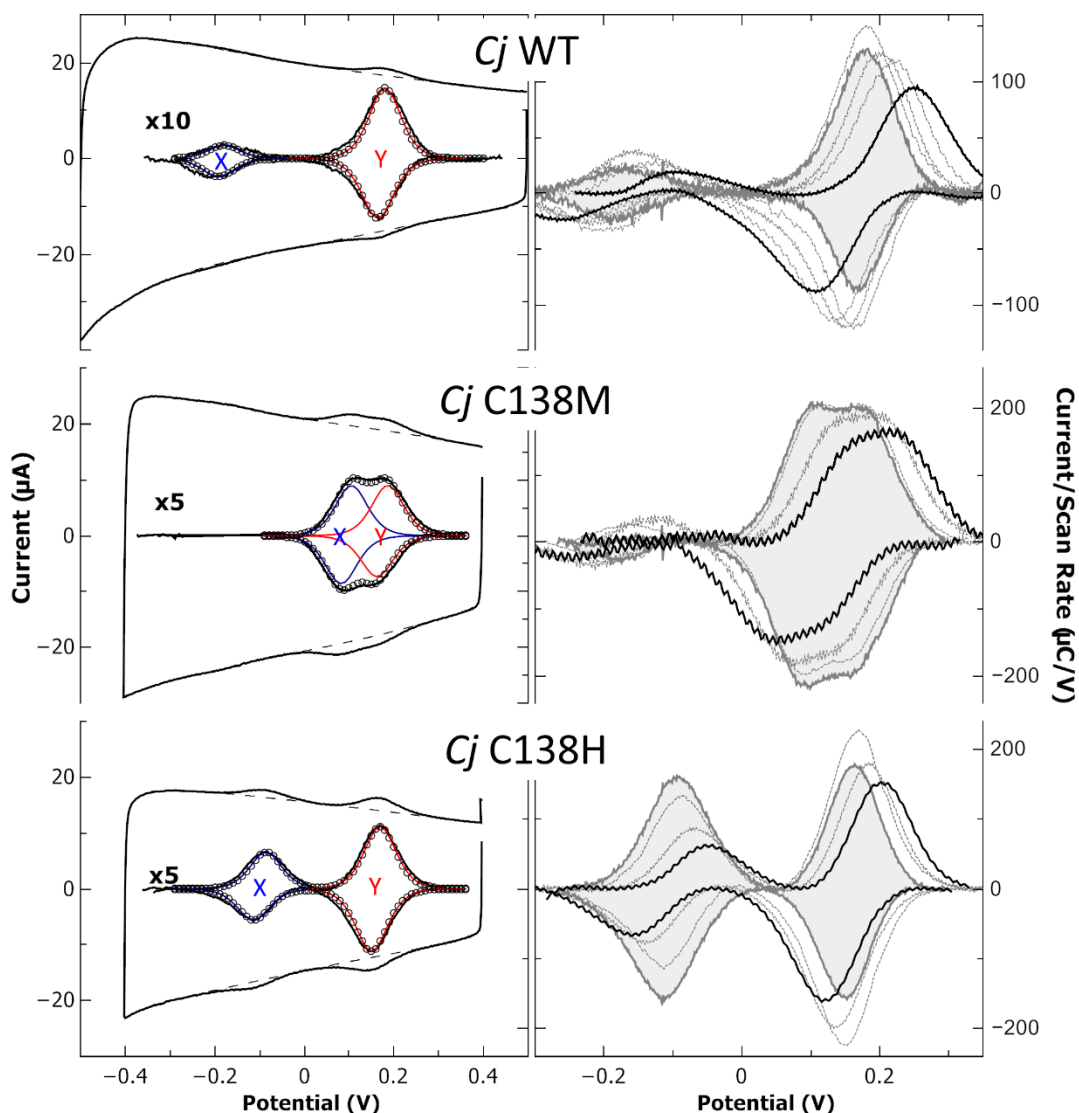


Figure 3.7 – Representative CV of *Cj* TsdA heme I variants. (Left) Raw data (outer black line) with baselines (dashed line) used to prepare baseline-subtracted CVs (inner black line) of *Cj* WT and C138M/H variants on IO-ITO electrodes. $\nu = 10 \text{ mV s}^{-1}$, $T = 277 \text{ K}$. Each peak has been fitted to two predicted $n=1$ theoretical responses (red and blue lines) and the sum of these contributions (black circles). (Right) Representative cyclic voltammograms recorded at $\nu = 5$ (grey line, shaded area), 10, 50 and 100 mV s^{-1} (black line) normalised by scan rate. All data recorded in 50 mM HEPES, 50 mM NaCl, pH 7, $T = 277 \text{ K}$.

Voltammetry of *Cj* C138H (Figure 3.7, bottom left) has a pair of peaks (X) with approximately 50% of the area of the $E_M = +160 \text{ mV}$ His/Met peaks (Y). The signals X are well described by a reversible $n = 1$ process with $E_M = -100 \text{ mV}$ and can be assigned as the electroactivity of His/His ligated heme I which is not reduced by ascorbate (Table 3.2).

For both *Cj* C138M and C138H the MCD signals and PFE peaks which were assigned to heme I with His/Cys⁻ ligation in *Cj* WT are absent. Those features are replaced by signals and peaks arising from heme ligated by the introduced ligands. MCD signals and peaks assigned to the unmodified His/Met ligated heme II in *Cj* WT are retained, giving further confidence in the ligation states and E_M values proposed for the *Cj* WT hemes (Table 3.2).

To be certain the scan rate chosen for experiments allows communication of all redox centres with the electrode, voltammograms were recorded over a range of scan rates. For surface adsorbed species current is directly proportional to scan rate⁵⁷. However, peak area expressed as the moles of electrons (N_{mol}) transferred in the corresponding process is independent of scan rate if total redox activity is the same for the scan rates in question. As a consequence, peak areas presented as current divided by scan rate (Figure 3.7, right panels) provide an immediate visual impression of any change in total redox activity as a function of change in scan rate. For ***Cj* WT**, although the total number of electrons transferred by heme I is always much less than heme II, these numbers remain constant for both hemes over the range of scan rates investigated. The moles of electrons transferred by either heme of ***Cj* C138M** also changes very little with scan rate. Contrastingly, for ***Cj* C138H** when the scan rate is lowered to 5 mV s⁻¹ the number of moles transferred during oxidation of heme I (X) is equal to that of heme II (Y). As scan rate increases the moles of electrons transferred by heme II does not change, however the moles of electrons transferred by heme I decreases as scan rate increases for both oxidation and reduction.

For *Cj* WT and all TsdA enzymes featured in this Thesis, there is separation of E_p values as $v > 30$ mV s⁻¹ indicative of rate limiting interfacial electron transfer at higher scan rates⁶³. This was visualised in a manner that allows side-by-side comparison each peak for each enzyme, by plotting the difference in peak separation (ΔE_p) at each scan rate (Figure 3.8). Each of these ‘trumpet’ plots⁶² has a similar shape and is well described by algorithmically predicted E_p values for a $n = 1$ process with $k^0 = 1.0 \pm 0.5$ s⁻¹. There is no evidence, therefore, that there is any difference in the rate that electrons are transferred between any of the TsdA hemes and the electrode, although there is clearly a discrepancy in the number of electrons transferred for *Cj* WT and *Cj* C138H at $v > 5$ mV s⁻¹. This suggests that for some molecules of *Cj* WT, heme I does not exchange electrons with the electrode even when heme II does. For *Cj* C138H, the electroactivity of heme I is instead being progressively ‘tuned out’ at faster scan rates. This phenomenon will be discussed further at the end of the following section (see below, 3.2.2).

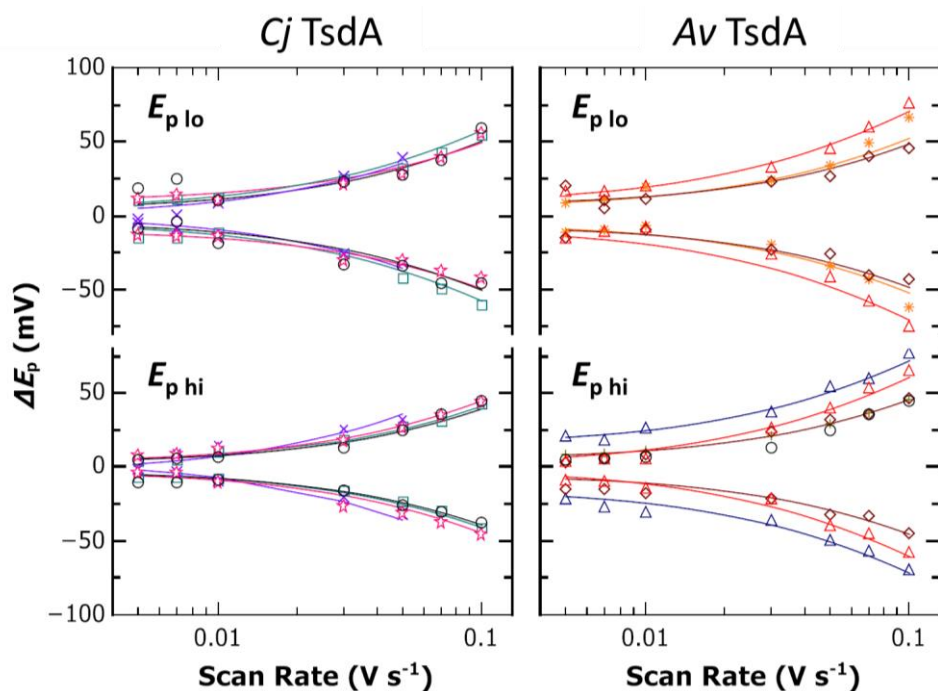


Figure 3.8 – Scan-rate dependency of peak potentials in TsdA voltammograms. Difference in peak potentials (ΔE_p) of low ($E_{p\ lo}$) and high ($E_{p\ hi}$) potential signals are shown for *Cj* WT (black circles), *Cj* C138H (cyan squares), *Cj* C138M (purple crosses), *Cj* N254K (pink stars), *Av* WT (red triangles), *Av* C96H (orange asterisks), *Av* C96M (blue triangles) and *Av* K208N (maroon diamonds). Positive (negative) values are determined from peak oxidative (reductive) currents. Lines show E_p predictions calculated from the Butler-Volmer equations (Equation 1.6) with $k^0 \approx 1\ \text{s}^{-1}$ using Jellyfit v2.1, Lars Jeuken, University of Leeds. All data recorded in 50 mM HEPES, 50 mM NaCl, pH 7, $T = 277\ \text{K}$.

3.2.2. *Av* TsdA Heme I Environment Cys-96 → Met and His Variants.

Variants were also investigated where the proposed heme I cysteine ligand of *Av* WT is substituted by histidine or methionine⁹. As with *Cj* C138M/H these variants are unlikely to participate in sulphur chemistry and are catalytically inactive both in solution assays⁹ (Figure 1.4) and on IO-ITO electrodes (data not shown). There was no opportunity to record MCD of these variants, so electronic absorbance spectroscopy and PFE have been used to infer information about heme spin- and oxidation states in these variants together with characterising their redox activity.

The electronic absorbance spectrum of as-isolated ***Av* C96M** (Figure 3.9, centre panel) has a Soret peak at 412 nm and a broad, low intensity $\alpha\beta$ band indicating low-spin ferric heme. The absence of high-spin signals is consistent with a strong field ligand binding to the heme I iron in place of the removed Cys-96. This is inferred to be the introduced Met-96 as this is likely to be the only suitable ligand within binding distance of the heme I iron, assuming the folding of this variant is not substantially changed from *Av* WT⁹. Incubation with ascorbate leads to the appearance of sharp $\alpha\beta$ bands and a more intense, red-shifted Soret arising from low-spin ferrous heme. Dithionite incubation increases the intensity of these features.

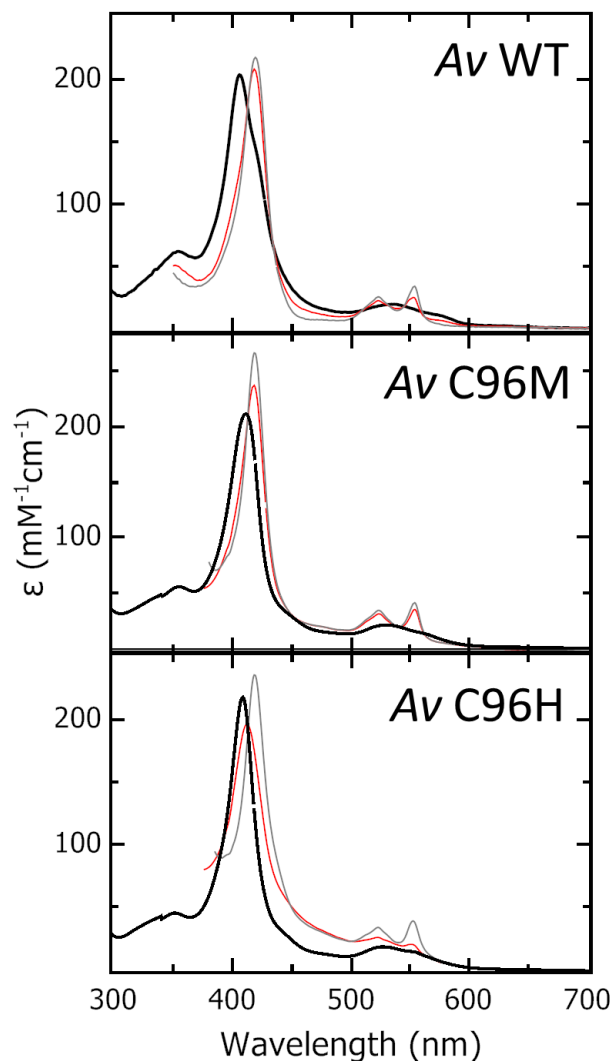


Figure 3.9 - Electronic absorbance spectra of Av TsdA Heme I variants. 17.6 μM Av WT, 62 μM Av C96M and 82 μM Av C96H as prepared (black line) or 17.6 μM Av WT, 4 μM Av C96M and 4 μM Av C96H incubated with 1.5 mM sodium ascorbate (red line) or 1.5 mM sodium dithionite (grey line). All samples in 50 mM HEPES, 50 mM NaCl, pH 7

It is assumed that this variant is fully reduced by dithionite as MCD of dithionite incubated Av WT (Figure 3.3, top panel) shows no trace of ferrous heme and the electronic absorbance of this sample has $\alpha\beta$ bands identical to those for dithionite incubated Av C96M (Figure 3.9, top panel). Comparing the intensity of the α peak after ascorbate incubation to that of dithionite-fully-reduced protein indicates $\sim 70\%$ reduction of the total heme population at $E = +60$ mV, suggesting that the majority of Av C96M heme electroactivity occurs at potentials above this. This observation is consistent with the E_M of heme I being raised by replacement of His/Cys⁻ with His/Met ligation.

A typical voltammogram recorded at $\nu = 10$ mV s⁻¹ for Av C96M shows complex signals with a clear difference between oxidation and reduction (Figure 3.10, centre left). There is one clear, reversible signal well described by an $n = 1$ process with $E_M = +94$ mV (X). No other variants have

peaks similar to this, so this signal is assigned as the electroactivity of His/Met ligated heme I. There is also a signal at higher potential with a larger oxidative than reductive area and a broad signal at lower potential with a larger reductive than oxidative area. Although the high potential signal is well described by a single $n = 1$ process with $E_M = +270$ mV (Y), the low potential signal is broader than one $n = 1$ process with $E_M = -173$ mV (Y'). The sum of the oxidative areas of Y and Y' is approximately equal to the sum of their reductive areas, so Y and Y' are assigned as His/Met and His/Lys ligated heme II respectively (Table 3.2). This assumes that the heme II electroactivity of Av C96M is similar to Av WT, as only the heme I environment has been intentionally modified. The broad appearance of Y' is rationalised if a dynamic Lys-208 to Met-209 ligand switch gives rise to non-reversible signals which are not appropriately described by the waveshapes presented in Chapter 1 (Equation 1.2) used for peak modelling.

The electronic absorbance of as-provided **Av C96H** (Figure 3.9, bottom panel) also has only low-spin heme bands, consistent with the introduced His-96 ligand coordinating heme I. The Soret band λ_{\max} is 411 nm and there is a broad $\alpha\beta$ band, both consistent with only low-spin ferric heme being present. The Soret peak is sharper than the same feature in Av WT and does not have the higher wavelength shoulder. This appearance is consistent with substituting thiolate ligation at heme I with a non-thiolate heme ligand, so that both hemes now give rise to similar features which are sharper than those arising from thiolate-ligated hemes.

Ascorbate incubation causes some heme reduction indicated by a small increase (~20%) of the α band intensity and a red shift of the Soret peak (Figure 3.9, red line). The Soret band of ascorbate-incubated Av C96H is narrower and sharper than ascorbate-incubated Av WT and Av C96M consistent with a (greater) population of bis-nitrogen-ligated ferrous heme in this variant. Dithionite incubated Av C96H (Figure 3.9, grey line) has similar intensity $\alpha\beta$ bands to ascorbate-incubated Av WT and C96M suggesting that this variant is also fully reduced at $E \approx -500$ mV. Unlike Av C96M, Av C96H is expected to be mostly electroactive at $E < 60$ mV consistent with the presence of a typically low E_M His/His heme in the latter protein.

A representative voltammogram for Av C96H (Figure 3.10, centre left) has one pair of broad signals at a low potential. The broad signals are well described as the sum of two pairs of reversible $n = 1$ contributions with equal areas and $E_M = -211$ mV (X) and -158 mV (Y). Assuming that the potential of His/Lys ligated heme II does not change significantly in this variant compared to Av WT, it can be inferred that Y arises from His/Lys ligated heme II. Unlike Av WT this signal has equal oxidative and reductive areas and there is no detectable electroactivity at $E > 0$ mV consistent with minimal reduction by ascorbate ($E = +60$ mV) in solution. There is therefore no evidence of a Lys-208 to Met-209 ligand switch at heme II in this variant. Assuming the E_M for heme I does not change substantially when Cys-96 is replaced by His-96 as a heme ligand, as is

observed in *Cj* C138H, it is possible to assign X as the electroactivity of His/His ligated heme I (Table 3.2).

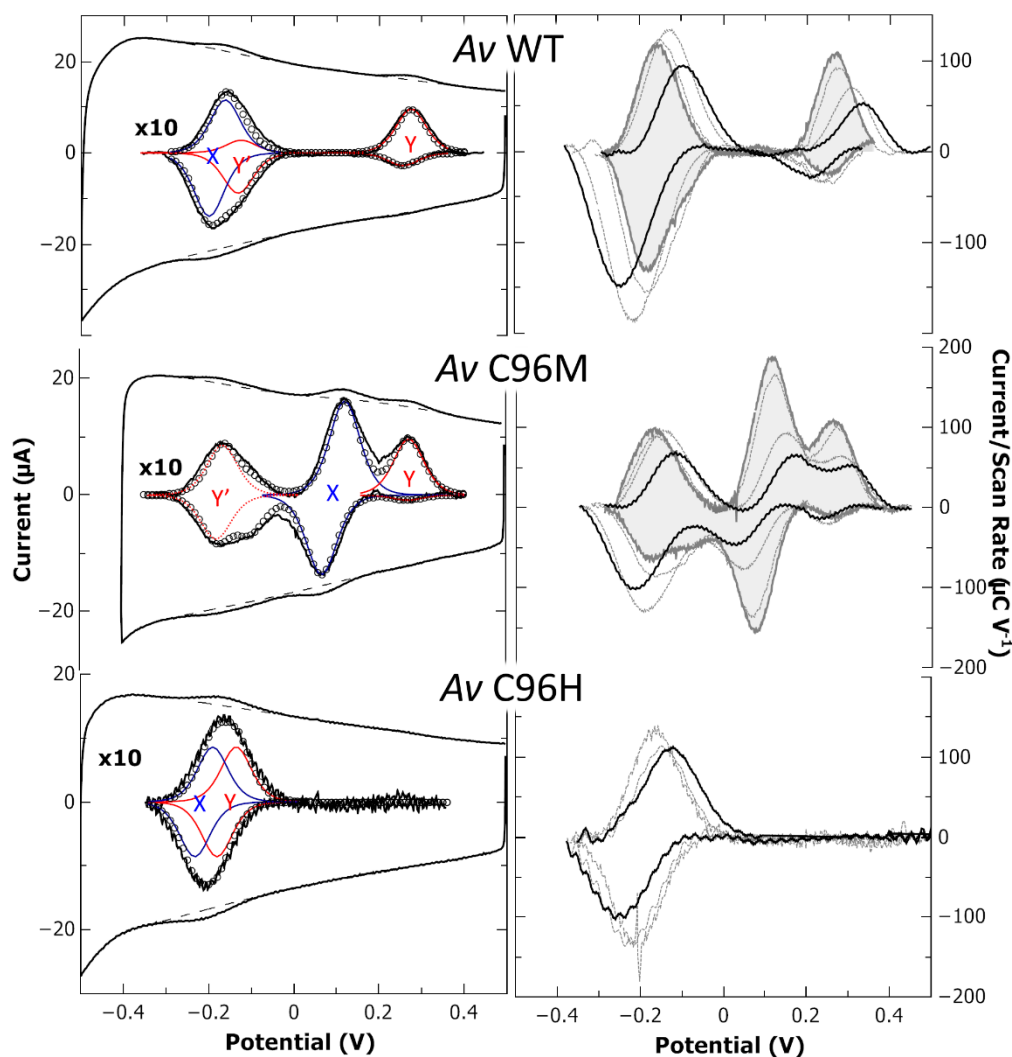


Figure 3.10 – Representative CV of *Av* TsdA heme I variants. (Left) Raw data (outer black line) with baselines (dashed line) used to prepare baseline-subtracted CVs (inner black line) of *Av* WT and C96M/H variants on IO-ITO electrodes. $\nu = 10 \text{ mV s}^{-1}$, $T = 277 \text{ K}$. Each peak has been fitted to two predicted $n=1$ theoretical responses (red and blue lines) and the sum of these contributions (black circles). (Right) Representative cyclic voltammograms recorded at $\nu = 5$ (grey line, shaded area), 10, 50 and 100 mV s^{-1} (black line) normalised by scan rate. All data recorded in 50 mM HEPES, 50 mM NaCl, pH 7, $T = 277 \text{ K}$.

As scan rate is varied from $\nu = 5 \text{ mV s}^{-1}$ to 100 mV s^{-1} , the number of electrons transferred by the hemes of ***Av* C96H** remains constant (Figure 3.10, bottom right) in a similar way to the *Cj* C138M variant. Contrastingly, the number of electrons transferred by heme I in ***Av* C96M** decreases as scan rate increases above 5 mV s^{-1} (Figure 3.10, centre right) whereas the total area of heme II signals remains constant. This behaviour is comparable to *Cj* C138H and may relate to both of these variants having a $\sim 200 \text{ mV}$ difference between their heme I and II E_M values, even considering the two possible heme II ligation states in *Av* C96M. The decreased thermodynamic driving force for inter-heme electron transfer due to this difference in E_M may therefore be one factor limiting electron transfer to heme I in these variants at $\nu > 5 \text{ mV s}^{-1}$.

Voltammetry for *Av* TsdA enzymes and variants was recorded over a range of scan rates (5 to 100 mV s^{-1}) in a similar way to *Cj* TsdA enzymes and variants. In ***Av* WT**, as scan rate increases the area of the oxidative peak for His/Met ligated heme II becomes smaller relative to the low potential oxidative peak(s). This implies that less of heme II is being oxidised with His/Met ligation at higher scan rates, rationalised if heme II is reduced (Figure 3.4, top blue arrow) faster than Lys-208 is displaced by Met-209 (Figure 3.4, right red arrow). Consistent with this, the area of the reductive peaks remains constant over the same range of scan rates.

Quantitative analysis of peak areas was used for greater insight into the information in the cyclic voltammograms. The dependence of all TsdA heme electroactive populations on scan rate was visualised by plotting the ratio of peak areas ($N_x/N_{y+y'}$) assigned to the electroactivity of heme I (X) and heme II (Y and Y') at each measured scan rate (Figure 3.11, bottom panel).

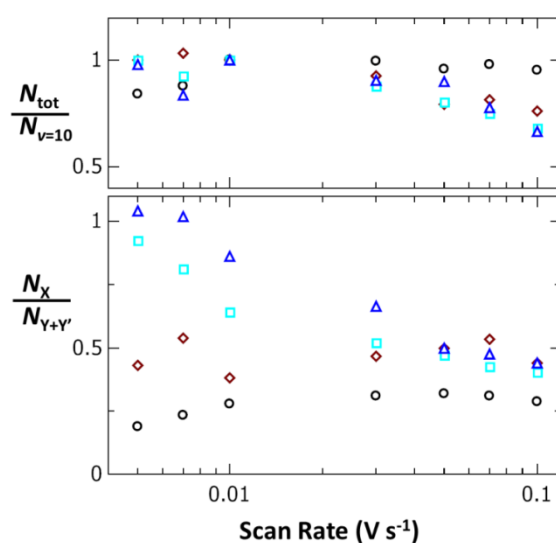


Figure 3.11 – Scan rate dependence of relative heme electroactive populations in TsdA variants. (Top) Total electroactivity (Q_{tot}) calculated from voltammetry peak areas normalised to $v = 10 \text{ mV s}^{-1}$ for *Cj* WT (black circles), *Cj* C138H (cyan squares), *Av* K208N (maroon diamonds), *Av* C96M (blue triangles). (Bottom) Average ratio of peak areas assigned to heme I (Q_x) to peak areas assigned to heme II ($Q_{Y+Y'}$) calculated from signal integration. All data recorded in 50 mM HEPES, 50 mM NaCl, pH 7, $T = 277 \text{ K}$.

For comparative purposes the total electroactive population normalised to $v = 10 \text{ mV s}^{-1}$ ($N_{\text{tot}}/N_{v=10}$) is also presented (Figure 3.11, top panel) and this does not change substantially with scan rate other than at $v > 50 \text{ mV s}^{-1}$ where the total electroactive population decreases modestly for *Cj* C138H (cyan squares) and *Av* C96M (blue triangles). For *Cj* WT (black circles) $N_x/N_{Y+Y'}$ remains approximately constant at < 0.5 over scan rates of 5 to 100 mV s^{-1} , however for *Cj* C138H and *Av* C96M this ratio decreases with scan rate from ~ 1 at $v = 5 \text{ mV s}^{-1}$ to ~ 0.5 at $v = 100 \text{ mV s}^{-1}$.

The ligation state of electroactive populations at heme II is visualised by plotting the ratio of peak areas for the lowest potential signals in voltammograms (Y' plus X when X is constant with

scan rate) (N_{lo}) to the highest (Y) potential signals in voltammograms (N_{hi}). For Av WT this ratio for reduction (Figure 3.12, open red triangles) does not change over $v = 5$ to 100 mV s^{-1} however for oxidation (closed red triangles) it increases with scan rate from ~ 1 at $v = 5 \text{ mV s}^{-1}$ to ~ 3 at $v = 100 \text{ mV s}^{-1}$. When $N_{lo}/N_{hi} \approx 1$ at 5 mV s^{-1} , ligand switching from His/Lys and His/Met is essentially complete in the time it takes to scan from $E = -129 \text{ mV}$ to $+266 \text{ mV}$ which is 227 s given the $E = -500 \text{ mV}$ to $+500 \text{ mV}$ potential window. This gives a lower limit on the Lys-208 to Met-209 switching rate of 0.004 s^{-1} . However, as switching His/Met to His/Lys is complete in the 8.6 s it takes to scan from $E = +266 \text{ mV}$ to -129 mV at $v = 100 \text{ mV s}^{-1}$, the Met-209 to Lys-208 switching rate is at least two orders of magnitude faster at $\geq 0.2 \text{ s}^{-1}$.

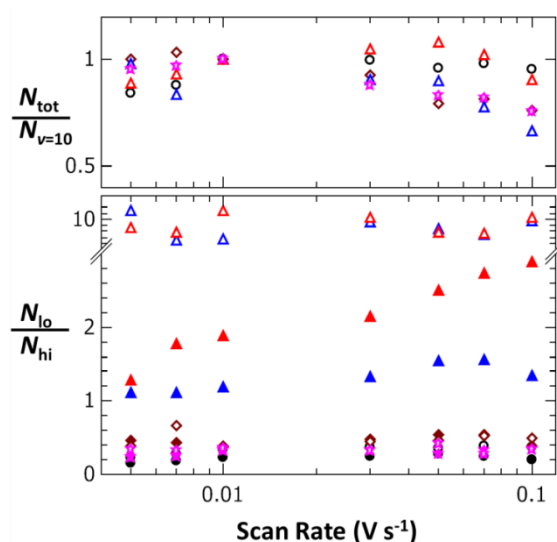


Figure 3.12 – Scan rate dependency of heme II electroactive populations in TsdA variants. **(Top)** Total electroactivity (Q_{tot}) calculated from voltammetry peak areas normalised to $v = 10 \text{ mV s}^{-1}$ for *Cj* WT (black circles), *Cj* C138H (cyan squares), *Cj* N254K (pink stars), Av WT (red triangles), Av K208N (maroon diamonds), Av C96M (blue triangles). **(Bottom)** Oxidative (filled symbols) or reductive (open symbols) low potential peak area (Q_{lo}) divided by low potential peak area (Q_{hi}). All data recorded in 50 mM HEPES , 50 mM NaCl , $\text{pH } 7$, $T = 277 \text{ K}$.

For Av C96M N_{lo}/N_{hi} for reduction (Figure 3.12, open blue triangles) is the same as Av WT over $v = 5$ to 100 mV s^{-1} ; the ferrous heme Lys-208 to Met-209 switching rate is $\geq 0.1 \text{ s}^{-1}$ and the ferric heme Met-208 to Lys-209 switching rate is $\geq 0.08 \text{ s}^{-1}$. For Av C96H, N_{lo}/N_{hi} for oxidation (closed blue triangles) is ~ 1 , the same as Av WT at $v = 5 \text{ mV s}^{-1}$. However, this ratio remains at ~ 1 and does not increase with scan rate as it does for Av WT (closed red triangles). For Av WT the frequency of the switch from His/Lys to His/Met ligation (0.004 s^{-1}) is 10^8 - or 10^6 -fold less than the turnover frequency for thiosulphate oxidation ($k_{cat} = 2010 \text{ s}^{-1}$) or tetrathionate reduction ($k_{cat} = 37 \text{ s}^{-1}$) respectively. Even considering the difference in temperature and pH between the non-turnover voltammetry recorded in this study and previous solution activity assays, these

observations alone would suggest that heme II in *Av* WT has exclusively His/Lys ligation during catalysis. Alternatively, the presence of substrate could have an effect on the frequency of the Lys → Met ligand switch.

3.2.3. *Av* TsdA Heme II Environment Lys-208 → Asn Variant.

A variant where the *Av* WT heme II ligand Lys-208 is substituted by non-ligating Asn⁹ was investigated by MCD and PFE, to determine if this variant lacks the electroactivity assigned to heme II ligand switching or displays *Cj* WT-like unequal heme electroactivity in an *Av* TsdA protein. *Av* K208N is catalytically active in solution assays⁹ (Figure 1.4) and on IO-ITO electrodes (Figure 5.2), suggesting that some of the protein film adsorbed on the latter is present in a native-like form.

MCD of oxidised ***Av* K208N** (Figure 3.13, bottom panel) shows two CT_{LS} bands in the nIR region consistent with there being two distinct heme chemical environments in this variant. One band has λ_{max} at 1140 nm with a vibrational feature at ~990 nm consistent with His/Cys⁻ ligation, the second band has λ_{max} at 1800 nm with a vibrational sideband at 1520 nm indicating His/Met ligation. In the UV/visible region signals indicative of only low-spin ferric heme are present consistent with these assignments. The Soret feature ($140 \text{ M}^{-1}\text{cm}^{-1}\text{T}^{-1}$) has a peak-to-trough intensity much less than *Av* WT ($277 \text{ M}^{-1}\text{cm}^{-1}\text{T}^{-1}$) but closer to *Cj* WT ($204 \text{ M}^{-1}\text{cm}^{-1}\text{T}^{-1}$), consistent with one thiolate-ligated heme and one methionine-ligated heme as deduced from the nIR MCD. Unlike *Cj* WT, there is no clear resolution of two separate $\alpha\beta$ signals, however there is a broad low-intensity negative peak at 720 nm assigned as a S(p) – Fe(d) CT band for His/Met ligation.

Incubation with ascorbate eliminates all intensity of the His/Met CT_{LS} band without modifying the His/Cys⁻ CT_{LS} band. There is also the appearance of a sharp α band at 552 nm with a peak-to-trough intensity of $283 \text{ M}^{-1}\text{cm}^{-1}\text{T}^{-1}$ and a red-shifted Soret band with a greater positive than negative intensity; both of these features are consistent with the presence of one ferrous heme per TsdA with methionine ligation. A lower wavelength shoulder on the Soret band indicates an overlapping broad signal from thiolate-ligated ferric heme. Incubation with dithionite eliminates all ferric heme signals and increases the intensity of the $\alpha\beta$ signal by $50 \text{ M}^{-1}\text{cm}^{-1}\text{T}^{-1}$ consistent with one methionine- and one thiolate-ligated ferrous heme per TsdA. These observations are consistent with *Av* K208N having His/Cys⁻ ligation at heme I and His/Met ligation at heme II as with *Cj* WT. Similarly, both hemes have electroactivity above -500 mV⁹⁷; heme I has an $E_M < +60 \text{ mV}$ and heme II has an $E_M > +60 \text{ mV}$.

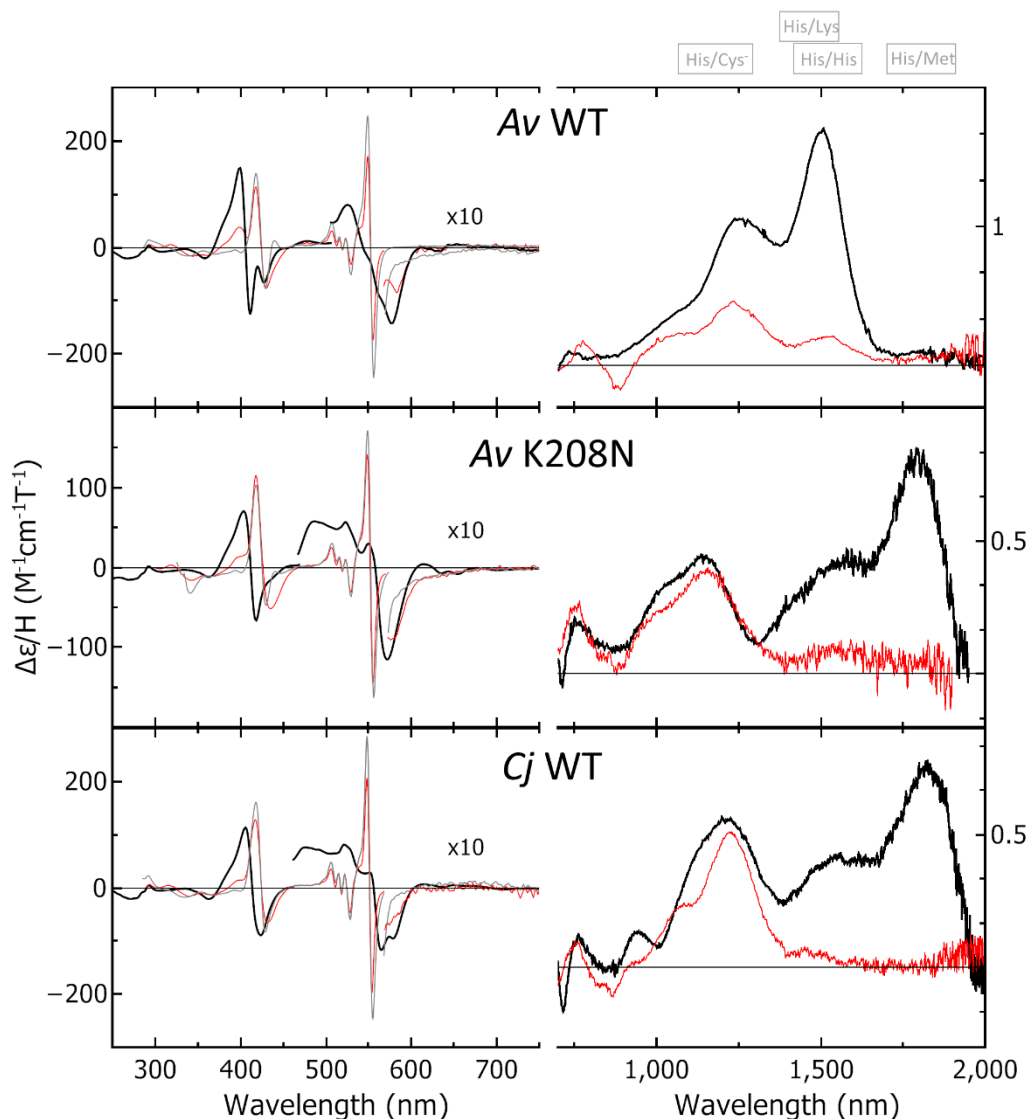


Figure 3.13 - MCD spectrum *Av* K208N. Room-temperature (left) UV/visible and (right) NIR MCD spectra of 17.6 μm (250-450 nm or 250-700 nm reduced), 163 μm (450-700 nm) and 123 μm (700-2000 nm) *Cj* WT; 35 μm (250-700 nm) and 350 μm (700-2000 nm) *Av* K208N. Samples are oxidised by sub-stoichiometric potassium ferricyanide (black) or reduced by 1.5 mM sodium ascorbate (red) or 1.5 mM sodium dithionite (5.0 mM for *Av* K208N) (grey). All data recorded in 50 mM HEPES, 50 mM NaCl, pH 7 or the same buffer in D_2O pH* 7 for NIR MCD.

A representative voltammogram recorded at $\nu = 10 \text{ mVs}^{-1}$ for ***Av* K208N** features two pairs of peaks well described by two reversible $n = 1$ processes with $E_M = -173 \text{ mV}$ (X) and $+264 \text{ mV}$ (Y). X is assigned to electroactivity of the non-ascorbate-reducible His/Cys⁻ heme I and Y is assigned to the ascorbate-reducible His/Met heme II. With Lys-208 replaced by Asn, there is now no evidence of any change in chemical environment between oxidation and reduction at heme II. Significantly, the area of X is much less (36%) that of Y in a similar manner to *Cj* WT. As the scan rate is varied ($\nu = 5 - 100 \text{ mV s}^{-1}$), the number of electrons transferred by each ***Av* K208N** heme does not noticeably change despite the disparity in heme I and heme II electroactive populations, there is peak separation and broadening at $\nu > 30 \text{ mV s}^{-1}$ indicating slow interfacial electron transfer at

these rates, similar to *Cj* WT. Thus in all aspects, the behaviour of *Cj* WT is introduced into *Av* TsdA when Lys-208 is substituted by Asn.

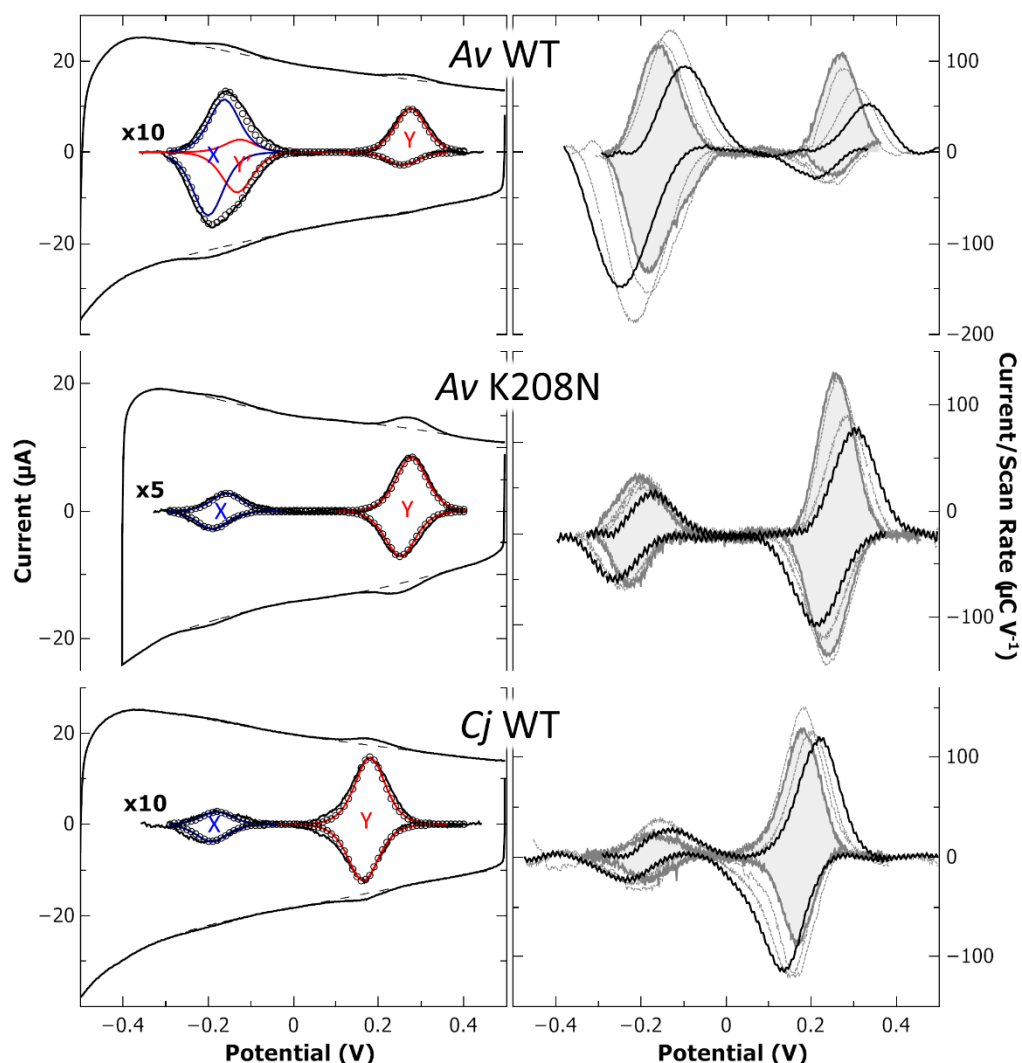


Figure 3.14 – Representative CV of *Av* K208N. **(Left)** Raw data (outer black line) with baselines (dashed line) used to prepare baseline-subtracted CVs (inner black line) of *Cj* WT and *Av* K208N on IO-ITO electrodes. $\nu = 10 \text{ mV s}^{-1}$, $T = 277 \text{ K}$. Each peak has been fitted to multiple predicted $n=1$ theoretical responses (red and blue lines) and the sum of these contributions (black circles). **(Right)** Representative cyclic voltammograms recorded at $\nu = 5$ (grey line, shaded area), 10, 50 and 100 mVs^{-1} (black line) are shown normalised by scan rate. All data recorded in 50 mM HEPES, 50 mM NaCl, pH 7, $T = 277 \text{ K}$.

3.2.4. *Cj* TsdA Heme II Asn-254 \rightarrow Lys Variant.

A *Cj* TsdA variant where Asn-254 is substituted for Lys⁹ was also investigated, to see if an *Av* TsdA-like ligand switch can be introduced in a *Cj* TsdA enzyme. *Cj* N254K is catalytically active in solution assays⁹ (Figure 1.4) and on IO-ITO electrodes (Figure 5.2), suggesting that some enzyme is present in a native-like conformation on the electrode.

The nIR MCD of oxidised **Cj N254K** has three overlapping contributions (Figure 3.15, bottom panel); all have only positive intensity indicating low-spin ferric heme with three different chemical environments. The CT_{LS} bands have λ_{\max} values of 1250 nm consistent with His/Cys⁻ ligation, 1530 nm consistent with bis-nitrogenous ligation and 1820 nm consistent with His/Met ligation.

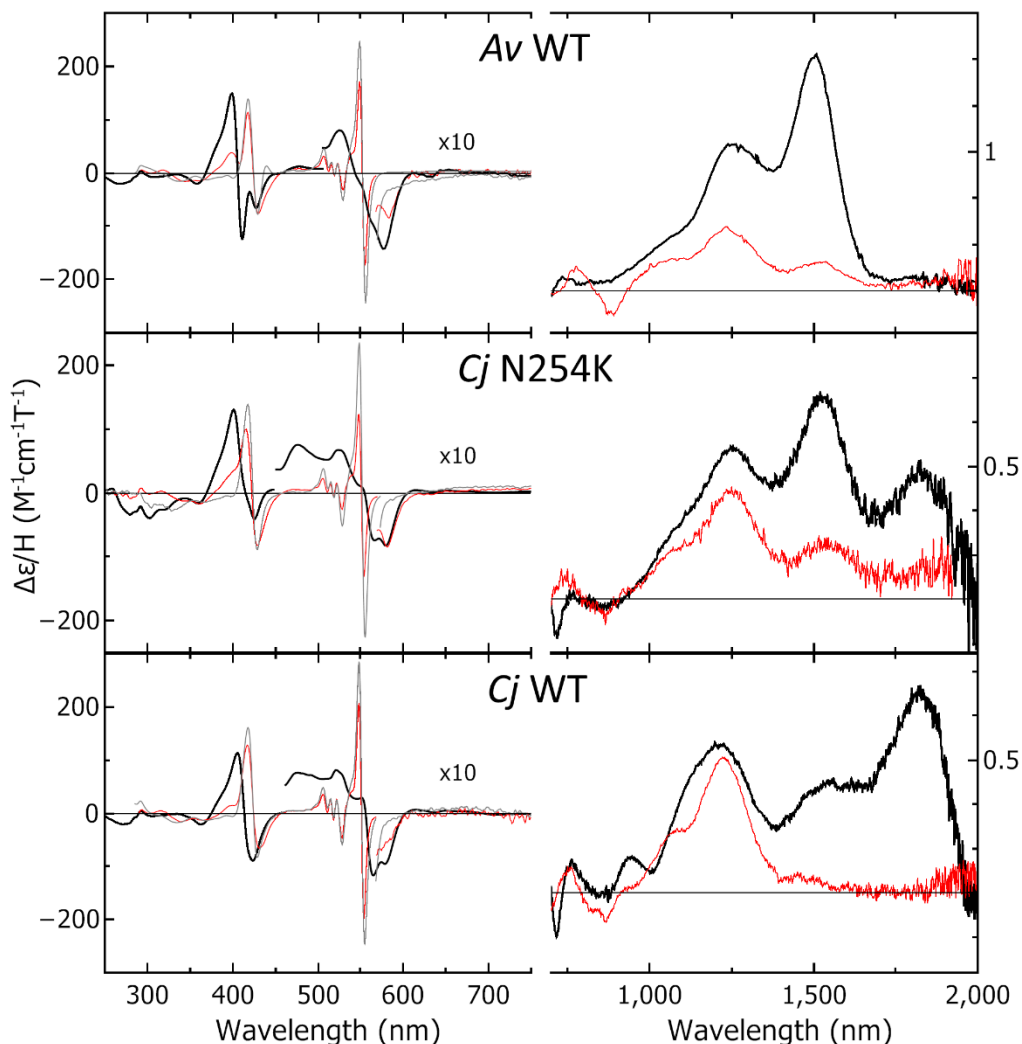


Figure 3.15 - MCD spectrum of *Cj* N254K. Room-temperature (left) UV/visible and (right) nIR MCD spectra of 30 μM (250-700 nm) and 170 μM (700-2000 nm) *Av* WT; 325 μM (700 nm – 2000 nm) and 47 μM (250 – 700 nm or 250 – 700 nm reduced) *Cj* N254K. Samples are oxidised by sub-stoichiometric potassium ferricyanide (black) or reduced by 1.5 mM sodium ascorbate (red) or 1.5 mM sodium dithionite (5.0 mM for *Cj* N254K) (grey). All data recorded in 50 mM HEPES, 50 mM NaCl, pH 7 or the same buffer in D₂O pH* 7 for nIR MCD.

As it is unlikely that His/Cys⁻ ligation at heme I has been displaced in this variant, the bis-nitrogenous species is assigned as His/Lys from the partial displacement of Met-255 as a ligand at heme II. Based on the intensities of these signals compared to the CT_{LS} bands in oxidised *Cj* WT and ascorbate-incubated *Av* WT (Table 3.2), there is an approximately 40:60 mixed His/Lys:His/Met ligation state at heme II. In the UV/visible region the Soret has a broad, asymmetric appearance, however this is likely to be due to three unresolved ferric signals rather

than ferrous heme as any presence of the latter would be clearly indicated by sharp signal(s) in the $\alpha\beta$ region. As with *Cj* WT, the negative intensity features of thiolate-ligated and non-thiolate-ligated low-spin ferric $\alpha\beta$ bands resolve at different wavelengths and there is a broad low-intensity negative peak at 720 nm likely to be the S(p) – Fe(d) CT band of a methionine heme ligand.

Incubation with ascorbate eliminates all of the intensity of the His/Met CT_{LS} band and all but ~25% of the His/Lys CT_{LS} band. Although there is an apparent decrease in the intensity of the His/Cys⁻ CT_{LS} band, this intensity is likely to have arisen from overlapping bands as the remaining signal has an intensity of 0.4 M⁻¹cm⁻¹T⁻¹ consistent with one heme per TsdA monomer. In the UV/visible region a sharp α band has appeared at 552 nm with a peak-to-trough intensity of 253 M⁻¹cm⁻¹T⁻¹ consistent with ~75% of a heme population of methionine-ligated low-spin ferrous heme. Incubation with dithionite eliminates all remaining low-spin ferric signals, and increases the peak-to-trough intensity of the 552 nm band to 460 M⁻¹cm⁻¹T⁻¹, almost identical to *Cj* WT and consistent with one thiol(ate)-ligated ferrous heme and one methionine-ligated ferrous heme. MCD data are therefore consistent with *Cj* N254K having His/Cys⁻ ligation at heme I with an E_M between -500 and +60 mV and a mixed His/Met:His/Lys ligation at ferric heme II which becomes exclusively His/Met ligated in the ferrous state.

Unlike all other TsdA variants featured in this thesis, the Faradaic peaks for voltammetry of ***Cj* N254K** have a different appearance on the first scan recorded with a fresh film; in the second and subsequent scans, these peaks do not change substantially. Voltammetry representative of the settled film at $\nu = 10$ mV s⁻¹ (Figure 3.16) features two pairs of peaks which are well described by the theoretical responses of $n = 1$ processes with $E_M = -115$ mV (X) and +203 mV (Y). As with *Cj* WT, the area of X is smaller (~40%) than Y. In the first scan the reductive peak of signal Y is smaller than the oxidative peak and there is an additional signal with a peak potential of -177 mV (Y') with a smaller oxidative than reductive peak. Voltammograms of *Cj* N254K, like *Cj* WT, do not vary across the range of scan rates recorded, except for some peak separation at $\nu > 30$ mV s⁻¹. There is no evidence of Y' in any scans other than the first.

Ascorbate incubation reduces all His/Met ligated heme II population in this variant leaving only His/Lys ligated ferric heme. This suggests a possible explanation for the redox behaviour of this variant seen by PFE; on the first reductive scan, heme II has mixed His/Met:His/Lys ligation which will reduce at a high and a low potential respectively. Once heme II is reduced, it then retains or switches to His/Met ligation for as long as redox cycling persists. From scan 2 onwards, Y can be assigned as exclusively His/Met ligated heme II and X is assigned as His/Cys⁻ ligated heme I with a *Cj* WT-like smaller electroactive population. The signal Y' only present on the first scan is therefore assigned as heme II with His/Lys ligation.

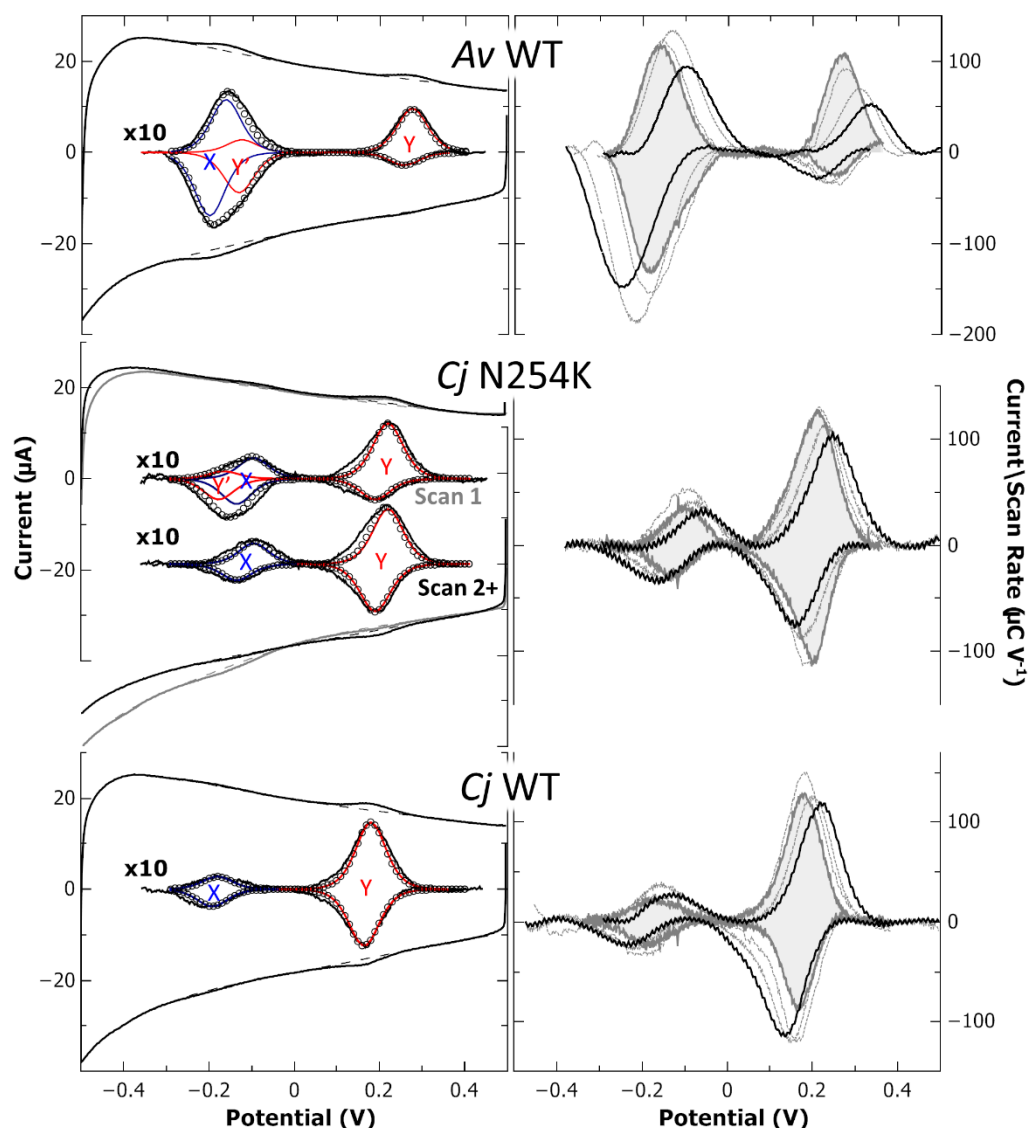


Figure 3.16 – Representative CV of *Cj* N254K. (Left) Raw data (outer black line) with baselines (dashed line) used to prepare baseline-subtracted CVs (inner black line) of *Av* WT and *Cj* N254K on IO-ITO electrodes. $\nu = 10 \text{ mV s}^{-1}$, $T = 277 \text{ K}$. Each peak has been fitted to multiple predicted $n=1$ theoretical responses (red and blue lines) and the sum of these contributions (black circles). The first scan for *Cj* N254K is shown above a scan which is representative of subsequent cycles and includes an additional fitted area (Y') which describes a single redox centre in combination with Y. (Right) Representative cyclic voltammograms recorded at $\nu = 5$ (grey line, shaded area), 10, 50 and 100 (black line) are shown normalised by scan rate. All data recorded in 50 mM HEPES, 50 mM NaCl, pH 7, $T = 277 \text{ K}$.

Voltammetry described above was recorded at $T = 277 \text{ K}$ to help preserve protein films, however *Av* WT has optimal catalytic activity at 303 K ^{9,29} and MCD and electronic absorbance spectroscopy were recorded at 293 K . To investigate the effect of temperature on the heme II ligand switch, similar PFE experiments were performed at $T = 293 \text{ K}$ using the same *Av* WT and *Cj* N254K coated IO-ITO electrodes used previously. A representative non-turnover voltammogram of *Av* WT recorded at $\nu = 10 \text{ mV s}^{-1}$ (Figure 3.16, left) has a very similar appearance at $T = 293 \text{ K}$ as

277 K, the only difference being a small (~15%) increase in overall electroactive area. This implies that there is little change in the electroactivity or rate of heme II ligand switching between these temperatures.

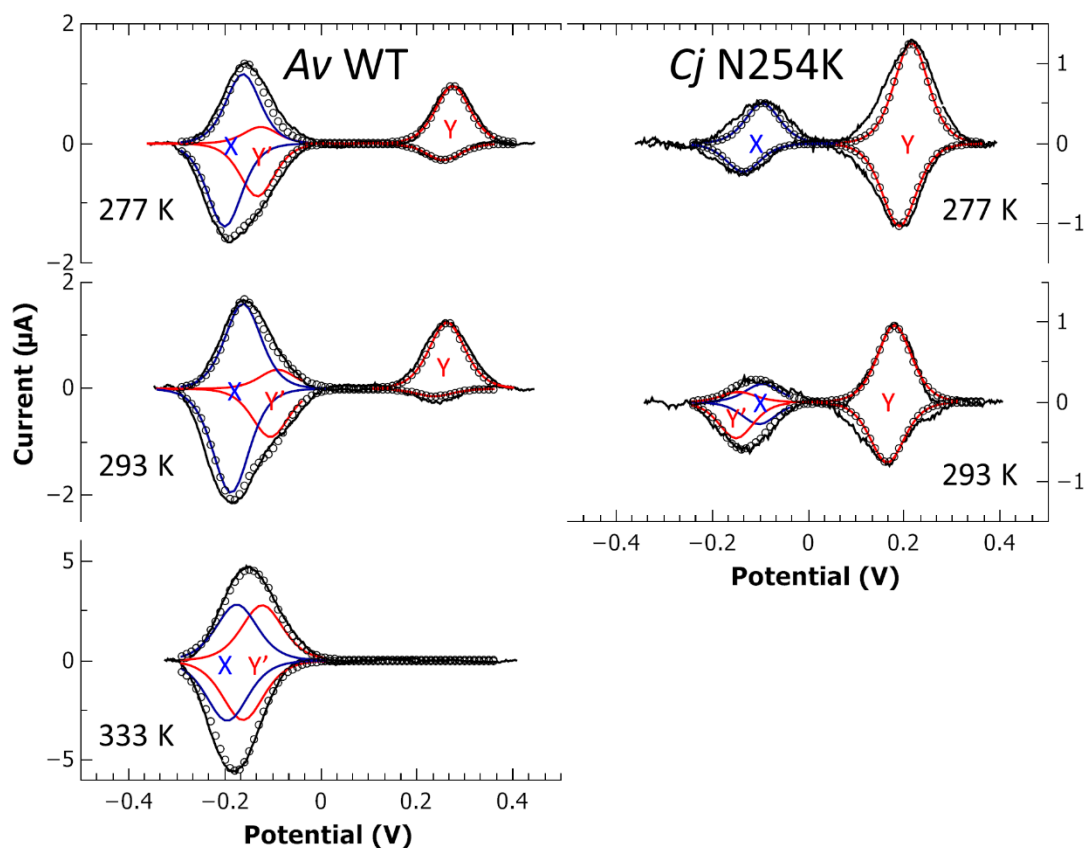


Figure 3.17 – Temperature dependence of Av WT and Cj N254K. Baseline-subtracted CVs (black line) of Av WT and Cj N254K on IO-ITO electrodes. $\nu = 10 \text{ mV s}^{-1}$, $T = 277, 293$ or 333 K as annotated. Each peak has been fitted to multiple predicted $n = 1$ theoretical responses (red and blue lines) and the sum of these contributions (black circles). All data recorded in 50 mM HEPES, 50 mM NaCl, pH 7.

Another Av WT coated IO-ITO electrode with greater electroactive coverage (~200%) giving rise to voltammograms with a similar appearance at $T = 277 \text{ K}$ was used to record CVs whilst temperature was increased. There are no significant changes in the appearance of the voltammogram until $T = 333 \text{ K}$ when the signal Y assigned to His/Met heme disappeared and Y' now has equal oxidative and reductive areas. The total areas of X and Y' are equal and the total area of the film increases by ~25% between $T = 277$ and 333 K . When subsequently cooled, the appearance of the non-turnover peaks does not return to its previous appearance, although the film still has some catalytic activity (data not shown) implying that even if some of the protein film has been damaged or permanently modified, it has not been entirely denatured.

A representative voltammogram of **Cj N254K** recorded at $T = 293 \text{ K}$ (Figure 3.17, right) still has two pairs of signals, however the low potential peak now has a broad appearance with more reductive than oxidative area. Similar to the first scan recorded with a fresh film at $T = 277 \text{ K}$, the

low potential peak is well described by a reversible $n = 1$ signal with $E_M = -99$ mV (X) and an $n = 1$ signal with a larger reductive than oxidative area and $E_M = -148$ (Y'). The high potential peak can be described by an $n = 1$ signal (Y) with $E_M = +173$ mV and a larger area for oxidation than reduction. The Faradaic response of the film does not change significantly over >30 scans, implying that at $T = 293$ K a small amount (~30%) of heme II becomes His/Lys ligated when oxidised during every cycle at $v = 10$ mV s⁻¹. Despite evidence of some Av WT-like ligand switching, the area of the heme I signal is still smaller (~25%) than the area of heme II like Cj WT.

3.3. Discussion

MCD and PFE have been used to investigate Av WT, Cj WT and several variants of both TsdAs. Heme axial ligands and E_M values have been assigned in many cases (Table 3.2). The ferrous/ferric heme II ligand switch proposed for Av TsdA from crystallographic⁹ and potentiometric³⁰ data has been confirmed by PFE and is sensitive to changes to both heme II and heme I environments. Furthermore, unequal heme electroactive populations have been identified in Cj WT that are not apparent in Av WT. These populations can be equal in Cj TsdA variants where the heme I environment is modified. Unequal heme electroactive populations are introduced in an Av TsdA variant where the heme II environment is modified. Each of these aspects is considered in more detail below.

3.3.1. Heme Ligation States and E_M Values.

Using MCD and PFE, the ligation states and E_M values of both hemes have been determined for Av and Cj WT and several variants where the heme I and heme II ligands have been substituted (Table 3.2). Both wild-type enzymes and the Cj N254K and Av K208N variants where only heme II ligands have been modified, are confirmed to have His/Cys⁻ ligation at heme I. E_M values for these hemes are between -100 and -200 mV (Figure 3.18, black triangles). Previously reported E_M values for His/Cys⁻ hemes, including those for the structurally similar SoxAX proteins (discussed further in Chapter 4) are more negative, ranging between -250 and -500 mV^{49,91–93,100} (Figure 3.18, black circles). There is evidence to suggest that the SoxAX heme with the lowest potential is ligated by cysteine persulphide⁹³ rather than cysteine, so this modification or modifications like it in the active site pocket may contribute to defining the lower E_M values of this enzyme. This difference in catalytic heme E_M values between enzymes could tailor each enzyme to the specific reaction it catalyses^{5,101}. Consequences on E_M of cysteine modifications in TsdA are explored in the work described in Chapter 4.

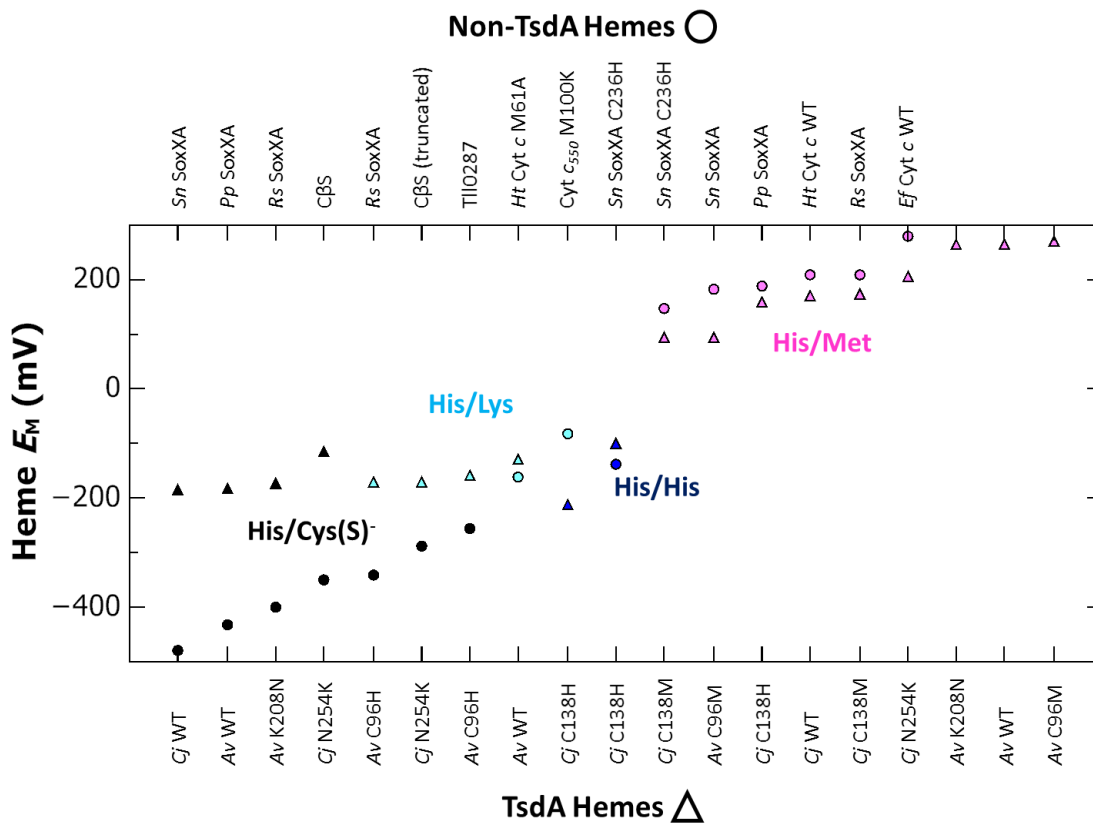


Figure 3.18 – TsdA Heme E_M values compared to previously reported examples. Reported heme E_M values are from *Starkeya novella* (Sn)¹⁰⁰, *Paracoccus pantotrophus* (Pp)⁹³ and *Rhodovulum sulfidophilum* (Rs)⁴⁹ SoxAX and variants, human Cystathione-β-synthase (CβS)⁹¹, *Thermosyneccoccus elongatus* TlI0287⁹², *Hydrogenobacter thermophilus* (Ht) cytochrome (Cyt) c M61A¹⁰², *Paracoccus versitus* Cyt c₅₅₀ M100K⁹⁶ and *Equus ferus* Cyt c³⁴.

With the exception of Av C96H, all TsdA variants investigated in this work feature His/Met ligation at heme II. For Av WT and C96M, His/Met ligation only predominates when heme II is in the ferrous state. The E_M values of all TsdA His/Met ligated hemes II range between +150 and +250 mV (Figure 3.18, pink triangles), consistent with E_M values reported for the His/Met hemes in SoxAX^{49,93,100} and for His/Met ligated monoheme c cytochromes^{34,103} (Figure 3.18, pink circles). Av WT, C96H, C96M (and Cj N254K) show evidence of (partial) His/Lys ligation at ferric heme II, this ligation state is entirely retained at ferrous heme II only in Av C96H. The E_M values for these His/Lys ligated hemes range from -130 to -170 mV (Figure 3.18, cyan triangles). There are few reported E_M values for His/Lys hemes which are not average values for hemes which switch to another ligation state when ferrous. The Cytochrome c₅₅₀ M100K variant from *Paracoccus versitus* is His/Lys ligated regardless of oxidation state and has an E_M of -81 mV⁹⁶ close to the observed range in TsdA proteins. Cytochrome c M61A from *Hydrogenobacter thermophilus* has an E_M within this range (-163 mV) and is proposed to have His/Lys ligation¹⁰³ (Figure 3.18, cyan circles).

Where cysteine has been substituted by histidine at the active site of *Cj* C138H and *Av* C96H, a His/His ligated heme I with $E_M = -100$ or -211 mV is present respectively. This difference in E_M values is unlikely to be due to variation in heme I environment as the E_M values for the wild-type His/Cys⁻ hemes are the same. One possibility is that the E_M of heme I is influenced by the heme II environment, which has His/Met ligation in *Cj* C138H and His/Lys ligation in *Av* C96H. Consistent with this, *Starkeya novella* SoxXA C236H has a His/His heme ($E_M = -137$ mV) equivalent to heme I in *Cj* C138H and a heme II equivalent ($E_M = +148$ mV) with His/Met ligation.

Consequently there is nothing unusual about E_M values of TsdA hemes for each ligand set. However the thiosulphate/tetrathionate couple proposed to be catalysed has an $E_M \sim 380$ mV higher than heme I in both enzymes. This would suggest suitable thermodynamics for tetrathionate reduction, but little driving force for thiosulphate oxidation. This may be explained if the form of heme I being interrogated by PFE is not the same as is present during catalysis. One possibility is that the covalent modification of cysteine proposed by Grabarczyk *et al.* as the first step in the TsdA catalytic mechanism⁵ also causes an increase in heme I E_M . Experiments that investigated this possibility are described in Chapter 5.

3.3.2. Ligand switch at heme II.

PFE provides compelling evidence that a His/Lys to His/Met heme II ligand switch does occur in *Av* WT as proposed by Brito *et al.*⁹ and MCD-monitored solution potentiometry is consistent with this. The signals present in *Av* WT and *Av* C96M assigned as evidence of ligand switching at heme II are absent in *Av* K208N, giving confidence in this assignment and confirming that Lys-208 is necessary for this behaviour. Introducing an *Av* WT-like heme II environment in *Cj* N254K introduces a mixed His/Met:His/Lys ligation at heme II, however Lys-254 is readily displaced by Met-255 upon reduction and the switch back does not occur during redox cycling at $T = 277$ K. Increasing the experimental temperature to 293 K does result in some (~25%) of heme II switching back to His/Lys upon oxidation, however it is clear that introducing an *Av* WT-like ligand switch in *Cj* TsdA requires more than just the introduction of a suitable Lys residue.

The results presented in this chapter suggest that the presence or absence of Lys at heme II is not simply an artefact of protein purification suggesting it is a feature of *Av* TsdA that differentiates it from the majority of TsdA enzymes. Ligand switching in *Av* WT occurs simply when heme II is redox cycled due to the affinity of methionine for ferrous heme and lysine for ferric heme, evidenced by the positive ratio of binding constants for these ligands ($K_d^{\text{red}}/K_d^{\text{ox}} = 5 \times 10^6$). It is apparent from the scan-rate dependency of peak areas that the switch from His/Met to His/Lys (0.2 s^{-1}) is faster than the switch from His/Lys to His/Met (0.004 s^{-1}). As a

result, the switch from His/Lys to His/Met ligation is unlikely to be fast enough for His/Met ligated heme II to be present during catalysis in both directions unless ligand switching is also influenced by other factors. Substituting Cys-96 with Met increases the rates of the His/Lys to His/Met ligand switch ($\geq 0.1 \text{ s}^{-1}$) and the His/Met to His/Lys ligand switch ($\geq 0.08 \text{ s}^{-1}$) so that the lower limit for all scan rates measured is the same. There is no evidence of His/Met ligation at heme II at all in Av C96H, even when the film is poised at a low potential for an hour or more (data not shown). It is therefore unlikely that the differences in the voltammetry of Av C96H compared to Av WT can be rationalised by a change in ligand switching rates; instead something more fundamental must have changed preventing the switch from occurring entirely. Similar behaviour is also observed in Av WT after temperature has been increased to 333 K, perhaps indicating some form of conformational change in the heme II environment is possible which prevents Met-209 ligation.

3.3.3. Unequal Electroactive Populations between Heme I and Heme II

Electron transfer between biological redox centres is typically thought to be dependent only on proximity and facile electron transfer is possible for any centres within 14 Å of each other⁶. Hemes I and II are within this distance in Av and Mp WT structures^{9,30,33} and this is not anticipated to be different in Cj WT. If facile electron transfer was possible as this inter-heme distance predicts, the number of electrons transferred by both hemes in voltammograms would be equal and this is seen for Av WT even though heme II has a redox-driven ligand switch. However, this is clearly not the case for Cj WT, so electron transfer between the TsdA hemes must either be controlled by more factors than distance alone, or the form of (some) Cj WT on the electrode is perturbed from the native conformation despite detectable catalytic activity. It is also clear that, while Cj WT heme II seemingly has reversible electron transfer with the IO-ITO electrode, heme I must not, otherwise when $E \approx -500 \text{ mV}$ in voltammograms, heme I would show more than trace reduction. The possibility that Cj WT heme I simply has $E_M < -500 \text{ mV}$ can be ruled out as samples poised chemically at this potential in solution become fully reduced. Furthermore, previous spectroelectrochemical experiments with Cj WT films on optically transparent SnO₂ electrodes also show full heme reduction at -600 mV ¹⁰⁴.

One rationalisation of this behaviour is the idea that Cj TsdA adsorbs with a preferential orientation on the electroactive surfaces of the IO-ITO structure, such that only heme II is in the $\leq 14 \text{ Å}$ range for direct electron transfer. All electrons passing to heme I would therefore have to be transferred *via* heme II (Figure 3.19). In this initial model, electrons may well pass with ease from heme I to heme II, the direction they would be expected to travel during thiosulphate oxidation, but they are somehow prevented from passing from heme II to heme I in 75% of the enzyme by more than just relative E_M values. Substitution of single, buried residues in Cj C138M/H

is unlikely to change the protein surface to the extent that this preferential electrode orientation would change, however facile inter-heme electron transfer is fully restored in both variants at slow scan rates ($\nu = 5 \text{ mV s}^{-1}$).

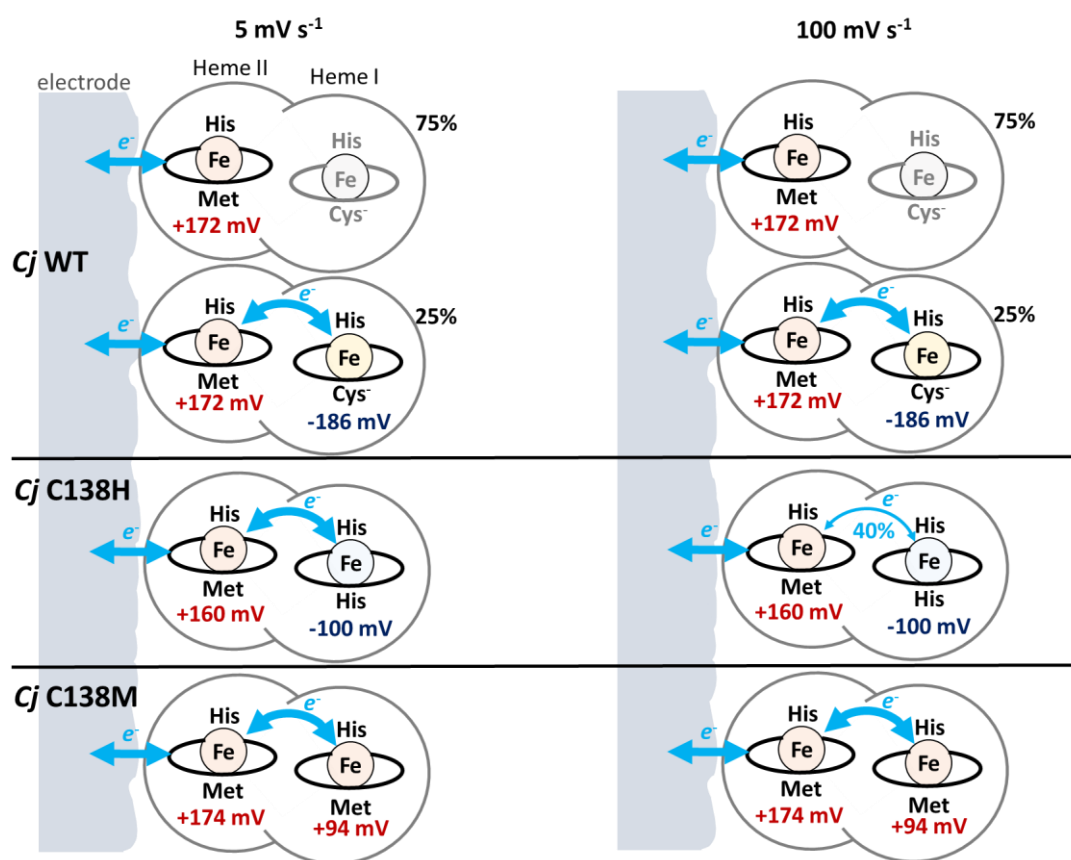


Figure 3.19 –Initial model of preferential orientation of *Cj* TsdA on an electrode surface that may rationalise electroactive behaviour. Blue arrows show redox events resolved by PFE, black-outlined hemes are electroactive in voltammetry and annotated with E_M values, positive (red) or negative (blue). Grey hemes are not electroactive in voltammograms. Fig. 4.12 presents a refined version of this model.

Since in *Av* WT the peak area for heme I signals is equal to the sum of peak areas assigned to both heme II environments, whatever prevents electron transfer to heme I of *Cj* WT is not present in *Av* WT. Despite some evidence of ligand switching in *Cj* N254K, the electroactive population of heme I is still smaller than for heme II. This implies that whatever prevents facile electron transfer to heme I in *Cj* WT is still present in *Cj* N254K and introducing an *Av* WT-like heme II environment into *Cj* WT does not replicate *Av*-like electroactivity. Conversely, in *Av* K208N the number of moles of electrons transferred by heme I is less than that of heme II, like *Cj* WT, so the absence of an *Av* WT-like heme II environment in *Av* K208N does appear to have replicated *Cj* WT-like redox properties in *Av* TsdA.

One rationalisation for this behaviour is that inter-heme electron transfer is highly dependent on the relative E_M values of heme I and II. In *Cj* C138M the heme E_M values are 80 mV

apart and in *Av* C96H these values are 53 mV apart and both of these variants show full electroactivity of both hemes which is not dependent on scan rate. For *Cj* WT the heme E_M values are 358 mV apart so inter-heme electron transfer could be largely prevented even at slow scan rates. *Cj* C138H has hemes with E_M values 260 mV apart and inter-heme electron transfer is now highly dependent on scan rate, 'tuning out' as this increases. *Av* C96M has similar 'tuning' and the heme E_M values are 176 to 266 mV apart depending on ligation, similar to the difference in values for *Cj* C138H. This model does not account for the observation that the number of electrons passed by heme I in *Cj* WT is unaffected by scan rate however (Figure 3.7).

Explaining these observations may be easier if there are differences in the heme I environment of *Av* and *Cj* WT which are also sensitive to the heme II environment. Although MCD confirms *Av* and *Cj* WT hemes as having His/Cys⁻ ligation it may be that modified forms of cysteine still competent as heme ligands, such as cysteine persulphide, are present. These may be chemically similar enough that the CT_{LS} of hemes ligated by these would resolve at the same wavelength as His/Cys⁻ giving similar MCD spectra and the appearance of homogeneity without eliminating the possibility that sub-populations are present with different electroactive properties. The explanation detailed above is therefore only one possible model of explaining the unequal electroactive heme populations observed in PFE, others, for example where cysteine modifications can affect E_M or electron transfer by heme I are discussed in subsequent chapters.

4. Cysteine Modifications of *Cj* WT and their Contributions to Spectroscopy and Electrochemistry

The first step of the mechanism proposed by Grabarczyk *et al.* for TsdA catalysis (Figure 1.8) involves modification of the heme I chemical environment. Specifically it is proposed that the heme I cysteine ligand covalently bonds a molecule of thiosulphate to form cysteine thiosulphonate⁵ which is unlikely to remain as a heme ligand. Chemical modification of cysteine is not unusual; arguably the most common modification is the condensation of two cysteines to form a disulphide bond:



Cysteine disulphides, or cystines, typically contribute to the structural stability of a protein. For example, the triple helix of animal collagen is stabilised by 'knots' of inter-helical cystines¹⁰⁵. Also significant is the thiol-disulphide redox activity of many proteins where the corresponding reaction (typically $E_M \approx -200 \text{ mV}^{52,106}$) contributes to maintenance of cellular redox homeostasis and metabolism¹⁰⁷, including *c*-heme insertion into proteins^{108,109}. However, a large number of post-translational modifications of cysteine are possible, many arising from the nucleophilicity of the cysteine thiol. Modifications most relevant to this thesis are summarised in Table 4.1.

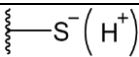
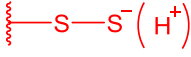
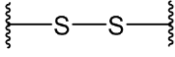
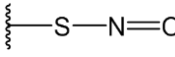
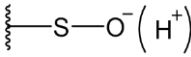
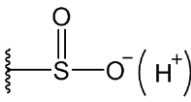
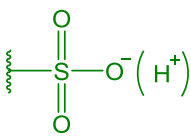
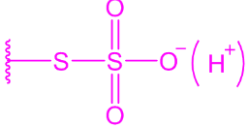
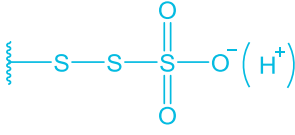
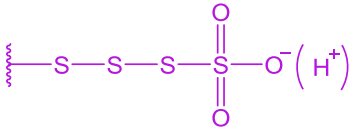
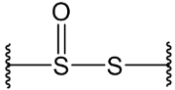
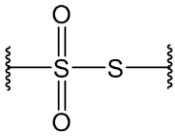
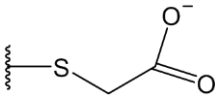
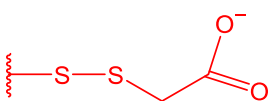
Modification(s) of *Cj* WT Cys-138 could result in heterogeneity in the heme I environment. In turn this heterogeneity may contribute to the much smaller electroactive population assigned to heme I compared to heme II in PFE (see above, 3.3.3) or influence the heme I (II) E_M values. This chapter begins by describing methods that identify cysteine modifications, followed by a brief review of previously reported post-translational cysteine modifications relevant to this work. Finally studies of *Cj* TsdA enzymes employing mass spectrometry, (magneto) optical spectroscopy and PFE are presented together with a hypothesis for the origin of the different peak areas resolved by PFE.

4.1. An Overview of Post-Translational Cysteine Modifications

4.1.1. *Methods that Identify Cysteine Modifications*

Ellman's reagent has long been used as part of a colorimetric assay to detect the presence or absence of free thiol(ate) groups¹¹⁰, however this technique does not reveal the nature of any chemical modifications that may be present which would prevent conventional reactivity of these residues. As a result, more informative methods are required. Post-translationally modified cysteine species can be detected and identified using several techniques. It is also possible to exploit the reactivity of thiols to manipulate these modifications *in situ* with chemical agents.

Table 4.1 –Cysteine modifications. Where multiple naming conventions exist, the terminology used in this thesis is marked in **bold**. Coloured text indicates modifications assigned in TsdA proteins based on mass changes detected by mass spectrometry. The same colour coding is used throughout this thesis.

Amino Acid Sidechain	Name (pK _a)	+Mass (Da)
	Cysteine (8.4)	
	Cysteine persulphide, cysteine sulphydride (6.2 ¹¹¹)	+32
	Cystine, cysteine disulphide	
	S-Nitrosocysteine	+30
	Cysteine sulphenic acid (6.6 ¹¹²)	+16
	Cysteine sulphinic acid, sulphinoalanine (≈2 ¹¹³)	+32
	Cysteine sulphonate	+48
	Cysteine sulphonate	+80
	Cysteine thiosulphonate	+112
	Cysteine thioperoxosulphonate	+144
	Cysteine thiosulphinic acid ester (7.3, 7.9 ¹¹⁴)	+16
	Cysteine thiosulphonate ester	+32
	Cysteine carboxymethylate	+57
	Cysteine persulphide carboxymethylate	+89

Additional electron density adjacent to a cysteine sulphur in a protein structure resolved by X-ray crystallography can often indicate post-translational modification of that residue³⁰. Chemically plausible adducts can be modelled to this electron density in order to identify the modification, although most experiments do not have sufficient resolution to determine protonation states. During protein crystallisation, samples often experience prolonged exposure to oxygen leading to adventitious formation of cysteine sulphinic and sulphonic acids⁹. Equally, high energy synchrotron X-rays can photoreduce disulphide bonds³⁶, potentially removing or damaging cysteine adducts during X-ray diffraction. As such, there can be ambiguity when relating a crystallographically-resolved protein structure to the same protein in solution when cysteine is present (Figure 1.6, C).

Post-translationally modified cysteine can also be detected from the mass increase *versus* unmodified cysteine. When other chemical adducts can be discounted, determining the intact mass of a protein can identify adducts present on one or more free cysteines. A popular technique for this is electrospray ionisation mass spectrometry (ESI-MS)⁸⁶ where (macro)molecules in solution are desolvated into gas-phase ions by spraying charged liquid into neutral gas at high pressure to create an ion beam¹¹⁵. This ion beam can then be electrostatically guided towards a mass/charge detector, such as a time-of-flight (TOF) chamber. This 'soft' ionisation technique is well-suited to large macromolecules, such as proteins¹¹⁶. Liquid chromatography mass spectrometry (LC-MS)⁸⁷ involves initial separation of proteins from salt or buffer molecules which might interfere with protein ionisation or form adventitious adducts. If multiple free cysteines are present in a single molecule, identification of individual modifications is ambiguous. One approach to resolving this ambiguity is tandem mass spectrometry (MS-MS), where proteins are proteolytically cleaved into multiple polypeptides prior to analysis and then fragmented further by high energy collisions within the instrument¹¹⁷. Sections of the protein sequence can then be identified from their fragmentation patterns, presenting the possibility of identifying sections of the protein where mass increases are present¹¹⁸.

Unambiguous identification of sulphur-based cysteine adducts from electron density or increases in mass is also possible if these species undergo detectable sulphur-specific chemistry. Disulphide bonds in proteins have traditionally been reduced using dithiothreitol, however, water soluble organophosphines, particularly tris(2-carboxyethyl)phosphine (TCEP) have recently gained popularity^{119,120}. TCEP stoichiometrically and irreversibly reduces disulphide bonds to give two thiols and tris(2-carboxyethyl)phosphine oxide (TCEPO) (Figure 4.1, A). Alkylating agents such as iodoacetate (and iodoacetamide) can also be used to cause irreversible and stoichiometric oxidation of free cystein(at)es and cysteine persulphides¹²¹, 'trapping' them as an alkylated species (Figure 4.1, B). The rate of this reaction has also been used as part of high-throughput

proteomics studies to identify hyperreactive cysteines, employing a iodoacetate-derived label tailored for high-throughput identification¹²².

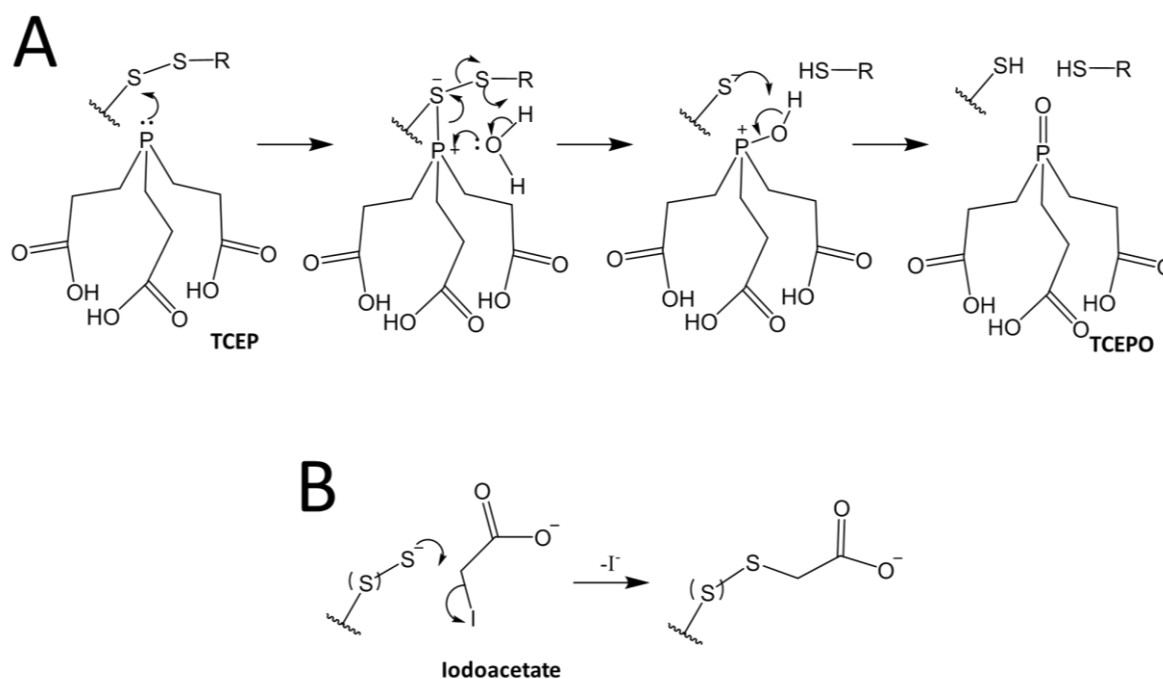


Figure 4.1 – Reactions used to interrogate cysteine residues. (A) Organophosphines (TCEP shown) in protic solvents irreversibly reduce and protonate disulphide bonds driven by the formation of a strong phosphorous-oxygen bond¹¹⁹. (B) Alkylating agents (iodoacetate shown) irreversibly oxidise cysteine and cysteine persulphide preventing further modifications from forming.

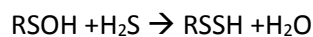
4.1.2. Cysteine Reactivity

Typically, cysteine reactivity features the formation of covalent bonds by the sulphur atom of the nucleophilic thiol group. Thiolates have even greater nucleophilicity, so cysteines with important mechanistic functions in proteins such the active sites of enzymes are often present in a protein environment that stabilises negative charge, lowering pK_a to a value where deprotonation is favoured under biological (neutral) conditions¹²². The pK_a of the thiol group of free cysteine in solution is 8.4, but protein environments can modify this substantially; values as low as 2¹²³ and as high as 12¹²⁴ have been reported. When cysteine is a heme ligand, ferric iron stabilises negative charge, so cysteinolate forms a stronger bond to ferric heme compared to ferrous⁴⁵ and deprotonation of cysteine often accompanies heme oxidation^{89,98}.

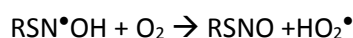
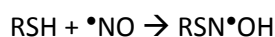
The nucleophilicity of cysteine can also result in the formation of covalent adducts, many of which have biological relevance. Cysteine sulphenic acid is a highly reactive, often transient species, formed *in vivo* from cysteine by reactive oxygen species such as hydrogen peroxide¹²⁵:



A stabilised cysteine sulphenic acid residue is formed by analogous reactions at the active site of peroxiredoxins, an ubiquitous family of enzymes that reduce cytotoxic reactive oxygen species¹¹². It is suggested that cysteine sulphenic acid is also a precursor for the sulphydration of cysteine by hydrogen sulphide:

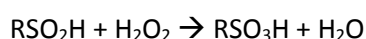
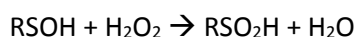


The product of this reaction is cysteine persulphide. Cysteine persulphide ($\text{pK}_a = 6.2$)¹¹¹ and cysteine sulphenic acid ($\text{pK}_a = 6.6$)¹¹² are largely deprotonated at neutral pH, increasing their nucleophilicity and the presence of lone pairs adjacent to the α -S or O, increases this further¹²⁶. Cysteine persulphide is more stable than cysteine sulphenic acid, and high concentrations of this species ($>100 \mu\text{M}$) are thought to be maintained in mammalian systems¹²⁷. In addition to facilitating non-enzymatic cystine formation, sulphydration can also increase^{128–130} or inhibit^{126,131} activity in enzymes with mechanistically-important cysteines. In this way, hydrogen sulphide is thought to act as a signalling molecule in higher organisms, similar to the more thoroughly characterised 'gasotransmitter' nitric oxide¹²⁸. Nitric oxide reacts directly with cysteine to form S-nitrosocysteine as a two-step process:

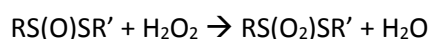
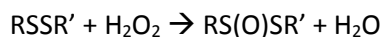


S-nitrosocysteine formation regulates a multitude of processes in mammalian systems, from neurotransmission, to DNA repair¹³². This modification, and therefore the nitric oxide 'signal', can be transferred to cysteines in glutathione or thioredoxin by disulphide exchange; S-nitrosogluthathione reductases or thioredoxin reductases then reverse this 'signal' by reducing S-nitrosocysteine back to cysteine¹³³.

As well as forming reversible modifications with well-characterised biological relevance, cysteine undergoes adventitious oxidation by reactive oxygen species which result in irreversible cysteine modifications. Cysteine sulphenic acid can be further oxidised to the more stable cysteine sulphinic acid, which in turn can be oxidised to cysteine sulphonc acid:



In mammalian systems undergoing ischemia, these species can arise when mitochondrial dysfunction produces excess reactive oxygen species¹³⁴. Analogous reactions with cystine form cysteine thiosulphinic acid and thiosulphonate esters¹³⁵:



Cysteine thiosulphinates can react with cysteine to form cystine and cysteine sulphenic acid, adventitious occurrence of the reverse of this reaction is one rationalisation for the short-lived nature of sulphenic acids in biology¹¹⁴.

4.1.3. Cysteine Chemistry of Sulphur-Cycle Enzymes

The bacterial sulphur oxidation (Sox) enzyme cycle, also known as the thiosulphate oxidising multi-enzyme system (TOMES), is a cascade of enzymes which oxidise thiosulphate and other reduced sulphur compounds to sulphate or elemental sulphur depending on the organism (Figure 4.2). Central to this process is SoxYZ, a carrier protein which is the *in vivo* substrate for the other enzymes in the cascade¹³⁶. SoxYZ features a cysteine residue on a flexible loop which is only presented to the active sites of the other enzymes, limiting adventitious sulphur chemistry. In the first reaction of the Sox cycle, this cysteine is post-translationally modified by the cytochrome SoxAX. SoxAX has two or three hemes depending on organism and shares many structural similarities with TsdA^{5,137}. In the active form of SoxYZ, the cysteine has already been modified to cysteine persulphide and the first step of the catalytic cycle is the thiosulphonation of this residue by SoxAX to form cysteine thioperoxosulphonate¹⁰¹. The active site heme of the SoxA subunit crystallises with His/CysS⁻ ligation, believed to be an off-pathway catalytic intermediate¹³⁸ and one proposed catalytic step is the displacement and thiosulphonation of the unmodified cysteine heme ligand⁴⁹. Thiosulphate oxidation by TsdA was initially investigated as an amenable analogue of SoxAX⁵, due to practical difficulties in the mechanistic analysis of the latter enzyme.

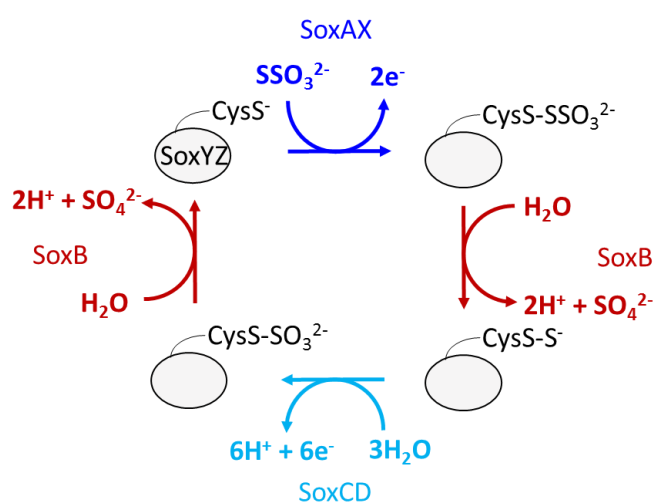


Figure 4.2 – Main bacterial Sox enzyme cycle proposed by Grabarczyk *et al.*¹⁰¹ The carrier protein SoxYZ has a cysteine persulphide residue on a flexible loop to which is further modified by SoxAX, SoxB and SoxCD. The eight total electrons released by each cycle enter the bacterial electron transfer chain *via* a *c*-type cytochrome.

When *Av* WT is incubated with thiosulphate or tetrathionate, the mass of the protein increases by 112 Da, consistent with cysteine thiosulphonate (Table 4.1) forming from Cys-96⁵. High-spin heme is detected in the electronic absorbance spectrum of cysteine thiosulphonate containing protein, consistent with the loss of Cys-96 as a heme ligand, however there is no loss of catalytic activity in this species *versus* the unmodified enzyme. Contrastingly, iodoacetate incubated *Av* WT also has high-spin heme with an appearance similar to tetrathionate treated protein, however catalytic activity is abolished. Based on this evidence, Grabarczyk *et al.* proposed a TsdA reaction mechanism⁵ where the formation of cysteine thiosulphonate is the first step (Figure 1.8).

Grabarczyk *et al.* also identified some forms of *Av* TsdA with a mass increase of 32 Da, proposed to be cysteine persulphide (Table 4.1) formed from the breakdown of cysteine thiosulphonate. No mechanism for this process has been proposed, however thiosulphate in aqueous solution is dismutated by water to form sulphuric acid and bisulphide¹³⁹. An analogous process is the dismutation of cysteine thiosulphate to cysteine persulphide, which would release a molecule of sulphuric acid. Alternatively, in TsdA electrons from the nearby ferrous hemes could reduce the S_α-S_β disulphide bond of an active site cysteine thiosulphate to form cysteine persulphide and one molecule of sulphite as a side-reaction of the Grabarczyk mechanism. An *Av* WT crystal soaked in sulphite resolves with cysteine persulphide ligating heme I and there is a molecule of sulphite modelled nearby⁹ (Figure 1.6, B). This observation is consistent with what would be expected from heme reduction of the S_α-S_β disulphide bond of an active site cysteine thiosulphonate, or X-ray photoreduction of the same. Other *Av* WT structures have Cys-96 present as cysteine sulphinic acid (Figure 1.6, C), most likely resulting from oxidative damage. TCEP is reported to remove or prevent the formation of all cysteine adducts in *Av* TsdA protein crystals⁹, although to date these structures have not been published.

4.2. LC-MS Reveals Multiple Cys-138 Modifications in *Cj* WT as Prepared, which are Removed by TCEP Treatment

LC-MS was used to detect and identify cysteine modifications of TsdA proteins. All samples were handled anaerobically (O₂ < 10 ppm) up to the point of denaturation by 10-fold dilution in 2% Acetonitrile, 0.1% Formic Acid. Mass spectra were deconvoluted from the mass/charge data (*e.g.* Figure 4.3). For clear visualisation of sample composition the relative intensities of the mass peaks are normalised, so the sum of their relative abundances is 100% for peaks obtained within 37,000 – 37,500 Da for *Cj* TsdA or 28,000 – 28,500 Da for *Av* TsdA. Therefore the intensity of a given peak corresponds with the relative abundance of that species in the sample. All spectra are annotated (grey font) to indicate the predicted mass of the protein containing two hemes, as

described below. Additional masses (coloured font) indicate species with a larger mass indicative of covalent cysteine modification (Table 4.1). A similar format is used for all mass spectra presented in this thesis.

LC-MS of *Cj* WT is more complex (see below), but LC-MS of ***Cj* C138M** and **C138H** revealed samples both comprised of a single species (Figure 4.2, right inset panels) consistent with there being no heterogeneity in the absence of cysteine. The difference in mass of these samples (10 Da) is similar to the difference in mass between methionine and histidine (6 Da). However, for each protein the observed mass is 99 Da larger than expected from the sequence of the diheme containing protein with an N-terminal Step II tag and four linker residues³². This additional mass was noted in the LC-MS of all *Cj* proteins analysed to date and could be a feature resulting from overexpression in *Escherichia coli*. The possible origin of this additional mass is suggested by the properties of minor peaks (<10% relative abundance) in some samples. These peaks had masses equal to those predicted for the diheme containing protein lacking 8 of the N-terminal residues. Thus, the additional 99 Da mass is assigned to a covalent adduct bound to the Strep II tag. This adduct is unlikely to be relevant to the chemistry of Cys-138 or the activity of TsdA and will therefore be regarded as a typical part of the unmodified mass of TsdA when rationalising mass increases.

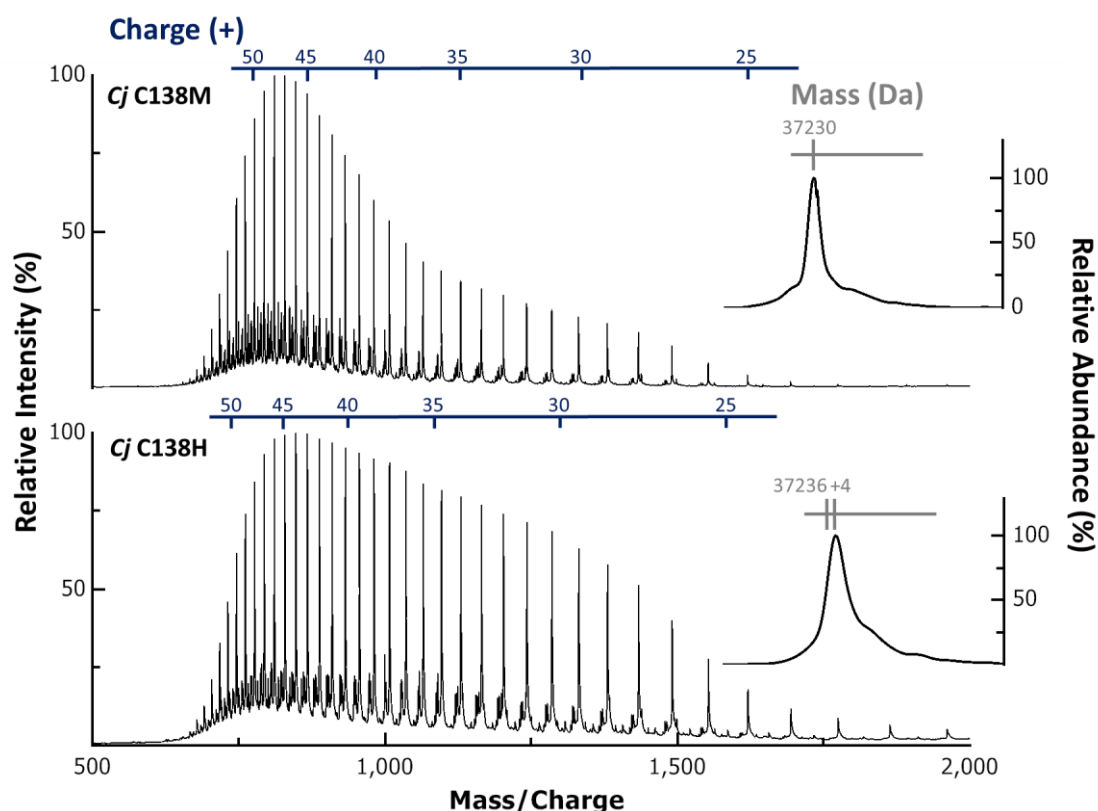


Figure 4.3 –Mass Spectra of *Cj* C138M/H variants. 30-50 μ M TsdA in pH 7 50 mM HEPES, 50 mM NaCl denatured for LC-MS by 10-fold dilution in 2% Acetonitrile, 0.1% Formic Acid.

The mass spectrum of **Cj WT** has multiple peaks (Figure 4.4, right inset). All of the peaks have a mass equal or greater to that predicted for the diheme containing protein with an N-terminal Strep II tag and a standard 99 Da adduct described above. Thus, the LC-MS provides compelling evidence for cysteine modification of some protein within the *Cj* WT sample. A peak at 37,202 Da represents 52% of the sample which has the mass predicted for the protein with unmodified Cys-138. One additional S or two additional O are predicted in 40% of the sample that displays a mass increase of +31 Da, which would correspond to the presence of cysteine persulphide or cysteine sulphinic acid respectively (Table 4.1). The remaining 10% of the sample has a mass increase of +110 Da, consistent with a sub-population of enzyme where Cys-138 has bound a thiosulphonate group. This adduct corresponds to that previously detected in thiosulphate or tetrathionate incubated *Av* WT⁵. Although no substrates were added during growth and overexpression³², the presence of this proposed catalytic intermediate may indicate *Cj* WT has adventitiously encountered sulphur compounds during or prior to purification.

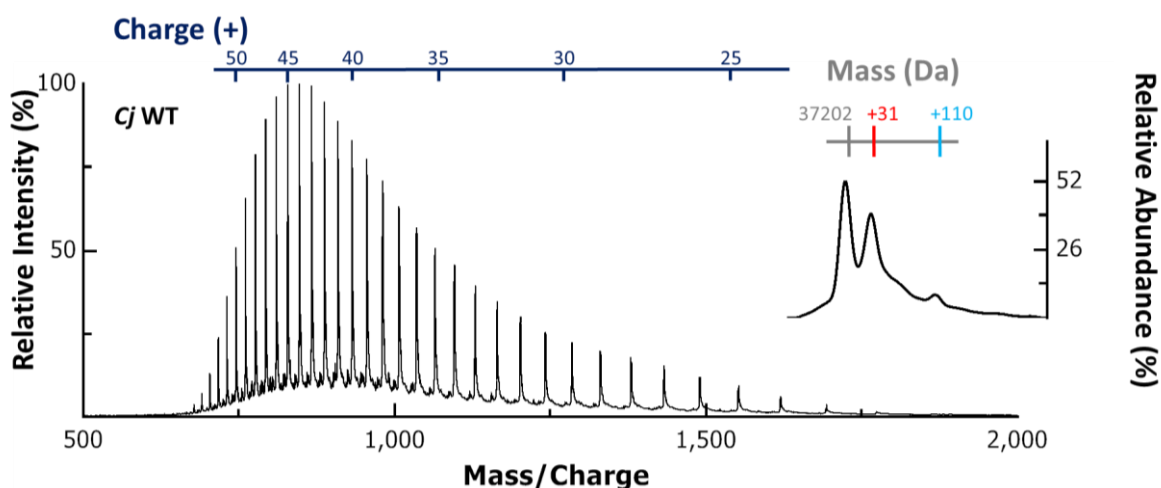


Figure 4.4 –Mass Spectrum of *Cj* WT. 30-50 μ M TsdA in 50 mM HEPES, 50 mM NaCl, pH 7, denatured for LC-MS by 10-fold dilution in 2% Acetonitrile, 0.1% Formic Acid. Mass increases are consistent with a percentage of the original sample has unmodified cysteine (grey) cysteine persulphide (red) or cysteine thiosulphonate (blue).

To be confident that the cysteine modifications proposed above were not formed by the denaturation and ionisation required by LC-MS, samples were analysed (Figure 4.5) after treatment with chemicals that should produce defined change in status of (modified) cysteine residues. Treatment with TCEP prior to iodoacetate should reduce all S-S bonds to produce a sample which only contains one unmodified cysteine that can then react with iodoacetate so that a single peak with a mass increase of 57 Da relative to prediction will be observed. In fact, *Cj* WT

incubated with TCEP and then iodoacetate displays two clear mass peaks (Figure 4.5, lower left). 80% of the sample has a mass +57 consistent with carboxymethylated Cys-138 while 20% of the sample has the mass predicted for unmodified Cys-138. Consistent with this proposal, it can be inferred that the reaction with TCEP has converted the sample to a homogenous state, containing only unmodified Cys-138, which has then partially reacted with iodoacetate to give the carboxymethylated enzyme. It is also possible that residual TCEP has acted as a modest inhibitor of the reaction with iodoacetate¹²⁰.

LC-MS of the sample reacted directly with iodoacetate reveals multiple species (Figure 4.5, upper left). As expected all of these species have a mass greater than predicted for the protein with unmodified Cys-138. The predominant peak (50% of the sample) has the mass predicted for protein with carboxymethylated Cys-138. Additional peaks represent 30% of the sample with carboxymethylated cysteine persulphide (+87 Da \approx +32 +57 Da) and 20% of the sample having cysteine thiosulphonate (+112 Da) which is unlikely to react with iodoacetate.

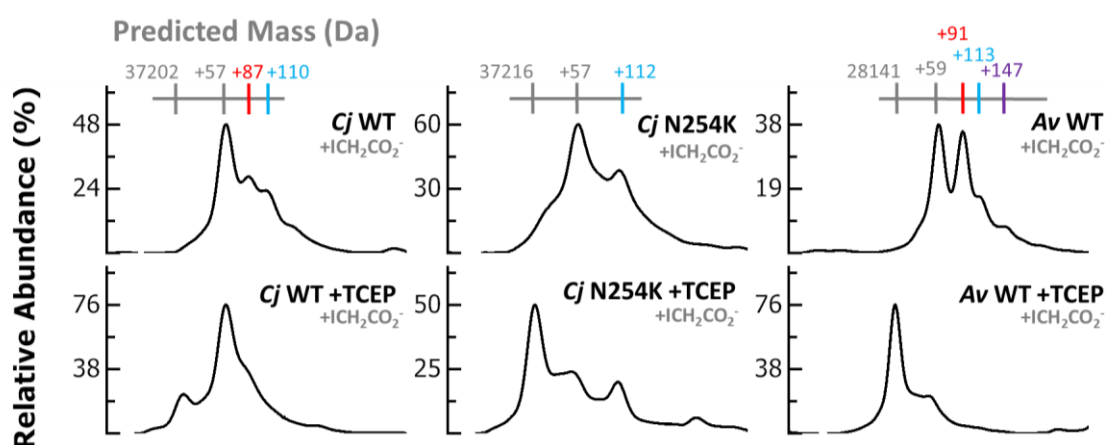


Figure 4.5 – Deconvoluted Mass Spectra of Av WT, Cj WT and N254K treated with TCEP. 30-50 μ M TsdA in pH 7 50 mM HEPES, 50 mM NaCl incubated for 1 hour with 75 μ M TCEP followed by incubation with 15 mM sodium iodoacetate. Samples were denatured for LC-MS by 10-fold dilution in 2% Acetonitrile, 0.1% Formic Acid. Mass increases are consistent with a percentage of the original sample has unmodified cysteine (grey) cysteine persulphide (red), cysteine thiosulphonate (blue) or cysteine thioperoxosulphonate (purple).

Cysteine sulphinic acid was a possible origin of the +32 Da species in Cj WT samples (Figure 4.3). However, this species is unlikely to react with iodoacetate and the absence of the +32 Da species in the iodoacetate treated sample makes it unlikely that cysteine sulphenic acid was present in the original sample. The proposed composition of as-provided samples of Cj WT and other proteins studied here is summarised in (Table 5.2).

Table 4.2 – Composition of cysteine modifications in TsdA samples as-provided and after TCEP treatment. Samples were prepared as indicated in pH 7 50 mM HEPES, 50 mM NaCl before incubation in 15 mM sodium iodoacetate and denaturation in 10-fold dilution in 2% Acetonitrile, 0.1% Formic Acid. Cysteine (persulphide) carboxymethylate and unmodified cysteine (persulphide) are proposed to originate from the same species in solution.

Sample	Relative Abundance (%)			
	Cys ⁻	Cys-S ⁻	Cys-SSO ₃ ⁻	Cys-SSSO ₃ ⁻
Mass Increase (Da)	+0, +57	+32, +89	+112	+144
<i>Cj</i> WT	50	30	20	-
<i>Cj</i> WT +TCEP	100	-	-	-
<i>Cj</i> N254K	60	-	40	-
<i>Cj</i> N254K +TCEP	80	-	20	-
<i>Av</i> WT	38	36	16	8
<i>Av</i> WT +TCEP	100	-	-	-

In order to assess the status of cysteine in other TsdA samples, those of *Cj* N254K and *Av* WT were studied (Figure 4.5, centre and right). It was expected that these samples, unlike *Cj* C138M/H would also display evidence for cysteine modification. Indeed, when incubated with TCEP, LC-MS is simpler and peaks at lower mass values are seen for both proteins. The predominant peak for *Cj* N254K treated with TCEP and iodoacetate indicates 60% of the sample has the mass predicted for protein where Cys-138 is entirely unmodified (+0 Da). There is a broad feature with a peak at +53 Da indicating ~25% of the sample has mass increase(s) that could indicate Cys-138 is carboxymethylated (or oxidised to cysteine sulphonic acid which is less likely). Unlike *Cj* WT there is still a peak with a mass +111 Da, (20% of the sample) indicating protein with cysteine thiosulphonate, for *Cj* N254K, TCEP incubation is inferred to only have homogenised cysteine in as much as 80% of the sample. *Cj* N254K incubated with iodoacetate (Figure 4.5, upper centre) has a mass peak equal to the predicted mass of the variant +57 Da, consistent with carboxymethylation of unmodified Cys-138 in 60% of the sample. The single additional peak (40% of the sample) has a +112 Da mass, indicating thiosulphonation of Cys-138. *Cj* N254K has catalytic activity comparable to *Cj* WT³² and has presumably undergone similar reactivity with adventitious sulphur compounds present during growth as *Cj* WT. Some His/Lys ligation at ferric heme II could increase the stability of the thiosulphonated form of Cys-138, explaining the absence of cysteine persulphide and the slower rate of TCEP reaction of this variant compared to *Cj* WT. His/Lys rather

than His/Met ligation at heme II lowers E_M and decreases the thermodynamic driving force for breaking disulphide bonds at Cys-138, consistent with this proposal.

Av WT incubated with TCEP and iodoacetate (Figure 4.5, bottom right) has one clearly resolved peak (76% of the sample) with a mass equal to the predicted mass of the unmodified protein (without the +100 Da mass increase present in *Cj* TsdA proteins). An additional peak with a mass +59 Da shows the remaining 36% of the sample has been carboxymethylated after all other modifications were removed. *Av* WT incubated with only iodoacetate has a mass peak (38% of the sample) equal to the predicted mass +59 Da indicating carboxymethylation of unmodified Cys-96. There is also a mass peak (36% of the sample) with +91 Da indicating persulphuration of Cys-96 prior to carboxymethylation. Two smaller mass peaks (16% and 8% of the sample respectively) with mass increases of +113 Da and +147 Da, assigned as enzyme where Cys-96 is respectively modified to cysteine thiosulphonate or thioperoxosulphonate. The technique used to detect cysteine modifications in *Cj* WT as purified has also detected similar modifications in *Av* WT consistent with similar cysteine chemistry occurring in both TsdA enzymes. TCEP incubation removes the majority of cysteine adducts like in *Cj* WT, but inhibits carboxymethylation, similarly to *Cj* N254K. This suggests that the presence of His/Lys ligation at heme II is not the only influence on the stability of disulphide bonds at the heme I cysteine.

4.3. (Magneto) Optical Spectroscopy of *Cj* WT with no Cys-138 Modifications

Having established that TCEP treatment of *Cj* WT produces a homogenous sample containing only unmodified cysteine, it was of interest to resolve the spectroscopic and electrochemical properties of this enzyme. Initial spectroscopic resolution of the consequences of TCEP reaction was provided by electronic absorbance (Figure 4.6, upper). For this experiment a 2000-fold molar excess of TCEP was introduced to an anaerobic sample of *Cj* WT in 50 mM HEPES, 50 mM NaCl, pH 7. Over 90 minutes spectroscopic changes consistent with heme reduction were monitored, namely the intensity of the α band centred on 552 nm. Spectra recorded at 2.5 minute intervals during this time show a clean transition from low-spin ferric to ferrous heme with no evidence of any detectable intermediates. The heme features of the spectrum recorded after this time are of a similar appearance to that of ascorbate treated *Cj* WT, suggesting that a single heme is being reduced in each TsdA monomer. Reduction of TsdA hemes by TCEP was not expected from the mechanism of cysteine reduction (Figure 4.1, A).

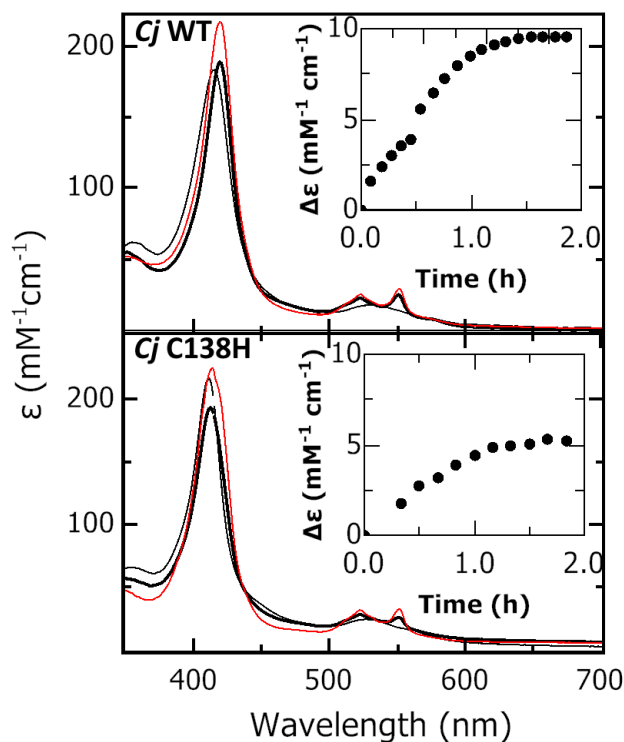


Figure 4.6 – Electronic absorbance spectrum of TCEP-treated *Cj* WT and C138H. 12 μM *Cj* WT or 15 μM *Cj* C138H before (thin black line) and after (thick black line) incubation with 30 mM TCEP for 120 minutes. 123 μM *Cj* WT or 168 μM *Cj* C138H incubated with 1.5 mM sodium ascorbate (thin red line) is shown for comparison. **Insets** – Intensity change at 552 nm over time after addition of TCEP. All samples in 50 mM HEPES, 50 mM NaCl, pH 7.

A possible origin is from products of the TCEP disulphide reaction, predicted to be bisulphide or thiosulphate, reforming disulphide bonds with Cys-138 in the oxidised protein. Each disulphide bond re-formed would release two electrons which could then reduce the TsdA hemes in di-ferric enzyme. Over time inter-monomer electron transfer in the bulk sample would result in electrons ultimately remaining on the higher E_M His/Met hemes only. No cysteine chemistry is possible for *Cj* C138H, however this variant is still reduced to $\sim 50\%$ the extent that *Cj* WT is by TCEP (Figure 4.6, lower). This suggests the reactivity of TCEP is more complex and direct reduction of hemes can occur when this agent is in excess.

To characterise the difference between *Cj* WT as prepared, which is predicted to have predominantly His/Cys S^- heme I ligation and *Cj* WT +TCEP, which is predicted to have entirely His/Cys S^- ligation, MCD was recorded of *Cj* WT treated anaerobically with TCEP and then re-oxidised with ferricyanide to permit resolution of CT_{LS} bands. In the nIR region the CT_{LS} band (Figure 4.7) previously assigned as arising from His/Cys S^- ligation is slightly red-shifted to 1250 nm, has a lower intensity ($0.4 \text{ M}^{-1} \text{ cm}^{-1} \text{ T}^{-1}$) and there is now clear resolution of a vibrational shoulder at 1080 nm similar to that observed after ascorbate incubation (Figure 3.3). There is no change to the His/Met CT_{LS} band at 1830 nm, except for an apparent increase in the intensity of the

vibrational shoulder due to overlapping intensity from the red-shifted His/Cys⁻ band. In the UV/visible region, the Soret band of the treated species is broader and less intense, and the trough at 579 nm assigned to thiolate-ligated low-spin ferric heme in untreated *Cj* WT in the $\alpha\beta$ region is now no longer clearly resolved. A small peak has appeared at 547 nm, which could indicate that a trace of low-spin ferrous heme is present from incomplete reoxidation of the hemes.

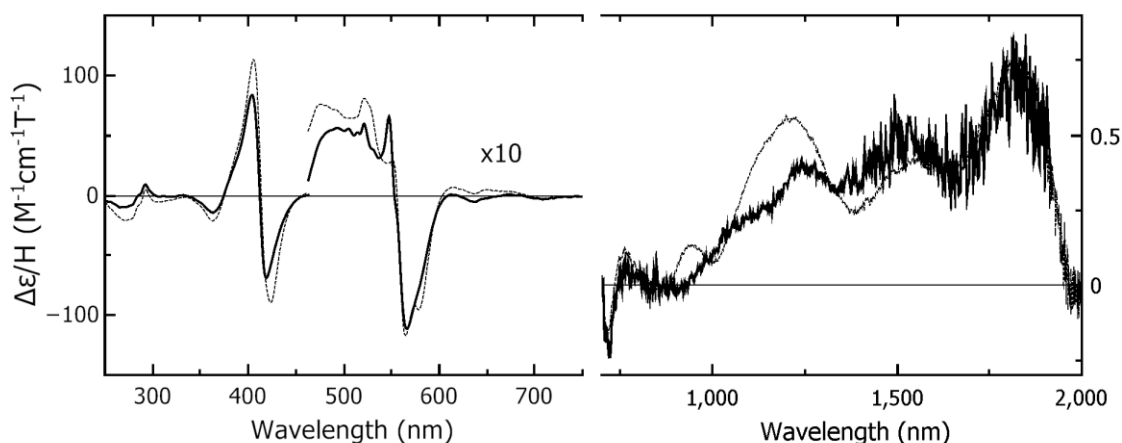


Figure 4.7 – MCD of oxidised TCEP-treated (black line) and as prepared (dashed grey line) *Cj* WT. Room-temperature (left) UV/visible and (right) nIR MCD spectra of 15 μM (250-450 nm) and 130 μM (450-2000 nm) *Cj* WT incubated with 80 μM TCEP and 17.6 μM (250-450 nm), 163 μM (450-700 nm) and 123 μM (700-2000 nm) *Cj* WT without TCEP. Both samples were fully oxidised with potassium ferricyanide after treatment. All data recorded at room temperature in 50 mM HEPES, 50 mM NaCl, pH 7 or the same buffer in D₂O pH* 7 for nIR MCD.

On the basis of LC-MS above, the bulk population of as-provided *Cj* WT is expected to have mixed His/Cys⁻ and His/Cys^S ligation at heme I and His/Met ligation at heme II. TCEP-treated *Cj* WT by contrast is expected to have homogenous His/Cys⁻ heme I ligation and identical His/Met ligation at heme II. MCD of oxidised TCEP-treated *Cj* WT is only subtly different from *Cj* as prepared, consistent with His/Cys⁻ and His/Cys^S ligated hemes having similar chemical properties. From comparing the two samples it appears that the *Cj* WT heme I with His/Cys^S ligation has a very slightly blue-shifted CT_{LS} band, a slightly narrower and more intense Soret, but a clearly distinctive negative $\alpha\beta$ feature at 579 nm that could be used to fingerprint this species given more examples of hemes with this ligation state.

4.4. PFE of *Cj* WT with no Cys-138 Modifications

The results presented above demonstrate how samples of *Cj* WT are heterogenous at the level of Cys-138 modifications. That heterogeneity can be removed by reaction with TCEP to produce samples containing only unmodified cysteine. As a consequence it was of interest to

assess the PFE of *Cj* WT containing only unmodified Cys-138. For these experiments PFE and LC-MS measurements were performed with the aim of providing detailed knowledge of cysteine status in samples used for PFE. PFE experiments were recorded with assistance from visiting researcher, Zuzana Bábková.

The protocol used was as follows. An anaerobic sample of *Cj* WT (~100 μM) in 50 mM HEPES, 50 mM NaCl, pH 7 was incubated with TCEP (30 mM) for 10 minutes at room temperature. Excess TCEP was removed by spin concentration against anaerobic 50 mM HEPES, 50 mM NaCl, pH 7. An aliquot of the sample was removed, treated with iodoacetate to trap reactive thiols, and analysed by LC-MS. The remainder of the sample was used to coat an IO-ITO electrode in anaerobic conditions and studied by PFE (5 to 100 mV s^{-1}). The adsorbed protein was then recovered from the electrode by applying a drop of iodoacetate solution (100 mM) to the electrode surface for 2 minutes, then scraping the entire mesoporous ITO layer into 2% acetonitrile, 0.1% formic acid. This suspension was then transferred to a container and allowed to sediment under gravity (typically ~5 minutes) so that ITO particles settle and permit extraction of only the liquid portion of the sample, which was then analysed by LC-MS. The corresponding LC-MS and PFE are presented in Figure 4.8.

LC-MS of *Cj* WT +TCEP used to coat the IO-ITO electrode shows the major species (50%) present in the sample was unmodified prior to carboxymethylation, with non-carboxylated protein and other sulphur adducts individually accounting for <20% of the sample. There is no indication for a significant change of Cys-138 status in the protein film recovered from the electrode. Representative voltammetry shows two pairs of peaks well described by $n = 1$ processes with $E_M = -83$ mV (X) and +195 mV (Y). The areas of X are now ~50% larger than for Y, respectively exchanging 210 (220) pmol electrons compared to 133 (115) pmol during the oxidative (reductive) scan.

The data presented above suggest that cysteine modification does indeed contribute to the electroactivity of *Cj* WT as revealed by PFE. A further experiment probed the properties of protein without TCEP treatment (Figure 4.8, B). The sample was treated as above but without the inclusion of TCEP. PFE showed behaviour consistent with that described in Chapter 3, where the peak area of X is smaller than that of Y, respectively exchanging 35 (45) pmol electrons compared to 140 (113) pmol during the oxidative (reductive) scan, which does not change as scan rate is varied. Importantly LC-MS of the protein as-adsorbed shows multiple mass peaks and after desorption the major species present (40%) in the sample is now cysteine persulphide, showing a clear link between the status of Cys-138 and the relative areas of signals in voltammetry.

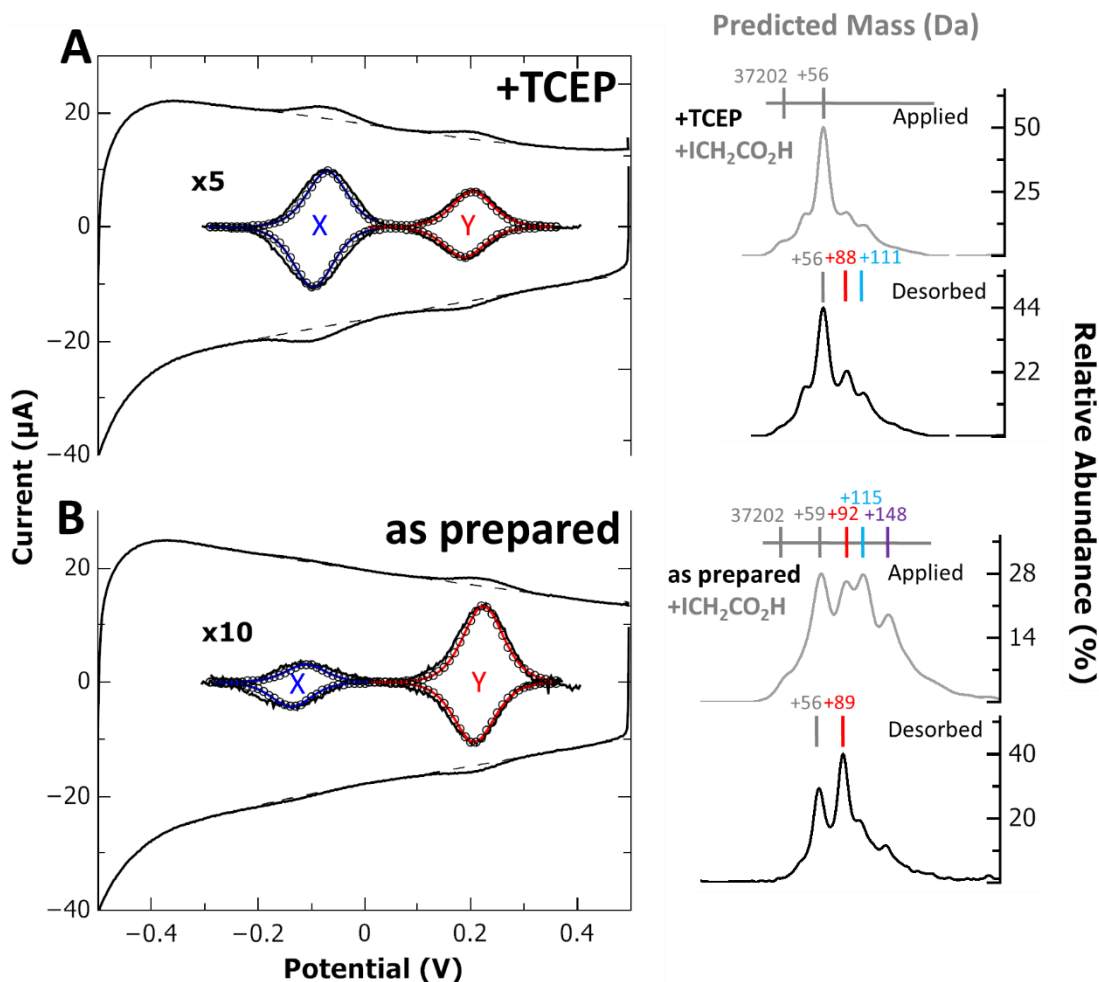


Figure 4.8 – Representative CV of *Cj* WT after TCEP incubation (A) and as prepared (B). (Left) Raw data (outer black line) with baselines (dashed line) used to prepare baseline-subtracted CVs (inner black line) of a *Cj* WT coated IO-ITO electrode either as prepared (top) or incubated with 75 μM TCEP and transferred to fresh buffer-electrolyte prior to adsorption (bottom). Each peak has been fitted to two predicted $n=1$ theoretical responses (red and blue lines) and the sum of these contributions (black circles). All data recorded in 50 mM HEPES, 50 mM NaCl, pH 7, $\nu = 10 \text{ mVs}^{-1}$, $T = 293 \text{ K}$. (Right) Mass spectra of stock solutions for voltammetry (upper panels) and desorbed protein (lower panels) incubated with 15 mM sodium iodoacetate. Samples were denatured for LC-MS by 10-fold dilution in 2% Acetonitrile, 0.1% Formic Acid. PFE recorded by Zuzana Bábková.

For LC-MS of the applied sample, 28% of Cys-138 was unmodified before carboxymethylation (+59 Da), 27% was persulphurated before carboxymethylation (+92 Da), 28% is thiosulphurated (+115 Da) and 17% is thioperoxosulphurated (+148 Da). This observation is consistent with cysteine thio(peroxo)sulphonate breaking down to cysteine persulphide, either during adsorption or redox cycling as electrons transferred from the (charged) electrode break disulphide bonds in the larger cysteine adducts, possibly *via* the TsdA hemes. Although PFE is largely identical, more heterogeneity is now visible in LC-MS (Figure 4.5, top left). There are more peaks at higher masses suggesting that more cysteine thio(peroxo)sulphonate is present in this sample and less cysteine persulphide, although this is rapidly reversed during adsorption and oxidation of the film. As this sample was taken at a later date from the same protein stock as the

first, it is likely that sulphur adducts have accumulated slowly over time in the purified protein, possibly originating from adventitious sulphur compounds present during growth which have bound non-covalently to the protein. This phenomenon is discussed further in Chapter 5.

To investigate if the link between cysteine modifications and electroactive heme populations is unique to *Cj* WT or is a general feature of TsdA enzymes, 400 μM TCEP was titrated into the buffer-electrolyte of the cyclic voltammetry experiments with IO-ITO electrodes coated with *Cj* WT, *Cj* N254K, *Av* WT and *Av* N254K. All of these films had previously displayed catalytic activity (Figure 5.2) giving confidence that they were in a native-like state. Catalytic activity was also detected after TCEP treatment (data not shown). To eliminate signals arising from direct oxidation of TCEP by the IO-ITO electrode, the experimental buffer-electrolyte was exchanged for fresh 50 mM HEPES, 50 mM NaCl, pH 7, before and after TCEP addition.

Representative baseline-subtracted voltammograms for TCEP-treated *Cj* WT, N254K and *Av* WT and K208N of all feature two pairs of peaks, where the lower potential peaks have a larger area than in voltammograms recorded prior to TCEP treatment (Figure 4.9).

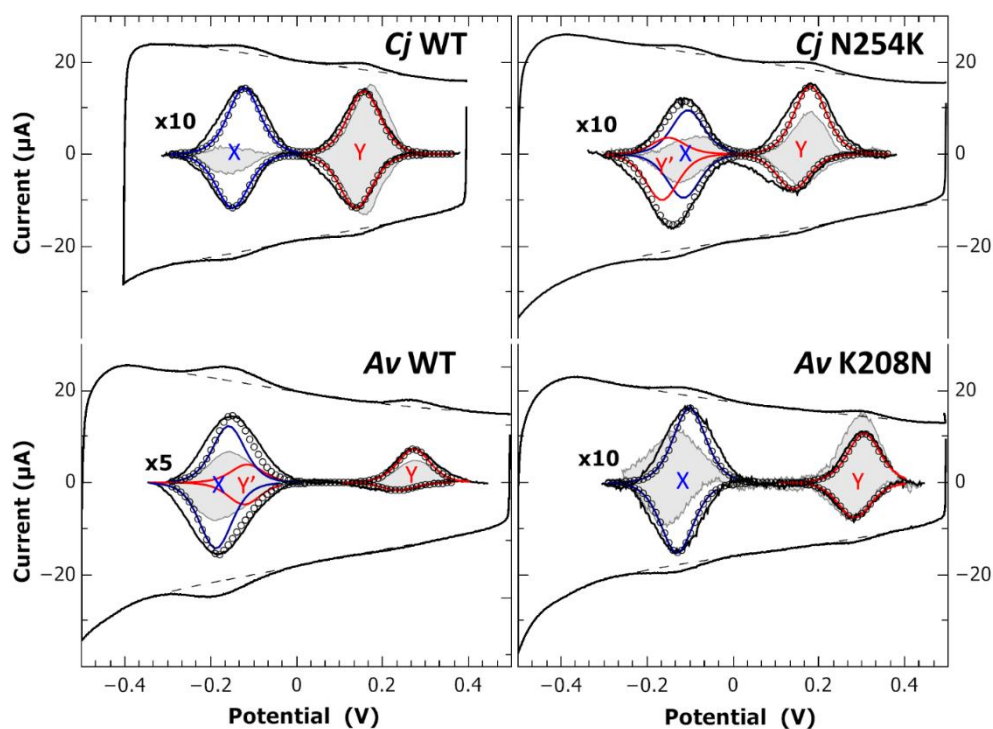


Figure 4.9 – Representative CV of TsdA enzymes after TCEP incubation. Raw data (outer black line) with baselines (dashed line) used to prepare baseline-subtracted CVs (inner black line) of TsdA coated IO-ITO electrodes titrated with 400 μM TCEP and transferred to fresh buffer-electrolyte. $T = 293\text{ K}$. Each peak has been fitted to predicted $n=1$ theoretical responses (red and blue lines) and the sum of these contributions (black circles). Also shown (grey, shaded area) is the response prior to TCEP incubation.

All voltammograms are well-described by theoretical $n = 1$ processes (X, Y and Y') centred on E_M values similar to those describing the electroactivity of the untreated enzymes, albeit with different areas indicating that the only change caused by TCEP is in the amounts of electrons passed by the TsdA hemes. For all enzymes the area of X is larger, indicating that heme I now transfers more electrons than it did prior to TCEP treatment. For *Av* K208N and to a lesser extent for *Cj* WT the area of Y is smaller, consistent with previous *Cj* WT voltammetry (Figure 4.8) and indicating heme II now transfers less electrons. Both *Av* WT and *Cj* N254K still have signals (Y and Y') consistent with His/Lys to His/Met ligand switching at heme II. The areas of these signals are larger after TCEP treatment, indicating that unlike *Cj* WT and *Av* K208N, heme II also transfers more electrons with the electrode. All TsdA enzymes investigated which have cysteine as a ligand to heme I therefore feature electroactivity which changes in the presence or absence of cysteine adducts.

4.5. Correlating Electroactivity and Cys Modification in *Cj* WT

The work presented above shows that in samples of *Cj* WT as prepared, Cys-138 has multiple post-translational modifications. Similar, but not identical modifications are found in the *Cj* N254K variant and *Av* WT, so it is proposed that they form in any TsdA enzyme with a heme I cysteine ligand. After redox cycling, the major species present in *Cj* WT is cysteine persulphide. Incubation with TCEP removes this and all other adducts, resulting in homogenous *Cj* WT where Cys-138 is unmodified. This species has a subtly different MCD spectrum to the as prepared enzyme. More striking is the difference in the number of electrons transferred by heme I (and possibly heme II) in PFE experiments comparing TCEP-treated and as-provided *Cj* WT. It is proposed that His/CysS⁻ ligated heme I does not readily transfer electrons with an IO-ITO electrode and His/Cys⁻ ligated heme I, by contrast, has reversible electron transfer. Heme II is unaffected by His/CysS⁻ ligation at heme I, however there is evidence that heme II transfers fewer electrons with an electrode than heme I when the latter has predominately His/Cys⁻ ligation.

If this observation is representative of a trend, it should be possible to correlate the relative abundance of post-translational modifications detected at Cys-138 using LC-MS with the areas of one or both pairs of peaks in voltammograms. To test this, *Cj* WT samples with different abundances of Cys-138 modifications were prepared with the assistance of Zuzana Bábková. In a number of experiments (examples given in Figure 4.10) *Cj* WT was incubated with TCEP to remove adducts, substrates to form adducts (see Chapter 5) or combinations of these. In some experiments chemical treatments were applied to the protein in solution prior to adsorption on IO-ITO electrodes, in which case an aliquot of this was incubated with iodoacetate and analysed by LC-MS as a control.

Alternatively, *Cj* WT was applied as-provided to the IO-ITO electrode and chemical treatments were applied to the enzyme film. PFE was then recorded in 50 mM HEPES, 50 mM NaCl, pH 7, typically over a range of scan rates (5 mV s⁻¹ to 100 mV s⁻¹).

The enzyme film was then treated with iodoacetate, recovered (see above, 4.4) and then analysed by LC-MS. Each voltammogram recorded featured two pairs of peaks centred on E_M values similar to those observed for all previous *Cj* WT coated electrodes. The notable difference between the voltammetry of each experiment was the areas of the low potential (N_{lo}) and high potential (N_{hi}) peaks, proportionate to the electroactivity of hemes I and II respectively. The theoretical lineshape for $n = 1$ processes (equation 1.2) was fitted to representative baseline-subtracted voltammograms ($v = 10$ mV s⁻¹) for each experiment and the average of the oxidative and reductive fitted areas for each pair of peaks was used as a measure of the heme I and heme II electroactive populations.

LC-MS mass peaks were then normalised so that the sum of the relative intensities of all peaks equalled 100% and each peak intensity represents the percentage of the bulk *Cj* WT population with that mass. These masses correspond to Cys-138 adducts as previously assigned (Table 4.1). For simplicity of analysis adducts were grouped into unmodified cysteine (Cys⁻, with or without carboxymethylation), cysteine persulphide (CysS⁻, with or without carboxymethylation) and higher mass cysteine adducts (CysSSX⁻) namely cysteine thiosulphonate and cysteine thioperoxosulphate (Table 4.1). A simple assumption is that depending on the status of Cys-138, each *Cj* WT monomer is either entirely electroactive, so that the area of the heme I voltammetric peak is proportional to the amount of that Cys-138 species present, or entirely inactive, so that no heme I signals can be assigned to the presence of that species at all.

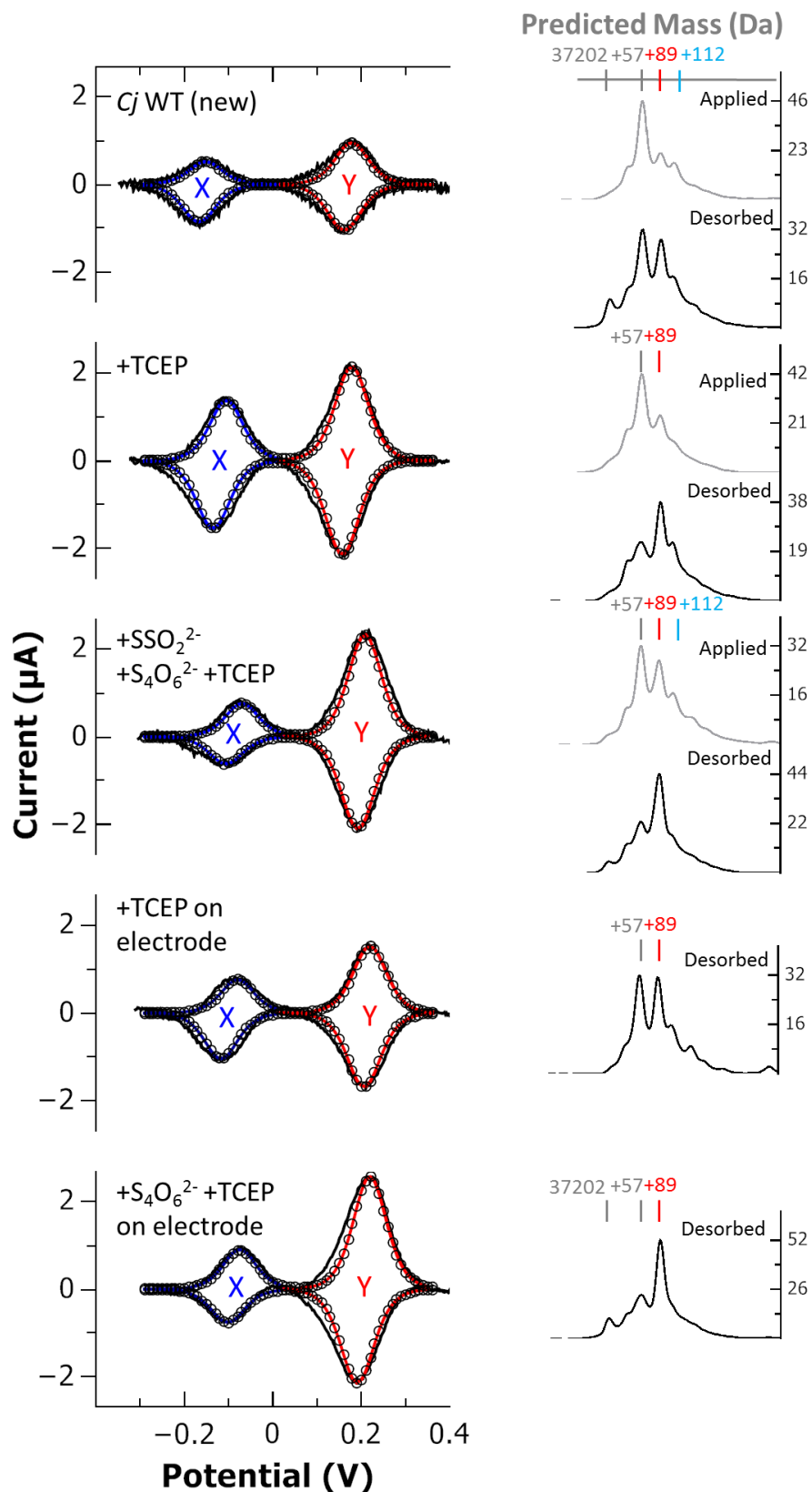


Figure 4.10 – Representative CVs and corresponding LC-MS of Cj WT films prepared with chemical agents. Baseline-subtracted CVs (black line) of Cj WT coated IO-ITO electrodes prepared as annotated. Each peak has been fitted to two predicted $n=1$ theoretical responses (red and blue lines) and the sum of these contributions (black circles). All data recorded in 50 mM HEPES, 50 mM NaCl, pH 7, $\nu = 10 \text{ mV s}^{-1}$, $T = 293 \text{ K}$. (Right) Mass spectra of stock solutions for voltammetry (upper panels) and desorbed protein (lower panels) incubated with 15 mM sodium iodoacetate. Samples were denatured for LC-MS by 10-fold dilution in 2% Acetonitrile, 0.1% Formic Acid. PFE recorded by Zuzana Bábková

Each permutation of each modification giving rise to active or inactive heme I was then plotted against the electroactivity of the film as follows. Electroactivity of modified forms of *Cj* WT was modelled from voltammograms in two ways. Both models assume there are two contributions to voltammograms giving rise to the two pairs of peaks (X and Y) observed (Figure 4.10). **Method A** assumes that when all of heme I (X) is active and gives rise to signals in voltammograms, none of heme II (Y) is active and *vice versa*. This model allows for the experimental observation that the peaks for heme I (X) can have a larger area than those of heme II (Y) (Figure 4.8, top). For method A, the electroactivity of heme I is expressed as the fitted area of heme I signals (N_x) divided by the total fitted electroactive area of the voltammogram (N_{tot}) expressed as a percentage. **Method B** assumes heme II is electroactive in both populations and the only difference is whether heme I is electroactive or not. Therefore, when heme I is fully electroactive, both hemes are active as with *Cj* C138M (Figure 3.6) and peaks in voltammograms are equal. For method B, the electroactivity of heme I is calculated from N_x divided by the area of heme II (N_y) expressed as a percentage.

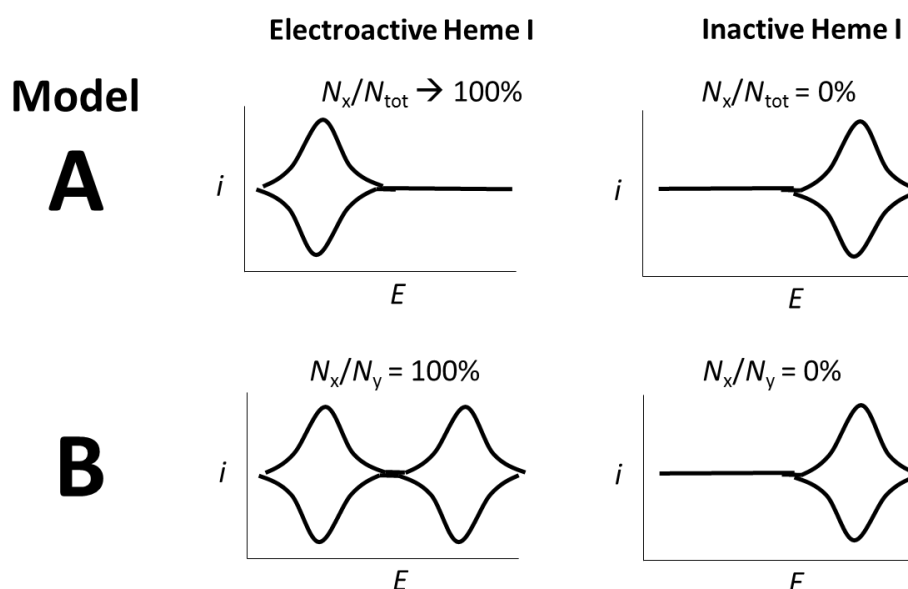


Figure 4.11 – Hypothetical models for the cysteine modification dependent electroactivity of *Cj* WT on IO-ITO electrodes. **A)** Assumes either heme I or heme II, but never both transfers electrons with an electrode for a given form of the enzyme. **B)** Assumes only electrons transferred by heme I are affected by cysteine modifications.

The percentage of electroactive heme I calculated from PFE using model A or B was then plotted against the LC-MS-determined percentage of each permutation of Cys-138 species present. The latter was either determined using LC-MS of the sample used to coat the IO-ITO electrode (Figure 4.12, right panels) or LC-MS of the desorbed enzyme (Figure 4.12, left panels). The strongest correlation between percentage of electroactivity and percentage of Cys-138

modification(s) is observed using method A, LC-MS of desorbed protein and with unmodified Cys⁻ as the only electroactive species (Figure 4.12, top left panel, red stars) with all other modifications resulting in inactive protein.

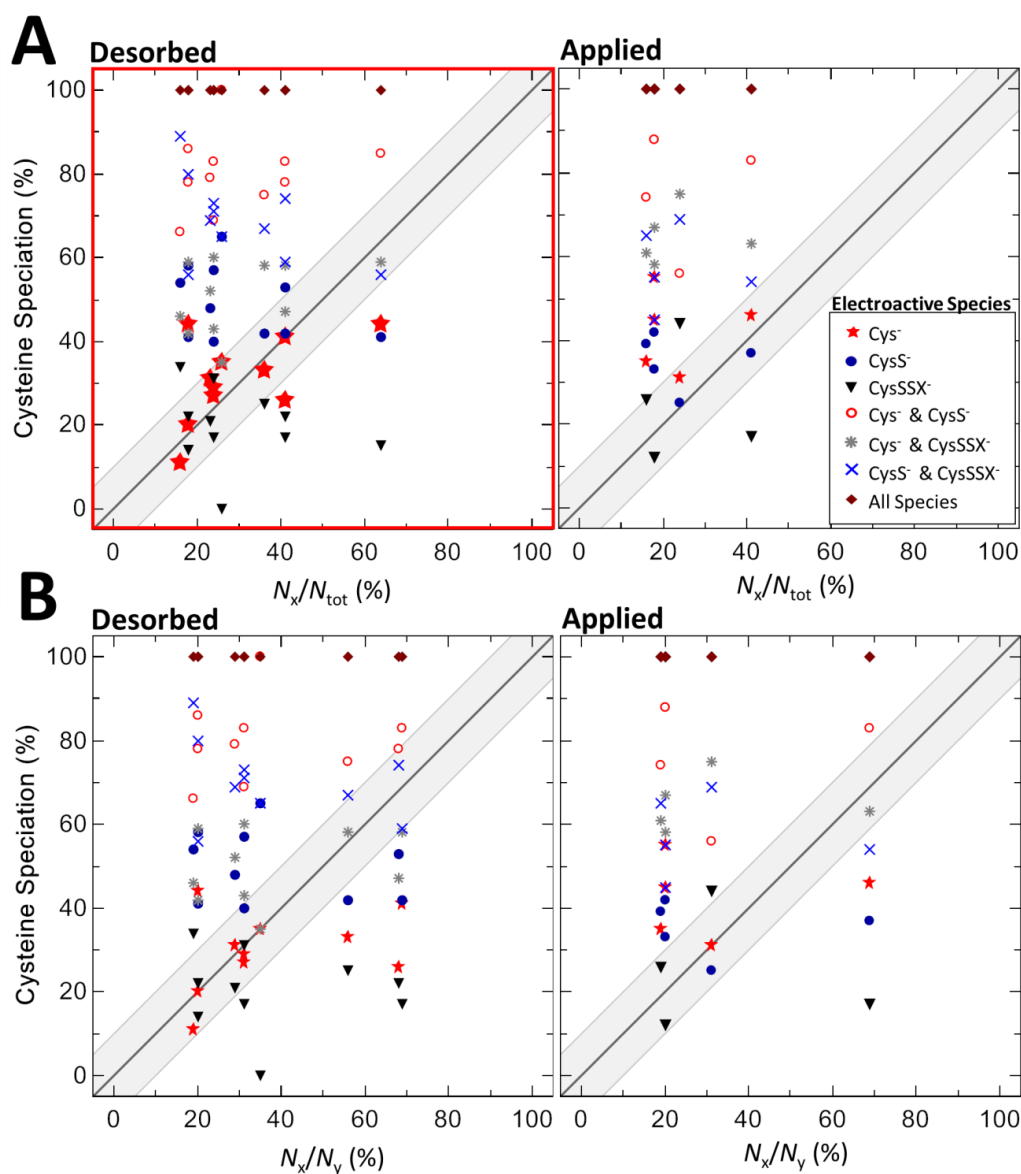


Figure 4.12 – Correlation of Cys-138 Modifications in *Cj* WT and heme I electroactivity. *Cj* WT samples were subject to chemical treatments intended to produce a range of Cys-138 modifications. The identity of these is calculated from relative intensity of LC-MS peaks from **(Left)** desorbed protein from IO-ITO electrodes following voltammetry or **(Right)** protein solutions used to coat electrodes. **A)** Heme I electroactive area (N_x) calculated as a percentage of total electroactive area (N_{tot}) from representative voltammograms **B)** Heme I electroactive area calculated as a percentage of heme II area (N_y). PFE recorded in 50 mM HEPES, 50 mM NaCl, pH 7, $v = 10 \text{ mV s}^{-1}$, $T = 293 \text{ K}$.

This suggests that when *Cj* WT has His/Cys⁻ ligation at heme I, heme I transfers electrons and heme II does not. When heme I has His/CysS⁻ or any other form of ligation, heme I does not transfer electrons and heme II does. Furthermore, this gives confidence that LC-MS of *Cj* WT

desorbed from the electrode is representative of the status of the enzyme film in PFE experiments.

4.6. Discussion

Correlating LC-MS and PFE data of chemically-treated *Cj* WT films supports the hypothesis that Cys-138 modifications affect electron transfer in *Cj* WT. Specifically only one heme transfers electrons with an IO-ITO electrode; when Cys-138 is unmodified, this is heme I, when Cys-138 is modified, this is heme II. By this model there is no inter-heme electron transfer in either form of the wild-type enzyme, despite the presumed close proximity of the TsdA hemes^{9,30,33}. All forms of *Cj* WT hemes present in the enzyme as-isolated are reduced by dithionite ($E \approx -500$ mV)⁹⁷ in solution, eliminating the possibility that a His/Cys⁻ ligated heme I simply has an E_M lower than the potential window for PFE, as is the case for SoxAX hemes proposed to have this ligation state^{49,93,100}. There is now clear evidence that both *Cj* WT hemes are capable of facile electron transfer with an IO-ITO electrode, even though this electroactivity is apparently mutually exclusive. It is therefore unlikely that heme I electron transfer is prevented simply by preferential orientation on the electrode surface (Figure 3.19) as it is unlikely that TCEP treatment would modify the surface of *Cj* WT and cause a large conformational change reversing the enzyme orientation. It is more likely that electron transfer to the TsdA hemes is instead controlled by factors other than distance. One rationalisation is that amino acid sidechains with partially unoccupied or conjugated orbitals within *Cj* WT, for example the conserved residues Tyr-161 and Trp-164, combine to provide a defined pathway for electron transfer through the protein (Figure 4.13). If Cys-138 thiol(ate) features in this pathway, it is possible to imagine a situation where the presence or absence of an additional sulphane sulphur atom, perhaps in combination with the flexibility of the cysteine sidechain, might somehow act as a switch for electron transfer through the protein depending on the size and orientation of this ligand and its interactions with surrounding residues. In variants where methionine or histidine replaces Cys-138, this path-limited electron transfer could either have been bypassed, or these larger residues might permit electron transfer to both hemes at once through perturbation of nearby residues.

In this model, dithionite or other chemical agents can still reduce both hemes regardless of the status of Cys-138 by diffusing directly to the hemes, bypassing the electron transfer path. Substrates would instead be expected to bind to the positively charged pocket⁵ in the vicinity of Cys-138 and only donate or accept electrons there. In this case, only His/Cys⁻ and not His/Cys^S ligated heme I is expected to participate in thiosulphate oxidation as the active site heme I is not available as an electron acceptor in the latter. This highly controlled electron transfer may have evolved in *Cj* TsdA to specifically limit or otherwise fine-tune the reactivity of heme I, similar to

how catalytic intermediates within the Sox enzyme cycle are bound to a persulphurated cysteine¹⁰¹.

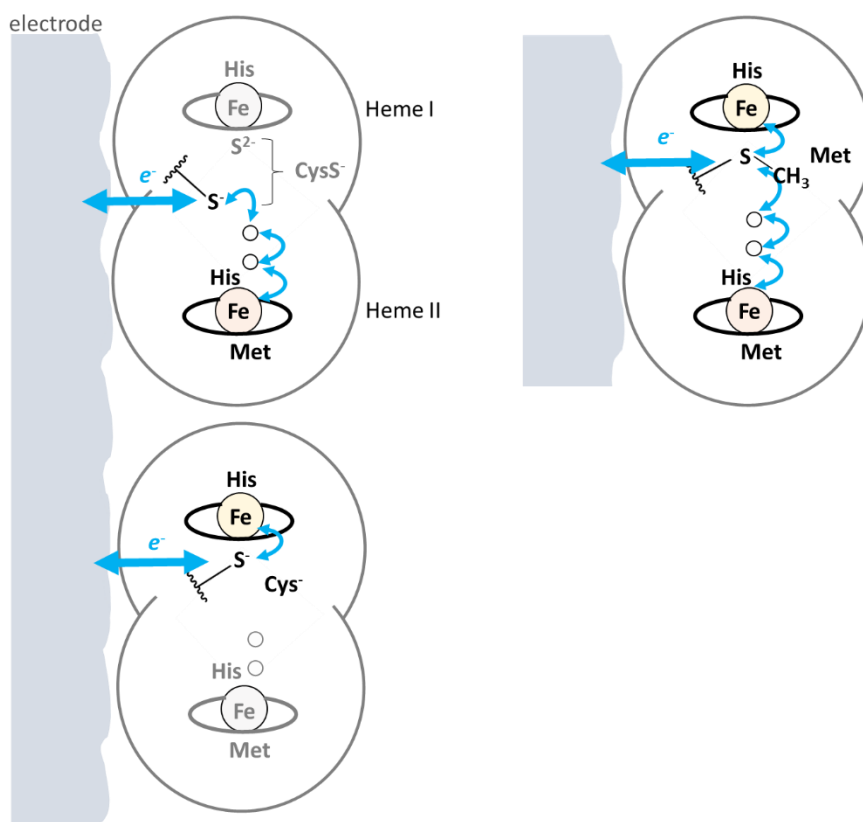


Figure 4.13 – Refined model for *Cj* WT electron transfer where persulphuration of Cys-138 could feature in a strictly controlled electron transfer path. Blue arrows show direction of electron transfer, black circles represent amino acid sidechains that provide a pathway for electron transfer. Hemes outlined in black are electroactive in voltammetry, grey hemes are not.

For the purpose of correlating Cys-138 modifications to heme I electroactivity, the analysis detailed above considers cysteine thio(peroxo)sulphonate identically to cysteine persulphide. Using this model it is difficult to reconcile how the cysteine thiosulphonate form of *Cj* WT has only one electroactive heme but can still act as a catalytic intermediate for a two-electron reaction. None of the desorbed *Cj* WT films have a large population of cysteine thio(peroxo)sulphonate, so one possibility is that this species has different electroactivity and simply breaks down to cysteine persulphide during redox cycling too rapidly have been accurately characterised in the experiments reported above. The above models also assume that E_M values for heme I (or II) are unaffected by cysteine modifications. Alternative descriptions are therefore possible such as the E_M of a modified form of heme I increasing to be equal or similar to that of heme II so that the signal Y in voltammograms features the electroactivity of more than one heme.

The following chapter reports on how substrates and substrate mimics were used in an attempt to prepare and characterise samples with larger populations of catalytically relevant or analogous Cys-138 adducts not expected to be competent as heme ligands which may give rise to more varied heme I environments.

5. Preparing and Characterising Catalytic Intermediates of *Cj* WT

PFE data recorded for *Cj* WT with and without the cysteine modifications found in the as-purified enzyme suggest that only one heme transfers electrons with IO-ITO electrodes at a time and inter-heme electron transfer is impossible, despite the $<14 \text{ \AA}$ distance between the hemes. If a two-electron reaction is catalysed by *Cj* WT, this suggests there must also be a form of the enzyme where electron transfer is possible to both hemes at once which has not been detected so-far. Replacing Cys-138 with methionine, or histidine at low scan rates, achieves this raising the possibility that the cysteine thiosulphonate catalytic intermediate proposed by Grabarczyk *et al.*⁵ might have similar electron transfer properties. As shown by the LC-MS presented in Chapter 4, some of Cys-138 is present as cysteine thiosulphonate in *Cj* WT as prepared, although this species only features in a small sub-population of monomers and readily decays to cysteine persulphide on an electrode. As such, experiments so-far are unlikely to feature enough of this species to accurately characterise its electroactive properties. One alternative to preparing *Cj* WT with more of this seemingly unstable species is to instead use an inhibitor of TsdA to form more stable analogous forms. If such a Cys-138 modification can be prepared in sufficient quantities, then this can be characterised to give insight into true catalytic intermediate(s).

Sulphite is a known inhibitor of TsdA enzymes¹⁴⁰, has a clear structural similarity to thiosulphate and has been resolved binding close to heme I in structures of *Av* TsdA⁹. This chapter presents mass spectrometry data which identified cysteine modifications formed in TsdA exposed to sulphite. Sulphite-reacted *Cj* WT was analysed by (magneto) optical spectroscopy and electrochemistry, these data are presented and it is proposed that this form of the enzyme is analogous to mechanistic intermediate(s). Similar experiments are then reported where cysteine modifications are formed by the presence of substrates. The data are discussed in terms of their effect on the TsdA hemes and their electroactivity. The appearance of previous voltammetry is then re-analysed with regards to the new findings of this chapter.

5.1. Catalytic Activity of TsdA.

Previous reports of the catalytic properties of TsdA proteins (Figure 1.4) are predominantly based on spectrophotometrically monitored solution activity assays^{5,9,31,32} although catalysis has also been investigated using PFE³⁰. The latter technique was also used to identify sulphite as an inhibitor of TsdA enzymes¹⁴⁰ and this section presents this unpublished work by Julia Kurth. To have confidence that TsdA films on IO-ITO electrodes are representative of the native-like protein, the results of catalytic PFE experiments using these are also reported. Following this, data from spectrophotometrically-monitored solution assays of TCEP-incubated TsdA enzymes are presented that provide evidence that cysteine modifications and the different relative

electroactive heme populations detected in PFE experiments have some relation to the catalytic activity of these enzymes.

5.1.1. PFE Investigations of *Cj* WT Catalysis and Sulphite Inhibition

The catalytic activity of *Cj* WT has been previously investigated using cyclic voltammetry of protein films adsorbed on pyrolytic graphite edge (PGE) electrodes³. Thiosulphate and tetrathionate independently added to separate protein films give rise to catalytic currents (Figure 5.1). A rotating disc electrode (RDE) system was used to provide constant convection of buffer-electrolyte across the protein-coated electrode surface to eliminate the effects of diffusion⁵⁷.

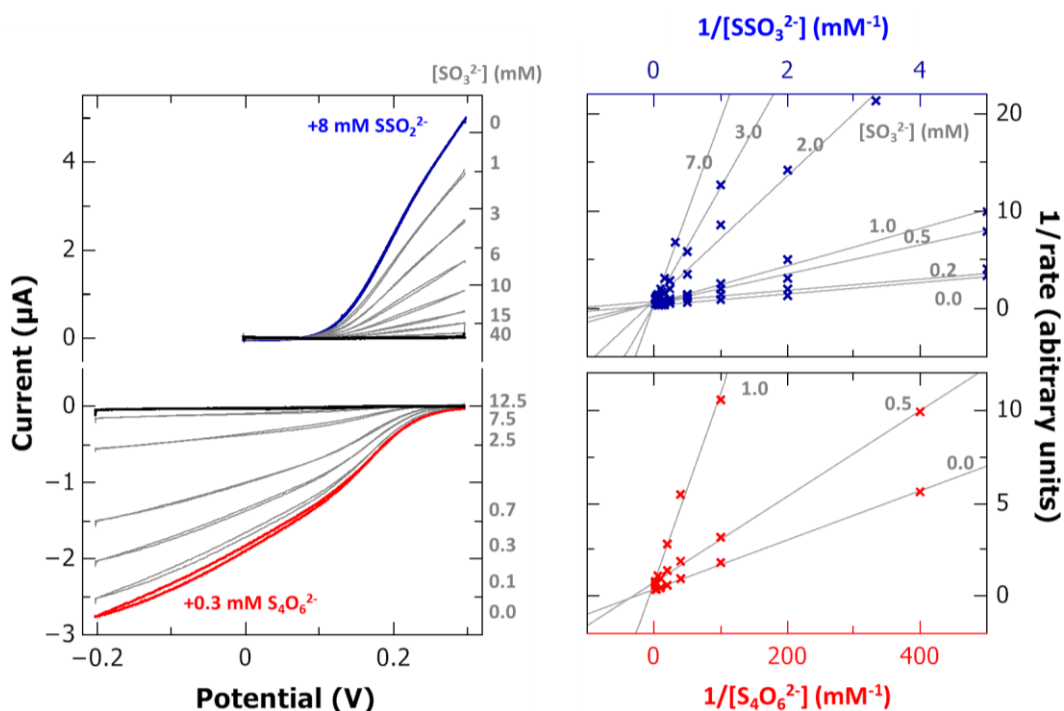


Figure 5.1 – Sulphite inhibition of tetrathionate reduction (top) and thiosulphate oxidation (bottom) in *Cj* WT. **Left**) Cyclic voltammograms of *Cj* WT films on PGE electrodes in the presence of 0.3 mM tetrathionate (red line) or 8 mM thiosulphate (blue line) and indicated concentrations of sulphite. **Right**) Similar PFE experiments performed in the indicated sulphite concentrations and varying tetrathionate (red crosses) or thiosulphate (blue crosses) concentrations indicate K_M increases with increasing sulphite concentration without affecting i_{max} and therefore inhibition is competitive. All experiments performed by Julia Kurth using *Cj* WT-coated PGE electrodes in 100 mM ammonium acetate, 50 mM NaCl, pH 5, $\omega = 500$ rpm, $\nu = 10$ mV s⁻¹, T = 315 K.

This catalytic current (i_{cat}), is proportional to the reaction velocity and was used to obtain a Michaelis constant for tetrathionate reduction ($K_M = 72 \pm 1 \mu\text{M}$), comparable to that observed for solution assays and 10-fold less ($K_M = 2.5 \pm 0.3$ mM) in the case of thiosulphate oxidation³². Sulphite (SO_3^{2-}) is a mimic of thiosulphate (SSO_3^{2-}) and lowers catalytic currents to a similar extent for both thiosulphate oxidation ($K_i = 1 \pm 0.1$ mM, Figure 5.1, upper left) and tetrathionate

reduction ($K_i = 4 \pm 0.8$ mM, Figure 5.1, lower left), consistent with sulphite inhibition of both reactions. Experiments performed using varying substrate and sulphite concentrations (Figure 5.1, right) determined that sulphite raises the K_M for the interconversion of thiosulphate and tetrathionate in either direction without affecting i_{max} (proportionate to v_{max}). Sulphite is therefore a competitive inhibitor of both thiosulphate oxidation and tetrathionate reduction in *Cj* WT. Based on this observation, it is likely sulphite may bind in an analogous way to thiosulphate in the TsdA active site, but does not progress any further through the catalytic cycle. As such, it may be possible to prepare a sulphite-bound species which is stable for a long enough time that spectroscopy and electrochemistry can be used to characterise this form.

5.1.2. Catalytic Activity of TsdA-Coated IO-ITO Electrodes.

Catalytic activity of TsdA enzymes is only expected when these are in a native-like form, so to have confidence that TsdA films on IO-ITO electrodes are not perturbed or denatured, aliquots of thiosulphate were titrated into the buffer-electrolyte during cyclic voltammetry experiments (Figure 5.2, blue lines). With the first thiosulphate addition a signal characteristic of a diffusing redox couple centred on $E_M \approx +200$ mV in solution appeared, which became more intense with each subsequent addition. This suggests the catalytic potential for thiosulphate oxidation on IO-ITO is equivalent to that previously detected on PGE electrodes³⁰.

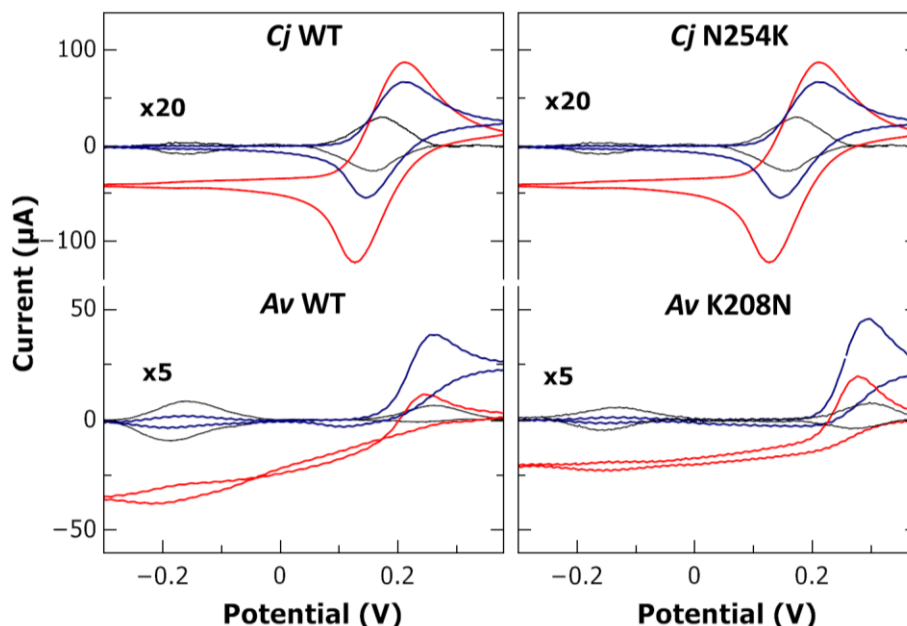


Figure 5.2 – Catalytic activity of TsdA on IO-ITO electrodes. Representative cyclic voltammograms of TsdA enzymes and variants as annotated in the absence of substrate (black line) or in the presence of 1.2 mM thiosulphate (blue line) or 1.2 mM tetrathionate (red line). All data recorded in 50 mM HEPES, 50 mM NaCl, pH 7, $v = 10$ mVs⁻¹, $T = 293$ K.

At higher potentials, the current does not return to baseline values, instead this oxidative current becomes more positive as more thiosulphate is added. These observations are consistent with catalytic thiosulphate oxidation by *Cj* WT. The negative peak centred on the E_M of the thiosulphate/tetrathionate couple (+198 mV)³ indicates re-reduction of some tetrathionate produced at the electrode, suggesting this product is not completely diffusing from the electrode over the timescale of the experiment. Overcoming the rate of diffusion would result in a sigmoidal voltammogram typical of a two-electron process¹⁴¹ (e.g. red and blue lines in the left panel of Figure 5.1), however this does not seem possible under the experimental conditions employed. Diffusion limitation may result from using a stationary electrode with only modest stirring or limited substrate access to a dense electroactive film on through a porous electrode material⁸⁴. The rate of substrate diffusion through mesoporous IO-ITO is likely to be slower than in solution, limiting the availability of substrate and resulting in the clearly diffusion-limited catalytic currents. There is also the possibility that only the enzyme molecules closest to the surface of the electrode undergo catalysis, converting all molecules of substrate and preventing them from diffusing any further into the electrode¹⁴². Catalytic signals also appear when the buffer-electrolyte is changed and tetrathionate is introduced into fresh buffer-electrolyte (Figure 5.2, red lines). In this case there is a negative current at potentials lower than $E_M \approx +200$ mV consistent with diffusion-limited tetrathionate reduction.

Over the range of substrate concentrations used v_{max} is never reached (Figure 5.3, black circles). Although the accurate determination of K_M values is not possible, it is clear that these are higher on the IO-ITO electrodes than in solution. From solution assays the K_M for thiosulphate oxidation is 0.3 mM and tetrathionate reduction is $K_M = 0.1$ mM³². The maximum turnover recorded in the presence of 1.2 mM thiosulphate is 8 s⁻¹, 100-fold less than k_{cat} determined by solution assays. In the presence of 1.2 mM tetrathionate there is a turnover of 23 s⁻¹, also ~100-fold less than k_{cat} . It is difficult to interpret these values due to likely diffusion limitations noted above. In addition catalytic activity is likely to be lower than in previously reported solution assays as the latter were conducted at pH values (pH 5.0 for *Av* TsdA, pH 6.5 or 5.0 for *Cj* TsdA) and temperatures ($T = 303$ K for *Av* TsdA, $T = 315$ K for *Cj* WT) optimal for catalytic activity^{5,9,32}, whereas all catalysis measured here has been conducted at pH 7, $T = 293$ K for consistency and to preserve protein films. Nevertheless, the presence of measurable catalysis is clear.

The same experiments were performed with ***Av* WT**, ***Cj* N254K** and ***Av* K208N**. All enzymes gave rise to clear, diffusion-limited catalytic currents in the presence of thiosulphate and tetrathionate. *Cj* N254K and *Av* K208N both have decreased thiosulphate oxidation activity relative to *Cj* WT, similar to their behaviour in solution assays. *Av* WT has a turnover of 2 s⁻¹ in the presence of 1.2 mM thiosulphate, 1000-fold less than k_{cat} in solution⁵ consistent with much lower

activity observed for this enzyme at the experimental pH 7 compared to pH 5 in previously reported solution assays⁹ and unpublished PFE experiments¹⁴⁰. Tetrathionate reduction by *Cj* N254K, *Av* K208N and *Av* WT on IO-ITO is approximately 10-fold less than k_{cat} in solution, suggesting the activity of these variants is limited in a similar way to that observed for *Cj* WT.

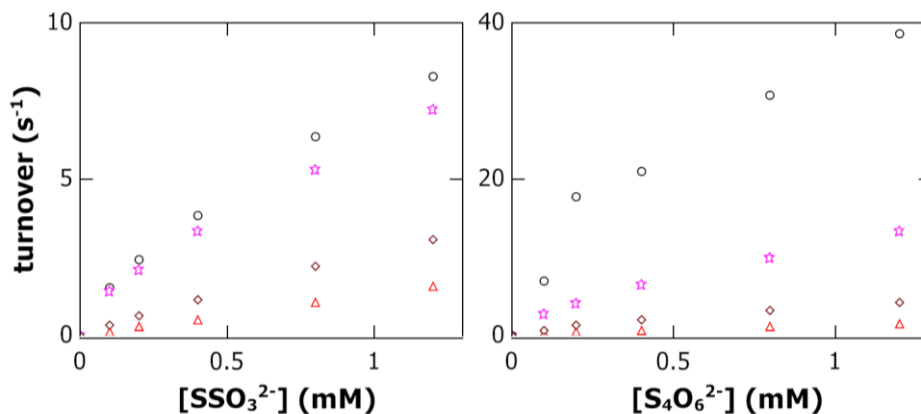


Figure 5.3 –Catalytic turnover for TsdA-coated IO-ITO electrodes. Catalytic turnover for thiosulphate oxidation (left) and tetrathionate reduction (right) by *Cj* WT (black circles), *Cj* N254K (pink stars), *Av* WT (red triangles), *Av* K208N (maroon diamonds) on IO-ITO electrodes calculated from peak catalytic currents, using half total moles of electrons transferred from integrated peak areas of voltammograms to indicate total moles of TsdA. All data recorded in 50 mM HEPES, 50 mM NaCl, pH 7, $\nu = 10 \text{ mVs}^{-1}$, $T = 293 \text{ K}$.

All TsdA enzymes featured in this thesis which are active in solution assays^{9,32} also display catalytic currents when adsorbed to IO-ITO electrodes. This gives confidence that some of the IO-ITO adsorbed enzyme is present in a native-like form. Unless this native-like population is too small to give rise to Faradaic currents in the absence of substrates, non-turnover voltammetry of TsdA-coated IO-ITO electrodes is reporting on the electroactivity of this native-like form and where signals are heterogenous, it is likely that the enzyme population is also. The diffusion limitation observed also implies that chemical treatments (eg. TCEP or sulphite incubation) are not able to access all of the adsorbed enzyme molecules. Therefore, such treatments are likely to be more effective when performed on a sample of TsdA in solution which is subsequently used for electrode coating.

5.1.3. The Effect of Cysteine Adducts on TsdA Catalytic Activity.

LC-MS of wild-type TsdA enzymes suggests that these exist in solution with multiple sub-populations with different cysteine modifications. If all of these can be interconverted in the presence of substrate it would be expected that as prepared enzymes with adducts and TCEP treated enzymes without them would feature identical catalytic activity. Alternatively, PFE

suggests that cysteine modifications are linked to the electroactivity of the TsdA hemes. If this is a feature of the native enzyme and is not just a consequence of adsorbing to IO-ITO, it would be expected that as prepared and TCEP-treated enzymes would have some difference in catalytic activity. To investigate this, spectrophotometrically-monitored solution assays were performed to monitor thiosulphate oxidation by TsdA with the assistance of visiting researcher Martin Ženka and Erasmus student Fabien Chappert. *Cj* and *Av* TsdA were assayed either as prepared or in the presence of equimolar TCEP, expected to remove any initial cysteine adducts present and become oxidised to inactive TCEPO in the process (Figure 4.1, A). PFE was not used as insufficient TsdA adsorbs to PGE electrodes for non-turnover currents that could be used to quantify electroactive TsdA population³ and the IO-ITO catalytic response is not free of mass transport limitation.

Activity of as-provided and TCEP-treated TsdA was assayed under anaerobic conditions using ferricyanide as a chromophore and electron acceptor. Catalytic turnover (Figure 5.4) for thiosulphate oxidation was calculated from the initial change in absorbance at 420 nm where ferricyanide, but not ferrocyanide, absorbs. Initial concentrations were 1 mM ferricyanide and 100 nM TsdA in 50 mM HEPES, 50 mM NaCl, pH 5 at T = 297 K to which varying concentrations (0.0675 to 18 mM) of substrate were added. Turnover at each thiosulphate concentration for *Av* WT is well-described by the Michaelis-Menten equation which has been normalised to TsdA concentration ([TsdA]):

$$TOF = \frac{k_{cat}[TsdA]}{(K_M + [TsdA])} \quad \text{Equation 5}$$

where *TOF* denotes turnover frequency in s⁻¹, *k_{cat}* is the maximum turnover frequency and *K_M* is the Michaelis constant representative of the affinity of the enzyme for substrate. *Cj* WT and *Cj* N254K data show evidence of substrate inhibition and the data for these is well-described the variant Michaelis-Menten equation featuring a dissociation constant for inhibition (*K_I*):

$$TOF = \frac{k_{cat}[TsdA]}{(K_M + [TsdA]) \left(\frac{1 + [TsdA]}{K_I} \right)} \quad \text{Equation 5.2}$$

Lines describing the recorded data (Figure 5.4, solid and dashed lines) have *K_M*, *k_{cat}* and where relevant *K_I* values summarised in Table 5.1. *K_M* falls within an order of magnitude for thiosulphate oxidation in all enzymes as-provided (0.4 to 0.7 mM) as expected from previous reports (0.1 mM to 0.3 mM)^{5,9,32}. *Cj* WT (130 s⁻¹) and *Av* K208N (160 s⁻¹) also have similar values for *k_{cat}*, consistent with the similar heme electroactivity observed for these in PFE (Figure 3.14).

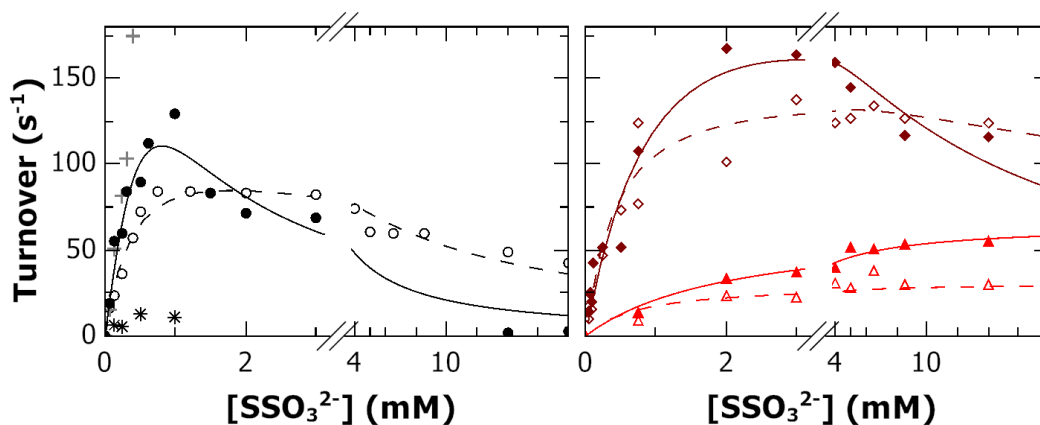


Figure 5.4 – Solution thiosulphate oxidation assays of TsdA enzymes as prepared (open symbols) or following TCEP treatment (closed symbols). *Cj* WT (left panel, black circles), *Av* WT (right panel, red triangles) and *Av* K208N (right panel, maroon diamonds) were assayed without (open symbols) or with (closed symbols) 100 nM TCEP by monitoring ΔA_{420} of 1 mM potassium ferricyanide after the addition of 0.0675 to 18 mM thiosulphate to 100 nM TsdA in 50 mM HEPES, 50 mM NaCl, pH 7, T = 293 K. Lines indicate the Michaelis-Menten equation with or without substrate inhibition fitted to data for as-provided enzymes (solid lines) or TCEP-treated enzymes (dashed lines) in QTI plot summarised in Table 5.1. Turnover data are also shown for ‘fresh’ *Cj* WT (left panel, grey crosses) and *Cj* WT after incubation with sulphite and ferricyanide (left panel, black stars). *Cj* TsdA experiments performed with assistance from Martin Ženka, *Av* TsdA experiments performed by Fabien Chappert.

Av WT (30 s^{-1}) has a k_{cat} value 4 to 5 times lower than *Cj* WT and *Av* K208N consistent with this enzyme being much less active at pH 7, T = 293 K than under optimised catalytic conditions, where it has a 10 to 100-fold greater k_{cat} for thiosulphate oxidation^{5,30}. Unlike *Av* WT, *Cj* WT ($K_{\text{I}} = 7.1 \text{ mM}$) and *Av* K208N ($K_{\text{I}} = 57 \text{ mM}$) show previously unreported evidence of substrate inhibition, although in the latter variant this is very modest and in neither case is $K_{\text{I}} < K_{\text{M}}$.

Table 5.1 – Catalytic parameters for thiosulphate oxidation by TsdA variants. Calculated from spectrophotometrically-monitored enzyme activity assays. ΔA_{420} of 1 mM potassium ferricyanide was monitored after the addition of 0.0675 to 18 mM thiosulphate to 100 nM TsdA in 50 mM HEPES, 50 mM NaCl, pH 7, T = 293 K.

Variant	K_{M} (mM)	k_{cat} (s^{-1})	K_{I} (mM)
<i>Cj</i> WT	0.4 ± 0.1	130 ± 10	7.1 ± 0.1
<i>Cj</i> WT +TCEP	1.6 ± 0.1	560 ± 10	0.4 ± 0.1
<i>Av</i> WT	0.7 ± 0.4	30 ± 2	-
<i>Av</i> WT +TCEP	2.0 ± 0.3	65 ± 3	-
<i>Av</i> K208N	0.4 ± 0.1	160 ± 10	57 ± 2
<i>Av</i> K208N +TCEP	1.3 ± 0.5	290 ± 10	8 ± 4

In the presence of TCEP, K_M increases slightly (3-4 times) however k_{cat} also doubles for *Av* WT and K208N and quadruples for *Cj* WT. This is consistent with there being an increase in the concentration of catalytically active enzyme in the presence of TCEP, which for the wild-type enzymes correlates approximately to the proportion of Cys-138 or Cys-96 expected to be present in these samples before and after TCEP treatment (Figure 4.5, right panels, Figure 4.8 lower right panels). TCEP incubation also causes a 7-fold decrease in K_I for *Av* K208N or a 18-fold decrease in K_I for *Cj* WT, which in the latter enzyme now makes $K_I < K_M$. TCEP treatment of all TsdA enzymes investigated therefore increases activity, but also increases substrate inhibition. During thiosulphate oxidation assays of *Cj* WT it was also apparent that enzyme assayed shortly after thawing from an aliquot of the as-purified protein has much greater activity (Figure 5.4, grey crosses) than the same protein stock assayed after 60+ minutes. Previous observations suggest purified protein samples accumulate cysteine modifications over time (see above, 4.4). It may be possible that immediately-thawed enzyme is initially free of all modifications and is therefore more active. It may alternatively be possible that some optimal proportion of cysteine modifications in the bulk enzyme population provides both high activity and protection from substrate inhibition.

Activity assays were also performed using *Cj* WT which had been incubated with excess sulphite and ferricyanide before being buffer exchanged extensively to remove unbound sulphite (Figure 5.4, black stars). This form of the enzyme has negligible catalytic activity, so it is likely that in addition to the competitive inhibition observed previously, extensively sulphite-treated *Cj* WT is incapable of further reaction with thiosulphate. This is rationalised if sulphite incubation of *Cj* WT modifies Cys-138 in a stable manner and the following section explores this possibility.

5.2. LC-MS of *Cj* WT Reveals Cys-138 Covalent Modification by Sulphite.

LC-MS of ***Cj* WT** incubated with two equivalents of sulphite (Figure 5.5, A) was recorded using the methodology detailed previously (see above, 4.2). The mass spectrum has two clear peaks, the more intense (60% of the sample) has a mass +113 Da greater than predicted, consistent with Cys-138 modified to cysteine thiosulphonate. The remaining peak (40% of the sample) has a mass +57 Da greater than the predicted, consistent with unmodified cysteine after carboxymethylation. Cysteine thiosulphonate is expected if persulphurated Cys-138 forms a covalent bond to one molecule of sulphite and the fact that this is the only obvious species that is likely to have formed from reaction with sulphite is consistent with cysteine persulphide being more nucleophilic than unmodified cysteine. When ferricyanide was included to fully oxidise a parallel sample in the presence of excess sulphite, the mass spectrum has one major peak (70% of the sample) at +81 Da, consistent with Cys-138 modified to cysteine sulphonate. The latter

species is expected if unmodified Cys-138 forms a covalent bond with one molecule of sulphite in an analogous manner to cysteine thiosulphonate formation observed after thiosulphate incubation of Av WT⁵. This species may also displace other Cys-138 modifications through disulphide exchange to explain how cysteine thiosulphonate is now no longer present.

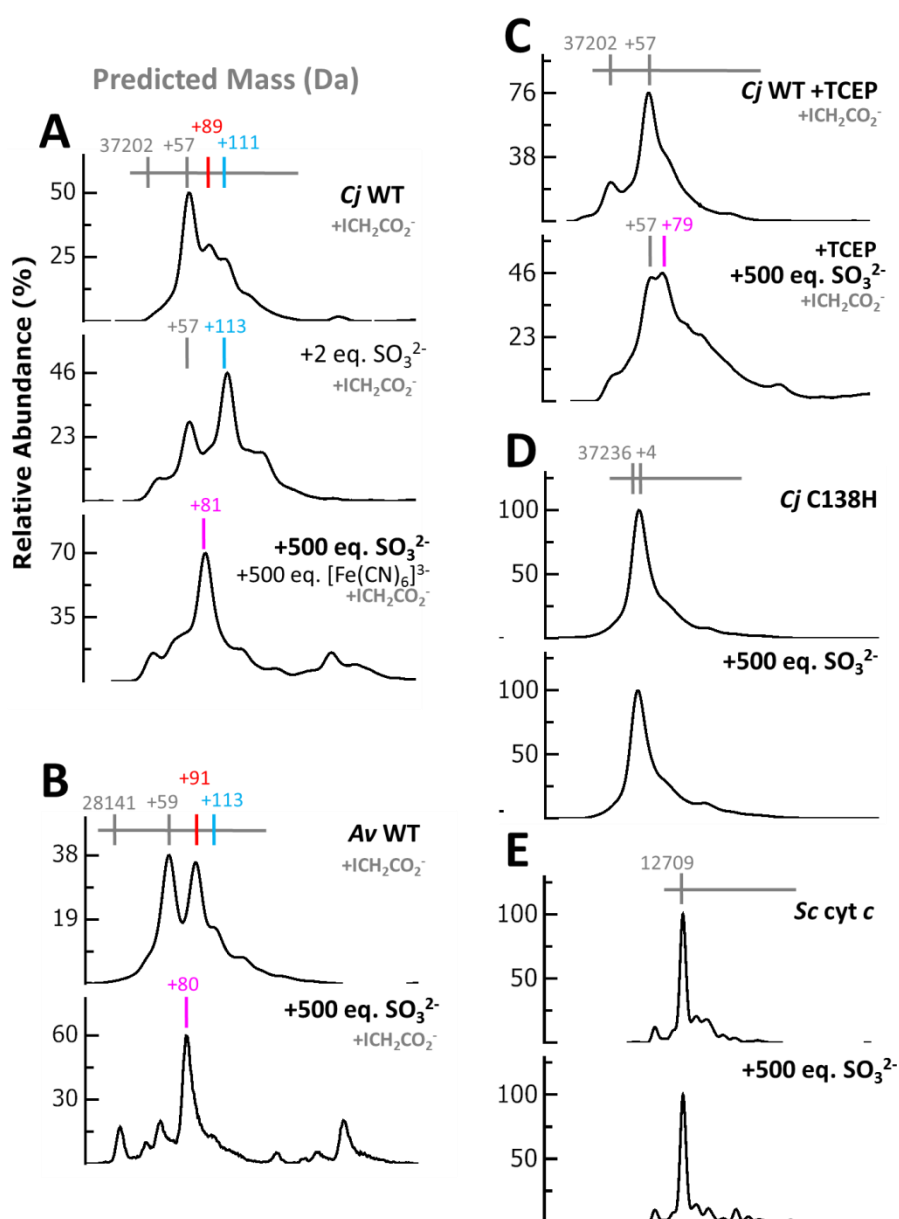


Figure 5.5 – Deconvoluted Mass Spectra of TsdA proteins with sulphite. 30-50 μ M TsdA or cyt c in pH 7 50 mM HEPES, 50 mM NaCl incubated for 1 hour with sodium sulphite (as annotated) followed by incubation with 15 mM sodium iodoacetate. Samples were denatured for LC-MS by 10-fold dilution in 2% Acetonitrile, 0.1% Formic Acid.

When *Cj* WT is first incubated with TCEP to remove all pre-existing cysteine modifications and is then incubated with excess sulphite (Figure 5.5, C), the mass spectrum has two major peaks of approximately equal intensity (each 46% of the sample). One peak has a mass increase of +57 Da

indicating unmodified protein which has been carboxymethylated and the other peak has a +79 Da mass increase consistent with sulphonation of Cys-138. The mass increases resulting from *Cj* WT incubation with sulphite as well as all other proteins and substrates investigated in this chapter are summarised in Table 5.2.

Table 5.2 – Composition of cysteine modifications in TsdA samples as-provided and after treatment with substrates and inhibitors. Samples were prepared as indicated in pH 7 50 mm HEPES, 50 mm NaCl before incubation in 15 mm sodium iodoacetate and denaturation in 10-fold dilution in 2% Acetonitrile, 0.1% Formic Acid. Cysteine (persulphide) carboxymethylate and unmodified cysteine (persulphide) are proposed to originate from the same species in solution.

Sample	Relative Abundance (%)				
	Cys ⁻	Cys-S ⁻	Cys-SO ₃ ⁻	Cys-SSO ₃ ⁻	Cys-SSSO ₃ ⁻
Mass Increase (Da)	+0, +57	+32, +89	+80	+112	+144
<i>Cj</i> WT	50	30	-	20	-
<i>Cj</i> WT +SO ₃ ²⁻	40	-	-	60	-
<i>Cj</i> WT +SSO ₃ ²⁻	-	100	-	-	-
<i>Cj</i> WT +S ₄ O ₆ ²⁻	-	6	-	44	50
<i>Cj</i> WT +TCEP	100	-	-	-	-
<i>Cj</i> WT +TCEP +SO ₃ ²⁻	54	-	46	-	-
<i>Cj</i> WT +TCEP +SSO ₃ ²⁻	56	44	-	-	-
<i>Cj</i> WT +TCEP +S ₄ O ₆ ²⁻	54	46	-	-	-
<i>Av</i> WT	38	36	-	16	8
<i>Av</i> WT +SO ₃ ²⁻	20	20	60	-	-
<i>Av</i> WT +SSO ₃ ²⁻	16	62	-	22	-
<i>Av</i> WT +S ₄ O ₆ ²⁻	14	24	-	62	-

To be confident that all mass increases in the presence of sulphite are due to modification of Cys-138 or Cys-96, ***Cj* C138H** which is lacking free cysteines, was also incubated with excess sulphite (Figure 5.5, D). There was no detectable change in the mass of the single peak deconvoluted before or after sulphite incubation, ruling out the adventitious formation of adducts with other residues. Similarly, *Saccharomyces cerevisiae* cytochrome *c* (*Sc* cyt *c*) which has a single free cysteine far from the single *c* heme in this protein¹⁴³, was also incubated with excess sulphite

(Figure 5.5, E). There is no detectable mass change in the single peak for this protein, suggesting that the formation of cysteine adducts is due to the reactivity of TsdA enzymes and is not simply sulphur chemistry that would occur at any free cysteine residue. **Av WT** was also incubated with excess sulphite (Figure 5.5, B) and the resulting sample has a single major peak (60% of the sample) with a +81 Da mass increase, consistent with sulphonation also occurring at Cys-96 in this enzyme and confirming that covalent modification of the heme I cysteine ligand is not unique to *Cj* TsdA.

5.2.1. (Magneto) Optical Spectroscopy of Sulphite-Bound *Cj* WT.

LC-MS data is consistent with the reaction of both *Cj* WT and *Av* WT with sulphite forming cysteine (thio)sulphonate at their heme I cysteine ligands. To investigate the effects of this reaction on the TsdA hemes, samples of *Cj* WT and *Av* WT were incubated with excess sulphite in solution and the electronic absorbance was monitored over time (Figure 5.6). After 1 hour, sharp, intense $\alpha\beta$ bands consistent with low-spin ferrous heme are visible in the spectrum of both proteins and there is a broad low-intensity band now present at ~ 630 nm consistent with high-spin ferric heme. The intensity at 552 nm was monitored over the incubation time as an approximation of overall heme reduction. The final intensity of the $\alpha\beta$ peaks for sulphite-incubated *Cj* WT (*Av* WT) is $\sim 80\%$ ($\sim 70\%$) of that of ascorbate-reduced protein, implying that less than one heme has been reduced, although hemes I and II are unlikely to have similar contributions to the extinction coefficient, so unambiguous assignment is not possible from electronic absorbance alone.

The change in extinction coefficient over time at 552 nm has a good fit to two exponential equations, suggesting that two first-order processes are occurring, for *Cj* WT there is one 'fast' ($k_1 = 3 \text{ s}^{-1}$) and one 'slow' ($k_2 = 440 \text{ s}^{-1}$). For *Av* WT, there is no 'fast' process, one of the first-order processes occurs at a similar 'slow' rate ($k_1 = 350 \text{ s}^{-1}$) and there is a slower process still ($k_2 = 2500 \text{ s}^{-1}$). Reduction of the TsdA hemes is consistent with the formation of a disulphide bond between the active site cysteine and sulphite, releasing two electrons and forming a cysteine (thio)sulphonate. This modified cysteine is likely to be displaced as a heme ligand by solvent and this could explain the appearance of high-spin ferric heme in the spectra of both proteins after 1 hour. Although this reaction is expected to release two electrons, full reduction of the protein is not observed, this feature of the results is discussed below.

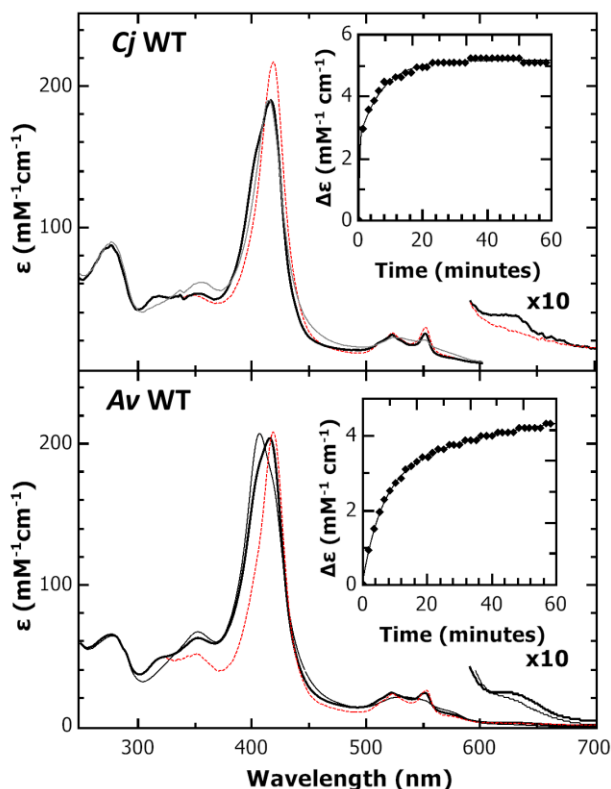


Figure 5.6 – Electronic absorbance spectra of TsdA before and after sulphite incubation. 66 μM *Cj* WT or 131 μM *Av* WT as prepared (grey line) was incubated with 1.5 mM sodium sulphite for 60 minutes (black line) under anaerobic conditions (<10 ppm O_2). *Cj* WT or *Av* WT incubated with 1.5 mM sodium ascorbate (dotted red line) is shown for comparison. **(Inset)** Change in extinction coefficient of 552 nm monitored over time fitted to two first order processes with $X = 2.6 \text{ M}^{-1} \text{ cm}^{-1}$, $k_1 = 3 \text{ s}^{-1}$ and $X = 3.6 \text{ M}^{-1} \text{ cm}^{-1}$, $k_2 = 440 \text{ s}^{-1}$ for *Cj* WT and $X = 2.6 \text{ M}^{-1} \text{ cm}^{-1}$, $k_1 = 350 \text{ s}^{-1}$ and $X = 2.0 \text{ M}^{-1} \text{ cm}^{-1}$, $k_2 = 2500 \text{ s}^{-1}$ for *Av* WT. Samples are in 50 mM HEPES, 50 mM NaCl pH* 7 in D_2O , $T = 293 \text{ K}$.

To interrogate the sulphite-incubated form of TsdA further, MCD spectra were recorded of *Cj* WT samples prepared in the same way. The UV/visible MCD spectrum of *Cj* WT incubated anaerobically with excess sulphite (Figure 5.7, black lines, upper panels) features a sharp derivative signal at 551 nm characteristic of low-spin ferrous heme. The peak-to-trough intensity of this feature is $320 \text{ M}^{-1} \text{ cm}^{-1} \text{ T}^{-1}$ indicating that $\sim 80\%$ of one heme has been reduced. Consistent with this, the His/Met CT_{LS} band at 1820 nm present in oxidised *Cj* WT is now absent. The His/Cys $^-$ CT_{LS} band which resolves at 1230 nm in *Cj* WT now only has 50% of the intensity it had prior to sulphite incubation. From the intensity of the 551 nm band it is clear that this heme population has not been reduced; however there is a high-spin ferric CT_2 band present at 636 nm consistent with His/ H_2O ligated heme⁴⁷. The corresponding His/ H_2O CT_1 band in the nIR region coincides with the His/Cys $^-$ CT band and is not clearly resolved. A low-intensity band is also present at 1530 nm, which is typical of low-spin, ferric heme with bis-nitrogenous co-ordination. As there are no obvious nitrogenous residues likely to provide this ligand in the pocket of hemes I or II this band is left unassigned.

Sulphite incubated *Cj* WT was then reoxidised with ferricyanide and from the UV/visible MCD it is clear that all traces of ferrous heme have now been eliminated (Figure 5.7, black lines, lower panels). In the nIR region, the ferrous His/Met band at 1820 nm has reappeared at the same intensity as the oxidised protein without sulphite incubation. The 1230 nm His/Cys⁻ CT_{LS} band is completely absent, replaced by a bisignate feature at 1120 nm consistent with the CT₁ band of high-spin, ferric heme with His/H₂O ligation⁴⁷. The corresponding CT₂ band is present at 636 nm and the trough at 580 nm assigned to low-spin, ferric heme with cysteine persulphide ligation (Figure 4.7) is absent.

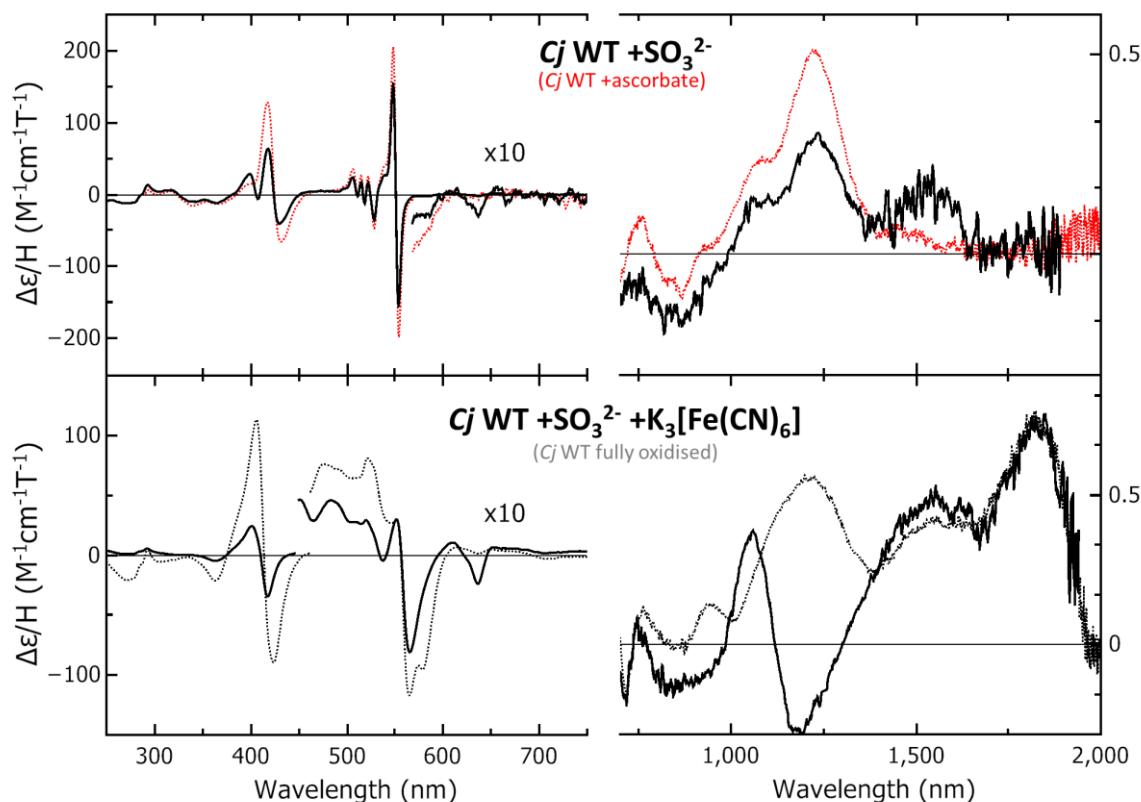


Figure 5.7 – MCD of sulphite-treated *Cj* WT. Room-temperature (left) UV/visible and (right) nIR MCD spectra of **(Top)** 34 μM (250-700 nm) and 104 μM (450-2000 nm) *Cj* WT incubated with 1.5 mM sodium sulphite (thick line) and 17.6 μM (250-450 nm), 163 μM (450-700 nm) and 123 μM (700-2000 nm) *Cj* WT incubated with 1.5 mM sodium ascorbate (red dashed line). **(Bottom)** 46 μM (250-450 nm), 144 μM (450-700 nm) and 109 μM (450-2000 nm) *Cj* WT incubated with 1.5 mM sodium sulphite and then fully oxidised with potassium ferricyanide and 17.6 μM (250-700 nm) and 123 μM (700-2000 nm) *Cj* WT (grey dashed line). All data recorded at room temperature in 50 mM HEPES, 50 mM NaCl, pH 7 or the same buffer in D₂O pH* 7 for nIR MCD.

These observations are consistent with sulphite incubation causing the reduction of the His/Met ligated heme II in the majority of the bulk population and the displacement of cysteine (persulphide) as a heme ligand by water in ~50% of heme I. In the presence of an oxidising agent, heme II is unaffected by the presence of sulphite, but now all of heme I becomes His/H₂O ligated, suggesting that now all of Cys-138 is a poor heme ligand. By comparison, MCD of *Cj* C138H

incubated with sulphite for 1 hour (Figure 5.8), shows little change, except the appearance of a bisignate feature at 552 nm with a peak-to-trough intensity of $32 \text{ M}^{-1} \text{ cm}^{-1} \text{ T}^{-1}$ consistent with a trace ($\sim 15\%$) of low-spin ferrous heme. This trace reduction is consistent with the protonated form of sulphite, bisulphite, acting as a mild reducing agent ($E_M = +0.170 \text{ mV}^{144}$) and being oxidised to sulphate in aqueous solution in the presence of a high potential His/Met ligated heme. Extensive reduction and displacement of the heme I ligand therefore only occurs when Cys-138 is present.

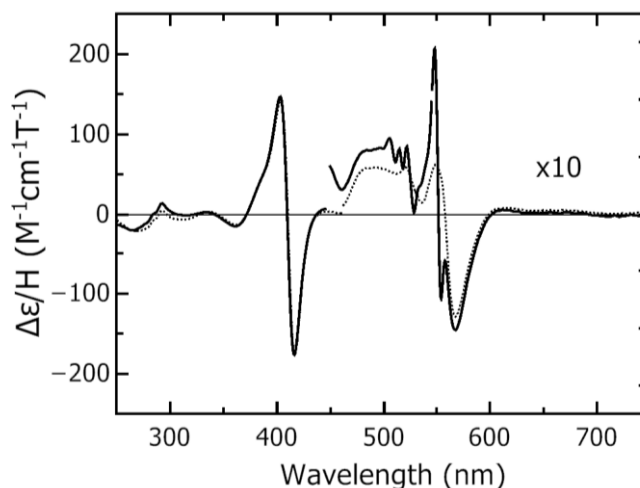


Figure 5.8 – MCD of sulphite-treated *Cj* C138H. Room-temperature UV/visible MCD spectra of $90 \mu\text{M}$ *Cj* C138H incubated with 1.5 mM sodium sulphite (thick black line) and $18 \mu\text{M}$ oxidised *Cj* C138H (grey dashed line). All data recorded at room temperature in 50 mM HEPES, 50 mM NaCl, pH 7.

5.2.2. Mechanism of Sulphite Binding to *Cj* WT.

To rationalise the observations from spectroscopy and mass spectrometry, the following mechanism is proposed: when *Cj* WT is incubated with sulphite, Cys-138 present as cysteine or cysteine persulphide forms a covalent bond to one molecule of sulphite to make cysteine (thio)sulphonate (Figure 5.9) which has a mass increase of $\sim 80 \text{ Da}$ (Figure 5.5, A, C). This reaction releases two electrons which reduce the TsdA hemes (Figure 5.6). Rapid inter-molecular electron exchange then results in an equilibrium being reached when the higher potential His/Met ligated heme II is reduced in all of the the bulk TsdA population (Figure 5.7). Monomers where the His/Met heme is reduced are also logically prevented from participating in further two-electron reactions, even where Cys-138 is unmodified. As such, each molecule of sulphite reduces two His/Met hemes, but only modifies one Cys-138 residue, explaining how $\sim 50\%$ of a sample gains the $\sim 80 \text{ Da}$ mass in mass spectra and there is 50% of a His/Cys⁻ heme CT_{LS} band in MCD of sulphite-incubated samples. When an electron acceptor is present, all hemes will be oxidised, allowing unreacted monomers to react with sulphite. This will result in a sample where all of Cys-

138 is modified and displaced as heme I ligand by water, consistent with reoxidised LC-MS samples where the majority of the sample has a ~80 Da mass increase (Figure 5.5) and MCD where high-spin His/H₂O heme signals entirely replace those assigned to low-spin His/Cys⁻ ligated heme (Figure 5.7, bottom panels).

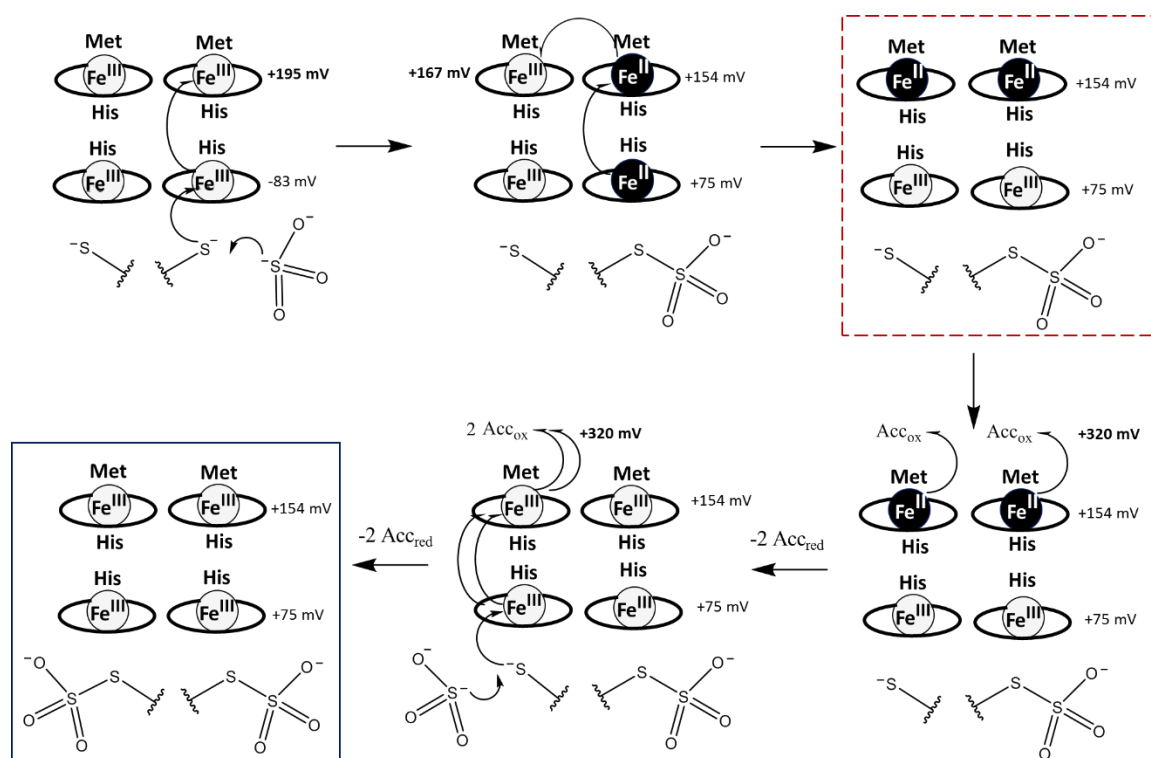


Figure 5.9 – Covalent modification of Cys-138 in *Cj* WT by sulphite. Ferric (ferrous) hemes shown in white (black). Red dashed box shows the form of the enzyme expected for samples incubated with excess sulphite. Blue box shows samples incubated with sulphite and ferricyanide or other high E_M electron acceptor (Acc). Analogous reactivity between sulphite and CysS-138 could form cysteine thiosulphonate.

If sulphite reacts preferentially with cysteine persulphide in *Cj* WT to form cysteine thiosulphonate, this proposed catalytic intermediate is unlikely to inhibit catalysis⁵ consistent with the competitive inhibition shown in catalytic voltammetry¹⁴⁰. This would also rationalise fitting two first-order processes (Figure 5.6) to the reduction of *Cj* WT by sulphite. The ‘slow’ phase ($k_2 = 440 \text{ s}^{-1}$) may be sulphite forming a covalent bond to cysteinate with the ‘fast’ phase ($k_1 = 3 \text{ s}^{-1}$) being sulphite reacting with cysteine persulphide. Conversely, *Av* WT reacts more slowly with sulphite, possibly due to the lower E_M of His/Lys ligated ferric heme II.

5.3. Electroactivity of Sulphite-Bound *Cj* WT.

To explore the electrochemical consequences of an analogue of a reaction intermediate present in the TsdA active site, *Cj* WT was incubated with excess sulphite and ferricyanide with the intent of producing a homogenous sample where Cys-138 is modified to cysteine sulphonate.

This sample was analysed with LC-MS and PFE using the same methodology used to interrogate TCEP-incubated enzyme (see above, 4.4). A representative voltammogram ($v = 10 \text{ mV s}^{-1}$) of an IO-ITO electrode coated with this sample has two pairs of broad peaks with an asymmetric appearance. These signals are broader than a single $n = 1$ lineshape at 293 K, but are a good fit to two reversible $n = 1$ processes with $E_M = +75 \text{ mV}$ (X) and $+154 \text{ mV}$ (Y). Both pairs of signals are similar in area, with X being approximately 80% that of Y.

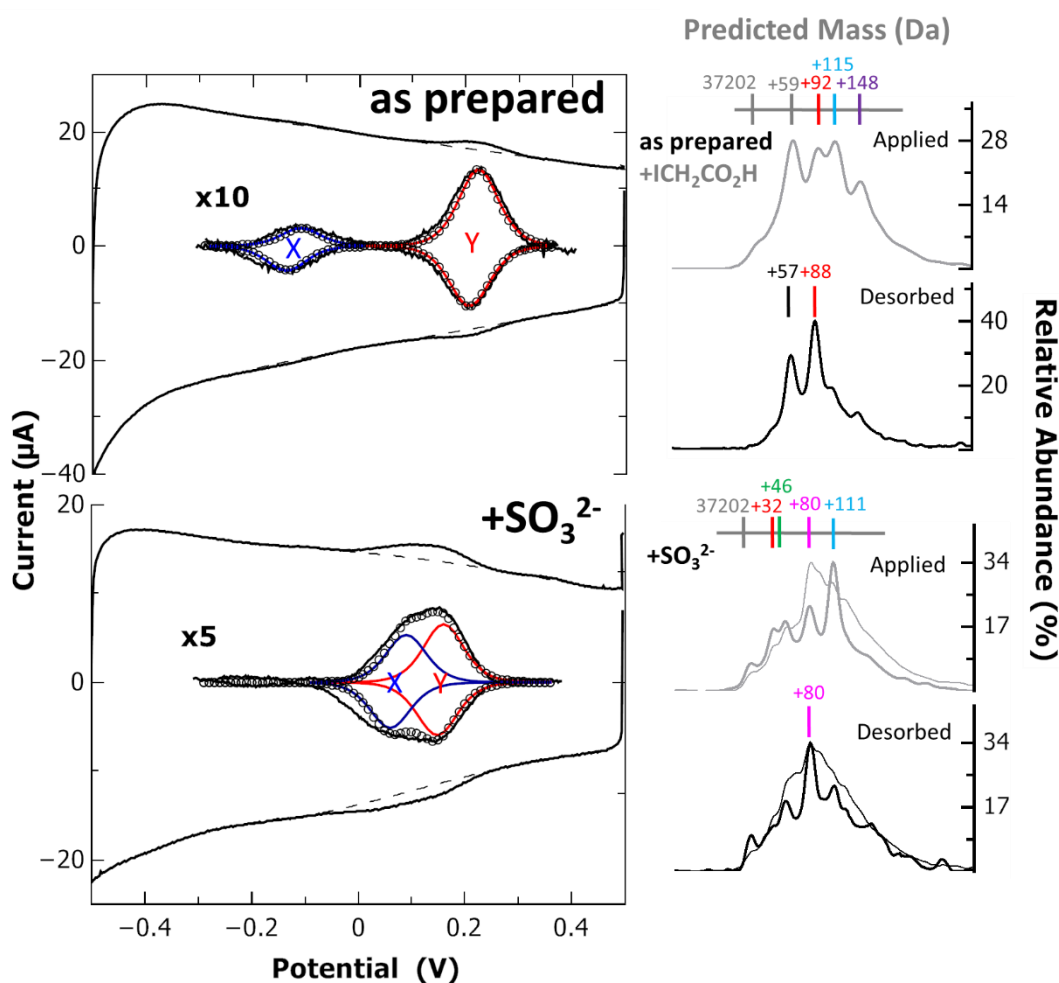


Figure 5.10 – Representative CV of *Cj* WT before and after sulphite incubation. (Left) Raw data (outer black line) with baselines (dashed line) used to prepare baseline-subtracted CVs (inner black line) of a *Cj* WT coated IO-ITO electrode either as prepared (top) or incubated with 20 mM sodium sulphite and 10 mM potassium ferricyanide, transferred to fresh buffer-electrolyte prior to adsorption (bottom). Each peak has been fitted to two predicted $n=1$ theoretical responses (red and blue lines) and the sum of these contributions (black circles). All data recorded in 50 mM HEPES, 50 mM NaCl, pH 7, $v = 10 \text{ mVs}^{-1}$, $T = 293 \text{ K}$. **(Right)** Mass spectra of stock solutions for voltammetry (thick grey lines) and desorbed protein (thick black lines) incubated with 15 mM sodium iodoacetate (*Cj* WT as prepared). LC-MS data corresponding to the *Cj* WT $+SO_3^{2-}$ voltammetry shown incubated with 15 mM sodium iodoacetate had poor ionisation giving rise to a noisy mass spectrum (thin lines). Clearly-resolved LC-MS of repeat experiment without iodoacetate also shown (thick lines). Samples were denatured for LC-MS by 10-fold dilution in 2% Acetonitrile, 0.1% Formic Acid.

The centre giving rise to Y has electroactivity at a similar E_M to heme II in *Cj* WT as-provided. The CT_{LS} band of the His/Met ligated heme is unchanged in MCD spectra of a similarly-treated sample (Figure 5.7) so this species is assigned as His/Met ligated heme II. The mass spectrum of the sample used to coat the electrode has a maximum intensity at +80 Da, consistent with sulphonation, but the appearance is broad and noisy (Figure 5.10, lower right, thin lines), which may be due to poor ionisation of the protein if the LC method used is not separating protein from charged small molecules such as iodoacetate and any remaining sulphur oxyanions. The mass spectrum of desorbed protein is largely identical. The experiment was repeated with a 10-fold lower concentration of sulphite and ferricyanide and no iodoacetate. Electrode coverage was poor, leading to ambiguous voltammetry (data not shown), however mass spectra resolved clearly (Figure 5.10, lower right, thick lines) and the most abundant species in the solution applied (34% of the sample) has a mass increase of +111 Da indicating protein with cysteine thiosulphate, with the next most abundant (23% of the sample) being protein with cysteine sulphonate. After redox cycling, there is less cysteine thiosulphonate (23% of the sample) and now cysteine sulphonate is the most abundant species (34% of the sample), consistent with the latter, inhibited species being more stable than the former.

The majority of the enzyme film on the electrode is therefore expected to have Cys-138 modified to cysteine (thio)sulphonate, so X is assigned as the electroactivity of high-spin His/H₂O-ligated Heme I. Unlike *Cj* WT as prepared or treated with TCEP, both hemes now give rise to signals of approximately equal area suggesting that both hemes are transferring electrons with the electrode at once when Cys-138 is modified to cysteine (thio)sulphonate. Furthermore, the E_M of heme I has increased by 168 mV and is now much closer to that of the thiosulphate/tetrathionate couple (+198 mV³). Assuming cysteine sulphonate and thiosulphonate are analogous in this sense, this rationalises how heme I acts as the catalytic site during tetrathionate reduction and thiosulphate oxidation by *Cj* TsdA and supports the catalytic mechanism proposed by Grabarczyk *et al*⁵.

5.4. LC-MS and MCD of *Cj* WT Reveals Modification of Cys-138 by Substrates.

Given the significant changes affected upon the E_M and ligation state of heme I by sulphite it was of interest to see if reaction products with natural substrates could be generated and characterised by a similar methodology. Firstly, LC-MS was recorded of TsdA samples incubated with substrates under anaerobic conditions to investigate any effect these had on the status of the active site cysteine. The mass spectrum of ***Cj* WT** incubated with thiosulphate for 1 minute followed by iodoacetate (Figure 5.11, A, black lines) has one clear peak with a mass +89 Da, indicating Cys-138 was entirely present as cysteine persulphide before carboxymethylation. This is

consistent with previous reports of Cys-96 in *Av* WT binding one molecule of thiosulphate to form cysteine thiosulphonate, which then breaks down to cysteine persulphide over time⁵. A repeat of this experiment using *Av* WT under the same conditions (Figure 5.11, B, black lines) results in a mass spectrum with one major peak (62% of the sample) which also has a mass increase of +91 Da indicating cysteine persulphide that has been carboxymethylated, giving further confidence that both TsdA proteins react similarly with thiosulphate over the timescale of the experiment. *Cj* WT +TCEP incubated with thiosulphate, then iodoacetate has two major peaks in the mass spectrum (Figure 5.11, C, black lines). One peak (44% of the sample) has a mass increase of +88 Da consistent with cysteine persulphide after carboxymethylation, whereas the other major peak (36% of the sample) has a mass increase of +57 Da indicating Cys-138 was unmodified before carboxymethylation. Modification of only ~50% of the sample is expected if thiosulphate binds to cysteine by a mechanism analogous to that of sulphite (Figure 5.9).

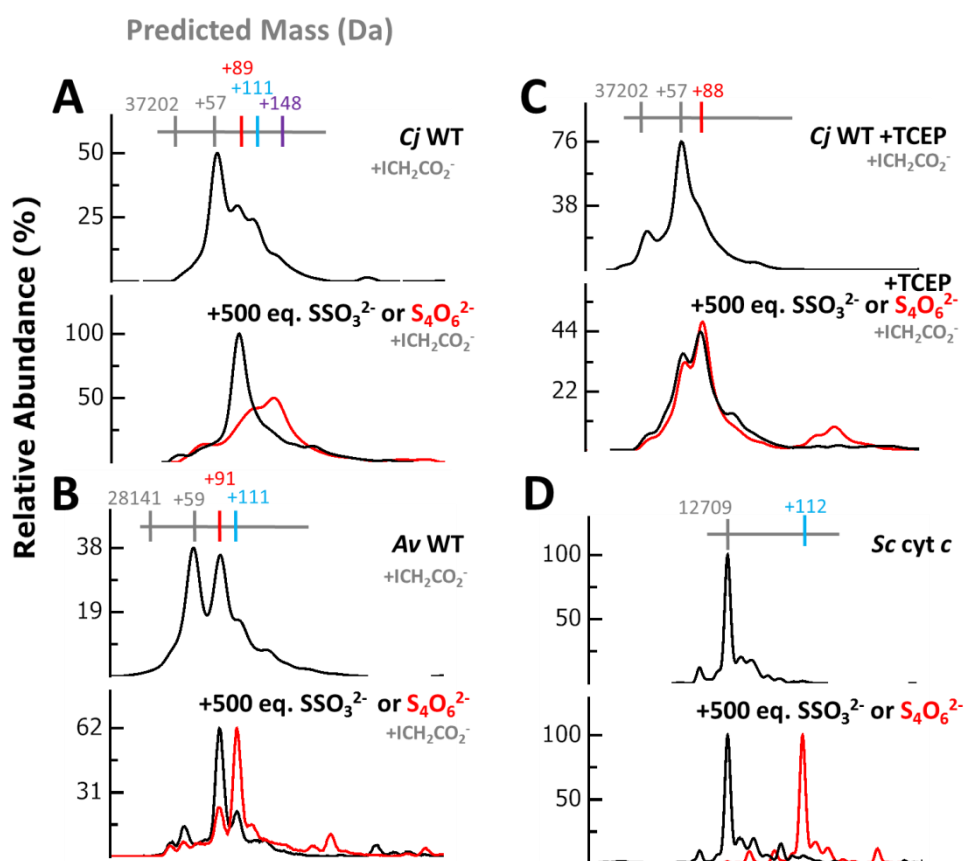


Figure 5.11 – Deconvoluted Mass Spectra of TsdA proteins with thiosulphate or tetrathionate (red lines). 30-50 μM TsdA or cyt c in pH 7 50 mM HEPES, 50 mM NaCl incubated under anaerobic conditions (<10 ppm O_2) for 10 minutes with sodium thiosulphate or tetrathionate (as annotated) followed by incubation with 15 mM sodium iodoacetate. Samples were denatured for LC-MS by 10-fold dilution in 2% Acetonitrile, 0.1% Formic Acid.

LC-MS of *Cj* WT incubated with excess tetrathionate shows two major peaks (Figure 5.11, A, red line), the most intense of which (50% of the sample) has the predicted mass +148 Da,

consistent with Cys-138 present as cysteine thioperoxosulphonate. The other major peak (44% of the sample) has a mass +111 Da, indicating Cys-138 is modified to cysteine thiosulphate. Cysteine thio(peroxo)sulphonate is likely to form if one molecule of tetrathionate undergoes nucleophilic attack from the Cys-138 (per)thiolate, breaking the central disulphide bond and releasing one molecule of thiosulphate. It is not expected that this process would involve any exchange of electrons, and therefore is expected to occur at any cysteine regardless of the electron transfer properties of the TsdA hemes. Consistent with this, *Sc* cyt *c* which has one free cysteine but no adjacent redox centre, incubated with tetrathionate (Figure 5.11, D) has a mass increase of +112 Da indicating thiosulphonation, whereas a parallel sample incubated with thiosulphate does not. Consistent with previous reports⁵, LC-MS of **Av WT** incubated with excess tetrathionate followed by iodoacetate (Figure 5.11, B, red line) results in a mass spectrum with one major peak (62% of the sample) with a mass +111 Da indicating the majority of Cys-138 has been modified to cysteine thiosulphonate. **Cj WT +TCEP** incubated with thiosulphate has a similar mass spectrum to TCEP and thiosulphate-incubated enzyme (Figure 5.11, C, red line). There are two major peaks, the most intense (46% of the sample) has a mass increase of +88 Da, consistent with Cys-138 being persulphurated and carboxymethylated. The other peak (35% of the sample) has a mass increase of +57 Da indicating only carboxymethylation.

For consistency and reflecting the focus on *Cj*-type TsdA³², all experiments in this thesis have been performed at pH 7. The catalytic activity of *Av* WT is, however, reported to be much greater at pH 5 (Brito), than under these standard pH 7 conditions. Therefore, two key LC-MS experiments (Figure 5.5, Figure 5.11, B) were repeated with *Av* WT samples exchanged into 50 mM sodium citrate, pH 5 (Figure 5.12) to identify any changes in catalytically or mechanistically relevant cysteine modifications at this lower pH value.

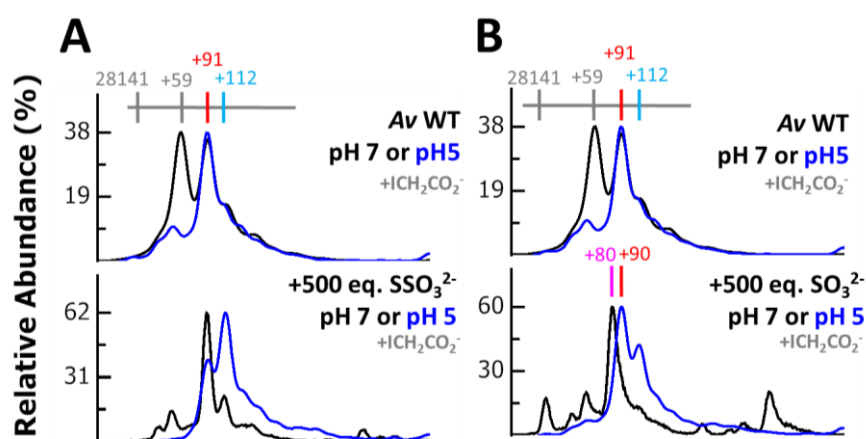


Figure 5.12 –Deconvoluted Mass Spectra of *Av* WT with thiosulphate or sulphite at pH 7 or pH 5 (blue lines). 30-50 μ M TsdA or cyt *c* in 50 mM HEPES, 50 mM NaCl, pH 7 or 50 mM sodium citrate, pH 5, incubated for 10 minutes with sodium thiosulphate or sulphite (as annotated) followed by incubation with 15 mM sodium iodoacetate. Samples were denatured for LC-MS by 10-fold dilution in 2% Acetonitrile, 0.1% Formic Acid.

Unlike the mass spectrum of Av WT recorded at pH 7 which has two major peaks, the pH 5 spectrum has only one (38% of the sample) indicative of enzyme where Cys-96 is persulphurated and then carboxymethylated. A parallel sample incubated with excess thiosulphate instead has two major peaks, one indicating thiosulphonated enzyme (62% of the sample) and one indicating persulphurated and carboxymethylated protein (38% of the sample).

Unlike *Cj* WT, there is therefore evidence that cysteine persulphide in Av WT can be displaced by thiosulphate. LC-MS of Av WT incubated with excess sulphite at pH 5 also features two clearly-resolved peaks, one indicating that 58% of the sample was persulphurated before carboxymethylation, the second indicating that 42% of the sample is carboxymethylated. At pH 5 there is no evidence for any formation of cysteine sulphonate which is the major species formed at pH 7. This suggests that, like *Cj* WT, Av WT under these conditions can form thiosulphate from cysteine persulphide and sulphite which may protect the enzyme from inactivation. Alternatively, sulphite at pH 5 is likely to be largely protonated and the reactivity of this species, bisulphite, may be different rendering the pH 5 and pH 7 experiments incomparable, but still of mechanistic interest.

MCD was also recorded of TsdA incubated with thiosulphate to investigate the effects of Cys-138 modification on the hemes (Figure 5.13). The spectrum of *Cj* WT incubated with thiosulphate has a sharp derivative feature at 552 nm indicating low-spin ferrous heme. The peak-to-trough intensity of this signal is $430 \text{ M}^{-1} \text{ cm}^{-1} \text{ T}^{-1}$, slightly more intense than the same signal in ascorbate-incubated enzyme consistent with the reduction of one methionine-ligated heme and perhaps a trace of thiol(ate) ligated heme.

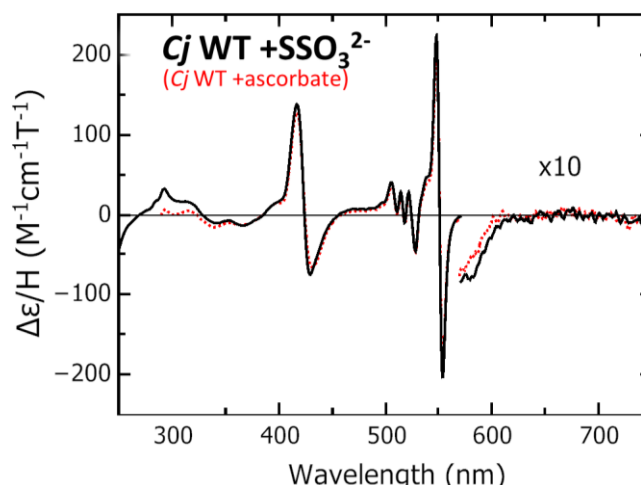


Figure 5.13 – MCD of thiosulphate-treated *Cj* WT. Room-temperature UV/visible MCD spectra of (Top) $34 \mu\text{M}$ (250-700 nm) and $104 \mu\text{M}$ (450-2000 nm) *Cj* WT incubated with 1.5 mM sodium sulphite (black line) and $17.6 \mu\text{M}$ (250-450 nm), $163 \mu\text{M}$ (450-700 nm) and $123 \mu\text{M}$ (700-2000 nm) *Cj* WT incubated with 1.5 mM sodium ascorbate (red dashed line). All data recorded at room temperature in 50 mM HEPES, 50 mM NaCl, pH 7 or the same buffer in D_2O pH* 7 for nIR MCD.

The trough of the $\alpha\beta$ 580 nm signal assigned to ferric persulphide-ligated heme in oxidised *Cj* WT is still clearly resolved, consistent with heme I having a significant proportion of His/Cys⁻ ligation, despite the reduction of some His/Cys⁻ heme. The major difference with sulphite and thiosulphate-treated *Cj* WT is that there are no features indicating the presence of any high-spin heme in the latter, unlike with the former. This is consistent with LC-MS data that suggests Cys-138 is modified to cysteine persulphide, expected to be a high field strength ligand to heme I giving rise to low-spin signals.

LC-MS and MCD data suggest that the active site cysteine ligand of TsdA initially reacts with thiosulphate in a manner analogous to the proposed mechanism for sulphite (Figure 5.9). The cysteine thiol forms a disulphide bond to the sulphane sulphur of a thiosulphate molecule, releasing two electrons to the TsdA hemes, reducing them both to the ferrous state. Inter-monomer electron exchange then results in mostly higher E_M His/Met ligated hemes II in the bulk population being ferrous, with hemes I mostly becoming reoxidised to the ferric state over time.

The active site of *Cj* WT has a higher affinity for thiosulphate ($K_M = 0.3 \text{ mM}^{32}$) than for sulphite ($K_I = 1 \text{ mM}^{140}$) so whilst rapid inter-monomer electron exchange may reduce one heme of ~50% of the unreacted sample at a significant rate compared to the binding of sulphite preventing further binding and reduction, thiosulphate binding is likely to be faster, resulting in a slightly greater overall population of ferrous heme. Furthermore, the reaction between cysteine and thiosulphate logically forms cysteine thiosulphonate, however only cysteine persulphide is detected on the timescale of LC-MS experiments. Thiosulphate reacting with cysteine also forms cysteine thiosulphonate, however this modification is seemingly more stable despite being chemically identical. The only difference between TsdA incubated with the two substrates is that tetrathionate incubation is unlikely to release electrons and tetrathionate treated TsdA will remain in the di-ferric state. It therefore follows that cysteine thiosulphonate only breaks down to cysteine persulphide in proximity to ferrous TsdA. The di-ferric hemes could reduce the β - γ disulphide bond *via* heme I, releasing one molecule of sulphite and leaving cysteine persulphide. Consistent with this, the only tetrathionate-incubated species where cysteine persulphide is present in a large proportion of a TsdA population is *Cj* WT pre-treated with TCEP, which has been demonstrated to reduce the TsdA hemes (Figure 4.6).

Consistent with the idea that *Cj* WT heme I does not participate in electron transfer when heme I is His/Cys⁻ rather than His/Cys^S- ligated, there is no evidence that thiosulphate reacts with cysteine persulphide to form cysteine thioperoxosulphonate. Conversely, persulphuration in *Av* WT is displaced by thiosulphate, but only at pH 5, suggesting this form of the enzyme may still be active in a pH-dependent manner which could explain its higher thiosulphate oxidation activity at pH 5⁹. Tetrathionate reacts by a disulphide exchange mechanism and there is evidence of

cysteine thioperoxosulphonate formation in *Cj* WT, but not in *Av* WT. It is not known, however if this species has any catalytic relevance, but could indicate that the persulphurated forms of both enzymes provide a molecular basis for their differences in catalytic activity^{3,9,32}. This idea is discussed further along with the mechanistic proposals in Chapter 6.

5.5. PFE used to Characterise Substrate-Bound *Cj* WT.

LC-MS data suggests that cysteine thiosulphonate is stable as long as the TsdA hemes are ferric. *Cj* WT was therefore incubated with tetrathionate to produce a sample with a large population of this proposed catalytic intermediate. This sample was then interrogated by a combination of LC-MS and PFE as previously used to characterise TCEP-incubated *Cj* WT (see above, 4.4) with the exception that the iodoacetate incubation step was omitted to limit the concentration of small charged molecules present in samples. Signals due to the redox activity of the enzyme film on IO-ITO electrodes change with each scan, so only four voltammograms were recorded at $\nu = 10 \text{ mV s}^{-1}$ before the film was recovered. The second baseline-subtracted voltammogram shows redox activity only between 0 and 400 mV. Oxidative signals are broader than an $n = 1$ process and there is structure suggestive of two peaks.

The reductive peak has maximum current at ~ 200 mV with a broad shoulder at ~ 100 mV and resolution of a second peak at ~ 300 mV. The signals are well described by a reversible $n = 1$ process with $E_M = 205$ mV (Y) and an $n = 1$ process with $E_M = 318$ mV (X), which has a reductive peak area 50% the size of the oxidative peak. An additional $n = 1$ signal with only reductive area is modelled $E_p = 115$ mV (X'). The reductive areas of X + X' equal the oxidative area of X, consistent with these features arising from the electroactivity of the same redox centre. Y is assigned to the redox activity of His/Met ligated heme II as it is identical to the peaks assigned to this species in *Cj* WT as prepared. LC-MS of the sample used to coat the electrode has several peaks, but the largest (26% of the sample) has a mass +148 Da indicating Cys-138 is present as cysteine thioperoxosulphonate and the second largest (24% of the sample) has a mass +112 Da consistent with cysteine thiosulphonate. Signals X and X' are therefore assigned as the redox activity of heme I where Cys-138 is likely to be displaced as a heme ligand by solvent.

LC-MS of protein recovered from the electrode has an unchanged cysteine thioperoxosulphonate peak, however the intensity of the cysteine thiosulphate peak is much less (14% of the sample) and there is now a clearly resolved peak at the predicted unmodified mass of the protein (13% of the sample) consistent with this species being reduced to unmodified cysteine when heme I is ferric. One rationalisation for X' is that some of heme I could be reduced at a lower potential during the (partial) reduction of cysteine thiosulphonate.

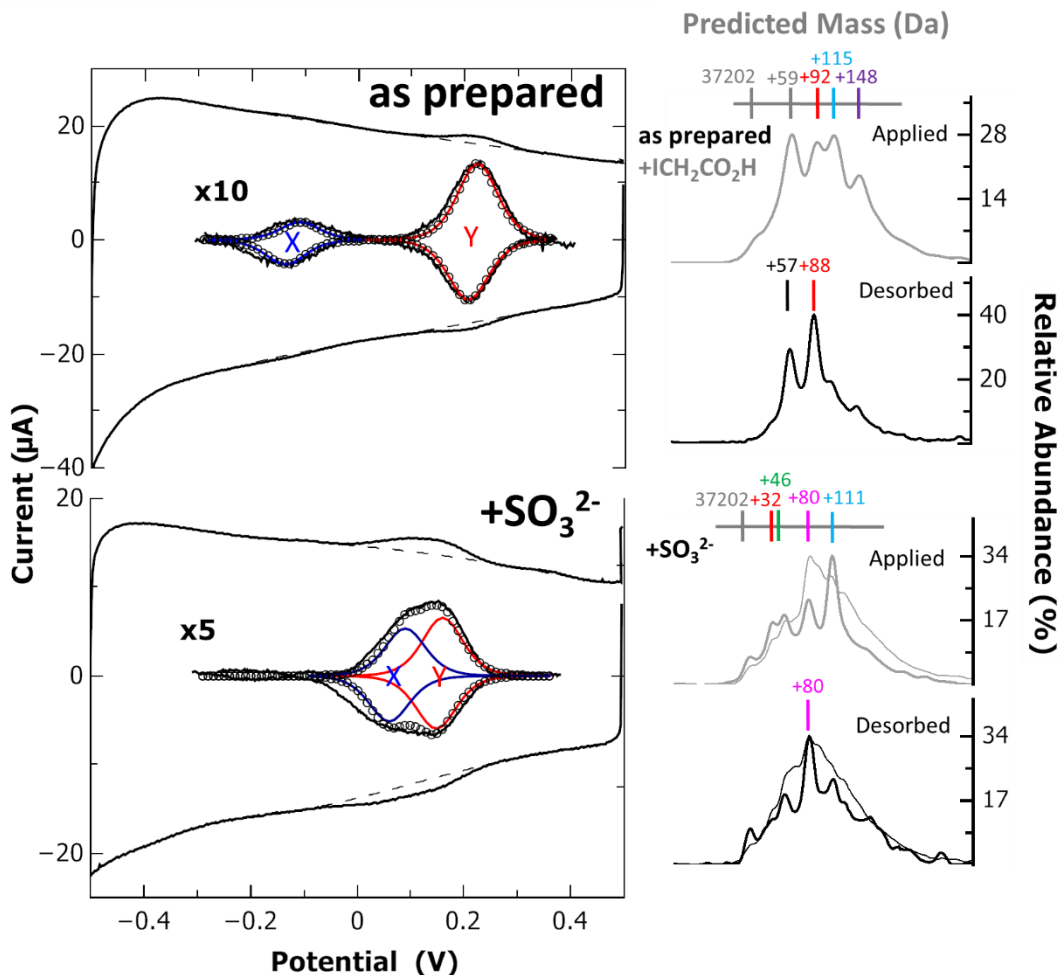


Figure 5.14 – Representative CV of *Cj* TsdA after tetrathionate incubation. **(Left)** Raw data (outer black line) with baselines (dashed line) used to prepare baseline-subtracted CVs (inner black line) of a *Cj* TsdA WT coated IO-ITO electrode incubated with 1.2 mM tetrathionate for 1 hour and then transferred to fresh buffer-electrolyte. T= 293 K. Each peak has been fitted to two predicted $n=1$ theoretical responses (red and blue lines) and the sum of these contributions (black circles). Also shown (grey, shaded area) is the response prior to tetrathionate incubation.

Similarly to when Cys-138 is modified to cysteine sulphonate, the areas of X plus X' are approximately equal to Y suggesting that cysteine thio(peroxo)sulphonate modification also enables electron transfer to both hemes at once. Furthermore the E_M of the majority of heme I is now higher than the E_M for the thiosulphate/tetrathionate couple (+198 mV³) suggesting this form of the enzyme would have a suitable thermodynamic driving force for thiosulphate oxidation. This is consistent with one or both of these modifications being a mechanistic intermediate for catalysis by TsdA enzymes.

5.6. Re-Evaluation of the Origin of *Cj* TsdA PFE

As previously presented in Chapter 4, several samples of *Cj* WT were prepared with chemical treatments to produce a range of Cys-138 modifications either before or after these

were used to coat IO-ITO electrodes. PFE was recorded for each electrode ($v = 10 \text{ mV s}^{-1}$, $T = 297 \text{ K}$) and then the enzyme film was recovered and the LC-MS of this measured (Figure 4.10). A simple comparison was made using these data that correlated moles of electrons transferred by peaks assigned as the electroactivity of heme I or II in PFE and the intensity of cysteine modifications determined by LC-MS. This analysis identified that when Cys-138 is unmodified, only heme I transfers electrons and when Cys-138 is persulphurated, only heme II transfers electrons (Figure 4.10). This simple model is now expanded with the observation that both *Cj* WT hemes appear to transfer electrons when Cys-138 is modified to cysteine sulphonate, thiosulphonate or thioperoxosulphonate (Figure 5.7, Figure 5.10). For samples with these modifications, the E_M of heme I also increases to be closer to that of heme II. Consequently, some of the electroactivity previously assigned to heme II in the simplified model, may actually originate from modified heme I.

Based on the results presented in this chapter, unmodified Cys-138 is expected to contribute one electroactive heme to the low potential peak observed in voltammograms, cysteine persulphide and cysteine sulphonate contribute one electroactive heme (see below) to the high potential peak and cysteine thio(peroxo)sulphonate contributes two hemes to the high potential peak. To test how well this revised model describes the effect of cysteine modifications on *Cj* WT heme electroactivity compared to the simpler description in Chapter 4, the ratio of electrons transferred at low potentials in voltammograms (now N_{lo} , previously N_x) was plotted against the LC-MS derived relative abundance of cysteine species expected to have electroactivity at high or low potentials by the previous method (Figure 5.15, red stars) and the revised method (open black stars). Both methodologies have a similar correlation, suggesting the complex description is at least as good a model.

Previously presented representative voltammograms for fourteen *Cj* WT PFE experiments recorded at $v = 10 \text{ mV s}^{-1}$ were therefore fitted to revised theoretical $n = 1$ lineshapes. The number of $n = 1$ lineshapes and the potentials over which these were fitted were based the hypothetical electroactivity of Cys-138 modifications present informed by experiments where films have one predominant modification (Figure 4.8, Figure 5.7, Figure 5.10). The rules for these fittings are summarised in Figure 5.16. The total relative area for each set of $n = 1$ lineshapes fitted to each voltammogram, representing moles of electrons transferred by enzyme with that modification, is based on the LC-MS determined percentage of that film with the modification in question.

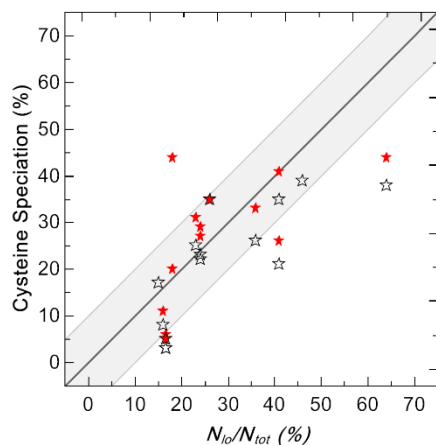


Figure 5.15 – Comparison of Chapter 4 Model (red stars) and Chapter 5 Model (open black stars) for the Correlation of Cys-138 Modifications in *Cj* WT with voltammetric signals. *Cj* WT samples were subject to chemical treatments intended to produce a range of Cys-138 modifications. The identity of these is calculated from relative intensity of LC-MS peaks from desorbed protein from IO-ITO electrodes following voltammetry. Low potential electroactive area (N_{lo}) calculated as a percentage of total electroactive area (N_{tot}) from representative voltammograms. Chapter 4 model assumes either heme I is active at low potential when Cys-138 is unmodified or heme II at high potential if Cys-138 is modified in any way. Chapter 5 model has both hemes at high potential in Cys-SSO₃²⁻ or Cys-SSSO₃²⁻ species. PFE recorded in 50 mM HEPES, 50 mM NaCl, pH 7, $v = 10 \text{ mV s}^{-1}$, $T = 293 \text{ K}$.

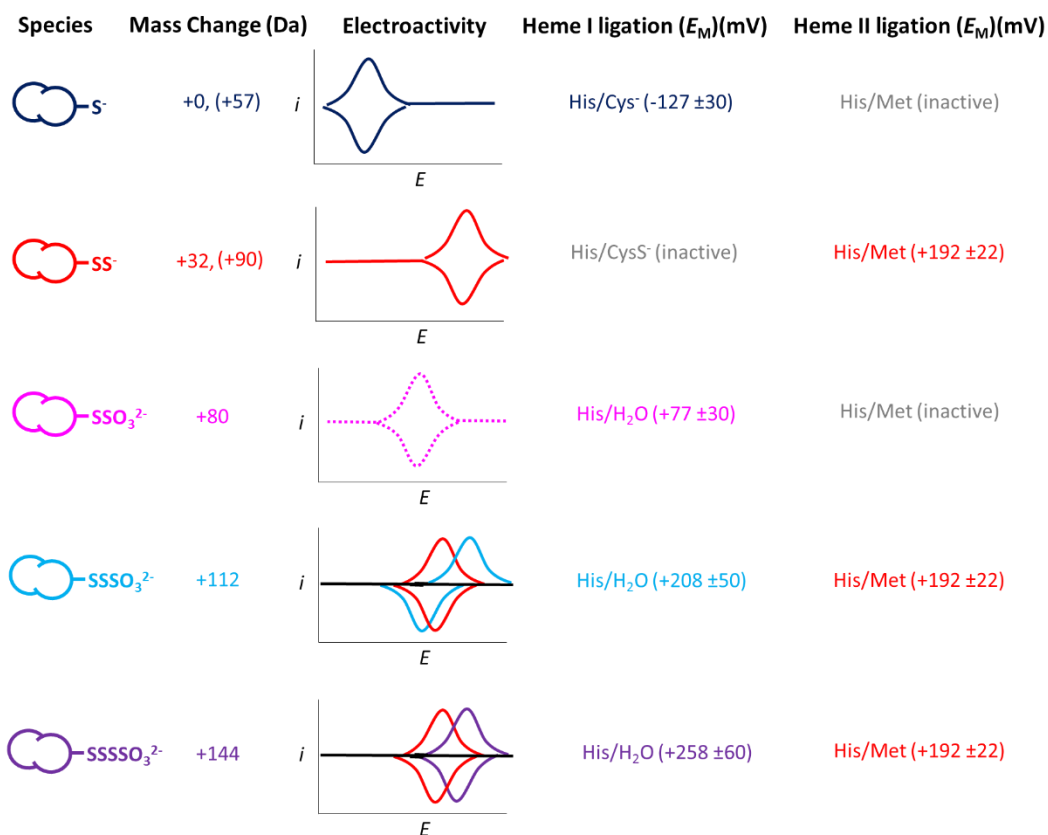


Figure 5.16 – Hypothetical electroactivity of Cys-138 modifications in *Cj* WT. Used as a guideline to fit theoretical $n = 1$ lineshapes to recorded voltammograms. LC-MS assignment of cysteine adducts is based on mass increases as stated, with carboxymethylated forms shown in parentheses. Average E_M values for all fitted lineshapes representing the electrons transferred by heme I (II) are given.

For the majority of experiments analysed this way, the electroactivity of unmodified His/Cys-138 ligated heme I is the only lineshape fitted to signals with $E_M < 0$. In most cases the observed peaks in voltammetry are well-described by the percentage unmodified cysteine present (Figure 5.17, dark blue lines). There are two conditions of samples which are exceptions to this. Firstly, both experiments using as-provided *Cj* WT coated electrodes treated with thiosulphate (Figure 5.17, lowest panels, dark blue lines). In the first experiment the area of the recorded signal is ~35% of the area of the fitted signal, in the second experiment the fitted signal is ~50% of the area of the recorded signal. The latter PFE film was recovered when the scan was stopped at $E = -500$ mV, for all other experiments scans were stopped at $E = +500$ mV. This difference suggests a rationale for the lack of correlation between unmodified Cys-138 and the area of the low potential signal as follows. Although the appearance of voltammograms treated with thiosulphate does not change over multiple scans in these experiments, the position of equilibrium between cysteine thiosulphate and cysteinate plus thiosulphate depends on the applied potential in the voltammogram. In this case the protein film recovered at the upper or lower limit of the potential window does not accurately describe the average bulk population of Cys-138 modifications over the entire scan in the same way that the voltammogram would.

Consistent with this, an average of the mass spectra recorded under these conditions predicts percentages of cysteine modifications which when translated into theoretical signals better describe the recorded data in both experiments (data not shown). The other outliers to this model are two experiments where *Cj* WT was incubated with TCEP prior to adsorption on electrodes. For these voltammograms, lineshapes based on the percentage of unmodified Cys-138 have less area than recorded signals. If, however, the population of Cys-138 present as cysteine thiosulphonate is also added to this, fitted lineshapes describe the recorded voltammograms more closely (Figure 5.17, third row from top). Based on previous solution LC-MS experiments (Figure 4.5) cysteine thiosulphonate is not expected to be present in TCEP-treated *Cj* WT, so it is possible that this species formed adventitiously during the recovery of these films from the electrode. In this case the LC-MS of the applied protein, rather than the recovered protein, more accurately describes Cys-138 species present during voltammetry (data not shown).

The His/Met ligated heme II is modelled as transferring electrons (Figure 5.17, red lines) with $E_M \approx 190$ for all Cys-138 modifications except for unmodified cysteine (and possibly cysteine sulphonate) and it is the only signal modelled when Cys-138 is persulphurated. For all experiments the fitted signal well-describes the recorded voltammetry. If hemes I and II transfer the same number of electrons when Cys-138 is modified to cysteine sulphonate as hypothesised (see above, 5.2), this does not result in a good fit to the recorded data.

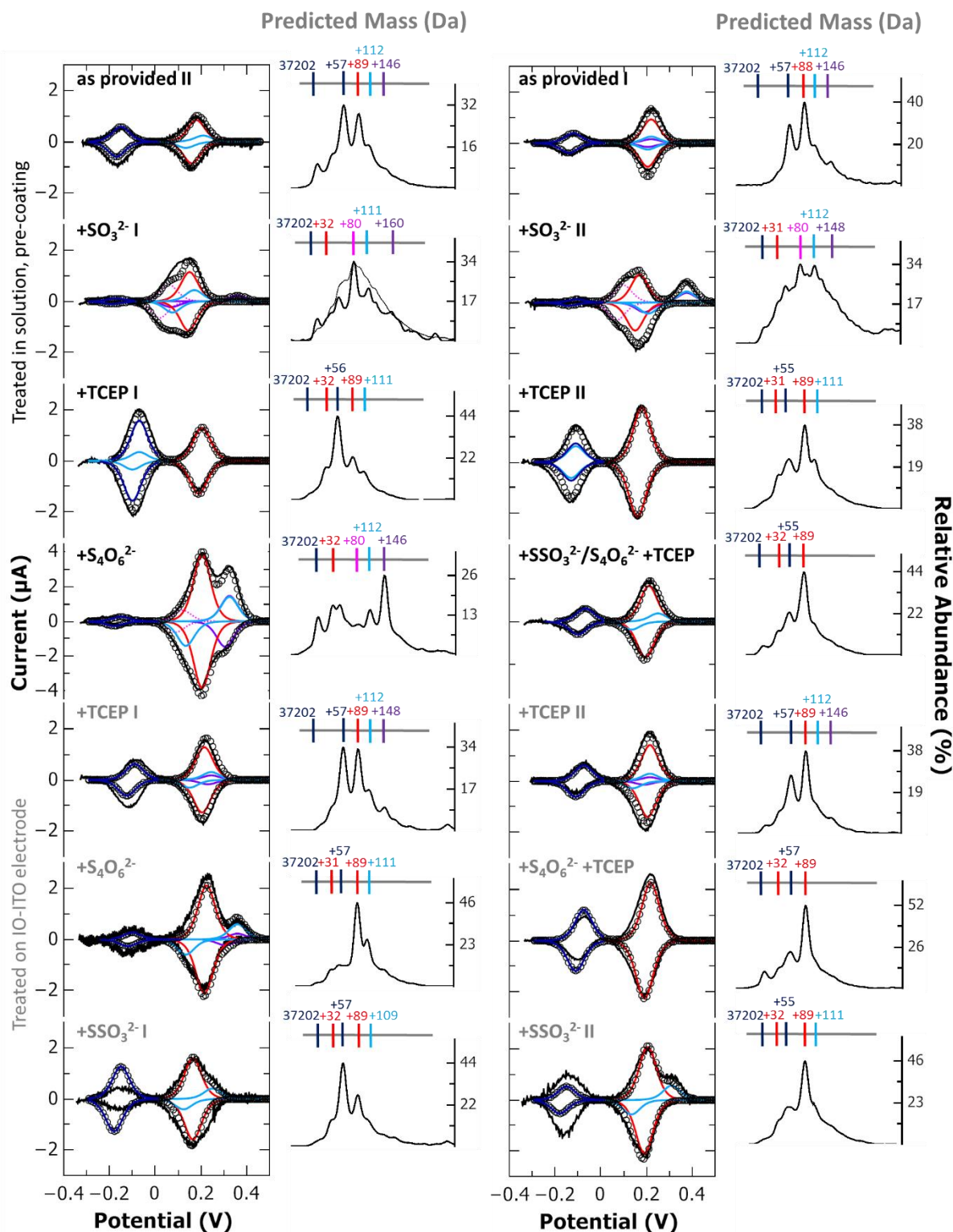


Figure 5.17 – Representative CVs and LC-MS (right of corresponding CVs) of *Cj* WT films prepared with chemical agents. Baseline-subtracted CVs (black line) of *Cj* WT coated IO-ITO electrodes prepared as annotated. Each PFE peak has been fitted to multiple predicted $n=1$ theoretical responses. Theoretical response areas to correlate to relative intensities of Cys-138 modifications detected by LC-MS (coloured lines correspond to coloured mass increases, fitting rules summarised in Figure 5.16). The sum of all fittings shown as black circles. All data recorded in 50 mM HEPES, 50 mM NaCl, pH 7, $\nu = 10$ mVs⁻¹, $T = 293$ K. (Right) Mass spectra of stock solutions for voltammetry (upper panels) and desorbed protein (lower panels) incubated with 15 mM sodium iodoacetate. Samples were denatured for LC-MS by 10-fold dilution in 2% Acetonitrile, 0.1% Formic Acid.

The electroactivity of the cysteine sulphonate form of *Cj* WT is instead modelled as one pair of peaks with $E_M \approx +80$ mV which could arise from heme I or II (Figure 5.17, dashed pink lines) but which is assumed to be heme I as heme II is generally unchanged in all other species where it is electroactive. This proposal is consistent with this form of the enzyme irreversibly losing all catalytic activity (Figure 5.4, grey stars), both because Cys-138 is blocked and because only one heme is active, preventing removal of cysteine sulphonate by reversal of its proposed mechanism of formation (Figure 5.9).

With the exception of experiments where *Cj* WT was treated with TCEP and then used to coat electrodes as mentioned previously, the electroactivity of Cys-138 modified to cysteine thio(peroxo)sulphonate has been modelled with both hemes transferring electrons. The behaviour of heme II is modelled identically its behaviour in the persulphurated form of the enzyme, whereas the behaviour of Heme I is modelled differently for the thiosulphonated and thioperoxosulphonated forms. The His/H₂O heme for *Cj* WT where Cys-138 is present as cysteine thioperoxosulphonate is modelled as an $n = 1$ lineshape with $E_M \approx +260$ mV (Figure 5.17, purple lines). Where Cys-138 is instead present as cysteine thiosulphate, this electroactivity is modelled centred on $E_M \approx +210$ mV but the reductive peak occurs at a potential up to ~ 200 mV less than oxidation (Figure 5.17, blue lines). This difference is approximately proportional to the percentage of cysteine thiosulphonate present and may be representative of a change in the heme I environment depending on if the heme iron is ferric or ferrous, possibly through flexibility of the sidechain or the nature of the ligand (likely water, hydroxide or nothing) that binds to the distal site of heme I. Heme I in both cysteine thiosulphonate and cysteine thioperoxosulphonate forms of the enzyme is oxidised at the same potential, but the former species reduces at a lower potential. This model implies there is stronger thermodynamic driving force for the reduction of the disulphide bond in cysteine thiosulphate to form thiosulphate than analogous reactions with cysteine thioperoxosulphonate, consistent with the former being a proposed step in the mechanism of tetrathionate reduction⁵.

5.7. Discussion

The results from PFE experiments and activity measurements suggest that electron transfer in TsdA proteins is dependent on adducts to the heme I cysteine ligand. There is some suggestion that this may be different in TsdA enzymes and variants with the possibility of His/Lys ligation at heme II, but the following observations apply to *Cj* WT which is assumed to be representative of the majority of TsdA enzymes which do not have this feature.

When the heme I cysteine ligand is unmodified, heme I transfers electrons at an E_M much lower than the tetrathionate/thiosulphate couple and heme II does not transfer electrons at all with an electrode (Figure 4.11). This form of the enzyme is catalytically active, but shows evidence of substrate inhibition at high thiosulphate concentrations. When unmodified cysteine is incubated with thiosulphate, the cysteine thiolate binds one molecule of thiosulphate forming cysteine thiosulphonate, which is displaced as a heme ligand (by solvent). The formation of this adduct now raises the E_M of heme I to be closer to the tetrathionate/thiosulphate couple and allows electron transfer to both hemes, suitable for a two-electron reaction to take place at heme I. Cysteine thiosulphonate bound to di-ferrous TsdA can also decay to cysteine persulphide, which is inferred to release one molecule of sulphite. Sulphite could be the source of substrate inhibition during thiosulphate oxidation as the unmodified heme I cysteine ligand can bind sulphite to form cysteine sulphonate, which is stable to further modification, may feature inactivation of heme II and is therefore catalytically inactive.

The cysteine persulphide form of the enzyme allows electron transfer only to heme II and not to heme I. This prevents thiosulphate from binding to cysteine persulphide to form cysteine thioperoxosulphonate. Therefore this form of the enzyme cannot oxidise thiosulphate and is catalytically inactive in this direction. Tetrathionate can form this species, so it is possible that catalytic activity may still occur in the reverse direction, otherwise this is may be a rationalisation for substrate inhibition in this direction. The cysteine persulphide form of the enzyme can, however, bind sulphite to form cysteine thiosulphonate which it does more readily than the unmodified form of the enzyme. This would return TsdA to a catalytically active form, so the presence of some TsdA with cysteine persulphide may be the reason that substrate inhibition is less severe when some of this species is present. There is evidence that sulphite present in the mammalian gut is harmful to bacterial growth¹⁴⁵ so the presence of cysteine persulphide may generally protect the bulk enzyme population from inhibition and provide a competitive advantage against other microorganisms. The following Chapter combines the findings of this Chapter, together with Chapters 3 and 4 to propose a revised catalytic mechanism for TsdA enzymes.

6. Conclusions and Implications for the Catalytic Mechanism of Cj TsdA

MCD spectroscopy has been used to confirm heme axial ligand assignments based on crystallography apply to *Av* TsdA in solution. Axial ligands have also been confirmed for *Cj* TsdA which is proposed to be more representative of the structure of the majority of this enzyme family and for which no crystallographic data is currently published. Ligation states for both these enzymes and several variants are summarised in Table 3.1. TsdA coated IO-ITO electrodes⁸⁴ allowed for clear resolution of Faradaic currents from the TsdA hemes in the absence of substrates such that E_M values could be determined in combination with MCD of parallel potentiometrically-poised samples. E_M assignments for TsdA enzymes and variants are summarised in Table 3.2. These experiments also confirmed a ligand switch in *Av* TsdA proposed from crystallography⁹ also occurs in solution, identifying a clear molecular basis for the difference between *Av* TsdA and *Cj* TsdA and adding to the known heme proteins which feature this phenomenon as part of their native activity^{34,35}.

Voltammetry of TsdA coated IO-ITO electrodes also identified differences in the number of electrons transferred at low and high potentials, which are assigned by MCD as the electroactivity of hemes I and II respectively. This observation suggests electron transfer in this protein depends much more on heme axial ligation than just the distance between redox centres⁶. Protein films on the IO-ITO electrodes used are sufficient to allow clearly resolved LC-MS of desorbed enzyme films. The native activity of TsdA features modulation of heme I ligation and therefore electron transfer, through sulphur adducts to the active site heme cysteine ligand. These adducts are analogous to those featured in the activity of the Sox enzyme cascade¹⁰¹ and were detected and identified by LC-MS and can be manipulated using chemical treatments, summarised in Table 5.2. Chemical treatments, non-turnover PFE and LC-MS of desorbed enzyme films were used to map the exquisitely controlled electroactivity of *Cj*-type TsdA. These insights allow a proposal for expansion of the active site chemistry and redox properties of these enzymes.

6.1. The Catalytic Mechanism of Cj-Type TsdA

A variety of previously discussed Cys-138 modifications appear in as-provided samples of *Cj* WT (Figure 4.8, B, upper right). This implies that *Cj* WT must be able to form each of these during overexpression and purification of the enzyme³² which is likely to involve encountering substrates that would also be present in the native cellular environment. LC-MS and MCD experiments (see above, 5.3) suggest how these modifications form and PFE and LC-MS experiments suggest which hemes are electroactive and their E_M values (Figure 5.16). It is therefore possible to combine these observations into a unified mechanism for catalysis expanding upon the proposal by Grabarczyk *et al.*⁵. The following is based on data from *Cj* WT but

is proposed to apply to all 'Cj-type' TsdA enzymes with Cj WT-like heme II environments (Figure 1.7). It is likely that Lys-208 in Av WT has an impact on this mechanism and this will be discussed subsequently.

The catalytic cycle for thiosulphate oxidation begins with unmodified, di-ferric TsdA which has His/Met ligation at heme II and His/Cys⁻ ligation at heme I. In this species only heme I transfers electrons (Figure 6.1, **A**, mechanism follows black arrows). One molecule of thiosulphate binds to the heme I pocket and the sulphane sulphur of this molecule is nucleophilically attacked by the thiolate of the heme I Cys⁻ ligand. This forms a disulphide bond releasing two electrons, the first of which transfers to the adjacent heme I iron. The inactivity of heme II prevents rapid inter-heme electron transfer whilst the active site cysteine is unmodified, causing one electron to remain associated with a transient cysteine thiosulphonyl radical species. This residue is no longer competent as a heme I ligand and is displaced by solvent, raising the E_M of heme I and allowing both heme I and II to transfer electrons (**B**). An electron can now transfer from ferrous heme I to ferric heme II and the radical from cysteine thiosulphonyl transfers to the now-ferric heme I iron. TsdA is now di-ferrous and both hemes can still transfer electrons (**C**). An electron acceptor (*eg.* ferricyanide, cytochrome *c*, TsdB) oxidises both hemes and a second molecule of thiosulphate binds to the heme I pocket. The sulphane sulphur of the second thiosulphate molecule attacks the thiosulphonate group of cysteine thiosulphonate (**D**), disulphide exchange occurs forming tetrathionate and leaving unmodified cysteine which re-ligates heme I, returning the enzyme to the start of the cycle.

In addition to the main catalytic cycle there are also off-pathway mechanistic steps that are relevant to the role of TsdA within a cell. When the transient cysteine thiosulphonyl radical is formed by the previous mechanism, heme I is ferrous, heme II is ferric and both hemes can transfer electrons (Figure 6.1, **E**, mechanism follows red arrows). Before ferrous heme I transfers an electron to heme II, possibly dependent on the rate of heme I ligand displacement, the sulphur radical can break an adjacent disulphide bond in concert with the electron from the ferrous heme II iron. Depending on which bond is broken, this reaction could regenerate the starting species, **A**, or it could produce cysteine persulphide and sulphite. If the latter occurs the now-His/CysS⁻ heme I of this species no-longer transfers electrons but heme II does. This persulphurated form of TsdA reacts with sulphite preferentially to unmodified cysteine, protecting the bulk TsdA population from irreversible inhibition by sulphite (Figure 5.6). The inactivity of heme I prevents this reaction occurring by analogous mechanism to thiosulphate binding to unmodified cysteine, instead suggesting a mechanism of disulphide exchange that does not release electrons to the hemes, forming thiosulphate and leaving TsdA with unmodified

cysteine. This would return the enzyme to the start of the catalytic cycle, most likely with a molecule of thiosulphate in the active site pocket ready to resume on-pathway catalytic turnover.

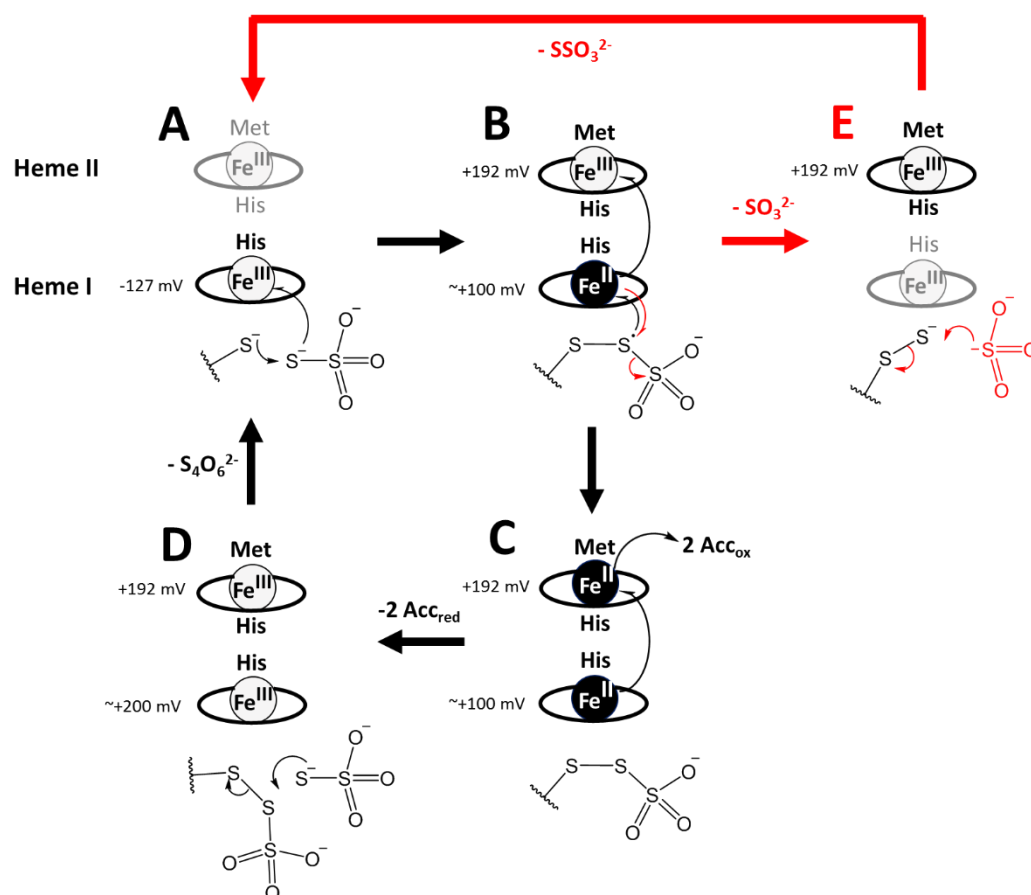


Figure 6.1 – Catalytic mechanism of *Cj* TsdA in the direction of thiosulphate oxidation (black arrows) – Ferric hemes shown in white when electron exchange is permitted and grey when it is prevented, ferrous hemes shown in black. Electroactive hemes show axial ligands and E_M values. Acc = Ferricyanide or other high E_M electron acceptor. Red arrows show cysteine persulphide formation and the mechanism by which it could prevent sulphite inhibition.

Unlike its reactivity with sulphite, di-ferric TsdA with His/Cys^S ligation at heme I is unlikely to react further with thiosulphate as heme I will not act as an electron acceptor and an analogous mechanism of disulphide exchange would produce disulphane monosulphonic acid, which is of unknown stability and reactivity. It is possible however, for cysteine persulphide to nucleophilically attack a molecule of tetrathionate and undergo disulphide exchange, forming cysteine thioperoxosulphonate and releasing one molecule of thiosulphate (Figure 6.2, F, blue arrows). Cysteine thioperoxosulphonate is no longer competent as a heme I ligand and is likely to be displaced by solvent and both hemes now transfer electrons. If an electron donor (eg. methyl viologen, physiological cytochrome donor) reduces both hemes to the ferrous state, it may be possible for these electrons to reduce the central disulphide bond in the

thioperoxosulphonate group to re-form cysteine persulphide and one molecule of thiosulphate (Figure 6.1, G, blue arrows) although the high E_M of heme I (+258 mV) suggests the thermodynamic driving force for this reaction will be low unless it is driven by a low E_M electron donor. By this mechanism it may be possible for *Cj* WT to turnover tetrathionate, but not thiosulphate in its persulphurated form.

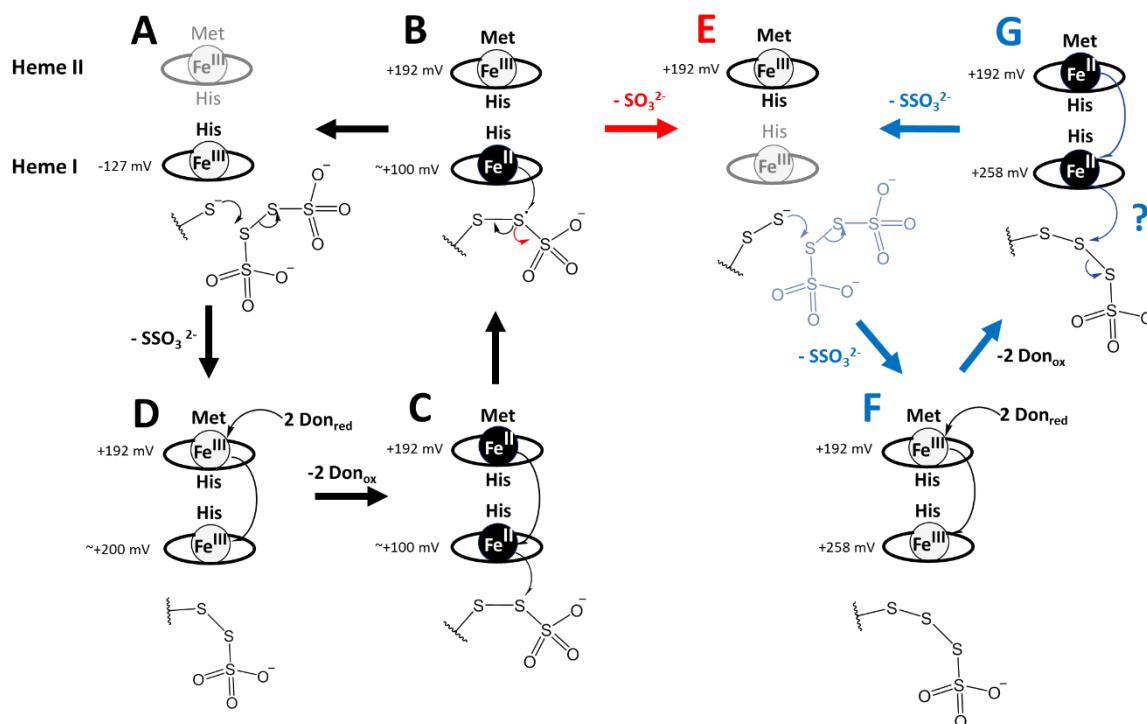


Figure 6.2 - Catalytic mechanism of *Cj* TsdA in the direction of tetrathionate reduction (black arrows) – Ferric hemes shown in white when electron exchange is permitted and grey when it is prevented, ferrous hemes shown in black. Electroactive hemes show axial ligands and E_M values. Don = Methyl viologen or other low E_M electron donor. Cysteine persulphide formation (red arrows) can lead to the formation of cysteine thioperoxosulphonate (blue arrows) which may also be catalytically active.

The hemes in *Cj* WT incubated with excess thiosulphate (Figure 5.13) are reduced to a greater extent than ascorbate. This is consistent with only the unmodified form of *Cj* WT (~50% of the sample) reacting with thiosulphate and becoming fully reduced (Figure 6.1, A to C), before electrons are re-arranged between monomers in the bulk sample such that all of the high potential His/Met hemes are ferrous. There is also likely to be some re-oxidation of the sample from the formation of cysteine persulphide (Figure 6.1, E) which can still form by this mechanism in monomers with an unmodified cysteine but a ferrous heme II. The prevalence of cysteine persulphide ligated heme I explains the lack of high-spin heme in the MCD, expected if a significant population of cysteine thiosulphonate is formed. Furthermore, cysteine persulphide is the only species observed in LC-MS of thiosulphate-incubated enzyme (Figure 5.11), consistent

with all of the sample eventually participating in this side-reaction when there is an excess of thiosulphate and no electron acceptor present. *Cj* WT incubated with an excess of tetrathionate forms cysteine thiosulphonate and thioperoxosulphonate (Figure 5.11) stable over the same timescale, consistent with unmodified cysteine going from step A to D and cysteine persulphide going from step E to F. *Cj* WT incubated with two equivalents of sulphite shows a mass change consistent with going from step E to B (Figure 5.5, A) and in the presence of an electron acceptor cysteine sulphonate is formed consistent with the enzyme going following the catalytic cycle round from E to A before being irreversibly sulphonated (Figure 5.9). *Cj* WT is more active in the thiosulphate oxidation direction after TCEP incubation to remove Cys-138 adducts (Figure 5.4, closed black circles), but is more susceptible to substrate inhibition, consistent with the cysteine persulphide side-reaction (step B to E) generating sulphite that can then irreversibly self-inhibit the enzyme. Where there is already a significant population of cysteine persulphide, this can react with sulphite to regenerate catalytic intermediates and therefore the enzyme as-provided is less active (Figure 5.4, open black circles), but less susceptible to self-inhibition during thiosulphate oxidation.

6.2. The Catalytic Mechanism of *Av*-Type TsdA

Although the majority of experiments reported in this thesis have focussed on elucidating mechanistic information for *Cj*-type TsdA, a number of key experiments have also been performed using *Av* TsdA which permit speculation on how the mechanism of *Av*-type TsdA is different. The main structural difference between these enzymes and *Cj* WT is the presence of a second heme II ligand, Lys-208. Characterisation of the *Av* variant lacking this residue suggests that this variant essentially re-creates *Cj*-like properties in *Av* TsdA (Figure 3.13, Figure 3.14). Any differences in the mechanism of *Av*-type TsdA enzymes are therefore likely to be due to the possibility of having a low E_M heme at heme II.

Although the number of moles of electrons transferred by heme I in voltammograms increases when an *Av* WT-coated (or *Cj* N254K) electrode is treated with TCEP (Figure 4.9), there is also an increase in the number of electrons transferred by heme II. This suggests that the form of the *Av* WT enzyme where Cys-96 is unmodified may have both hemes active unlike the proposal for *Cj* WT. If inter-heme electron transfer is influenced by relative heme E_M values, as *Cj* C138H/M and *Av* C96H/M suggest (Figure 3.7, Figure 3.10), the low E_M value of His/Lys ligated heme II may permit electron transfer to heme II when Cys-96 is unmodified. Although this heme environment does not imply a strong driving force for thiosulphate oxidation and the upper limits for ligand switching in *Av* WT suggest that the ligand switch is much slower than the turnover of the enzyme, data from *Av* C96M suggests that the rate of the ligand switch increases when the heme I

E_M becomes more positive (Figure 3.12). Therefore one possibility is that if the formation of cysteine thiosulphonate at heme I raises the E_M of this heme in the same way that it does for *Cj* WT, this will increase the rate of heme II ligand switching so that Met-209 will ligate ferrous heme II in this form. Together these observations were used to propose a variant catalytic mechanism for *Av* WT, which is assumed to apply to other TsdA enzymes which share its heme II environment.

The mechanism in the direction of thiosulphate oxidation begins with di-ferric TsdA where heme I has His/Cys⁻ ligation, heme II has His/Lys ligation and both hemes transfer electrons (Figure 6.3, A). Thiosulphate forms a disulphide bond to the heme I cysteine ligand, releasing two electrons which reduce both TsdA hemes *via* heme I (Figure 6.3, B). Cysteine thiosulphate is then displaced by solvent as a heme I ligand, causing the E_M of this centre to become more positive, permitting heme II to switch from His/Lys to His/Met ligation (Figure 6.3, C). Electron transfer is still possible at both ferrous hemes so an electron acceptor (*eg.* ferricyanide or high-potential iron-sulphur protein³⁰) can then oxidise these. A second molecule of thiosulphate then binds to the heme I pocket and reacts with cysteine thiosulphonate to form tetrathionate and cysteine by disulphide exchange (Figure 6.3, D). This step leaves di-ferric TsdA which returns to having His/Cys⁻ ligation at heme I and may retain His/Met ligation at (now inactive) heme II, binding another molecule of thiosulphate to continue catalysis *via* a *Cj* TsdA-like mechanism (Figure 6.3, A' to B', green arrows). Alternatively heme II ligation may switch from His/Met to His/Lys now that this heme is oxidised, returning to the start of the catalytic cycle.

As in the *Cj*-type mechanism, the di-ferrous enzyme where the active site is thiosulphonated may undergo an off-pathway reaction to form cysteine persulphide and sulphite (Figure 6.3, B to E). The low E_M of His/Lys ligated heme II increases the driving force for this reaction and so this reaction is only likely to occur from this form. LC-MS suggests that this species does not react with tetrathionate to form thioperoxosulphonate, but does form cysteine thiosulphonate in the presence of thiosulphate (Figure 5.12). Heme I is also likely to be inactive in this form. One molecule of thiosulphate could nucleophilically attack the β sulphur of cysteine persulphide, forming cysteine thiosulphonate and releasing sulphide to the distal pocket of heme I by disulphide exchange (Figure 6.3, E, blue arrows). As sulphide is likely to be unstable at all but very basic pH values, it is likely that this species becomes (di-)protonated, forming bisulphide (or hydrogen sulphide) rationalising how cysteine thiosulphonate is found as a greater percentage of thiosulphate-incubated *Av* WT samples at pH 5 compared to pH 7 (Figure 5.12). There is evidence that bisulphide (or hydrogen sulphide) can bind to ferric hemes¹⁴⁶ and the heme I environment of dithionite-soaked *Av* WT crystals features such a species (although protonation is not resolved)⁹. Water could subsequently displace this, returning the enzyme to the main

catalytic cycle. The reason that this reaction does not occur in *Cj*-type TsdA and cysteine thioperoxosulphonate is formed is unlikely to be due to the possibility of His/Lys ligation at heme II, as it is likely that the inactive heme I prevents anything but disulphide exchange reactions. Instead, it could be speculated that differences in the shape of the heme I binding pocket between enzymes may sterically control which reactions are possible.

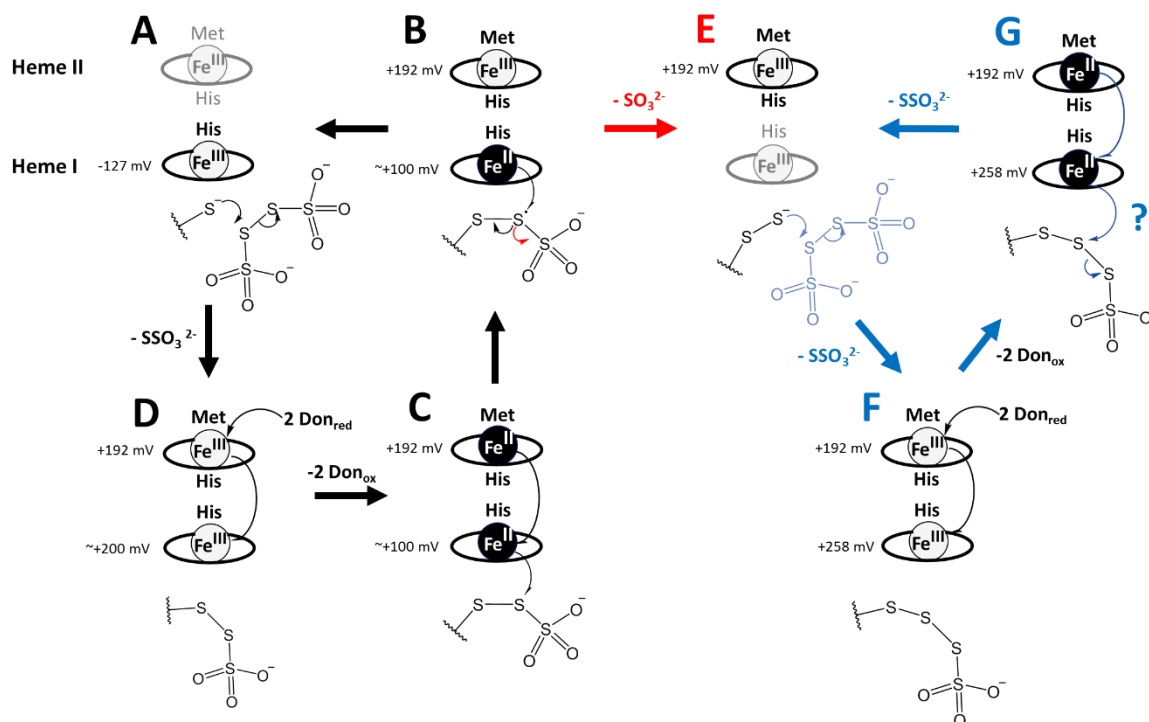


Figure 6.3 – Catalytic mechanism of *Av* TsdA in the direction of thiosulphate oxidation (black arrows) – Ferric hemes shown in white when electron exchange is permitted and grey when it is prevented, ferrous hemes shown in black. Electroactive hemes show axial ligands and E_M values. Acc = Ferricyanide or other high E_M electron acceptor. Red arrows show cysteine persulphide formation and the mechanism by which it could prevent sulphite inhibition. Blue arrows show possible mechanism of persulphide displacement by thiosulphate. Green arrows show how His/Met ligation may be retained at heme II allowing catalysis to proceed *via* a *Cj*-TsdA-like mechanism

At pH 7, when proton-dependent steps E to D are likely to be slow, *Av* WT has poor thiosulphate oxidation activity compared to *Cj* WT, however this activity increases after TCEP incubation (Figure 5.14) expected to convert the ~50% cysteine persulphide population present to unmodified cysteine, returning it to the main catalytic cycle. Unlike *Cj* WT, *Av* WT even after TCEP treatment shows no evidence of substrate inhibition during thiosulphate oxidation, consistent with a mechanism where sulphite is unlikely to be produced during constant turnover. The thiosulphate oxidation activity of *Av* WT and *Cj* WT is comparable when these enzymes are at optimum pH, consistent with them having essentially the same catalytic mechanism during rapid turnover (if A' to B' is possible). The apparent absence of the ability to form cysteine

thioperoxysulphonate in *Av* WT may mean that the persulphurated form of this enzyme is catalytically inactive during tetrathionate reduction, whereas the same is not necessarily true for *Cj* WT (Figure 6.2, G to E). This would explain the relatively low rate of tetrathionate reduction observed in previous *Av* WT activity experiments compared to *Cj* WT^{9,32}. It is also consistent with substrate inhibition observed for this reaction in both enzymes as the high E_M of the thioperoxosulphonated intermediate in *Cj* WT is still likely to mean that the persulphurated form of *Cj* WT has a slower turnover.

6.3. Further Studies

The mechanisms above feature modification of the heme I cysteine ligand and rationalise the purpose of strictly-controlled electron transfer to the TsdA hemes. Also proposed are a number of apparent side-reactions in the TsdA mechanism which may help *Cj* TsdA to fulfil its biological role and provide an evolutionary advantage over organisms which lack this enzyme. Heme ligand switching in *Av*-type TsdA enzymes is also proposed to relate to the modulation of electron transfer through the TsdA hemes and a variant of the 'standard' TsdA catalytic cycle has been proposed which accounts for a number of the observed differences between *Av* TsdA and *Cj* TsdA. To either support or dismiss these proposals, a number of further experiments could be performed.

MCD could be used to confirm heme ligation in *Av* C96M and *Av* C96H which has currently only been inferred from electronic absorbance. Unambiguous characterisation of these variants is likely to be informative as both are proposed to have the same heme II environment, but PFE signals suggest the His/Lys to His/Met ligand switch that occurs in the former is not present in the latter. The lack of a cysteine heme I ligand in both of these variants suggests that, like *Cj* C138H (Figure 5.8), they are unlikely to be significantly reduced by sulphite (or substrates). As such, resolution of ferrous CT bands by nIR MCD in sulphite or substrate incubated *Av* C96H/M should be possible and may determine if the presence of these in the heme I binding pocket affects the ligation at heme II.

Little MCD characterisation of cysteine-containing TsdA enzymes and variants has taken place with defined cysteine modifications, so the techniques described in this thesis for preparing samples with large populations of a given modification could valuably be used to begin setting benchmarks for the MCD spectra of these species in combination with LC-MS to confirm modifications. One issue with this is that if nIR MCD is to be recorded, samples would have to be prepared in D₂O which may lead to variable levels of isotope exchange with the protein, making LC-MS of these samples more ambiguous. One benefit of LC-MS in D₂O is that the mass change for

deuteration, rather than protonation of proteins is within the resolution limit of a mass spectrometer comparable to the one used in this thesis. Knowledge of the deuteration state of cysteine modifications could offer additional levels of information.

Currently the only evidence for a change in heme I E_M value when the TsdA active site cysteine is sulphonated or thio(peroxo)sulphonated is from PFE. To confirm if high E_M electroactivity does arise from a likely His/H₂O ligated high-spin heme, MCD or electronic absorbance of potentiometrically poised *Cj* WT samples prepared with these modifications could be recorded in combination with LC-MS of these samples to confirm cysteine status. It is expected from LC-MS that tetrathionate incubated *Cj* WT would have one high-spin His/H₂O ligated heme and one low-spin His/Met ligated heme (Figure 5.11). Both of these hemes would be substantially reduced by ascorbate (+60 mV) if they have $E_M > +60$ mV as predicted by PFE (Figure 5.17). Although this species is expected to rapidly decay to cysteine persulphide, reoxidising both hemes, removing all traces of high-spin heme and leaving two low-spin ferrous hemes with His/CysS⁻ and His/Met ligation respectively. Monitoring a suitable spectral change over time could even allow resolution of the kinetics of this process.

The enzyme activity assays performed in this thesis have been limited to thiosulphate oxidation in as-prepared or TCEP cleaned samples. LC-MS resolution of cysteine modifications in samples subsequently used in assays, especially if these were treated so that they feature one major species, may allow specific kinetic characterisation of each modified form of TsdA in a similar way to the characterisation of electroactivity by PFE and LC-MS. Tetrathionate reduction assays using reduced methyl viologen as an electron donor would be necessary to complete this characterisation and to prove or disprove the hypothesis that *Av* and *Cj* TsdA have different activities for these due to their persulphurated forms. Further to this performing these experiments at different pH values would also give more information on whether the proposed mechanism for displacement of persulphide in *Av* TsdA (Figure 6.3, B to E) is plausible and if the same occurs in *Cj* TsdA.

The combination of PFE and LC-MS analysis used to propose the electroactivity of forms of *Cj* WT could be repeated using films of *Av* TsdA to see if similar proposals can be made for the electroactivity of cysteine-modified forms of this enzyme. One complication of this is the variable nature of heme II signals which could lead to some ambiguity in modelling, especially if the extent of heme I ligand switching is dependent on heme I cysteine modifications.

Possibly the most difficult, but most useful question to answer about TsdA enzymes is the mechanism by which electron transfer to hemes is rendered active or inactive. Several conserved inter-heme residues exist in *Av* TsdA⁹ (Figure 1.7) that could plausibly provide a pathway for electron transfer. Variants of these characterised by PFE may identify changes in heme

electroactive populations which are not due to heme I E_M or cysteine modifications. It is also of interest to see if the related enzyme, SoxAX has any evidence of different heme electroactive populations or if this is just a feature of TsdA enzymes. If the molecular origin for such properties could be identified, this might allow for the introduction of switch-like capability into engineered proteins, which may have biotechnological applications.

References

- (1) Smith, A. J. *J. Gen. Microbiol.* **1966**, 42 (3), 371.
- (2) Hensen, D.; Sperling, D.; Trüper, H. G.; Brune, D. C.; Dahl, C. *Mol. Microbiol.* **2006**, 62, 794-810
- (3) Kurth, J. M.; Dahl, C.; Butt, J. N. *J. Am. Chem. Soc.* **2015**, 137 (41), 13232.
- (4) Liu, Y. W.; Denkmann, K.; Kosciow, K.; Dahl, C.; Kelly, D. J. *Mol. Microbiol.* **2013**, 88 (1), 173.
- (5) Grabarczyk, D. B.; Chappell, P. E.; Eisel, B.; Johnson, S.; Lea, S. M.; Berks, B. C. *J. Biol. Chem.* **2015**, 290 (14), 9209.
- (6) Page, C. C.; Moser, C. C.; Chen, X.; Dutton, P. L. *Nature* **1999**, 402 (6757), 47.
- (7) Rich, P. R.; Rich, P. *Biochem. Soc. Trans.* **2003**, 1095.
- (8) Maia, L. B.; Moura, J. J. G. *Chem. Reviews* **2014**, 114, S273-S357.
- (9) Brito, J. A.; Denkmann, K.; Pereira, I. S. A. C.; Archer, M.; Dahl, C. *J. Biol. Chem.* **2015**, 290 (14), 9222.
- (10) Ferguson, S. *J. Biochem. Soc. Trans.* **2001**, 29, 629.
- (11) Kappler, U.; Aguey-Zinsou, K.-F.; Hanson, G. R.; Bernhardt, P. V; McEwan, A. G. *J. Biol. Chem.* **2004**, 279 (8), 6252.
- (12) Von Jagow, G.; Sebald, W. *Annu. Rev. Biochem.* **1980**, 49, 281.
- (13) Raw, I.; Da Silva, A. A. *Exp. Cell Res.* **1965**, 40 (3), 677.
- (14) Hooper, A. B.; Maxwell, P. C.; Terry, K. R. *Biochemistry* **1978**, 4, 2984-2989.
- (15) Shimada, H.; Orii, Y. *FEBS Lett.* **1975**, 54 (2), 237.
- (16) Arciero, D. M.; Hooper, A. B. *J. Biol. Chem.* **1993**, 268 (20), 14645.
- (17) Ullrich, V.; Ruf, H. H.; Wende, P. *Croat. Chem. Acta* **1977**, 49 (2), 213.
- (18) Chreifi, G.; Baxter, E. L.; Doukov, T.; Cohen, A. E.; McPhillips, S. E.; Song, J. *Proc. Nat. Ac. Sci.* **2015**, 113, 1226-1231.
- (19) Rigby, S. E. J.; Moore, G. R.; Gray, J. C.; Gadsby, P. M.; George, S. J.; Thomson, A. *J. Biochem. J.* **1988**, 256, 571.
- (20) Munro, A. W.; Girvan, H. M.; Mclean, K. J.; Cheesman, M. R.; Leys, D. *Heme and Hemoproteins*, **2009**, Landes Bioscience, pp. 411-434.
- (21) Collins, M. J.; Arciero, D. M.; Hooper, A. B. *J. Biol. Chem.* **1993**, 268 (20), 14655.

- (22) Cedervall, P.; Hooper, A. B.; Wilmot, C. M. *Biochemistry* **2013**, 52 (36), 6211.
- (23) Maalcke, W. J.; Dietl, A.; Marritt, S. J.; Butt, J. N.; Jetten, M. S. M.; Keltjens, J. T.; Barends, T. R. M.; Kartal, B. J. *Biol. Chem.* **2014**, 289 (3), 1228.
- (24) Pettersen, E. F.; Goddard, T. D.; Huang, C. C.; Couch, G. S.; Greenblatt, D. M.; Meng, E. C.; Ferrin, T. E. *J. Comput. Chem.* **2004**, 25 (13), 1605.
- (25) Tezcan, F. A.; Winkler, J. R.; Gray, H. B. *J. Am. Chem. Soc.* **1998**, 120 (51), 13383.
- (26) Nicolet, Y.; Rohac, R.; Martin, L.; Fontecilla-Camps, J. C. *Proc. Natl. Acad. Sci.* **2013**, 110 (18), 7188.
- (27) Davis, K. M.; Kosheleva, I.; Henning, R. W.; Seidler, G. T.; Pushkar, Y. *Journal of Physical Chemistry B.* **2013**, pp 9161–9169.
- (28) Wickstrand, C.; Dods, R.; Royant, A.; Neutze, R. *Biochim. Biophys. Acta - Gen. Subj.* **2015**, 1850 (3), 536.
- (29) Denkmann, K.; Grein, F.; Zigann, R.; Siemen, A.; Bergmann, J.; van Helmont, S.; Nicolai, A.; Pereira, I. A. C.; Dahl, C. *Environ. Microbiol.* **2012**, 14 (10), 2673-2688.
- (30) Kurth, J. M.; Brito, J. a.; Reuter, J.; Flegler, A.; Koch, T.; Franke, T.; Klein, E. M.; Rowe, S. F.; Butt, J. N.; Denkmann, K.; Pereira, I. A. C.; Archer, M.; Dahl, C. *J. Biol. Chem.* **2016**, 291 (48), 24804.
- (31) Kurth, J. M.; Schuster, A.; Seel, W.; Herresthal, S.; Simon, J.; Dahl, C. *FEMS Microbiol Lett* **2017**, 364 (2), 1.
- (32) Kurth, J. M.; Butt, J. N.; Kelly, D. J.; Dahl, C. *Biosci. Rep.* **2016**, 36 (6), e00422.
- (33) Brito, J. A.; Gutierrez, A.; Denkmann, K.; Dahl, C.; Archer, M. *Acta Crystallogr. Sect. F, Struct. Biol. Commun.* **2014**, 70 (Pt 10), 1424.
- (34) Bradley, J. M.; Silkstone, G.; Wilson, M. T.; Cheesman, M. R.; Butt, J. N. *J. Am. Chem. Soc.* **2011**, 133 (49), 19676.
- (35) Van Wonderen, J. H.; Knight, C.; Oganessian, V. S.; George, S. J.; Zumft, W. G.; Cheesman, M. R. *J. Biol. Chem.* **2007**, 282 (38), 28207.
- (36) Wherland, S.; Pecht, I. *Proteins Struct. Funct. Bioinforma.* **2018**, 86 (8), 817.
- (37) Gouterman, M. *J. Chem. Phys.* **1959**, 30 (5), 1139.
- (38) Gouterman, M. *J. Mol. Spectrosc.* **1961**, 6 (C), 138.
- (39) Yang, T. C.; McNaughton, R. L.; Clay, M. D.; Jenney, F. E.; Krishnan, R.; Kurtz, D. M.; Adams, M. W. W.; Johnson, M. K.; Hoffman, B. M. *J. Am. Chem. Soc.* **2006**, 128 (51), 16566.

- (40) McKnight, J.; Cheesman, M. R.; Reed, C. A.; Orosz, R. D.; Thomson, A. J. *J. Chem. Soc.* **1991**, 0, 1887-1894.
- (41) Cheesman, M. R.; le Brun, N. E.; Kadir, F. H.; Thomson, a J.; Moore, G. R.; Andrews, S. C.; Guest, J. R.; Harrison, P. M.; Smith, J. M.; Yewdall, S. J. *Biochem. J.* **1993**, 292, 47.
- (42) Rønne, C.; Åstrand, P.-O.; Keiding, S. R. *Phys. Rev. Lett.* **1999**, 82 (14), 2888.
- (43) Buckingham, A.; Stephens, P. *Annu. Rev. Phys. Chem.* **1966**, 17, 399.
- (44) Berka, V.; Palmer, G.; Chen, Pe.-F.; Tsai, A.-L. *Biochemistry* **1998**, 37 (98), 6136.
- (45) Zhong, F.; Lisi, G. P.; Collins, D. P.; Dawson, J. H.; Pletneva, E. V. *Proc. Natl. Acad. Sci.* **2014**, 111 (3), E306.
- (46) Thomson, A. J.; Gadsby, P. M. *J. Chem. Soc. Dalton. Trans.* **1990**, 10, 1921.
- (47) Cheesman, M. R.; Greenwood, C.; Thomson, A. J. *Advances in Inorganic Chemistry* **1991**, 36, 201-255.
- (48) Marritt, S. J.; Kemp, G. L.; Xiaoe, L.; Durrant, J. R.; Cheesman, M. R.; Butt, J. N. *J. Am. Chem. Soc.* **2008**, 130, 8588.
- (49) Bradley, J. M.; Marritt, S. J.; Kihlken, M. A.; Haynes, K.; Hemmings, A. M.; Berks, B. C.; Cheesman, M. R.; Butt, J. N. *J. Biol. Chem.* **2012**, 287 (48), 40350.
- (50) Van Wonderen, J.; Li, D.; Piper, S.; Lau, C.; Piper, L.; Hall, C.; Clarke, T.; Watmough, N.; Butt, J. N. *ChemBioChem* **2018**.
- (51) Yu, Y.; Mukherjee, A.; Nilges, M. J.; Hosseinzadeh, P.; Miner, K. D.; Lu, Y. *J. Am. Chem. Soc.* **2014**, 136 (4), 1174.
- (52) Adamson, H.; Robinson, M.; Bond, P. S.; Soboh, B.; Gillow, K.; Simonov, A. N.; Elton, D. M.; Bond, A. M.; Sawers, R. G.; Gavaghan, D. J.; Parkin, A. *Anal. Chem.* **2017**, 89 (3), 1565.
- (53) Pettigrew, G. W.; Meyer, T. E.; Bartsch, R. G.; Kamen, M. D. *BBA - Bioenerg.* **1976**, 430 (2), 197.
- (54) Kurnikov, I. V.; Ratner, M. A.; Pacheco, A. A. *Biochemistry* **2005**, 44 (6), 1856.
- (55) George, P. *J. Biol. Chem.* **1953**, 201 (1), 427.
- (56) Stankovich, M. T. *Anal. Biochem.* **1980**, 109 (2), 295.
- (57) Bard, A. J.; Faulkner, L. R. *Electrochemical Methods, 2nd ed.*; John Wiley & Sons Inc., **2001**.
- (58) Clarke, T. A.; Dennison, V.; Seward, H. E.; Cole, J. A.; Hemmings, A. M.; Richardson, D. J. *J. Biol. Chem.* **2004**, 279 (40), 41333.

- (59) Armstrong, F. A.; Hill, H. A. O.; Oliver, B. N.; Psalti, I. S. M.; Bond, A. M. *J. Am. Chem. Soc.* **1989**, 111 (26), 9185.
- (60) Armstrong, F. A.; Heering, H. A.; Hirst, J. *Chem. Soc. Rev.* **1997**, 26 (3), 169.
- (61) Armstrong, F. A.; Camba, R.; Heering, H. A.; Hirst, J.; Jeuken, L. J. C.; Jones, A. K.; Léger, C.; McEvoy, J. P. *Faraday Discuss.* **2000**, 116, 191.
- (62) Hirst, J.; Duff, J. L. C.; Jameson, G. N. L.; Kemper, M. A.; Burgess, B. K.; Armstrong, F. A. *J. Am. Chem. Soc.* **1998**, 120 (8), 7085.
- (63) Laviron, E.; Roullier, L. *J. Electroanal. Chem.* **1980**, 115 (1), 65.
- (64) Xu, L.; Armstrong, F. A. *Energy Environ. Sci.* **2013**, 6 (7), 2166.
- (65) Plumeré, N.; Rüdiger, O.; Oughli, A. A.; Williams, R.; Vivekananthan, J.; Pöller, S.; Schuhmann, W.; Lubitz, W. *Nat. Chem.* **2014**, 6 (9), 822.
- (66) Armstrong, F. A.; Wilson, G. S. *Electrochim. Acta* **2000**, 45 (15-16), 2623.
- (67) Weber, K.; Creager, S. E. *Anal. Chem.* **1994**, 66, 3164.
- (68) Jenner, L. P.; Butt, J. N. *Curr. Opin. Electrochem.* **2018**, 8, 81-88.
- (69) Blanford, C. F.; Armstrong, F. A. *J. Solid State Electrochem.* **2006**, 10 (10), 826.
- (70) Lockwood, C. W. J.; Burlat, B.; Cheesman, M. R.; Kern, M.; Simon, J.; Clarke, T. A.; Richardson, D. J.; Butt, J. N. *J. Am. Chem. Soc.* **2015**, 137 (8), 3059.
- (71) Xu, L.; Armstrong, F. A. *RSC Adv.* **2015**, 5 (5), 3649.
- (72) Adamson, H.; Simonov, A. N.; Kierzek, M.; Rothery, R. A.; Weiner, J. H.; Bond, A. M.; Parkin, A. *Proc. Natl. Acad. Sci.* **2015**, 112 (47), 14506.
- (73) Baffert, C.; Sybirna, K.; Ezanno, P.; Lautier, T.; Hajj, V.; Meynial-Salles, I.; Soucaille, P.; Bottin, H.; Léger, C. *Anal. Chem.* **2012**, 84 (18), 7999.
- (74) Muguruma, H.; Iwasa, H.; Hidaka, H.; Hiratsuka, A.; Uzawa, H. *ACS Catal.* **2017**, 7 (1), 725.
- (75) El Kasmi, A.; Wallace, J. M.; Bowden, E. F.; Binet, S. M.; Linderman, R. J. *J. Am. Chem. Soc.* **1998**, 120 (1), 225.
- (76) Stieger, K. R.; Feifel, S. C.; Lokstein, H.; Lisdat, F. *Phys. Chem. Chem. Phys.* **2014**, 16 (29), 15667.
- (77) Hwang, E. T.; Sheikh, K.; Orchard, K. L.; Hojo, D.; Radu, V.; Lee, C. Y.; Ainsworth, E.; Lockwood, C.; Gross, M. A.; Adschiri, T.; Reisner, E.; Butt, J. N.; Jeuken, L. J. C. *Adv. Funct. Mater.* **2015**, 25 (15), 2308.

- (78) Ashur, I.; Schulz, O.; McIntosh, C. L.; Pinkas, I.; Ros, R.; Jones, A. K. *Langmuir* **2012**, 28 (13), 5861.
- (79) Reuillard, B.; Ly, K. H.; Hildebrandt, P.; Jeuken, L. J. C.; Butt, J. N.; Reisner, E. *J. Am. Chem. Soc.* **2017**, 139 (9), 3324.
- (80) Yang, X.-Y.; Chen, L.-H.; Li, Y.; Rooke, J. C.; Sanchez, C.; Su, B.-L. *Chem. Soc. Rev.* **2017**, 46 (2), 481.
- (81) Mersch, D.; Lee, C. Y.; Zhang, J. Z.; Brinkert, K.; Fontecilla-Camps, J. C.; Rutherford, A. W.; Reisner, E. *J. Am. Chem. Soc.* **2015**, 137 (26), 8541.
- (82) Peters, K.; Lokupitiya, H. N.; Sarauli, D.; Labs, M.; Pribil, M.; Rathousky, J.; Kuhn, A.; Leister, D.; Stefik, M.; Fattakhova-Rohlfing, D. *Adv. Funct. Mater.* **2016**, 26 (37), 6682.
- (83) Shen, B.; Martin, L. L.; Butt, J. N.; Armstrong, F. A.; Stout, C. D.; Jensen, G. M.; Stephens, P. J.; La Mar, G. N.; Gorst, C. M.; Burgess, B. K. *J. Biol. Chem.* **1993**, 268 (34), 25928.
- (84) Sokol, K. P.; Mersch, D.; Hartmann, V.; Zhang, J. Z.; Nowaczyk, M. M.; Rögner, M.; Ruff, A.; Schuhmann, W.; Plumeré, N.; Reisner, E. *Energy Environ. Sci.* **2016**, 9 (12), 3698.
- (85) Guilhaus, M.; Selby, D.; Mlynski, V. *Mass Spectrom Rev* **2000**, 19 (2), 65.
- (86) Yamashita, M.; Fenn, J. B. *J. Phys. Chem.* **1984**, 88 (20), 4451.
- (87) Whitehouse, C. M.; Dreyer, R. N.; Yamashita, M.; Fenn, J. B. *Anal. Chem.* **1985**, 57 (3), 675.
- (88) McKnight, J.; Cheesman, M. R.; Thomson, A. J.; Miles, J. S.; Munro, A. W. *Eur. J. Biochem.* **1993**, 213 (2), 683.
- (89) Cheesman, M. R.; Little, P. J.; Berks, B. C. *Biochemistry* **2001**, 40 (35), 10562.
- (90) Gadsby, P. M. A.; Peterson, J.; Foote, N.; Greenwoodt, C.; Thomson, A. J. *Biochem. J.* **1987**, 246, 43.
- (91) Singh, S.; Madzellan, P.; Stasser, J.; Weeks, C. L.; Becker, D.; Spiro, T. G.; Penner-Hahn, J.; Banerjee, R. *J. Inorg. Biochem.* **2009**, 103 (5), 689.
- (92) Motomura, T.; Suga, M.; Hienerwadel, R.; Nakagawa, A.; Lai, T.; Nitschke, W.; Kuma, T.; Sugiura, M.; Boussac, A.; Shen, J. *J. Biol. Chem.* **2017**, 292, 9599.
- (93) Reijerse, E. J.; Sommerhalter, M.; Hellwig, P.; Quentmeier, A.; Rother, D.; Laurich, C.; Bothe, E.; Lubitz, W.; Friedrich, C. G. *Biochemistry* **2007**, 46 (26), 7804.
- (94) Miller, J. E.; Grădinaru, C.; Crane, B. R.; Di Bilio, A. J.; Wehbi, W. a.; Un, S.; Winkler, J. R.; Gray, H. B. *J. Am. Chem. Soc.* **2003**, 125 (47), 14220.
- (95) Scott Mathews, F. *Prog. Biophys. Mol. Biol.* **1985**, 45 (1), 1.

- (96) Ubbink, M.; Canters, G. W.; Campos, A. P.; Teixeira, M.; Hunt, N. I.; Hill, H. A. O. *Biochemistry* **1994**, 33 (33), 10051.
- (97) Mayhew, S. G. *Eur. J. Biochem.* **1978**, 85 (2), 535.
- (98) Perera, R.; Sono, M.; Sigman, J. A.; Pfister, T. D.; Lu, Y.; Dawson, J. H. *Proc. Natl. Acad. Sci. U. S. A.* **2003**, 100 (7), 3641.
- (99) Vincent, K. A.; Tilley, G. J.; Quammie, N. C.; Streeter, I.; Burgess, B. K.; Myles, R. *Chem. Comm.* **2003**, 2590.
- (100) Kilmartin, J. R.; Bernhardt, P. V.; Dhouib, R.; Hanson, G. R.; Riley, M. J.; Kappler, U. *J. Inorg. Biochem.* **2016**, 162, 309.
- (101) Grabarczyk, D. B.; Berks, B. C. *PLoS One* **2017**, 12 (3), 1.
- (102) Levin, B. D.; Walsh, K. A.; Sullivan, K. K.; Bren, K. L.; Elliott, S. *J. Inorg. Chem.* **2015**, 54 (1), 38.
- (103) Levin, B. D.; Can, M.; Bowman, S. E. J.; Bren, K. L.; Elliott, S. *J. Phys. Chem. B* **2011**, 115 (40), 11718.
- (104) Rowe, S. F.; Kurth, J. M. *Unpubl. Work.*
- (105) Barth, D.; Musiol, H. J.; Schütt, M.; Fiori, S.; Milbradt, A. G.; Renner, C.; Moroder, L. *Chem. - A Eur. J.* **2003**, 9 (15), 3692.
- (106) Jocelyn, P. C. *Eur. J. Biochem.* **1967**, 2 (3), 327.
- (107) Gat, Y.; Vardi-Kilshtain, A.; Grossman, I.; Major, D. T.; Fass, D. *Protein Sci.* **2014**, 23 (8), 1102.
- (108) Fabianek, R. A.; Hofer, T.; Thöny-Meyer, L. *Arch. Microbiol.* **1999**, 171 (2), 92.
- (109) Thöny-Meyer, L. *Biochem Soc Trans* **2002**, 30 (4), 633.
- (110) Ellman, G. L. *Arch. Biochem. Biophys.* **1959**, 82 (1), 70.
- (111) Park, C.; Weerasinghe, L.; Day, J. J.; Fukuto, J. M.; Xian, M.; States, U.; Park, R.; States, U. *Mol. Biosyst.* **2016**, 11 (7), 1775.
- (112) Hugo, M.; Turell, L.; Manta, B.; Botti, H.; Monteiro, G.; Netto, L. E. S.; Alvarez, B.; Radi, R.; Trujillo, M. *Biochemistry* **2009**, 48 (40), 9416.
- (113) Reddie, K. G.; Carroll, K. S. *Curr. Opin. Chem. Biol.* **2008**, 12 (6), 746.
- (114) Nagy, P.; Lemma, K.; Ashby, M. T. *J. Org. Chem.* **2007**, 72 (23), 8838.
- (115) Iribarne, J. V.; Thomson, B. A. *J. Chem. Phys.* **1976**, 64 (6), 2287.

- (116) Loo, J. A.; Udseth, H. R.; Smith, R. D. *Anal. Biochem.* **1989**, 179 (2), 404.
- (117) Hunt, D. F.; Yates, J. R.; Shabanowitz, J.; Winston, S.; Hauer, C. R. *Proc. Natl. Acad. Sci.* **1986**, 83 (17), 6233.
- (118) Bowman, L.; Flanagan, L.; Fyfe, P. K.; Parkin, A.; Hunter, W. N.; Sargent, F. *Biochem. J.* **2014**, 458 (3), 449.
- (119) Burns, J. A.; Butler, J. C.; Moran, J.; Whitesides, G. M. *J. Org. Chem.* **1991**, 56 (8), 2648.
- (120) Getz, E. B.; Xiao, M.; Chakrabarty, T.; Cooke, R.; Selvin, P. R. *Anal. Biochem.* **1999**, 273 (1), 73.
- (121) Bosron, W. F.; Yin, S. J.; Dwulet, F. E.; Li, T. K. *Biochemistry* **1986**, 25 (8), 1876.
- (122) Weerapana, E.; Wang, C.; Simon, G. M.; Richter, F.; Khare, S.; Dillon, M. B. D.; Bachovchin, D. A.; Mowen, K.; Baker, D.; Cravatt, B. F. *Nature* **2010**, 468 (7325), 790.
- (123) Alcock, L. J.; Perkins, M. V.; Chalker, J. M. *Chem. Soc. Rev.* **2018**, 47 (1), 231.
- (124) Mavridou, D. A. I.; Stevens, J. M.; Ferguson, S. J.; Redfield, C. *J. Mol. Biol.* **2007**, 370 (4), 643.
- (125) Lo Conte, M.; Carroll, K. S. *J. Biol. Chem.* **2013**, 288 (37), 26480.
- (126) Francoleon, N. E.; Carrington, S. J.; Fukuto, J. M. *Arch. Biochem. Biophys.* **2011**, 516 (2), 146.
- (127) Ida, T.; Sawa, T.; Ihara, H.; Tsuchiya, Y.; Watanabe, Y.; Kumagai, Y.; Suematsu, M.; Motohashi, H.; Fujii, S.; Matsunaga, T.; Yamamoto, M.; Ono, K.; Devarie-Baez, N. O.; Xian, M.; Fukuto, J. M.; Akaike, T. *Proc. Natl. Acad. Sci.* **2014**, 111 (21), 7606.
- (128) Mustafa, A. K.; Gadalla, M. M.; Sen, N.; Kim, S.; Mu, W.; Gazi, S. K.; Barrow, R. K.; Yang, G.; Wang, R.; H, S. *Science Signalling* **2009**, 96, 2, 1-8.
- (129) Vandiver, M. S.; Paul, B. D.; Xu, R.; Karuppagounder, S.; Rao, F.; Snowman, A. M.; Seok Ko, H.; Il Lee, Y.; Dawson, V. L.; Dawson, T. M.; Sen, N.; Snyder, S. H. *Nat. Commun.* **2013**, 4, 1.
- (130) Krishnan, N.; Fu, C.; Pappin, D. J.; Tonks, N. K. *Sci. Signal.* **2011**, 4 (203), 1.
- (131) Tsuyoshi, T.; Tsuchiya, Y.; Ida, T.; Sawa, T.; Akaike, T.; Watanabe, Y. *Nitric Oxide* **2014**, 42, 99.
- (132) Broillet, M. C. *Cell. Mol. Life Sci.* **1999**, 55 (8-9), 1036.
- (133) Nikitovic, D.; Holmgren, A. *J. Biol. Chem.* **1996**, 271 (32), 19180.

- (134) Kang, P. T.; Chen, C. L.; Lin, P.; Zhang, L.; Zweier, J. L.; Chen, Y. R. *J. Mol. Cell. Cardiol.* **2018**, 121, 190.
- (135) Allison, W. S. *Acc. Chem. Res.* **1976**, 9 (8), 293.
- (136) Bamford, V. A.; Bruno, S.; Rasmussen, T.; Appia-Ayme, C.; Cheesman, M. R.; Berks, B. C.; Hemmings, A. M. *EMBO J.* **2002**, 21 (21), 5599.
- (137) Allen, J. W. A.; Cheesman, M. R.; Higham, C. W.; Ferguson, S. J.; Watmough, N. J. *Biochem. Biophys. Res. Commun.* **2000**, 279 (2), 674.
- (138) Bamford, V. A.; Angove, H. C.; Seward, H. E.; Thomson, A. J.; Cole, J. A.; Butt, J. N.; Hemmings, A. M.; Richardson, D. J. *Biochemistry* **2002**, 41 (9), 2921.
- (139) Xu, Y.; Schoonen, M. A. A. *Geochim. Cosmochim. Acta* **1995**, 59 (22), 4605-4622.
- (140) Kurth, J. M. *Unpubl. Work* **2015**.
- (141) Fourmond, V.; Baffert, C.; Sybirna, K.; Lautier, T.; Abou Hamdan, A.; Dementin, S.; Soucaille, P.; Meynial-Salles, I.; Bottin, H.; Léger, C. *J. Am. Chem. Soc.* **2013**, 135 (10), 3926.
- (142) Siritanaratkul, B.; Megarity, C. F.; Roberts, T. G.; Samuels, T. O. M.; Winkler, M.; Warner, J. H.; Happe, T.; Armstrong, F. A. *Chem. Sci.* **2017**, 8 (6), 4579.
- (143) Finzelt, B. C.; Poulos, T. L.; Kraut, J. *J. Biol. Chem.* **1984**, 259 (21), 13027.
- (144) Latimer, W. M. *Oxidation Potentials*; **1952**, Prentice Hall, pp. 74.
- (145) Irwin, S. V.; Fisher, P.; Graham, E.; Malek, A.; Robidoux, A. *PLOS One* **2017**, 12 (10), 1-14.
- (146) Pietri, R.; Roma, E.; Lo, J. *Antioxidants and Redox Signalling*, **2011**, 15 (2).